Final Technical Report

Federal Agency to which Report is submitted: DOE EERE – Wind & Water Power Program
Recipient: The University of Toledo, DUNS Number: 051623734
Award Number: DE-EE0003540
Project Title: Advanced Offshore Wind Turbine/Foundation Concept for the Great Lakes
Project Period: 06/01/2010 through 05/31/2013

Principle Investigator: Dr. Abdollah Afjeh, Professor and Chair, Dept. of Mechanical, Industrial, Manufacturing Engineering, College of Engineering (419) 530-8205, Abdollah.Afjeh@utoledo.edu

Date of Report: August 29, 2013

Working Partners:

The University of Toledo
Dr. Abdollah Afjeh, Professor and Chair, Dept. of Mechanical, Industrial, Manufacturing Engineering, College of Engineering (419) 530-8205
Abdollah.Afjeh@utoledo.edu

Nautica Windpower
Dr. Larry Viterna, President, (440) 452-3732
viterna@gmail.com

OCC|COWI
Joseph Marrone, COWI Project Director, (203) 268-5007
joma@ocean-coastal.com

Nordic Windpower
Thomas Wagner, Head of Engineering, (518) 852-4898
twagner@nordicwindpower.com

Cost-Sharing Partners: The University of Toledo
Nautica Windpower
Nordic Windpower USA, Inc.

DOE Project Team:

DOE HQ Program Manager - Jose Zayas
DOE Field Contract Officer - Pamela Brodie
DOE Field Grants Management Specialist - Michael P. Hahn
DOE Field Project Officer – Laura Merrick
DOE/CNJV Project Monitor – Meghan Rodwell

Signature of Submitting Official: Dr. Abdollah Afjeh/electronic signature

Advanced Offshore Wind Turbine/Foundation Concept for the Great Lakes

Mechanical, Industrial and Manufacturing Engineering Department

The University of Toledo

August 29, 2013

Executive Summary

The availability of high, steady winds; vast real estate; and proximity to large shoreline population centers potentially make extracting offshore wind energy a highly lucrative enterprise. Although land-based wind turbines today largely employ 3-bladed rotor configurations, a 2-bladed rotor design offers significant inherent design advantages, which can be exploited to reduce the cost of offshore wind energy. Advantages include lower cost of the rotor with one less blade, lower torque on the turbine drivetrain, and lower transportation, maintenance and installation costs.

The objective of the project presented in this report was to investigate a conceptual 2-bladed rotor wind turbine design and to assess its feasibility for installation in the Great Lakes. The levelized cost of energy was used for this purpose.

Since wind turbine system design is site specific, a location in Lake Erie near the coast of Cleveland, Ohio was selected as the application site in this study. The loading environment was defined using wind and wave data collected at a weather station in Lake Erie near Cleveland. In addition, the probability distributions of the annual significant wave height and wind speed were determined. A model of the dependence of the above two quantities was also developed and used in the study of wind turbine system loads. This model predicts maximum loads more accurately than conventional models that assume independence. Loads from ice floes and ridges can be significant for the Great lakes sites and can drive the foundation design. These data were also obtained for and used in ice load analysis in this study.

The NREL 5 MW 3-bladed rotor wind turbine concept was used as the baseline design in this study. The cross sections of the baseline 5 MW wind turbine were selected using reference paper studies. The turbine design employs variable pitch blade control with tip-brakes and a teeter mechanism. The rotor diameter, rated power and the tower dimensions were selected to closely match those of the NREL 5 MW wind turbine.

A semi-floating gravity base foundation was designed for this project primarily to adapt to regional logistical constraints to transport and install the gravity base foundation with locally available equipment in Lake Erie. This semi-floating gravity base foundation consists of, from bottom to top, a base plate, a buoyancy chamber, a taper zone, a column (with ice cone), and a service platform. A compound upward-downward ice cone was selected to secure the foundation from moving because of ice impact.

The turbine loads analysis was based on International ElectroTechnical Committee (IEC) Standard 61400-1, Class III winds. The NREL software FAST was the primary computational tool used in this study to determine all design load cases. More advanced load modeling tools such as Automatic Dynamic Analysis of Mechanical Systems (ADAMS) are available for modeling wind turbine loads; however, an initial set of studies of the dynamics of wind turbines demonstrated that FAST and ADAMS load predictions were comparable. Because of its relative simplicity and short run times, FAST was selected for the purposes of this conceptual design study. For ice load calculations, a method was developed and implemented in FAST to extend its capability for ice load modeling.

A computer code was developed to efficiently manage computer simulations using FAST. This code interfaces with FAST to compute the response of a wind turbine to multiple load cases. For each case, this tool computes significant parameters, such as wind turbine annual energy production, blade deflection, maximum lifetime bending moments in the rotor blades, and forces and moments that are transmitted from the tower to the foundation. This information, together with the ice load data was used to design the turbine foundation.

Both upwind and downwind 2-bladed rotor wind turbine designs were developed and studied. When compared with the NREL 5 MW baseline turbine, the new rotor has one rotor blade removed, the blade twist angle distribution modified and a new pitch control algorithm implemented. The coning and tilt angles were selected for both the upwind and downwind configurations to maximize the annual energy production. The risk of blade-tower impact is greater for the downwind design, particularly under a power grid fault; however, this risk was effectively reduced by adjusting the tilt angle for the downwind configuration.

Conclusions

***Cost of Energy*:** This study demonstrated that the levelized cost of energy of the 2-bladed downwind design is considerably lower than that of the baseline 3-bladed design. Specifically, the cost of the 2-bladed design with redesigned blades is $0.1308/kWh and that of the optimized design is $0.117/kWh, while the cost of the baseline is $0.1453/kWh. The cost can be further reduced to $0.0868 by replacing the gravity foundation with a floating one. Two main reasons for the cost reductions are:

- The decrease in the cost of one blade and the attendant increases in reliability and availability and the reduction of the transportation and installation costs
- The substitution of the gravity foundation with a floating foundation

Overall, the evidence from this study supports the conclusion that cost of energy from offshore wind turbines can be reduced considerably by removing a blade and redesigning the remaining two without compromising safety. Developing a floating foundation would create greater opportunities for further cost reduction.

***Annual Energy Production*:** At the selected site the baseline NREL 5 MW design produces 16.9 GWh AEP, while the 2-bladed upwind and downwind designs produce between 2% to 7% less energy. However, factoring in the cost of the wind turbine itself, the predicted cost per kilowatt hour of the two-blade designs is lower than the baseline turbine. In addition, the lower torque on the 2-bladed turbine drive train is expected to reduce the maintenance costs and enhance reliability of that configuration. No significant difference in the cost of energy was found for the upwind and downwind 2-bladed turbine configurations.

***Ice Loads*:** Loads due to ice floes and ridges are significant and can drive the foundation design. A methodology was developed and implemented to calculate ice loads and predict the response of a turbine foundation. To study the significance of ice impact, FAST simulations were performed to compare the loads on an offshore wind turbine exposure to (1) only wind loads and (2) combined wind and ice loads. For this study, the 50-year ice thickness for the site was applied to a simple circular cross-section foundation. The available data indicate that ice

thickness is 61.8 cm, and ice ridge is 92.7 cm with a 11.2 m deep rubble keel. Compared with wind only loads, a 61.8 cm ice sheet increases the shear force at the foundation base by 330% and 260% for upward and downward ice breaking cones, respectively. The foundation base bending moment increases by approximately 50% for either ice cone shape. Likewise, ice thickness of 92.7 cm with an ice keel of 11.2 m produces an increase in foundation base shear forces of 1180% and 1060%, and the foundation base bending moment increases by 150% for upward and 200% for downward ice breaking cones.

Accurately modeling ice loads is an important challenge for offshore wind energy in Lake Erie to design the wind turbine foundation that can sustain these loads.

***Structural Integrity*:** The proposed 2-bladed downwind design is practically as safe as the baseline 3-bladed turbine. The 2-bladed design, however, is subjected to slightly higher loads. The predicted bending moments in the blades of the 2-bladed turbine configurations were higher than those in the NREL 5 MW baseline design. Additionally, shear forces, axial forces, root bending and torsional moments on the blades of the 2-bladed design was approximately 5% higher than the NREL baseline design. This was expected, because the rotor of the 2-bladed rotor turbines rotates faster than the NREL baseline turbine, and the blades of the former are more twisted than those of the latter design.

Acknowledgement

The following graduate students in the department of Mechanical, Industrial and Manufacturing Engineering at the University of Toledo contributed to the work reported in this final technical report: Brett Andersen, Musarrat Jehan, Jin Woo Lee, Mahdi Norouzi, Adrian Sescu, and Quiying Zhao.

Table of Contents

List of Figures

List of Tables

List of Acronyms

AEP	Annual Energy Production
BOPT	Blade OPTimized (Optimized blade)
BOS	Balance Of System
BUT	Blade of the University of Toledo
CAE	Computer Aided Engineering
CDF	Cumulative Density Function
CFD	Computational Fluid Dynamics
CM	Center of Mass
DC	Direct Current
DLC	Design Load Case
DNV	Det Norske Veritas
DOF	Degree Of Freedom
DOWEC	Dutch Offshore Wind Energy Converter
DU	Delft University
ECD	Extreme Coherent gust with Direction change
EDC	Extreme Direction Change
EOG	Extreme Operating Gust
ESS	Extreme Sea State
ETM	Extreme Turbulence Model
EWM	Extreme Wind speed Model
EWS	Extreme Wind Shear
FAST	Fatigue, Aerodynamics, Structures, and Turbulence (NWTC CAE code for HAWTs)
FAST_ICE	Enhanced FAST to model ice loads
FAST_SM	FAST Simulation Manager
FORTRAN	FORmular TRANslation programming language
GBF	Gravity Base Foundation
HAWT	Horizontal Axis Wind Turbine
HSS	High-speed-shaft
IEC	International Electrotechnical Committee
LEADERS	Leadership for Educators: Academy for Driving Economic Revitalization in Science
LCOE	Levelized Cost of Energy
LSS	Low-speed-shaft
MIME	Mechanical, Industrial and Manufacturing Engineering
NACA	National Advisory Committee for Aeronautics
NAWEA	North American Wind Energy Academy
NDBC	National Data Buoy Center
NOAA	National Oceanic and Atmospheric Administration
NREL	National Renewable Energy Laboratory
NSS	Normal Sea State
NTM	Normal Turbulence Model
NWP	Normal Wind Profile model

NWTC	National Wind Technology Center
PDS	Project-Based Science
PDF	Probability Density Function
RMS	Root Mean Square
RPM	Revolution Per Minute
SCADA	Supervisory Control And Data Acquisition
SNL	Sandia National Lab
TAG	Transfer Assurance Guides
TSR	Tip Speed Ratio
USACE	US Army Corps of Engineers
UT	University of Toledo
WIS	Wave Information Studies

List of Symbols

A	Swept area
A_1, A_2, A_3, A_4	Dimensionless coefficients for cone angle of ice cone of foundation
B_1, B_2	Dimensionless ice to cone friction coefficients of ice cone of foundation
a	Acceleration
b	Baseline model
C	Copula function
C_D	Drag coefficient
C_M	Inertia coefficient
C_p	Coefficient of power
c	Cohesion within the keel
D	Diameter
D_c	Cone diameter at the waterline
D_w	Diameter of the structure at the waterline
d	Water depth
D_j^{Life}	Extrapolated lifetime damage due to j^{th} time series
D_T	Diameter at the narrow end of the cone (same as the tower diameter)
E	Module of elasticity
$E(v)$	Mean value of v
F	Force
$F(H_{s50})$	Probability of not exceeding H_{s50}
$F(V_{e50})$	Probability of not exceeding V_{e50}
$f(v)$	Probability density function of the wind speed in one year
FDD	Cumulative Freezing Degree-days
F_U, F_V	Cumulative distribution functions of U and V
G	Gravitational acceleration
g	Gravitational acceleration
H	Wave height
H_d	Horizontal force
H_s	Significant wave heights
H_{s1}	1-year extreme significant wave height
H_{s50}	50-year extreme significant wave height
$\bar{H}$	Mean value of significant wave height
h	Ice sheet thickness
h_c	Consolidated layer thickness
h_{ice}	Ice thickness
h_k	Total draft of the keel as measured from the waterline
h_{keel}	Depth of the ice keel
I	Moment of inertia

i	Index of load effect for various load effect types at locations of interest for weighted percent difference calculation
j	Model number
K	Stiffness matrix
K_p	Passive pressure coefficient of the rubble
k	Shape parameter of Weibull distribution
k_1	Shape factor of the structure where the ice is hitting it
k_2	Contact factor between the ice and support structure
k_3	Aspect ratio factor, given as $\sqrt{1+5h/D_w}$, where h is the ice thickness
L	Wave length
L_{ji}^{R}	Load range about mean L_{ji}^{M} for i^{th} cycle in j^{th} time-series
L^{MF}	Fixed load-mean
L^{ult}	Ultimate design load of the component
M	Moment
m	Wohler exponent of the component
N	Total number of kinds of load effects considered
N_{ij}	Cycles to failure
n	Size of the population
n_{ij}^{Life}	Extrapolated cycle counts
$P(v)$	Generated power at a given wind speed
P_r	Rated power
P_w	Water density
$(P\|v_{\text{bin}})$	Power generated at the wind speed v_{bin}
p	Exponent of weight term
q	Factor that determines the importance of each load effect
R	Rotor radius
S	Effect of any surcharge
s	Scale for normalization
T	Wave period
T_p	Wave period
Tp	Power spectral period
$T_{p\,\max}$	Maximum wave period
$T_{p\,\min}$	Minimum wave period
t_c	95% percentile value of the Student distribution
V	Wind speed
V_{e1}	1-year extreme wind speed
V_{e50}	50-year extreme wind speed
V_{hub}	Wind speed at hub height
V_{in}	Cut-in wind speed
$V_{\max}$	Maximum wind speed

$V_{\min}$	Minimum wind speed
V_{out}	Cut-out wind speed
V_r	Rated wind speed
V_T	Measured mean wind speed over period *T*
$\bar{V}$	Average value of the maximum annual speeds
v	Wind speed
v_{bin}	Wind speed for a bin
$v_{\text{bin max}}$	Upper bound of the wind speed of the bin
$v_{\text{bin min}}$	Lower bound of the wind speed of the bin
v_{in}	Cut-in speed
v_{out}	Cut-out speed
v_r	Rated wind speed
W_e	Effective structure width
X_{50}	50-year extreme wind speed
x	Penetration distance of the foundation into the keel
x_b	x direction of blade root coordinate system
x_p	x direction of tower top coordinate system
x_s	x direction of LSS coordinate system
x_t	x direction of tower base coordinate system
xy_b	xy plane of blade root coordinate system
xy_p	xy plane of tower top coordinate system
xy_s	xy plane of LSS coordinate system
xy_t	xy plane of tower base coordinate system
y_b	y direction of blade root coordinate system
y_p	y direction of tower top coordinate system
y_s	y direction of LSS coordinate system
y_t	y direction of tower base coordinate system
z	Hub height
z_b	z direction of blade root coordinate system
z_p	z direction of tower top coordinate system
z_r	Height at which the wind speed is measured
z_s	z direction of LSS coordinate system
z_t	z direction of tower base coordinate system

α	Exponent of the power law (shear factor)
β	Wave direction
γ	Threshold of 3-parameter lognormal distribution
γ_{eff}	Effective buoyant density of the keel rubble, including effects of porosity
δ	Threshold of 3-parameter Weibull distribution
δ	Displacement
θ	Angular deformation
θ'	Dependence variable
θ_k	Angle that the keel rubble makes with the horizontal
η_{DT}	Efficiency of drive train

η_m	Weighted percent difference
λ	Scale parameter of Weibull distribution
μ	Location parameter of 3-parameter lognormal distribution
ξ	Load effect value
ϱ	Scale parameter of 3-parameter lognormal distribution
σ	Standard deviation
σ_b	Ice bending strength
σ_c	Crushing strength of the ice
ρ	Density of air
ρ_w	Water density
ϕ	Cone angle
ϕ_f	Internal friction angle of the rubble
ψ	Shaft tilt angle

1 Objective

The objective of the project is to conduct a preliminary design of a downwind 2-bladed rotor turbine concept and to assess its feasibility for application in the Great Lakes. The levelized cost of energy is used to measure the merit of the design.

The above objectives are achieved by comparing the safety and cost of the following configurations:

1. A 5 MW 3-bladed wind turbine design developed by NREL (NREL 5 MW)
2. 2-bladed upwind and downwind variants of the above turbine

The following tasks were to be completed to achieve the project objective:

1. Design a two-blade upwind, and downwind configuration for the Lake Erie environment. This involves the following steps:
    - Design the rotor
    - Develop a power control method. This involves the PI control for the 2-bladed downwind configuration.
    - Define the blade properties
        - Geometry: blade geometry chord, thickness-to-chord-ratio and twist distribution for the two-blade rotor.
        - Structural properties: mass and stiffness distribution for new blade geometry.
        - Analyze natural frequencies of new blades
    - Optimize cone and tilt angles to maximize energy production while minimizing the risk of a blade impact with the tower
    - Define the teeter mechanism properties
    - Model tower shadow effects
    - Optimize the blades twist angle
2. Develop or collect the requisite tools to assess the safety and efficiency of the designs in this study. These include:
    - A simulation manager code that enables the user to create input files for simulations of the turbine operation in an automated fashion
    - Post processing tools
    - Add to the FAST code the capability to model ice impact and determine the ice loads
    - Tune the control algorithm for a 2-bladed rotor configuration
    - Develop a cost model to compute the levelized cost of turbine and its components
3. Select the most suitable foundation type and design it
    - Optimize the dimensions to minimize the wave and ice load effects.

4. Review and model the loading environment at the location of the turbine. Consider the following loads for this purpose:
    - Wind
    - Wave
    - Ice

    This step involves estimation of the probability distributions of the wind speed and wave height, and the statistical dependence of these quantities.

5. Perform simulation to assess the load effects on the blades, the tower and the foundation. In this step, the investigators will quantify the risk of failure due to first excursion, fatigue damage accumulation and blade impact. They will compare these risks for the three alternative designs in this project.

6. Consider future opportunities for improving the offshore wind turbine concept. Make a plan to:
    - Optimize the blades, tower, teeter mechanism
    - Develop independent pitch control
    - Estimate the levelized cost of new concepts, which could be more suitable for the Lake Erie environment.

2 Introduction

2.1 Multi-megawatt Offshore Wind Turbines

This section will cover the following topics:

- Importance of wind energy as a potential renewable energy source
- Limitations of on-shore wind turbines, and potential advantages off-shore turbines
- Challenges in the development of large off-shore wind turbines

The need to harness energy from renewable sources is on the rise. Wind energy has already been recognized as a potential alternative option to traditional energy sources such as coal and nuclear power plants. However, the main challenge for wind energy to compete economically with other relatively cheap energy sources is the reduction of the cost per kWh.

In order to produce wind energy at a comparable cost to that from traditional sources, wind turbines need to produce more power, which demands bigger turbines. However, for onshore wind turbines, the size of the turbine is restricted by the noise concerns as well as their visual impact on the environment.

On the other hand, off-shore wind energy technology is more viable than the onshore wind technology as there are fewer limitations in terms of noise and visual concerns. Off-shore turbines are limited in size only by the availability of appropriate technology.

Yet, the installation and maintenance cost of a conventional large off-shore wind turbines is substantially greater than that of an onshore wind turbine with same power production capacity. Moreover, these turbines are subjected to significantly greater loads than their onshore counterparts. These include loads due to waves and ice impact, whose intensity increases with the turbine size.

Therefore, it is critical to develop new design concepts that are simpler and more economical than traditional designs. Examples include 2-bladed upwind and downwind configurations and flexible, floating designs. In order to study these designs we need accurate computational tools for modeling the loading environment, predicting the applied loads and their effects on an offshore wind turbine, and assessing their structural integrity.

2.2 Review of the 3-bladed 5 MW wind turbine

For the purposes of this study, the central basin of Lake Erie defined by a band three to five miles off the Cuyahoga County shore, close to the city of Cleveland, Ohio was considered as the wind turbine site. The water depth at this location varies between 13-17 m. The main sources of environmental data used here are from the National Oceanic and Atmospheric Administration (NOAA) buoy 45005, a wind resource report by Dykes et al., [2008], and a Great Lakes feasibility study document by Marshall et al., [2009]. Both Marshall's and Dykes' studies were

conducted for the same location. To define the load cases, the historical data from the buoy were used in conjunction with the report by Marschall et al., [2009].

To support the research and development in the field of wind energy, the National Renewable Energy Laboratory (NREL) has developed a 5-MW wind turbine concept [Jonkman et al., 2009]. This is a conventional three-bladed upwind variable-speed variable blade-pitch-to-feather-controlled turbine. The properties are summarized in Table 2.1.

Table 2.1. Properties of NREL 5 MW baseline wind turbine.

Rating	5 MW
Rotor Orientation, Configuration	Upwind, 3 Blades
Control	Variable Speed, Collective Pitch
Rotor, Hub Diameter	126 m, 3 m
Hub Height	90 m
Cut-In, Rated, Cut-Out Wind Speed	3, 11.4, 25 m/s
Rated Rotor Speed	12.1 RPM
Rotor Mass	110 tons
Nacelle Mass	240 tons
Tower Mass	347.5 tons

The structural properties of the blades in the NREL concept are based on the properties of the blades from the Dutch Offshore Wind Energy Converter (DOWEC) concept project [Kooijman et al., 2003]. The rated power of the DOWEC project is 6 MW, so the blades were adjusted for 5 MW rated power. The structural properties of the blades at different sections are summarized in Jonkman et al., [2009]. The aerodynamic properties of the airfoils used in the blades are also based on the concept developed by DOWEC [Kooijman et al., 2003].

The Nacelle and the Hub properties of the NREL concept are summarized in Table 2.2.

Table 2.2. Nacelle and Hub properties [Jonkman et al., 2009].

Elevation of Yaw Bearing above Ground	87.6 m
Vertical Distance along Yaw Axis from Yaw Bearing to Shaft	1.96256 m
Distance along Shaft from Hub Center to Yaw Axis	5.01910 m
Distance along Shaft from Hub Center to Main Bearing	1.912 m
Hub Mass	56.780 kg
Hub Inertia about Low-Speed Shaft	115,926 kg.m^2
Nacelle Mass	240,000 kg
Nacelle Inertia about Yaw Axis	2,607,890 kg.m^2
Nacelle CM Location Downwind of Yaw Axis	1.9 m
Nacelle CM Location above Yaw Bearing	1.75 m
Equivalent Nacelle-Yaw-Actuator Linear-Spring Constant	9,028,320,000 Nm/rad
Equivalent Nacelle-Yaw-Actuator Linear-Damping Constant	19,160,000 Nm/(rad/s)
Nominal Nacelle-Yaw Rate	0.3 °/s

The tower structure of the land based NREL 5 MW concept consists of a tapering tube with the top diameter of 3.87 m and the thickness of 19 mm. The base diameter is circular with the diameter equal to 6 m and the thickness equal to 27 mm. The modulus of elasticity was assumed to be 210 GPa, the shear modulus was assumed to be 80.8 GPa, and the density of the steel was

considered to be 8,500 kg/m^3 [Jonkman et al., 2009]. For more information about the tower distributed properties refer to Table 2.1,2 in Jonkman et al., [2009].

The NREL 5 MW baseline design consists of two major controllers. The blade-pitch controller regulates the generator speed above the rated operating point. Other controller acts below rated operating point and tries to maximize capturing energy by controlling the torque in the generator. More detail can be found in Section 7.3 as well as in Jonkman et al., [2009] and Jonkman [2007] with regards to developing those controllers.

The full system natural frequencies can be obtained either by FAST or by MSC ADAMS as shown in Table 2.3.

Table 2.3. Natural frequencies of the baseline NREL 5WM turbine [Jonkman et al., 2009].

Mode	Description	FAST	ADAMS
1	1st Tower fore-aft	0.3240	0.3195
2	1st Tower side-to-side	0.3120	0.3164
3	1st Drivetrain torsional	0.6205	0.6094
4	1st Blade asymmetric flapwise yaw	0.6664	0.6296
5	1st Blade asymmetric flapwise pitch	0.6675	0.6686
6	1st Blade collective flap	0.6993	0.7019
7	1st Blade asymmetric edgewise pitch	1.0793	1.0740
8	1st Blade asymmetric edgewise yaw	1.0898	1.0877
9	2nd Blade asymmetric flapwise yaw	1.9337	1.6507
10	2nd Blade asymmetric flapwise pitch	1.9223	1.8558
11	2nd Blade collective flap	2.0205	1.9601
12	2nd Tower fore-aft	2.9003	2.8590
13	2nd Tower side-to-side	2.9361	2.9408

2.3 Comparison of Two-blade and Three-blade Wind Turbines

In turbine design, number of blade is a major consideration. While most modern wind turbines have three blades, the idea of reducing one blade arose primarily from cost reduction point of view. Ideally, one less blade means less weight and hence less overall cost. Also each blade causes wake for the other blades, in that respect 2-bladed turbines are advantageous over 3-bladed turbines. However in reality, number of blades on a wind turbine is a trade-off and both 2-bladed and 3-bladed turbines have their advantages and disadvantages.

Because of one less blade, a 2-bladed turbine has lower loads on the gear box and hence lower torque so lighter components such as tower, low speed shaft can be used for 2-bladed turbines. But, in order to produce the same amount of energy, a 2-bladed rotor has to rotate faster than a 3-bladed rotor which increases blade noise and causes more loads on blades. Downwind configuration of a rotor can be advantageous as the blades can be coned away from the tower and reduces chance of impact between the blade and the tower. Conning of rotor helps balancing the centrifugal forces on the blades with the thrust from the wind. On the other hand downwind turbines produce unpleasant noise as the blades rotate past the tower.

The pros and cons of 2-bladed vs. 3-bladed turbines is further discussed in Section 3.1

2.4 Offshore Foundation Types

There are three foundation categories for offshore wind:

- Shallow Water (up to 30 m depth)
- Transitional (between 30 and 60 m depth)
- Deep Water (beyond 60 m)

There are two main types of Shallow Water foundations:

- Monopole (steel is driven into sea floor)
- Gravity Foundation (uses concrete and gravity to keep it in place)

There are many different designs for transitional foundations. Transitional foundations are not commonly used. A few designs are:

- Tripod Tube Steel
- Guyed Tube (Guy wires are used to keep tower stable)
- Truss
- Suction Bucket

Deep Water foundations are also called floating foundations. This is the leading edge of wind turbine technology. There are two floating foundations in operation (Hywind in Norway, and WindFloat in Portugal). A floating foundation possibly offers the benefit of putting wind turbines out of site of the coast line.

Lake Erie is a shallow fresh water lake. It is known to freeze over during winter. For this reason, a gravity foundation is considered the best option. A gravity foundation offers the benefit of an ice cone. An ice cone is an angled structure that dissipates the load effects of ice impact. Similar technology was used in the fresh water lake wind turbine installation in Lake Vanern, Sweden.

2.5 Outline of This Report

The rest of this report is organized as follows. Chapter 3 first provides an overview of a general methodology for the preliminary design of an offshore wind turbine and the application of this methodology to develop a downwind 2-bladed wind turbine concept. Then it briefly describes the computational tools that are used for preliminary design of the wind turbine. These include a preprocessor and a postprocessor for preforming FAST simulations, a code for calculation of ice loads, fatigue analysis software, blade pitch controllers and programs for estimation of the annual energy production and cost of annual energy. Chapter 4 provides detailed descriptions of these computational tools.

Chapter 5 describes the tentative site of the turbine, and provides an overview of the loading environment. Then it describes a methodology to estimate the probability distributions of the wind and waves using NOAA data. Ice loads are an important consideration in the design of the

foundation. A method for modeling these loads and estimating the applied forces on the foundation is presented in the same chapter. Chapter 5 explains the design load cases for both the foundation and the turbine. These are based on the DNV standards (foundation) and the IEC standards (turbine).

Chapter 6 explains the design of the 2-bladed downwind turbine. This process is applied to the rotor, power control method, tower and blades. Chapter 7 describes the design of the gravity foundation.

Cost of energy is the critical attribute of a turbine design, besides safety. Chapter 8 provides a methodology for cost estimation. Then it applies it to the estimation the cost of the proposed 2-bladed design, and optimized version thereof. It also estimates the cost of a tentative design on a floating foundation.

Chapter 9 presents and discusses the results of the assessment of safety and cost of the alternative designs in this project. The chapter has four sections. The performance of the wind turbines in this study is presented in Section 9.1. This includes analyses and comparisons of maximum forces and moments, fatigue life, tower-to-blade clearance and teeter angle of various wind turbine models. In addition, the effect of changes in the number of blades, rotor position relative to the tower (upwind and downwind), teeter parameters, rotor brake, shaft tilt and cone angles, and changes in the blade designs are discussed. Section 9.2 presents the forces and moments applied to the foundation for the three turbine configurations in the project. Section 9.3 presents and compares the annual energy production and cost of energy. Based on the results, a final 2-bladed downwind design is proposed. Chapter 10 presents the development of the wind energy educational program during the project, including the curriculum activities completed and hands-on laboratory experiments advanced. The chapter also discusses the academic and outreach activities conducted during the course of this project. Finally, Chapter 11 summarizes the main observations and conclusions.

3 Turbine Design Methodology

Wind turbines must compete with alternative systems for energy production such as fossil fuel and nuclear power plants. A wind turbine must be designed to produce energy at a low cost and operate safely over its lifetime. Therefore, it is critical for a designer to have a suite of accurate and efficient computational tools for prediction of turbine loads and estimation of the cost of energy.

This chapter consists of four sections. Section 3.1 is an overview of a general methodology for the preliminary design of an offshore wind turbine and the application of this methodology to develop a downwind 2-bladed wind turbine concept for this project. In Section 3.2, optimization formulation is outlined. Section 3.3 lists the computational tools that are used for preliminary design of the wind turbine. An overview of the preliminary design of wind turbine is outlined in Section 3.4 of this chapter.

3.1 Design Requirements and Procedure

Section 3.1 presents an overview of the preliminary design methodology in this project. Manwell et al., [2009], describe a wind turbine preliminary design methodology consisting of eight steps. The first is the selection of the site of the turbine. In this project, the turbine is designed to be installed at a location in Lake Erie approximately 10 miles off the coast of Cleveland, Ohio. The design rated power of the wind turbine is 5 MW.

Table 3.1. NREL 5MW 3-bladed baseline wind turbine model description [Jonkman, 2009].

Feature	Description
Rating	5 MW
Wind Regime	IEC 61400-3 (Offshore) Class 1B/ Class 6 winds
Rotor Orientation and Number of Blades	Upwind, 3 blades
Control	Variable Speed, Collective Pitch
Drivetrain	High speed, Multiple-stage gearbox
Rotor Diameter/ Hub Diameter	126m/ 3m
Hub Height / Design	90m / Rigid hub
Maximum Rotor/ Generator Speed	12.1 rpm / 1,173.7 rpm
Maximum Tip Speed	80 m/s
Overhang/ Shaft Tilt/ Precone	- 5 m/ - 5 deg/- 2.5 deg
Rotor Mass	110,000 Kg
Nacelle Mass	240,000 Kg
Tower Mass (Deep water)	347,460 kg
Reference Site	National Data Buoy Center (NDBC) Buoy 44008
Cut-in, rated, cut-out wind speed	3 m/s, 11.4 m/s, 25 m/s
Cut-in, rated rotor speed	6.9 rpm, 12.1 rpm

Previous designs are identified and reviewed in the second step. The proposed design concept is developed by modifying the NREL 5 MW reference turbine [Jonkman, 2009]. This turbine has been studied extensively, and thus provides an excellent baseline design for comparative evaluation of the proposed downwind 2-bladed wind turbine concept. Table 3.1 shows the main characteristics of the NREL reference wind turbine.

In the third step, the overall layout of the design is defined. In this study, the rotor arrangement was selected to be a downwind configuration and the number of blades was specified as two. The bending moments in the blades of a downwind rotor are lower than those in an upwind rotor. This is because of the counteraction of the centrifugal and wind induced bending moments. Moreover, because the blades deform away from the tower under wind loads, they are less likely to hit the tower during the normal turbine operation. Reducing the number of blades from three to two has potential cost savings; however, 2-bladed rotor wind turbines are typically rotating faster than a 3-bladed counterpart in order to produce comparable power. This increases the blade loads. Also the cyclic rotor thrust variations are higher for 2-bladed machines because of their faster rotation. Finally, faster rotation of a 2-bladed turbine may appear more disturbing to an observer than the rotation of a 3-bladed turbine.

As will be shown later, a 2-bladed wind turbine, rigid-hub design does not provide significant performance benefits over a 3-bladed machine of the same rotor diameter. However, introducing a teeter mechanism between the rotor and the low-speed shaft can yield potential benefits. A teeter mechanism reduces the out-of-plane fatigue loading on the rotor blade. Also the teeter hinge prevents the out-of-plane rotor aerodynamic moments to transfer to the low speed shaft, resulting in large reductions in the operational loads on the shaft, nacelle and yaw drive.

The fatigue life of the components of a 2-bladed turbine must be carefully evaluated. The turbine blades and the low speed shaft are examples of such components. In preliminary design fatigue loading is quantified by the Damage Equivalent Load (DEL) which is defined as the equivalent constant-amplitude load that inflicts the same fatigue damage as the true random load.

The mass moment of inertia of a 2-bladed rotor depends on the rotor position, which leads to higher loads on the yaw system. Shaft tilt also causes unequal loads on the blades and therefore increases the risk of dynamic impact on a 2-bladed turbine compared to a 3-bladed turbine. The rotor symmetry in case of a 2-bladed turbine causes some additional dynamic load from wind shear. When the two blades are in the vertical position, the loading on the upper portion of the rotor is significantly higher than the lower portion. Therefore, nacelle nodding moment is moderately higher when the blades are in the vertical position than in the horizontal position, where there is unequal loading from wind shear. It should also be noted that for a rigid hub turbine, cyclic shaft moments due to gravity is cancelled out by the cyclic shaft moments due to wind shear, so the teeter mechanism adds no benefit considering those two loads. While introducing a teeter mechanism can reduce the load on the driveshaft and potentially reduce drivetrain maintenance and replace costs, additional costs will be incurred to acquire, install and maintain the teeter system. The teeter mechanism is further discussed in Section 6.7.

Table 3.2 summarizes the main features of the design in this study.

Table 3.2. Main features of the 2-bladed concept wind turbine design.

Feature	Description
Rating	5 MW
Rotor Orientation and Number of Blades	Downwind, 2 blades
Control	Variable Speed, Collective Pitch
Drivetrain	High speed, Multiple-stage gearbox
Rotor Diameter/ Hub Diameter	126m/ 3m
Hub Height / Design	90m / Teetering hub
Maximum Rotor/ Generator speed	16 rpm /
Maximum Tip Speed	105.78 m/s
Overhang/ Shaft Tilt/ Precone	5 m/ 5 deg/ 2.5 deg
Rotor Mass	92,260 Kg
Nacelle Mass	240,000 Kg
Tower Mass (Deep water)	347,460 kg
Reference Site	National Data Buoy Center (NDBC) Buoy 45005
Cut-in, rated, cut-out wind speed	3 m/s, 11.4 m/s, 25 m/s
Cut-in, rated rotor speed	6.9 rpm, 12.1 rpm

Design load cases are selected in step 4 to assess the safety of the turbine operation. A subset of the load cases used in [Jonkman & Matha, 2010] to evaluate the safety of the NREL 5 MW 3-bladed upwind design was adopted in this study.

A tentative design is developed in the next step (Step 5). This includes subsystems, and principal components as listed in Table 3.3.

Table 3.3. Primary components and their subsystems of 2-bladed turbine system.

Principal component	Major subsystems
Rotor	Blades, hub
Drive train	Low speed shaft, high speed shaft, gearbox, generator, mechanical brakes
Nacelle & main frame	
Yaw system	
Support system	Tower, foundation

For this study, as mentioned earlier in this chapter, the existing baseline NREL 5MW turbine was altered by removing one rotor blade and by changing the rotor configuration from upwind to downwind. A tower shadow model was used to take into account the influence of the tower shadow on the 2-bladed downwind rotor wind turbine. Drivetrain, generator and nacelle components were adopted unchanged from the NREL 5 MW baseline design. The yaw system of the concept turbine also remained unchanged from the baseline turbine. A semi-floating type gravity-based foundation with a compound downward ice cone was used for this study and is described in detail in Chapter 7.

The next two steps (steps 6 and 7) involve estimation of the generated power and evaluation of the safety of the design against two failure modes: 1) ultimate failure due to extreme loads, and 2) fatigue failure due to cyclic loads. In the latter step, steady loads, cyclic and transient loads are considered. In the last set, loads due to the tower shadow effect are considered. These effects are important for the downwind turbine design.

The last step (Step 8) is an assessment of the economic viability of the design by calculating the cost of energy per kWh. The national average residential electricity rate was 12¢/kWh in the U.S. in April 2012 (http://www.eia.gov/electricity/monthly/).

3.2 Optimization Formulation

The objective is to minimize the cost per KW energy produced by the wind turbine by changing the design variables so that the constraints are satisfied.

The design variables include the following items;

- Rating
- Number of blades
- Wind direction
- Blade model
- Application of tip-brake
- Shaft tilt angle
- Conning angle
- Teeter parameters
- Application of tower shadow effect

The constraints considered in this study are, blade to tower clearance should be larger than 3.5 m, the load effects such as bending moments should be less than the capacity of the turbine components, and damage should be less than. Finally the feasible design or designs are selected.

3.3 Available Design Tools and Methods

Computational tools that are important in wind turbine design can be classified into four categories according to their application:

Turbulent Wind Modeling

Turbulent winds are modeled by calculating aerodynamic forces and moments on blades. These include TurbSim, Airfoil Prep, WT_perf, and AeroDyn

TurbSim uses a statistical model to numerically simulate time series of stochastic, full field, three-component turbulent wind. The wind files generated by TurbSim are used to model normal turbulent model (NTM) load case situations. [Kelley & Jonkman, 2006].

AirfoilPrep is a spreadsheet that is used to generate the airfoil data files needed for AeroDyn and WT_Perf. The latter program predicts the performance of wind turbines using blade-element momentum theory. [Hansen, 2012]

AeroDyn is a plug-in type code that is used to generate aerodynamic loads on a wind turbine blade segment at a certain location and time [Laino & Hansen, 2001].

Dynamic Analysis of Turbine Structure and Drivetrain

BModes, PreComp, FAST, and ADAMS are used for the analysis.

BModes is a finite-element code that uses the specified rotor speed, blade geometry, coning angle, pitch control setting and blade structural property distribution along the blade length as inputs and generates dynamically coupled modes for a blade or a tower [Bir, 2005]. The structural properties used as inputs can be produced by PreComp.

PreComp code computes the cross-coupled stiffness properties, inertia properties, and offsets of the blade shear center, tension center, and center of mass with respect to the blade pitch axis of a composite blade [Bir, 2005]. ProComp uses the blade external shape (such as airfoil geometry, chord and twist distribution along the blade length) and internal structural detail (such as laminates constituent properties, orientation of fibers in each laminate) as inputs. These properties produced by ProComp are then used as inputs for FAST, ADAMS to properly model the blades, tower and drivetrain shaft. [Damiani, 2012]

FAST is a comprehensive aero-elastic simulator that can predict both the extreme and fatigue loads of wind turbines. These are important for predicting the probabilities of ultimate and fatigue failure [Jonkman & Buhl, 2005].

ADAMS is the popular MSC software that is used for multibody dynamics analysis. ADAMS is used as an alternative solver for FAST.

Assessment of Safety against First Excursion and Fatigue Failure

MLife, MSC NASTRAN, ADAMS, FAST, FAST_SM, and DLC post-processor are used for the assessment of safety.

MLife is a MatLab-based tool used to generate fatigue-life estimates for loads analysis [Hayman & Buhl, 2012].

NASTRAN is a program to solve stress-strain behavior, dynamic response and nonlinear behavior of components.

FAST_SM is a user interface for automated analysis of the wind turbine responses operating under multiple design load cases (DLCs). This computer code is used to manage and perform a large number of simulations for this study. The output data are post-process with DLC post-

processor code. The FAST_SM and DLC post-processor codes are introduced in Section 4.1 and Section 4.2, respectively.

3.4 Overview of the Preliminary Design of Wind Turbine

Primarily, the NREL 5 MW 3-bladed upwind turbine is considered as the baseline turbine design. Then various design options are explored. In this study, the number of blades, blade design, turbine configuration, type of hub, pre-cone and tilt angle, tip brake and tower design are considered as design variables and load effects at different turbine locations are analyzed.

Figure 3.1 shows the computational flow chart and the tools used in the preliminary design study of the proposed wind turbine concept. The role of each tool in the design process is explained below. In this figure, gray boxes present input information, blue boxes represent software, and yellow boxes correspond to calculation results.

First, wind resource data for the specific site is collected from the published buoy data and wind input data files are created using TurbSim or IEC wind. The designers use the airfoil description provided for the baseline design to generate airfoil coordinate files. Wind input files and airfoil coordinate files together are used to create AeroDyn input files. Similarly, blade input data files are generated by BModes using the distributed structural properties of the baseline turbine.

AeroDyn input files and blade input files are used to prepare FAST input files which are used to generates time history of load effects. Load effects are evaluated by analyzing FAST output files. Power production is also produced from the FAST output files and AEP (annual energy production) is estimated using this data and the wind resource. FAST output files are used as input files for MLife to predict damage.

Calculation of the wind energy cost per kWh requires calculation of the AEP. The AEP of a model is found using power production results from FAST simulation output files. The power production results are collected for various wind speeds. Steady winds are used for the AEP simulations. The power generation results are integrated with the PDF of the wind speed of Lake Erie site to estimate the AEP of a model. The details of this method are described in Section 4.6. Validation of the simulation based AEP prediction method and AEP results of each wind turbine model are shown in Section 9.3.1.

A design is considered feasible if the structural capacities of the turbine components are much higher than the corresponding load effects, and the average damage at any location is less than one. Another criterion for feasibility is that the blade tip to tower clearance should not be less than 3.5 m. Finally, the AEP and the cost per kWh are calculated. A new iteration is performed by changing the design variables if the design is infeasible or the cost per kWh is high.

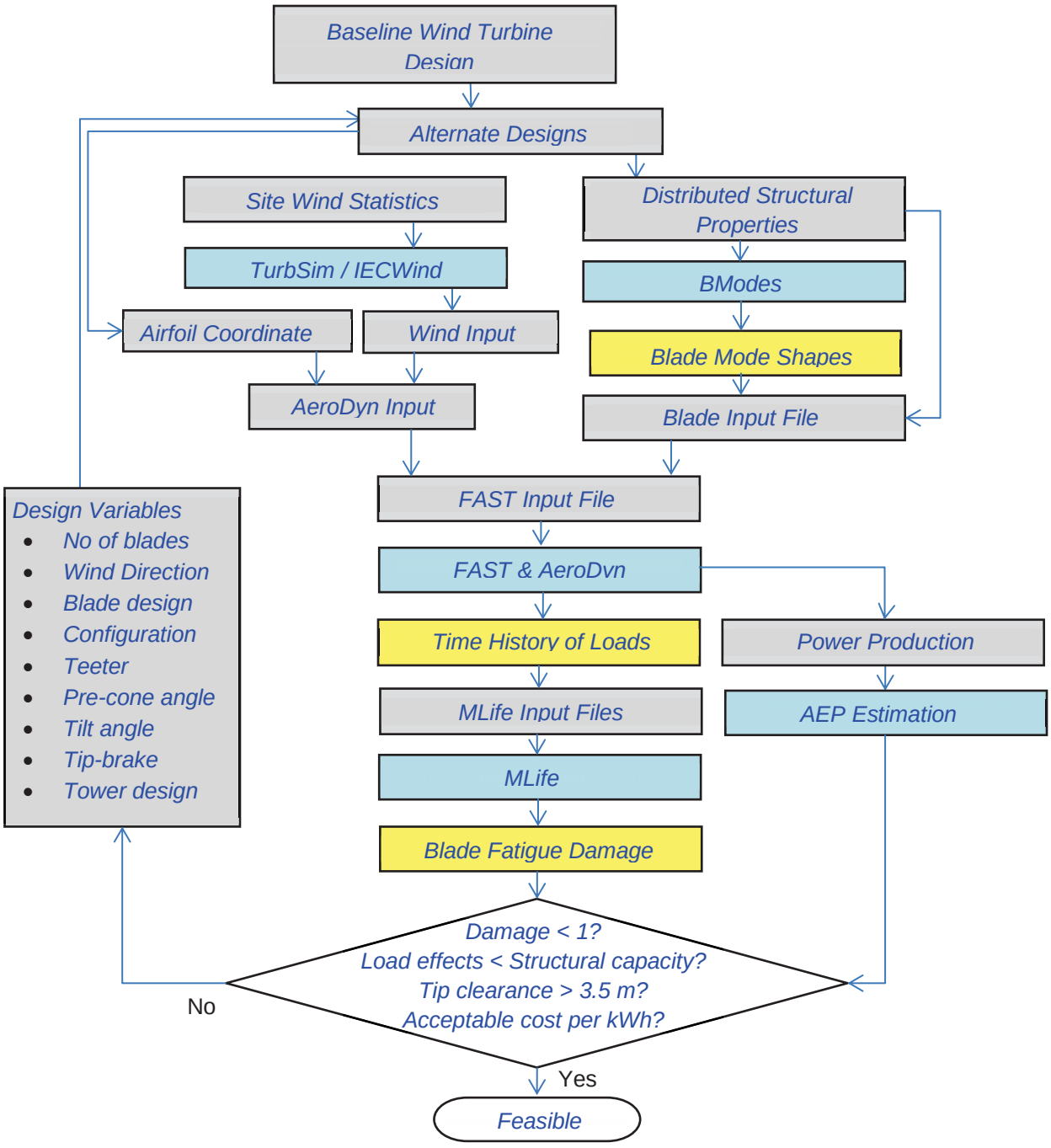

Figure 3.1. Computational tools used for wind turbine design.

The design iteration procedure starts with a preliminary baseline design as shown in Figure 3.1. Initially, a set of input files are prepared. This set includes a material input file, a structural lay-up input file and a set of aero-foil coordinate input files. The material file contains a list of commercially available materials and their properties.

The structural lay-up input file contains the description of the blade internal structural layup, such as the number of laminates, the number, sequence, and material of the laminas in each

laminate, the number of plies, the principal material direction, and the material type in each lamina. A ply is also described by its thickness, material type, and orientation of its principal material direction with respect to the blade axis.

Airfoil data files contain the x- and y- coordinates of points describing the airfoil profile to completely describe the corresponding blade section.

The main input file for PreComp is created using the above airfoil data files. Then PreComp computes the blade's distributed stiffness properties along the blade length. The stiffness properties are used as input for BModes to calculate the blade mode shapes. The blade mode shape properties generated by BModes together with the blade distributed properties generated by PreComp completely define the blade input files required for FAST. The latter program also requires AeroDyne input files. To create these files, the airfoil distribution and wind input files are needed. There are two types of wind input files: (1) hub-height wind files and (2) files with simulated full-field wind data that represent all three components of the wind vector varying in space and time to model turbulence.

FAST computes the time histories of loads and bending moments at different locations of the turbine components. The time history data are then post-processed to determine the blades' fatigue damage. If the analysis shows that the concept blade design meets the specified expected life, then the design is final. Otherwise, the preliminary design will be updated and the above process is repeated for the refined design.

4 Computational Design Tool Development

In this chapter, the computational tools that are used in this report are described. Some of these tools are developed using the existing tools that are available from the NREL, and others are developed by the team at UT.

In Section 4.1, the FAST_SM, a simulation manager, is explained. This tool enables running FAST under different parametric conditions. Section 4.2 introduces a post-processing tool that was used to process results from FAST. Section 4.3 explains the FAST_ICE code which adds the ice impact modeling capability to FAST code. Section 4.4 discusses the tools and the methodologies to estimate the fatigue damage inflicted on the turbine structure. Section 4.5 describes a tool that can be used to tune the blades' pitch control for the new wind turbine design. Finally, Section 4.6 discusses a tool that can be used to calculate Annual Power Production (AEP).

4.1 Development of FAST Simulation Manager (FAST_SM)

A simulation manager program (FORTRAN code) called FAST_SM is developed to perform parametric simulations of wind turbine operations efficiently. FAST_SM allows the user to conduct repetitive FAST simulations for a given set of wind and wave conditions without requiring manual user intervention. The code allows us to predict the wind turbine responses from recurrent random seeds for various wind and wave conditions. Also, FAST_SM can provide post processing capability such as probing the FAST standard output results to organize the data in a desired form or compute needed supplementary parameters. This code allows efficient setup of FAST simulations and analysis of FAST-computed data. Moreover, FAST_SM can manage files to systematically catalog simulation runs; users only need to specify a few key input files to perform the desired tasks consistently.

FAST_SM is configured mainly in three parts: a pre-processor, a FAST simulation executive and a post-processor. The program functionality is readily expandable; it is designed to run any program for pre-processing or post-processing that can be executed in command prompt.

Figure 4.1 summarizes a system simulation process using FAST_SM. A simulation is performed for a prescribed set of wind and wave conditions and wind turbine settings. The term *simulation condition* is used to denote this set. For each simulation condition, the user specifies the wind type, average wind speed, wind direction, significant wave height, wave period, and wave direction. In addition, the user specifies the number of replications needed in order to estimate the response of the turbine with acceptable confidence. The user also provides a set of seeds for each replication. FAST_SM pre-processes the input data before running each replication. After completing the simulation, FAST post-processes the results from each replication and simulation condition.

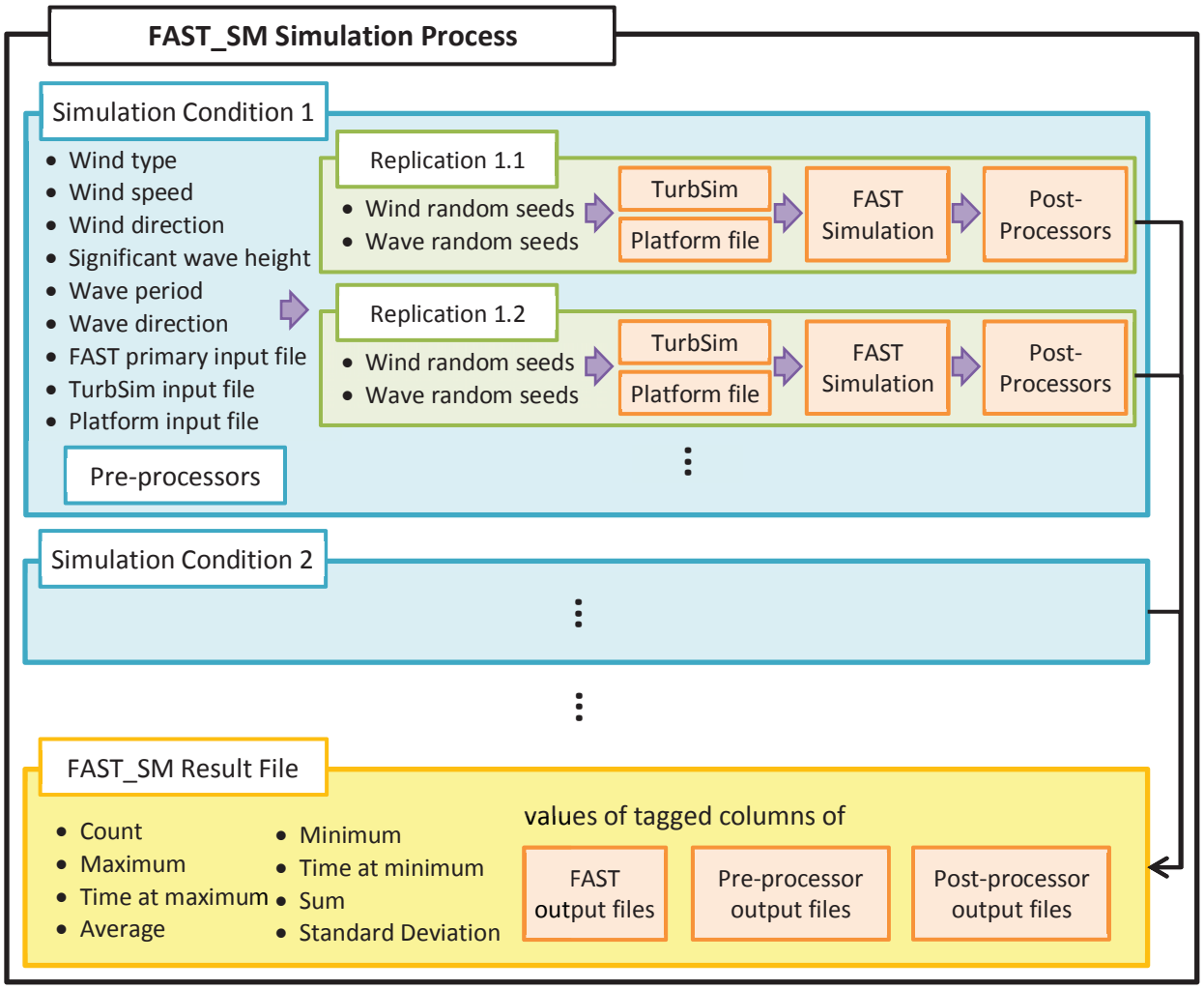

Figure 4.1. FAST_SM simulation process.

The FAST_SM pre-processor implements functions that update the wind and wave input data for each simulation condition and random seed for each replication. If deterministic winds are used, FAST_SM simply replaces the wind file referred to in the AeroDyn input file with the desired deterministic wind file specified in the FAST_SM input file. When random winds are specified, FAST_SM executes the TurbSim with random seeds and a given random wind condition. The generated random wind file is then connected to the AeroDyn input file. Similarly, the platform input file can be updated with wave condition parameters and random seeds when the platform module is enabled in the FAST primary input file. Moreover, FAST_SM is capable of incorporating a custom baseline FAST primary input file, platform input file, and TurbSim input file for each simulation condition. This capability enables the user to control all parameters of a FAST simulation for each simulation condition.

Data columns of the FAST output files for each replication can be tagged for post-processing using FAST_SM. The post-processor can perform a number of tasks including the following: sort or calculate count, maximum value, time at maximum value, minimum value, time at minimum value, average value, sum, and the standard deviation of values for the tagged columns.

Afterwards, the sorted data are saved in a single file. In short, the post-processor facilitates the analysis of the large amounts of computed data.

4.2 DLC Post-processor

Multiple simulations are performed for various DLCs using FAST_SM. Because each DLC generates its own FAST_SM post-processed data, a program is required to sort out data globally. Thus, a DLC post-processor FORTRAN code is developed to sort out result data globally and automatically. This code sorts locally post-processed data from various DLCs globally.

The sorting process is performed throughout four different levels: replication, simulation condition, DLC, and group, from the lower to upper level. A ranking system is imported in the DLC post-processor except at the replication level. One of the three different options can be selected in a level: ascending order, descending order, or averaged value. Therefore, the maximum value, minimum value, and averaged value can be found at each level. Consequently, the sorting processes are performed from the lower level to the upper level. DLCs can be grouped in normal operating, fault, or parked condition. Within a defined group, result values can be sorted.

The DLC post-processor also includes a function that can list corresponding outputs for the sorted result values. This function allows a user to track the corresponding output parameter results for the sorted result value from tagged columns. For example, if a user requests to sort out maximum bending moments at the blade root, the program can trace back the DLC and find the wind speed, tower base bending moment, teeter angle, and tower-to-tip clearance at the instant when the bending moment is a maximum. This is possible when the FAST_SM post-processor tags these output parameters. This capability helps the user to understand what is happening in the wind turbine when the structural integrity is threatened.

4.3 FAST_ICE

The FAST_ICE code adds ice impact modeling capability to FAST. The modeling procedure implemented follows the [IEC 61400-3, 2009] recommendations. In this context, the ice loads exerted on the structure from a stationary ice sheet (due to the wind action on the ice sheet, or to the thermal ice pressure, or to the changes of the water level) are smaller than the loads imparted by a moving ice sheet and or a moving ice ridge. Therefore, stationary ice sheets were not covered in this implementation. The ice loads calculation was performed for a generic cylindrical structure fitted with an ice breaking cone at the water surface, such as monopile foundations. Based on the same general procedure, the program can be adapted to cover more complex geometries.

The calculation of the loads was applied in two steps:

- Calculation of the maximum loads and location using ice failure models;
- Generation of a dynamic load profile and application to the structure based on the previously determined loads.

Both steps are performed when running the FAST simulation.

Implementation in FAST

The ice loads calculations were incorporated in FAST using the tower loading subroutine "UserTwrLd," which is part of the FAST source code. UserTwrLd was adapted to calculate the loads and apply them to the tower during the time simulation. UserTwrLd limits the application of external loads to even load distributions over individual tower segments (which is synonymous to the application of the external loads in the central nodes of the tower elements). Because the ice loads are not necessarily uniformly distributed or centered at the tower nodes, the ice load distribution as calculated using the ice failure models had to be redistributed to satisfy the UserTwrLd limitations while preserving the load effects (shear and bending moments) on the structure at the resolution level limited by the tower discretization elements.

Consider a horizontal load acting on the tower at a location situated between two tower nodes. To preserve both the resulting bending moment and the total horizontal force while at the same time applying the force evenly over individual tower elements, two approaches were considered:

- Application of the load at the closest tower node location with an additional concentrated bending moment to account for the error in the bending moment due to the inaccuracy in the force location. Simulations showed that this method may introduce artificial (numerical) disturbances when the location of the load moves in time (such as when an ice ridge of non-uniform thickness advances against the tower).
- Distribution of the load between the two adjacent tower nodes. This method did not introduce disturbances so was preferred for moving ice ridges.

The magnitude of the ice load was determined using the procedure recommended in IEC 61400-3 (2009). The following equations were used to calculate the horizontal load from a moving ice sheet against a vertical cylindrical structure, horizontal load against a conical structure and vertical load against a conical structure, respectively [Ralston, 1977].

$$H_d = k_1 k_2 k_3 h D_w \sigma_c \tag{4.1}$$

$$H = A_4\left[A_1 \sigma_b h^2 + A_2 \rho_w g h {D_c}^2 + A_3 \rho_w g h \left({D_c}^2 - {D_T}^2\right)\right] \tag{4.2}$$

$$V = B_1 H + B_2 \rho_w g h \left({D_c}^2 - {D_T}^2\right) \tag{4.3}$$

where,

H_d = horizontal force

D_w = the diameter of the structure at the waterline

k_1 = shape factor of the structure where the ice is hitting it

k_2 = contact factor between the ice and support structure

k_3 = aspect ratio factor, given as $\sqrt{1+5h/D}$, where h is the ice thickness

σ_c = crushing strength of the ice

A_1, A_2, A_3, A_4, B_1 and B_2 are dimensionless coefficients; these are functions of the cone angle and the ice to cone friction coefficient.

σ_b = ice bending strength

h = ice sheet thickness

ρ_w = water density

g = gravitational acceleration

D_c = cone diameter at the waterline

D_T = diameter at the narrow end of the cone (same as the tower diameter)

For downward breaking cones, the water density is replaced by $\rho_w/9$, which approximates the difference between the densities of water and ice. Coefficients A_i and B_i are calculated using a procedure from [Ralston, 1977] that is also described in [Wells, 2012].

The horizontal load from a keel is calculated following a procedure described in [C-Core, 2008] and [Timco et al., 1999]. The forces occurring from the local failure of the ice keel (crushing) and from the global failure of the ice keel along plug failure planes are calculated and compared. The acting load is then determined to be the minimum load between the two modes of failure. When the ice keel starts making contact with the cylindrical (submerged) structure, the force from the local failure mechanism is small compared to the global mechanism, and thus the keel is crushed against the structure. As the ice keel advances and becomes thicker, the local failure force increases while the global force decreases, because the plug planes become shorter. At some point the two forces become equal to each other and according to the model, the failure mechanism switches from local to global.

The local failure force is calculated as [C-Core, 2008] and [Timco et al., 1999]:

$$F_{local}(x) = W_e \left(1 + \frac{2h_e}{3W_e}\right)\left(\frac{h_e^2 \gamma_{eff} K_p^2}{2} + 2ch_e K_p\right) \tag{4.4}$$

where,

$$h_e = x tan\theta_k \left(1 + \frac{SW_e}{h_k - h_c}\right) \tag{4.5}$$

and

W_e = effective structure width

x = penetration distance of the foundation into the keel

c = cohesion within the keel (submerged portion of the ridge formed of ice rubble)

S = effect of any surcharge; C-CORE Report does not specify what this is

θ_k = angle that the keel rubble makes with the horizontal

h_k = total draft of the keel as measured from the waterline

h_c = consolidated layer thickness

γ_{eff} = effective buoyant density of the keel rubble, including effects of porosity

$K_p = tan(45° + \frac{\phi_f}{2})$ = passive pressure coefficient of the rubble

ϕ_f = internal friction angle of the rubble

The global failure force is calculated as the sum of two forces as [C-Core, 2008]

$$F_{global}(x) = F_{side}(x) + F_{top}(x) \tag{4.6}$$

$$F_{side}(x) = K\gamma_{eff} \tan(\phi) \left[(h_k - h_c)^2 \left(\frac{w_k - w_b}{3} + w_b \right) - \frac{x(xtan(\theta_k))^2}{3} \right] + c[(w_k - w_b)(h_k - h_c) - x^2 tan(\theta_k)] \tag{4.7}$$

$$F_{top}(x) = W \left[\gamma_{eff} \tan(\phi) \left[(w_k - w_b)(h_k - h_c) - x^2 tan(\theta_k) + c(w_k - x) \right] \right] \tag{4.8}$$

More details about the procedure are presented in [Wells, 2012].

It should be noted that, according to [Brown & El Seify, 2005] who used the data from the Confederation Bridge Monitoring Program, the ice keel load calculated using the above procedure overestimates the observed loads on the Confederation Bridge Pier. Therefore, for a gravity foundation, the industrial partner decided to use the unified model proposed by Brown & El Seify [2005].

The step-by-step implementation procedure in FAST following the model presented in [C-Core, 2008] is described below.

For each time step of the simulation using FAST, the UserTwrLd subroutine is called to calculate the ice load occurring at each tower node. When the UserTwrLd is called for the first time, a data file is opened and case specific data are read from that file; these values are then retained in the memory such that the file is accessed only once. The data file is organized similarly to other data files used by FAST, using values related to ice sheet/ice keel geometry and properties. Figure 4.2. shows this data file. The significance of each value is self-explanatory inside the file, similarly to other data files used by FAST.

```
=========Tower Properties============================================
107.6       tower height (meters) (found on line 87 of fst input file;
            includes tower draft on line 19 from platform dat file)
25          number of tower nodes (found on line 134 of fst input file)
11.04       D ! diameter (warterline)
6.0         DT ! diameter (tower)
0.8727      alpha!  cone angle (50 deg is 0.8727 radians)
=========Ice/Tower Properties=======================================
0           ConeType (0 is Cylinder; 1 is upward breaking Cone;
            2 is downward breaking cone)
20.0        targetH (meters) This is the distance from the base of
            the tower at which the ice sheet hits the tower
0.0         force angle (radians from x axis towards y axis)
0.15        mu !  ice/cone coefficient of friction
=========Ice Properties=============================================
0.927       t ! ice thickness (meters) (if ice keel is present,
            put the consolidated layer thickness as the ice thickness)
1770e3      sigmaF ! ice flexural strength, pascals
4400e3      sigmaC ! ice crushing strength, pascals
999.552     rhow ! water density, kg/m3 (divide regular water by
            nine to get downward breaking cone)
916.0       rhoi ! ice density, kg/m3
60.0        startTime, seconds
9999.0      endTime, seconds
0.20        iceSpeed (meters per second)
0.7         rampPercent (fraction of the reptime during which the triangular load increases)
true        userRep (user specifies period of dynamic ice loading profile, true/false)
2.5         repTime, seconds (used only if UserRep is true)
=========Keel Properties============================================
11.2        hk ! keel draft from waterline (meters)
43.301      wk ! total keel width (meters)
0.523598    thetaK ! keel angle (radians)
true        useKeelAngle (if true, hk and theta are used to determine keel size,
            wk is inferred; if false, hk and wk are used to determine keel size, theta is inferred)
6.0         We ! effective structure width (meters)
            (assuming the submerged structure is cylindrical,
            this is its diamter, used to find keel forces)
80.0        keelstart (seconds) (time for the onset of keel forces to begin)
0.7         phi ! internal friction angle (radians)
1.0         kSoil (unitless)
5000.0      c ! ice rubble cohesion (pascals)
0.25        nVoid ! ice void ratio
```

Figure 4.2. Sample Ice Properties Input File [Wells, 2012].

Some other calculations are also only performed at the first call of the UserTwrLd subroutine and then retained in memory for later use. These are the maximum force (horizontal and vertical components) imparted by the advancing ice sheet on the structure, the location of the force on the tower (this calculation is based on the water level depth), the bending moment excess or deficit because of the error in mapping the horizontal force from the ice sheet on the tower nodes, and the bending moment generated by the vertical component generated by the ice sheet on the ice cone. As shown above, these two force components and two bending moment components represent the peak loads from a moving ice sheet.

For subsequent calls of the UserTwrLd subroutine (time steps), based on the IEC recommendation (see Figure 4.3), the magnitude of the saw tooth function is calculated as a value between zero and one. For the saw tooth function the load increases from zero to one for the first 70% of the cycle and then decreases back to zero for the remaining 30% of the cycle; the 70% value is an input value in the ice data file. The saw tooth function is then used to scale the

peak load components calculated at the first call of the subroutine UserTwrL, thus generating the dynamic load from an ice sheet. The first cycle can start at an arbitrary time, which is user specified in the data file.

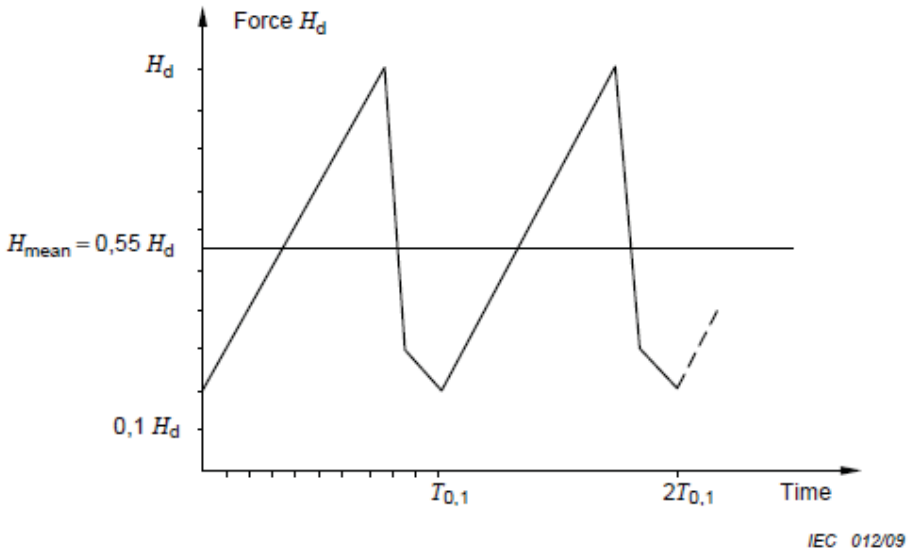

Figure 4.3. Suggested Dynamic Horizontal Load Profile from [IEC 61400-3, 2009].

The load generated by an ice ridge is also dynamic, not just because of the failure mechanism of the ice, but also because the ice keel is modeled as having some variable thickness. IEC suggests a triangular shape for the keel thickness. As a result, as the keel advances against the foundation and is penetrated by it, the contact height between the ice keel and the structure (effective height, as shown in Figure 4.4) changes over time – first it increases from zero to the maximum keel height, then it decreases. Thus at each time step, the effective height is recalculated knowing the penetration distance and the keel geometry (data regarding the keel geometry is included in the data file). Also, since the pressure from the keel is assumed to have a triangular shape (zero at the lower edge of the effective height and maximum at the water line) the force required to penetrate the keel is assumed to act at one third of the keel's effective height from the waterline. This location changes relative to the tower elements and is also recalculated at each time step using Eqs. (4.12) - (4.16). As mentioned before, when acting between tower nodes, the load imparted by the ice keel on the structure is divided among the adjacent nodes to preserve the resulting bending moment on the structure and to avoid artificial excitation of the tower as the location of this load moves along the tower/foundation height.

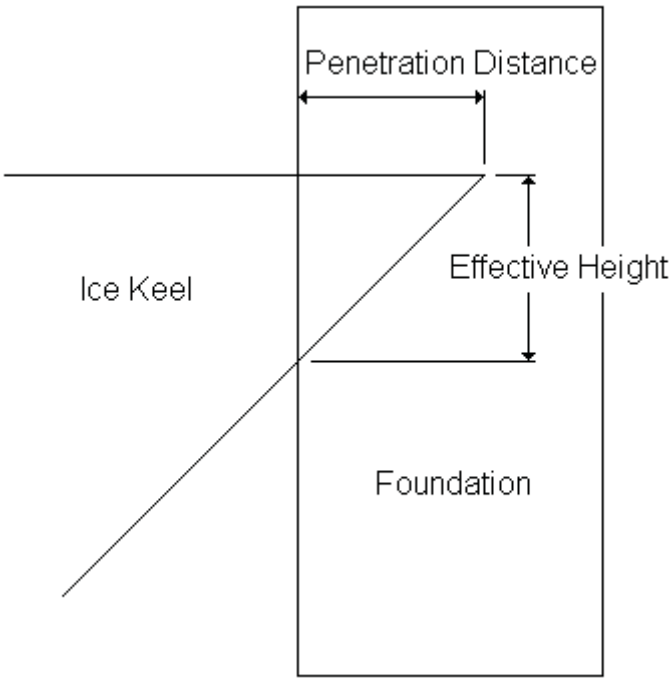

Figure 4.4. Ice keel effective height [Wells, 2012].

The failure mechanism of the ice ridge assumes that the load is calculated as the minimum between two local failure (crushing) and global failure (ridge breaking). Once the global failure becomes the prevalent mechanism, the load from the ice keel drops to zero and remains zero for subsequent time steps.

It should be noted that the ice ridge/keel does not occur alone, but together with the ice sheet; the implemented model reflects this reality. Therefore, when ice loads are included in the turbine simulations, it is assumed that either an ice sheet is present, or an ice sheet together with an ice ridge is present. Also note that when the ice ridge is present, a consolidated ice sheet must be used, which is thicker than the standard ice sheet; the consolidated ice typically has a 50% larger thickness than the ice sheet. The thickness of the ice sheet (either consolidated or normal), together with the triangular geometry of the ice keel, are provided in the ice loads data file.

Discussion

The implementation described above was validated by comparing the simulation results with MSC Software ADAMS. ADAMS uses a finite element approach for the elastic structure and does not rely on mode shape functions as FAST does. Therefore, ADAMS is intrinsically more accurate (at least when using the same number of elements to discretize the tower). Therefore the comparison can provide a guideline on the possibility of using FAST to simulate foundation-tower ensembles as a continuous structure.

To exemplify the capabilities of the implementation, Figure 4.5 shows an example of a simulation using FAST for the 5MW NREL turbine. In this simulation, a sheet of freshwater ice with a thickness of 61.8 cm advances against a monopile structure with an upward or downward

breaking cone. The bending moment at the tower base (soil level) is shown compared with the case when no ice is present. In all cases, the turbine is subjected to a wind of 11.3 m/s (rated wind speed). The ice load is applied at a distance of 20 m from the base (water level), and the ice advances at a velocity of 0.2 m/s, which results in a breaking period of about 17.5 s. The waterline diameter of the ice cone is 11m and the cone has 50 degree angle from the horizontal. The downward breaking cone generates a slightly larger maximum load (bending moment) compared to the upward breaking cone. On the other hand, the upward breaking cone also provides a beneficial stabilizing vertical load, while the downward breaking cone results in a detrimental uplifting vertical load. The bending moment at the soil level is about 50% higher compared with wind alone (no ice).

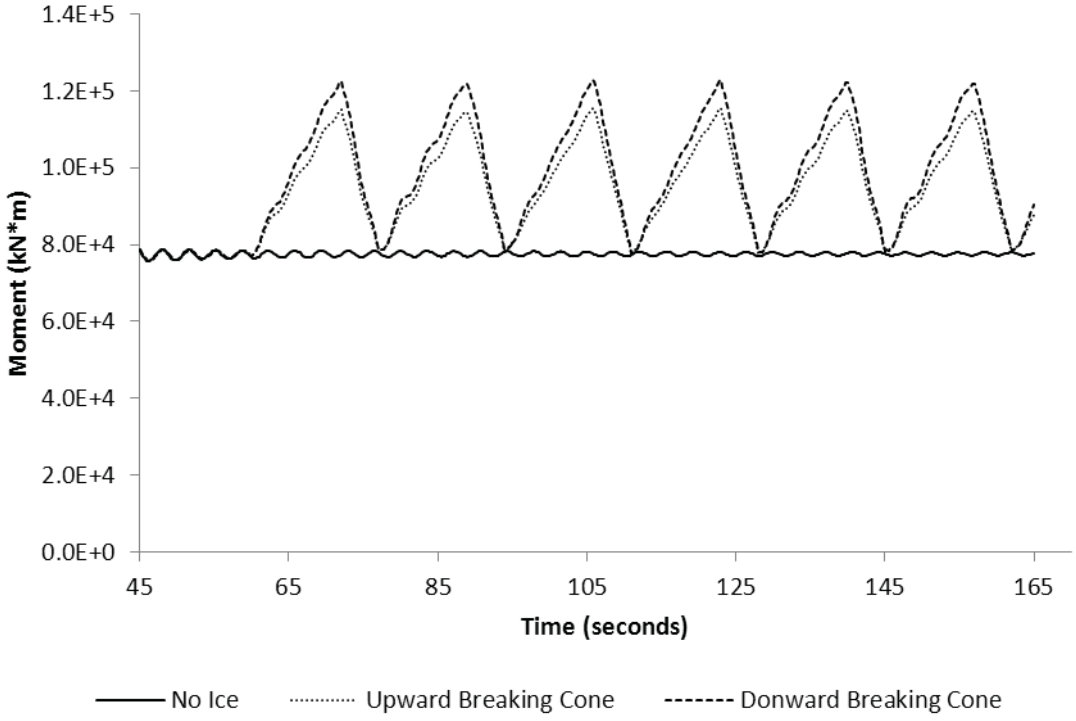

Figure 4.5. Foundation Base Bending Moment for a 61.8cm thick ice sheet, for the two ice breaking cones [Wells, E., 2012].

A similar simulation result is shown in Figure 4.6. This is an extreme case where a consolidated ice sheet of 92.7 cm thickness with an ice keel of 11.2 m depth advance against the tower. All the other elements (geometry of the structure, ice properties, ice speed are the same is before. The frequency of the ice breaking is lower (corresponding to about 25 seconds time period) because the ice is thicker. Also the keel increases the overall load because of its increased effective thickness. The keel makes contact with the structure at 80 seconds and then, because of its shape, the load from the keel increases the load because of the periodically breaking ice sheet. At about 155 seconds, the keel breaks and the ice load drops, generating a shudder in the tower.

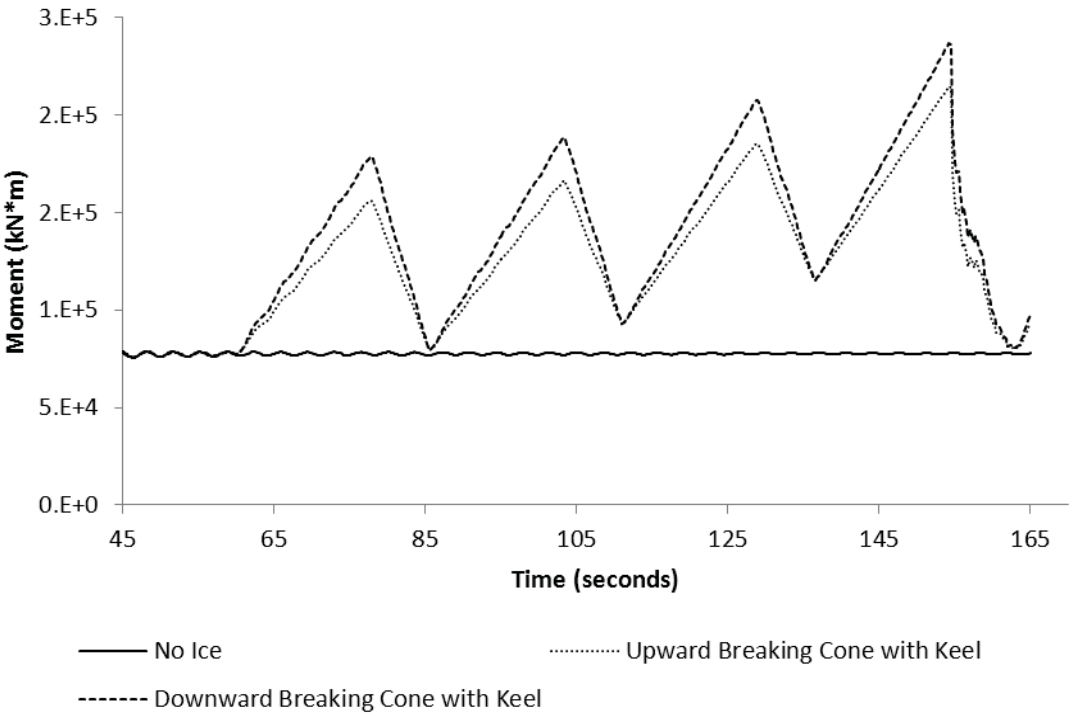

Figure 4.6. Foundation Base Bending Moment for 92.7 cm thick ice sheet and 11.2 m deep keel, for the upward cone and downward cone [Wells, 2012].

A comparison of FAST with ADAMS shows good agreement between the two methods (within 10% difference for the top tower displacement). However, as the foundation becomes stiffer and heavier than the tower, the difference between the results from FAST and ADAMS increases. The reason is that mode shape functions cannot accurately describe the deformation pattern of a structure that has sections with dissimilar properties. For more details, the reader should consult [Wells, 2012].

4.4 Method for Fatigue Life Assessment

Fatigue damage is calculated using MLife, a MatLab-based tool developed by NREL. FAST simulations were run at each mean wind speed to produce characteristic fluctuating load time histories. The fatigue damage caused by those fluctuating loads over the design life of the wind turbine is accumulated using the techniques defined in Annex G of IEC 61400-1 edition 3. These fluctuating loads are then counted by the rain flow algorithm [Downing & Socie, 1982] and the cycles are characterized by a load-mean and range and extrapolated to estimate turbine lifetime damages. Damage accumulation is assumed to be linear with each of these cycles according to Miner's Rule [Palmgren-Miner,1945].

The following inputs listed in Table 4.1 needed to be provided to MLIfe in order to calculate damage.

Table 4.1. Turbine input features required for damage calculation.

Inputs for MLife
Load time histories output from FAST simulation
Ultimate (static) loading of turbine components that causes failure in one cycle
Weibull shape and scale factor for wind speed distribution
Design life of turbine (20 years)
Availability: The percent time the turbine is online and producing power when the wind speed is in the range between cut-in and cut-out speed.
Fixed Mean Load: The fixed mean load is the aggregated mean of the load channels across all input files using the specified Weibull distribution.

Fatigue damage calculation requires detailed geometry and material properties of the turbine structure. However, when the detailed geometry of the turbine structure is not well defined and material properties are not known at conceptual design level, fatigue damage calculation may have major assumptions involved. Since the detail geometry and material properties are not well known for the proposed turbine components at this stage, they are calculated based on the limit loads calculated from the simulations.

Since the 5MW 3-bladed NREL turbine is a well-established design, it is used as a reference baseline design for this research. FAST simulations are run for different design load cases and maximum load effects are estimated for each load effect at critical locations of the turbine. The maximum loads on critical turbine locations found from the simulations are multiplied with safety factors to estimate the limit load (safe limits) on the turbine components for each corresponding load effect. These limit loads are used as a substitute of true, ultimate load in fatigue damage calculations for this research for comparison purposes only. Limit load calculations are described in Appendix 5 of this report and are listed in Table 4.2. For example, the ultimate shear force at the tower base is 1594 kN. This means that a lateral force at the tower base of 1594 kN will cause failure in one cycle.

Table 4.2. Ultimate loading on turbine components.

Turbine location	Description	Ultimate Load Effect
Tower base	Shear force (kN)	1594
	Bending moment (kN m)	126821
	Axial force (kN)	-7878
	Torsional moment (kN m)	18
Tower top	Shear force (kN)	1594
	Bending moment (kN m)	17308
	Axial force (kN)	- 4766
	Torsional moment (kN m)	12529
Blade root	Shear force (kN)	672
	Bending moment (kN m)	24923
	Axial force (Max) (kN)	1367
	Axial force (Min) (kN)	- 201
	Torsional moment (Max) (kN m)	197
	Torsional moment (Max) (kN m)	-276
Low-speed-shaft	Shear force (kN)	1556
	Bending moment (kN m)	19796
	Axial force (kN)	1473
	Torsional moment (kN m)	9641

Theory

Lifetime damage from all cycles,

$$D^{Life} = \sum_j D_j^{Life} \tag{4.9}$$

Accumulation of damage using one or more input time-series,

$$D_j^{Life} = \sum_i \frac{n_{ji}^{Life}}{N_{ji}} \tag{4.10}$$

where,

index i is used to specify the ith cycle

D_j^{Life} is the extrapolated damage over the design lifetime due to the j^{th} time series

n_{ij}^{Life} is the extrapolated cycle counts

N_{ij} is the cycles to failure and

$N_{ji} = \left(\frac{L^{ult} - |L^{MF}|}{\left(\frac{1}{2} L_{ji}^{RF}\right)} \right)^m$

Goodman correction is considered to account for variable load means of the actual load cycles.

Goodman correction for a Goodman exponent equal to one is,

$$L_{ji}^{RF} = L_{ji}^{R} \left(\frac{L^{ult} - |L^{MF}|}{L^{ult} - \left|L_{ji}^{M}\right|} \right) \tag{4.11}$$

Where,

L_{ji}^{R} is range about a load mean of L_{ji}^{M} for the i^{th} cycle in the j^{th} time-series,

L^{ult} is the ultimate design load of the component,

L^{MF} is the fixed load-mean,

m is the Wohler exponent of the component.

The lifetime damage is then accumulated for all cycles and time-series,

$$D^{Life} = \sum_j \sum_i \frac{n_{ji}^{Life}}{N_{ji}} \tag{4.12}$$

The total damage from all cycles

$$D = \sum_i \frac{n_i}{N_i (L_i^{RF})} D^{Life} \tag{4.13}$$

Extrapolation of cycle counts depends on the design load cases (DLC). Three fatigue-related major classes of DLC from IEC 61400-1 [2005] are considered in MLife for damage calculation. These DLCs are

- Power production (DLC 1.2)
- Parked (DLC 6.4)
- Discrete events (DLCs 2.4, 3.1 and 4.1)

The fatigue cycle counting presented in this report only considers the power production DLC.

4.5 Controller Generation Code

The Control Generator is more an order of operations than a code. It uses the programs WT_Perf, FAST_Linear, Excel and a FORTRAN compiler. It is organized into three main objectives:

1. Find highest Cp and TSR for blade and "wind speed – pitch angle" couples for above rated power.
2. Find pitch sensitivity and best-fit line of pitch sensitivity results
3. Calculate values needed for controller and Compile .dll.

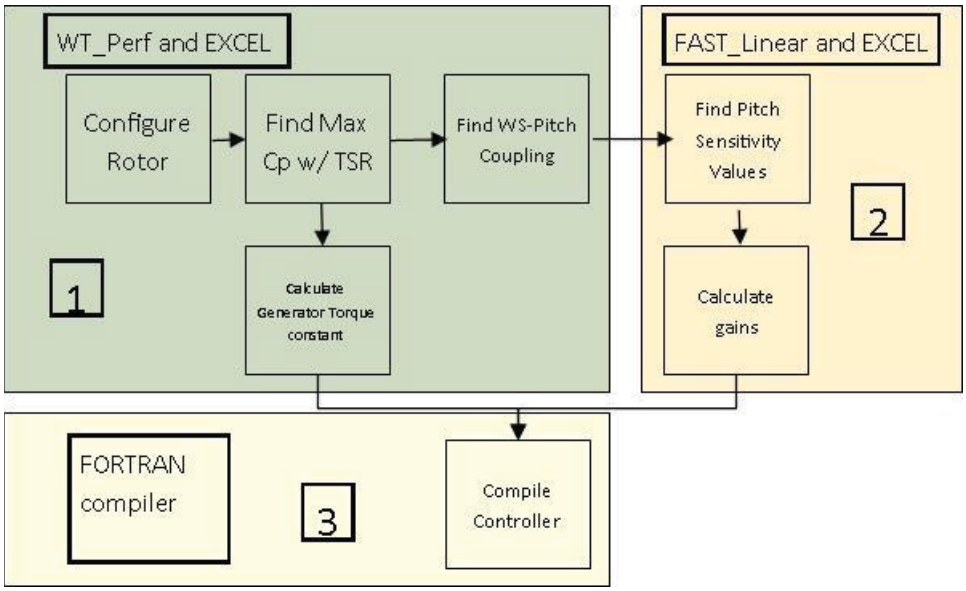

Figure 4.7. Controller generation code block diagram.

Looking at the order of operations as a list with corresponding subsection

- Remove one blade from the NREL baseline 5MW rotor
- Run WT_Perf to find highest Coefficient of Power and corresponding tip-speed ratio (1)
- Calculate Generator-Torque Constant with Cp and TSR (1)
- Run WT_Perf over a range of wind speeds and pitch angles (1)
- Determine pitch angle -wind speed couples for desired rated power (1)
- Generate files for FAST_Linear at wind speed and pitch angle found in previous step (2)
- Run FAST_Linear to find pitch sensitivity (2)
- If possible find linear approximation from FAST_Linear pitch sensitivity results (2)
- Find minimum pitch angle, and generator rpm at rated power (2)
- Find proportional and integral gains based on linear approximation (2)
- Compile .dll controller with Generator-Torque Constant, and proportional and integral gains (3)

It is in development to bring all three main operations together into one code.

4.6 Simulation Based Annual Energy Production Estimation Method

A method for estimating the annual energy production (AEP) from wind turbine simulation results is developed. The traditional theoretical AEP estimation method uses the coefficient of power, C_p, to characterize the power generated. However, it is challenging to find accurate coefficient of power values, C_p, for many alternative designs. Therefore, a method that can estimate AEP from simulation results that does not require coefficient of power value for the AEP estimation is required. This method directly accounts for any change in a wind turbine model. Using this method, a user can compare the AEPs of alternative wind turbine designs. In this section, a theoretical method for AEP estimation and an alternative method that uses simulation results are introduced and compared.

Theoretically, the AEP can be obtained using Eq. (4.14)

$$\text{AEP} = (24\text{hr/day})(365\text{day/yr})\int_{v_{\text{in}}}^{v_{\text{out}}} P(v)f(v)dv \tag{4.14}$$

where, v_{in} is the cut-in speed, v_{out} is the cut-out speed, v is wind speed, $P(v)$ is the generated power at a given wind speed, and $f(v)$ is probability density function (PDF) of the wind speed in one year.

The generated theoretical power can be calculated from Eq. (4.15) for a speed greater than the cut-in speed, v_{in}, and less than the rated wind speed, v_r.

$$P(v) = \frac{1}{2} C_p \rho A v^3 \tag{4.15}$$

where, C_p is the coefficient of power, ρ is density of air which equals to 1.22 kg/m^3, and A is the swept area. Once the wind speed reaches the rated wind speed, the generated power becomes constant, equal to the power at cut-out wind speed, v_{out}. The swept area in Eq. (4.15) can be calculated as follows:

$$A = \pi\big(R\cos(\phi)\big)^2 \cos(\psi) \tag{4.16}$$

where, R is rotor radius, ϕ is cone angle, and ψ is shaft tilt angle. The swept area A used in Eq. (4.16) is the projected swept area on a vertical plane. Jonkman et al., [2009] used a swept area without the $\cos(\psi)$ term in Eq. (4.16). However, the projected swept area is used in this study to account for the shaft tilt.

The wind speeds at NOAA Buoy 45005 at 90m height on Lake Erie are distributed according to the histogram in Figure 4.8. These wind data are collected from year 1980 to 2011. Although the wind speed data for 1986 and 1987 were excluded because the records are not reliable. Thus, wind speed data over 30 years are used. The wind speeds measured at 5m above the water level are converted to wind speeds at 90 m height using the power law with a shear factor of 0.14. The 3-parameter lognormal distribution fit best to the data. The location parameter, μ, the scale parameter, ϱ, and the threshold, γ , are found equal to 2.612, 0.3020, and -6.505, respectively.

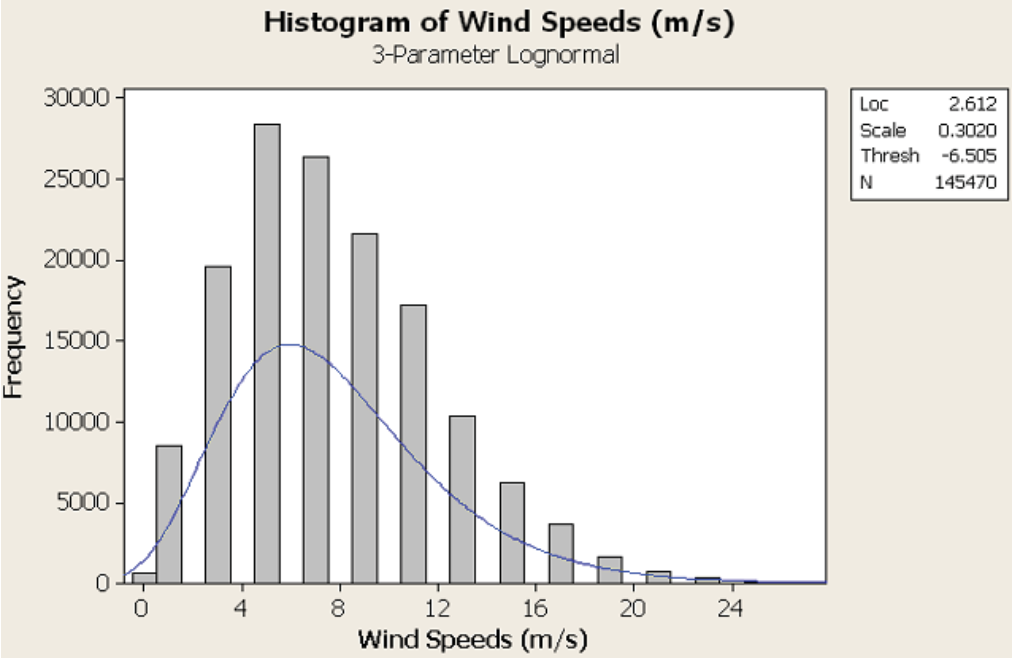

Figure 4.8. Histogram and PDF of wind speeds at buoy 45005 at 90m height.

The PDF of the 3-parameter lognormal is defined in Eq. (4.17). Its mean value can be found using Eq. (4.18). The mean value at the location of buoy 45005 at 90 m height is equal to 7.76 m/s.

$$f(v;\mu,\varrho,\gamma)=\frac{1}{(v-\gamma)\varrho\sqrt{2\pi}}\exp\left\{-\frac{[\ln(v-\gamma)-\mu]^2}{2\varrho^2}\right\} \tag{4.17}$$

$$\text{Mean}(V)=E(V)=\gamma+\exp\left(\mu+\frac{\varrho^2}{2}\right) \tag{4.18}$$

According to the specification of the NREL 5MW wind turbine in [Jonkman et al., 2009], a coefficient of power value C_p=0.482 can be used for the AEP calculation of the baseline NREL 5MW wind turbine. The theoretical AEP of the baseline NREL 5MW wind turbine at buoy 45005 can be calculated by Eq. (4.19). Because the wind turbine will maintain rated power from the rated to the cut-out wind speed, the integral is divided in to two parts.

$$\begin{aligned}\text{AEP}_{\text{theory}} &= (8760\text{hr})\left\{\int_{v_{\text{in}}}^{v_r}\left(\frac{1}{2}C_p\eta_{DT}\rho A v^3\right)f(v)dv+\int_{v_r}^{v_{\text{out}}}P_r f(v)dv\right\} \\ &= 17.1216\ \text{GWh}\end{aligned} \tag{4.19}$$

where, the v_r is the rated wind speed that is v_r=11.4 m/s, the η_{DT} is the efficiency of drive train that is η_{DT}=0.944, and P_r is the rated power that is equal to 5MW. The drive train efficiency, η_{DT}, is added in the below rated wind speed term because the coefficient of power, C_p, does not include effects of drive train efficiency for the wind turbine model considered in this project.

The AEP is calculated using the power generation results from the FAST simulations. The operation of NREL 5MW 3-bladed upwind turbine in steady winds from 3 m/s to 25 m/s with 2 m/s intervals is simulated. The AEP is calculated by using Eq. (4.20). The difference between Eq. (4.14) and Eq. (4.20) is that the power generated term of Eq. (4.14) is replaced with the power generation results from simulations for the Eq. (4.20). Equation (4.14) is converted into a discretized form in Eq. (4.20). This is because, in most of cases, we can get discrete power generated results from simulations rather than continuous results for a wind speed region. Eq. (4.20) sums AEPs for each bin, that is product of power generation of each wind speed bin and the histogram of the wind speed and then multiplies by the sum of hours in a year, which is 8760 hours. On the other hand, Eq. (4.14) integrates the product of the PDF of the wind speed and power generated and then multiplies by number of hours in a year.

$$\text{AEP}=(24\text{hr/day})(365\text{day/yr})\sum_{v_{\text{bin}}=v_{\text{in}}}^{v_{\text{out}}}(P|v_{\text{bin}})\cdot\left(\int_{v_{\text{bin min}}}^{v_{\text{bin max}}}f(v)dv\right) \tag{4.20}$$

where, the v_{bin} is wind speed for a bin, the $(P|v_{\text{bin}})$ is the power generated at the wind speed in the corresponding bin from simulations, the $v_{\text{bin max}}$ is the upper bound of the wind speed of the bin, and the $v_{\text{bin min}}$ is lower bound of the wind speed of the bin.

Generally, a power generated value at a wind speed bin, $(P|v_{\text{bin}})$, can be obtained by running FAST simulations with a steady wind profile for a wind speed in a wind speed bin. FAST generates electrical power production in time domain. The average value of the generated power

results of a wind speed bin can be used for the $(P|v_{\text{bin}})$ value of a wind speed bin. By running multiple simulations, $(P|v_{\text{bin}})$ values can be found for various wind speed bins.

One of the advantages of the AEP estimation using simulation results is that the type of winds are not limited to steady wind. Because this method reflects any conditions applied on wind turbine simulation, any kind of wind profile can be used for AEP estimation for the wind condition. For example, if someone wants to estimate AEP of a wind turbine under a wind profile with random turbulence, by just plugging in the average value of generated power result from the wind turbine simulation into Eq. (4.20), AEP can be estimated.

The simulation-based AEP estimation method is validated by comparing its results with those from theory. The 5MW 3-bladed upwind baseline design (5MW3UB00) is used for this validation. The unconditional probability distribution of the wind speed in Lake Erie is presented in Table 4.3 for various wind speed bins. This table also compares the generated power and AEP estimated from both theory (Eq. (4.19)) and simulation (Eq. (4.20)).

The AEP estimated using simulation is 1.22% less than the theoretical AEP value. This difference may be because of the approximations in the wind turbine simulation model. Another reason may be that a constant coefficient of power value, C_p, from the cut-in to rated wind speed is used for the theoretical method. The actual coefficient of power value may vary with the wind speed. Finally, the coefficient of power value that is used for the theoretical method, which is C_p=0.482 is approximate. If the theoretical power generated at the rated wind speed of 11.4 m/s is calculated using Eq. (4.15), then the power generated at the rated wind speed is $P(v_r)$=5.098 MW, after a value of 0.944 for the drive train efficiency, η_{DT}, is applied. This value exceeds 5 MW. Thus, the coefficient of power given in [Jonkman, 2009] is approximate, and the error in the approximation could be about 1.96%. Moreover, it is reasonable that the AEP estimated from simulation is smaller than the theoretical value because the theoretical generated power at the rated wind speed is estimated to be larger than 5 MW. In addition, if the C_p value that has exactly 5 MW at rated wind speed is calculated, the coefficient of power value calculated equal to C_p=0.473 for the case 0.944 η_{DT} value is applied. In this case, the simulation based AEP value is only 0.19% less than the theoretical value.

Because the percent difference is relatively small, the AEP estimation from simulation is reasonable. Using the simulation method, the designer will be able to calculate the AEP for various wind turbine configurations without finding a new coefficient of power value for each new wind turbine design using the theoretical approach.

Table 4.3. Annual energy production comparison of theory and simulation values.

v_{bin}	$v_{\text{bin min}}$	$v_{\text{bin max}}$	Integrated PDF	Hours	Power generation (kW)		Annual Energy Production (MWh)	
(ms)	(m/s)	(m/s)	(-)	(Hr)	Theory	Simulation	Theory Eq. (4.19)	Simulation Eq. (4.20)
	-∞	0	0.00717	63	0	0	0	0
	0	3	0.10933	958	0	0	0	0
3.5	3	4	0.07800	683	148	95	105	65
5	4	6	0.19357	1696	430	394	769	668
7	6	8	0.19389	1698	1180	1160	2027	1970
9	8	10	0.15520	1360	2509	2457	3394	3340
11	10	12	0.10739	941	4580	4449	4139	4185
13	12	14	0.06744	591	5000	4997	2954	2952
15	14	16	0.03968	348	5000	4997	1738	1737
17	16	18	0.02233	196	5000	4998	978	978
19	18	20	0.01220	107	5000	4998	534	534
21	20	22	0.00653	57	5000	4998	286	286
23	22	24	0.00345	30	5000	5000	151	151
24.5	24	25	0.00105	9	5000	5000	46	46
	25	∞	0.00276	24	0	0	0	0
Total			1	8760			17122	16912
%Difference							0	-1.22

4.7 Cost Estimation and System Modeling Code

Purpose of Code

The purpose of the cost estimation code outlined here is to estimate the levelized cost of energy of the wind turbine system. A wind turbine system is a reference to not only the costs of the tangible components of the wind turbine, but the total costs involved in erecting, commissioning, operating and maintaining an offshore wind turbine.

The Levelized Cost of Energy (LCOE) is the total cost of the wind turbine system divided by the total net amount of the energy produced

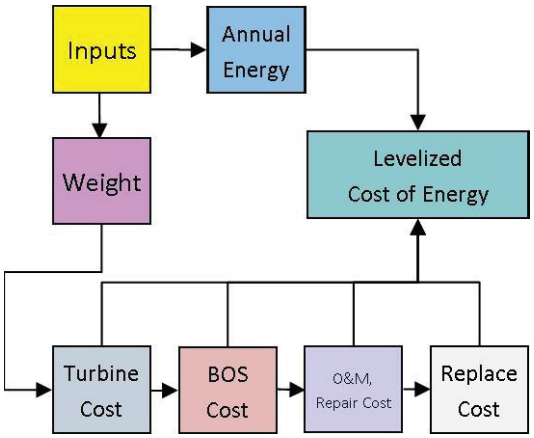

Figure 4.9. Block Diagram of Cost Estimation Code.

Brief Description of Cost Estimation

The cost code used in this report is divided into eight main categories:

- Inputs
- Turbine Capital Costs
- Balance of Station (BOS) Capital Costs
- Operation and Maintenance & Repair Costs
- Replacement Costs
- Annual Energy Production
- Levelized Cost of Energy

Built in MATLAB, the estimates are largely based on equations from NREL (a list of references used in the analysis can be found in the cost portion of the report). The code needs, environmental (average wind speed, location, and etc., wind turbine (rotor diameter, rated power, and etc.), financial (size of farm, interest rates…), operation (time between repairs, days to repair, and etc.) and replacement (time to replacement, days to replace) data.

The code will return the costs associated with the main categories mentioned above, or by individual components, or tasks such as installation or repair. Please see a more detailed description of codes outputs in Chapter 8 of the report.

5 Modeling of Environment and Design Loads

This chapter describes the information and methods used to characterize the loading environment of the wind turbine site considered in this study. The scope of this discussion is limited to developing the information needed for offshore wind turbine design load case studies based on the IEC standards. Section 5.1 discusses the standards, Section 5.2 introduces the site of study and Section 5.3 reviews the available data. Finally, Section 5.4, using the available data, specifies the load cases that are to be used for the concept turbine design studies.

5.1 Wind Turbine and Foundation Design Standards

In order to perform wind turbine load analysis, the International Electrotechnical Commission (IEC) standards are used. IEC 61400-1 [2005] is used primarily to predict land-based wind turbine loads, and the IEC 61400-3 [2009] is used to determine the offshore wind turbine system loads. For the foundation, the DNV-OS-J101 standard was used to determine the loads. The IEC 61400-3 and DNV-OS-J101 standards have almost similar DLCs. The DLCs of DNV-OS-J101 standard correspond to DLCs of IEC61400-3 [2009] standard, and for each DLC in the first set of standards there is a corresponding one in the second.

Different wind conditions, including deterministic and turbulent are characterized in the IEC 61400-1 [2005] standard. The wind load cases are divided into "Normal" and "Extreme" conditions, and in each category several loading cases are specified as follows:

1) Normal wind conditions
    a. Normal Wind Profile model (NWP)
    b. Normal Turbulence Model (NTM)
2) Extreme wind conditions
    a. Extreme Wind speed Model (EWM)
    b. Extreme Operating Gust (EOG)
    c. Extreme Turbulence Model (ETM)
    d. Extreme Direction Change (EDC)
    e. Extreme Coherent gust with Direction change (ECD)
    f. Extreme Wind Shear (EWS)

The mathematical formulation of the above wind cases are described in IEC 61400-1 [2005] standard. National Renewable Energy Laboratory (NREL) has developed computational tools to generate design load cases in accordance with the IEC standards for a wind farm. One code, IECWind, generates deterministic wind cases, and the other code, TurbSim [Jonkman & Kilcher, 2012] generates random wind load cases. Both codes are open source and can be downloaded from the NREL website. Figure 5.1 demonstrates the wind conditions and the tools that can be used to generate the IEC wind parameters.

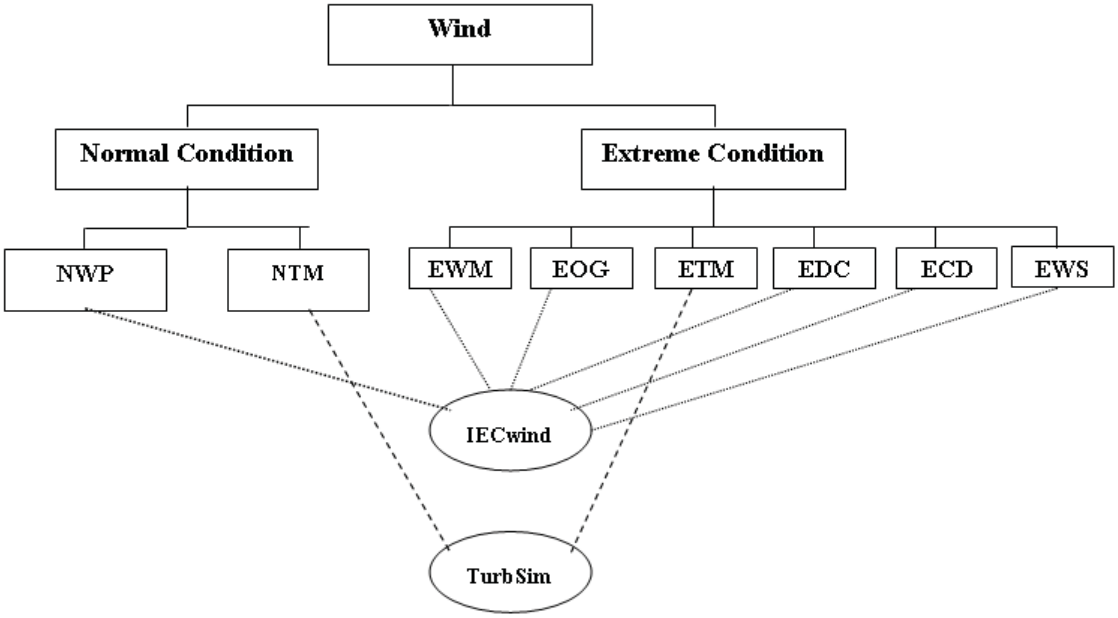

Figure 5.1 Different wind load cases and the tools to generate them.

5.2 Study Site

For the purposes of this study, the central basin of Lake Erie defined by a band three to five miles off the Cuyahoga County shore, close to the city of Cleveland, Ohio was considered as the wind turbine site. The water depth at this location varies between 13-17 m. The main sources of environmental data used here are from the National Oceanic and Atmospheric Administration (NOAA) buoy 45005, a wind resource report by Dykes et al., [2008], and a Great Lakes feasibility study document by Marshall et al., [2009]. Both Marshall's and Dykes' studies were conducted for the same location. To define the load cases, the historical data from the buoy were used in conjunction with the report by Marschall et al., [2009].

5.3 Environmental Conditions

5.3.1 Wind & Wave

The main source of the wind data in the Great Lakes feasibility study conducted by Masrchall et. al., [2009] is the wind resource assessment study by Dykes et al., [2008]. The measurements were collected at the Cleveland water intake crib, which is located 3.5 miles from the shore. A picture of the structure is found in Figure 5.2. The crib is located at the Cleveland bay, which is sheltered by the natural depression of the shore. Thus, the accuracy of readings of wind speed should be evaluated for potential wind farms farther from shore in Lake Erie.

Since the raw data from either the wind resource assessment studies by Dykes et. al., [2008] or the study by Marchall et. al., [2009] were unavailable for this work, the wind and wave data collected at the buoy 45005 were used in order to calculate the environment loading condition

based on the IEC standards. Moreover, using data from buoy to model the dependence between wind and wave is advantageous as the data were collected at the same location and the wind and wave measurements were synchronized. The disadvantage of these data, however, is that the buoy does not operate during winter time; therefore, there are no wind data corresponding to the cold months. For those months, the wind data from the crib, summarized in Marchall et. al., [2009] were used..

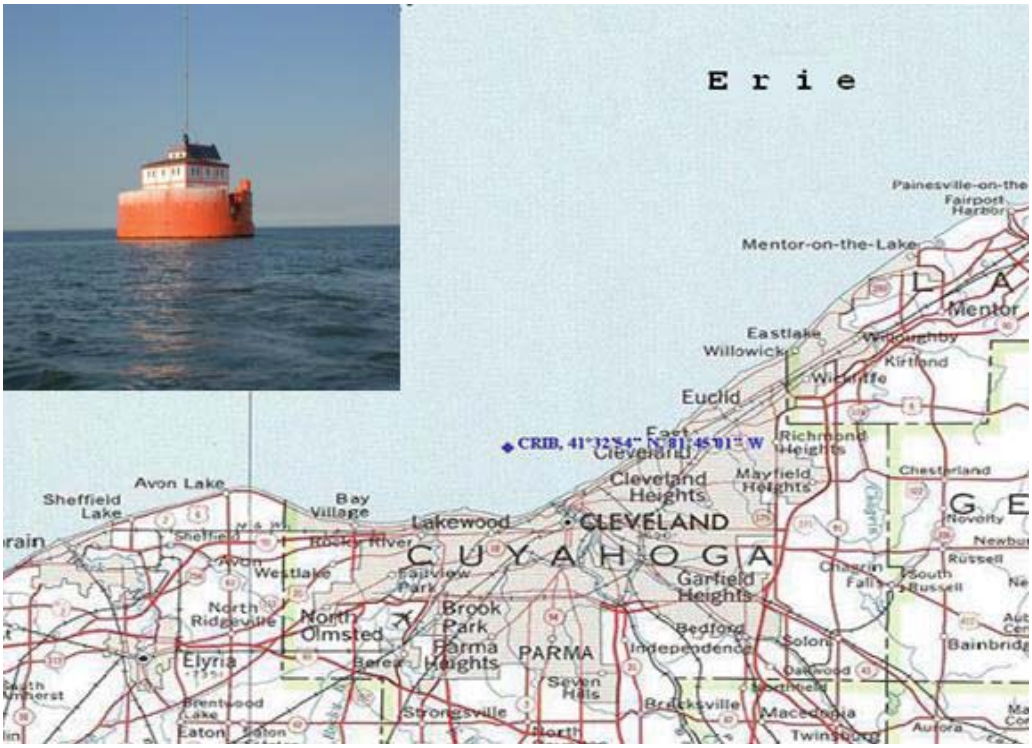

Figure 5.2 Cleveland water intake crib [Marchalls et. al, 2009].

Figure 5.3 shows the buoy with the Data Acquisition and Control Telemetry payload, which is located at position 41.677 N 82.398 W (see Figure 5.4). Table 5.1 lists the main characteristics of this buoy.

Figure 5.3 Picture of the buoy.
[courtesy of NOAA website]

Figure 5.4. Location of the reference buoy in Lake Erie.
[courtesy of Google Earth]

Table 5.1. Main buoy characteristics.

Site elevation	173.9 m above mean sea level
Air temp height	4 m above site elevation
Anemometer height	5 m above site elevation
Barometer elevation	173.9 m above mean sea level
Sea temp depth	0.6 m below site elevation
Water depth	12.6 m
Watch circle radius	36 yards

Thirty two years' historical data for wind speed, wave elevation, and dominant wave period are available in the NOAA website for the buoy 45005. However, the data for the following six years are ignored because they were not usable: 1986, 1987, 1996, 2007, 2008 and 2010. Therefore, information from the remaining 26 years was used in order to construct the probabilistic models of the wind speed and wave height. Note that since the buoy did not operate during the winter, the wind and wave data do not represent the environment conditions during winter.

The measured wind speed at the buoys is reported by averaging the speed data over an eight-minute period. Similarly, the significant wave height is calculated during a 20-minute sampling period. The dominant wave period is the period of the waves with maximum energy. In the wind industry ten-minute period wind speeds are typically used. In order to convert the eight-minute average wind speeds, the following equation can be used, which is based on DNV-OS-J101 [2007] standard.

$$V_{10} = V_T \left(1 - 0.047 \ln\left(\frac{T}{10}\right)\right) \tag{5.1}$$

where V_T is the measured mean wind speed over period T. The averaging of the measurements from buoy is performed over 8 minutes. Therefore, to obtain the corresponding wind speeds over ten minutes or one hour the wind speeds should be adjusted by scaling them by 0.99 or 1.10, respectively.

A sample scatter diagram corresponding to year 2002 data is shown in Figure 5.5. Every dot represents a sample pair of wind speed and significant wave height taken during that year. The point at the rightmost corner is selected as the extreme condition for that year. This process was repeated to select the extreme pair for each year, as summarized in Table 5.2.

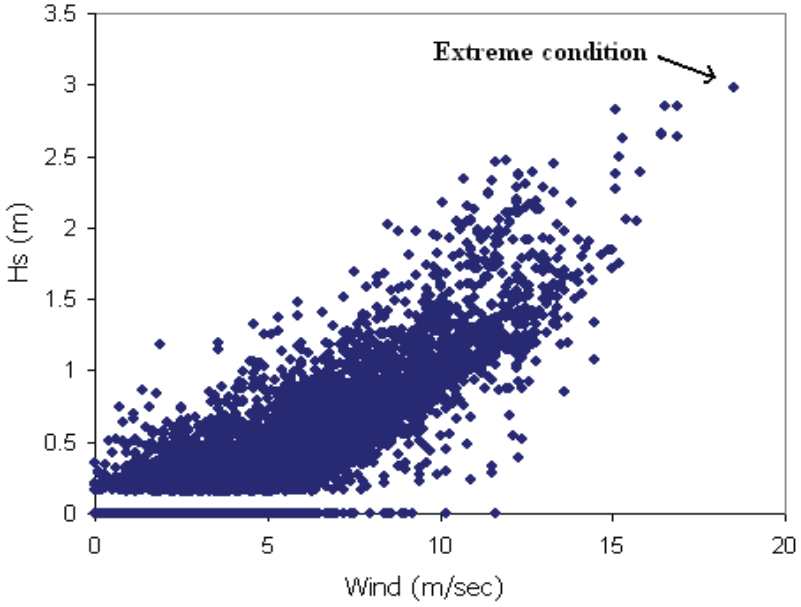

Figure 5.5. Scatter diagram of wind speed versus significant wave height for the data recorded in 2002 [Norouzi, 2012].

Table 5.2. Extreme wind, wave and period.

Year	Wind speed (m/s)	Significant wave height (m)	Wave period (s)
1980	14.7	2.20	5.00
1981	17.4	2.50	5.00
1982	15.7	2.30	4.80
1983	13.8	2.30	5.00
1984	16.1	1.90	4.50
1985	12.9	2.10	5.90
1988	18.4	1.00	3.60
1989	13.4	1.10	3.80
1990	16.9	2.40	5.60
1991	15.3	2.50	2.90
1992	18.0	2.70	5.60
1993	17.3	2.50	5.00
1994	16.8	2.00	5.60
1995	17.1	3.40	8.30
1997	18.0	2.60	5.88
1998	19.0	2.85	6.25
1999	16.4	2.11	4.55
2000	16.6	2.26	5.56
2001	18.3	2.45	5.88
2002	18.5	2.98	5.24
2003	18.8	2.97	6.25
2004	17.6	2.54	5.56
2005	17.6	2.72	5.56
2006	17.4	2.29	5.00
2009	17.7	2.70	5.88
2011	19.4	3.23	7.14

Figure 5.6 and Figure 5.7 show the wind roses corresponding to the periods of 1980-1994 and 1995-2008 respectively. These wind roses were constructed using the buoy data.

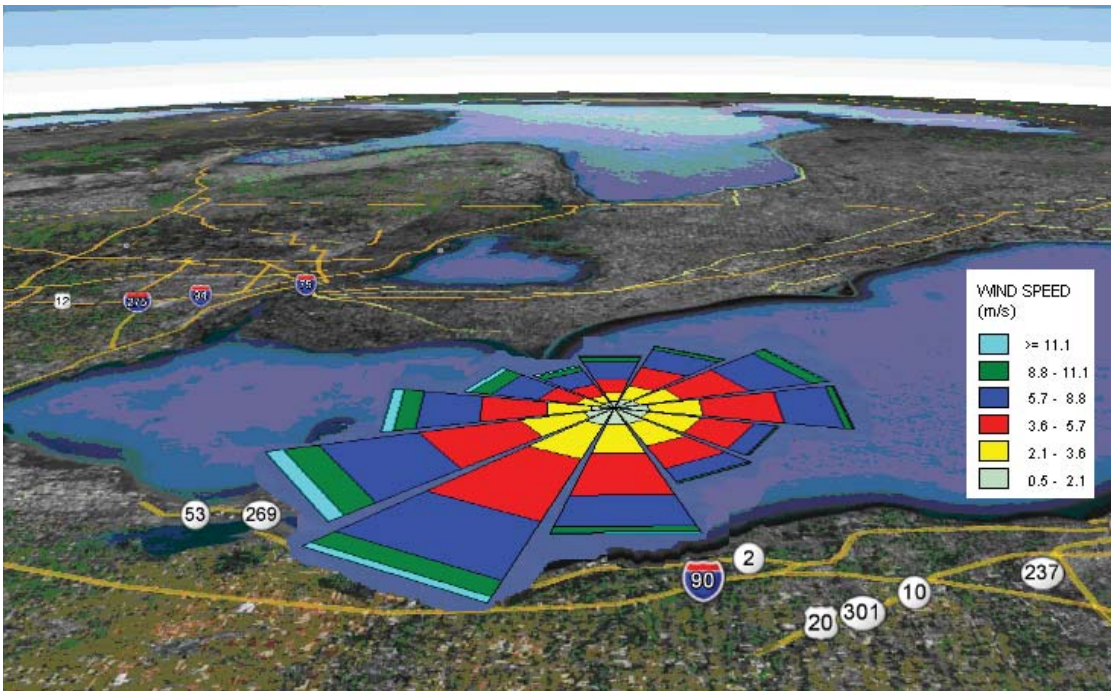

Figure 5.6. Wind rose from year 1980 to 1994 (measured at the NOAA buoy 45005).

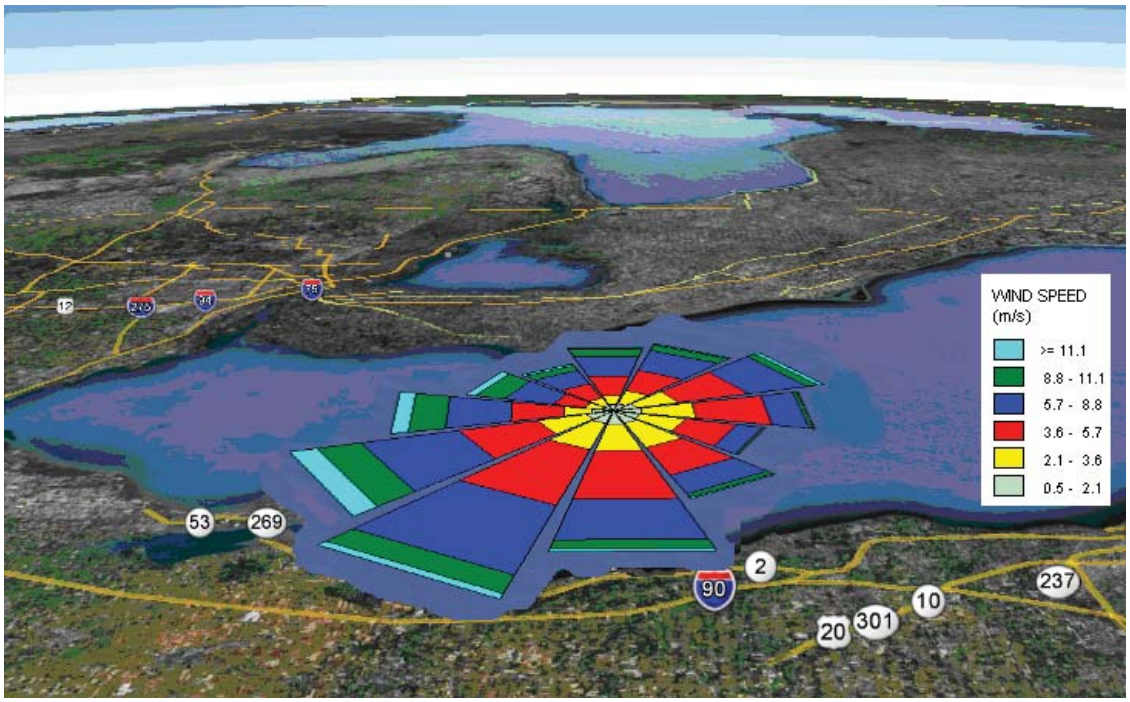

Figure 5.7. Wind rose from year 1995 to 2008 (measured at the NOAA buoy 45005).

Figure 5.8 presents the wind rose for the time period from 1995 to 2008.

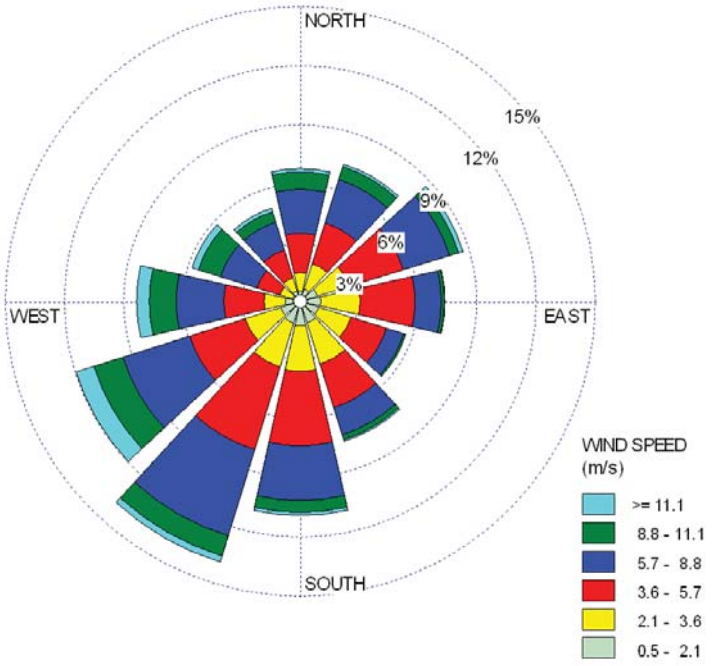

Figure 5.8. Wind rose for period of 1995-2008.

The wind speeds at the buoy were measured at 5 m height, which corresponds to the top of the buoy. The power law, Eq. (5.2), was used to estimate the corresponding wind speed at the hub height.

$$V(z) = V(z_r)\,(z/z_r)^{\alpha} \tag{5.2}$$

where V is the wind speed, z is the hub height, z_r is the height at which the wind speed is measured, and α is the exponent of the power law (shear factor).

Figure 5.9. Frequency Rose for Crib data shows the wind rose from Marschall et al., [2009]. This rose was constructed from the data collected at the crib by Dykes et al., [2008]. Although the buoy is approximately 20 miles from the water crib, the data shows trends for dominant winds similar to those reported by Marschall et al., [2009]. The wind rose shown in Figure 5.9, presents the wind speed at 70 m hub height.

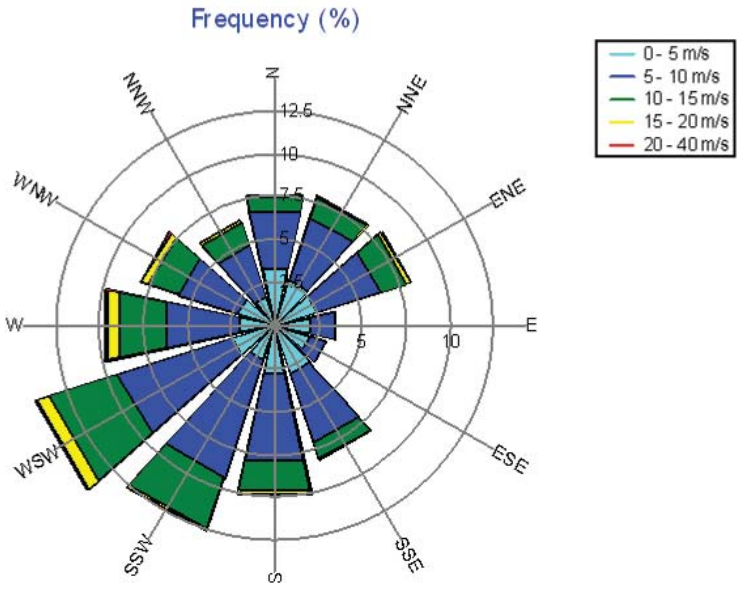

Figure 5.9. Frequency Rose for Crib data [Marschall et al., 2009].

Approach 1: Characterization of Wind and Wave Dependency

Wind and wave are dependent as large waves are always associated with high winds. There are different methods to model this dependence in an offshore wind farm. Herein this work, a method was adopted based on copula functions. Copulas are functions that couple the one-dimensional marginal probability density functions of a set of random variables to the joint density of these variables [Nelsen, 2006]. Here copulas were applied to obtain the distribution of the joint wind speed and significant wave height utilizing data from buoy, which recorded wind speeds and wave heights simultaneously. For more details about this process refer to Norouzi [2012] or Nikolaidis et al., [2011].

Sklar's theorem builds the foundation for the application of copulas. Based on this theorem, for two dependent variables u and v, there is a copula function (C) such that for all combinations of values of the cumulative probability distribution functions (CDF) of u and v the following relationship holds:

$$F_{UV}(u, v) = C\big(F_U(u), F_V(v)\big) \tag{5.3}$$

For continuous CDFs, F_U and F_V, C will be unique. Conversely, if C is a copula and F_U and F_V are distribution functions, then function F defined by Eq. (5.3) is a joint distribution function with margins F_U and F_V.

In order to model the dependence between wind and waves using a copula, as a first step one needs to estimate the marginal PDFs of the wind speed and the significant wave height from the data. Well-known distributions such as Gumbel, Generalized Extreme and Weibull distributions can be good candidates for modeling marginal PDFs [Nikolaidis et al., 2011].

Using Weibull distribution, by considering the location parameter as zero, the shape and scale parameters would be 13.87 and 17.47, respectively. Similarly, if Weibull distribution is fitted to the wave data, the shape and scale parameters are estimated to be 5.63 and 2.57. Figure 5.10 shows the corresponding CDFs of the wind speed and significant wave height.

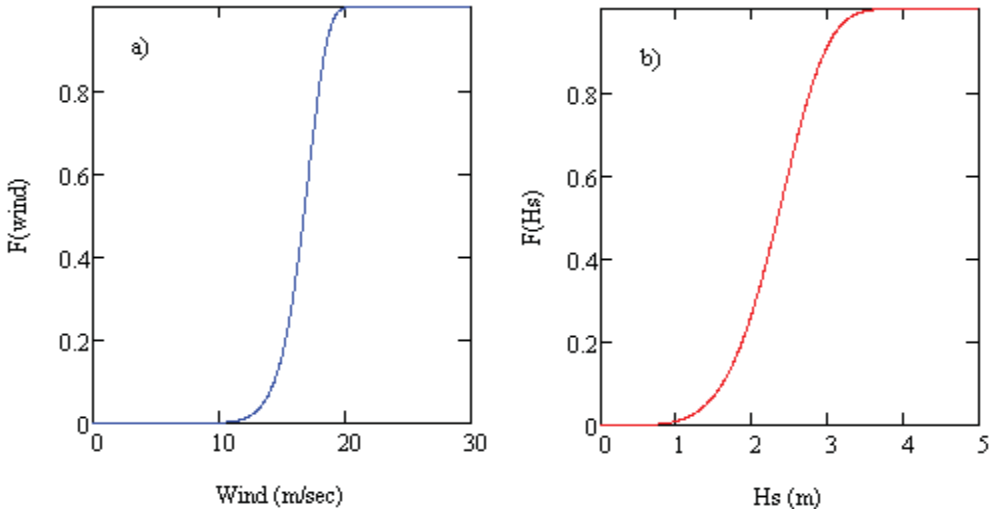

Figure 5.10. The CDF of a) wind speed b) significant wave height (Hs) [Norouzi, 2012].

The next step is to integrate the CDFs using a copula function. There are several copulas in the literature; in this study Frank's copula was selected to build the joint distribution [Nelsen, 2006]. In Frank's copula the dependence is measured by a single parameter, θ', as in Eq. (5.4)

$$C_{\theta'}(u,v) = \log_{\theta'}\left\{1 + \frac{(\theta'^{u} - 1)(\theta'^{v} - 1)}{\theta' - 1}\right\} \tag{5.4}$$

where u and v are the values of the CDFs of the wind speed and significant wave height. Zero value for θ' means perfect dependence while unit value means perfect independence.

The value of parameter θ' can be estimated from data. The method based on maximizing the pseudo-likelihood function was used to estimate the dependence [Nikolaidis et al., 2011]. A pseudo-likelihood function is defined as follows,

$$L(\theta') = \prod_{i=1}^{n} C_{\theta'}(u,v) \tag{5.5}$$

where, $c_{\theta'}(u,v)$ is the joint PDF calculated by,

$$C_{\theta'}(u,v) = \frac{\partial^2 C_{\theta'}(u,v)}{\partial u \partial v} \tag{5.6}$$

This function equals to 1 for unit θ', and

$$C_{\theta'}(u,v) = \frac{\theta'^{u+v}\ln(\theta')(\theta'-1)}{(\theta' + \theta'^{u+v} - \theta'^{u} - \theta'^{v})^2} \tag{5.7}$$

otherwise.

The value of θ' is found by maximizing the logarithm of the likelihood function. For the copula corresponding to the wind and wave data from the buoy, a value of θ' equal to 0.0087 was obtained. This means that there is a strong dependence between the wind speeds and the wave heights. Figure 5.11 shows the joint PDF of the wind speed and the significant wave height that was obtained using the copula function. This shows that it is more likely to observe large waves while the wind speeds are high and vice versa, as expected.

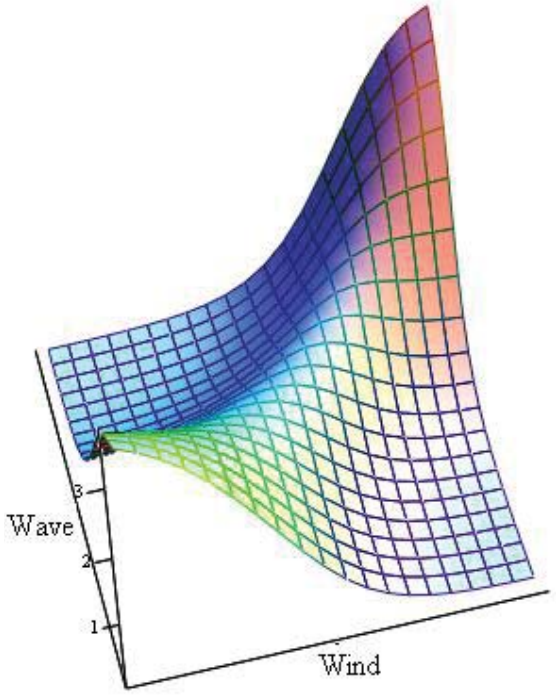

Figure 5.11. The PDF of wind speed and significant wave height [Norouzi, 2012].

In order to assess the quality of the model, 50 pairs of wind speeds and wave heights were simulated, which are shown in Figure 5.12. These pairs are compared with the 26 pairs of measurements from the Lake Erie site. This figure supports a conclusion that the copula model is accurate.

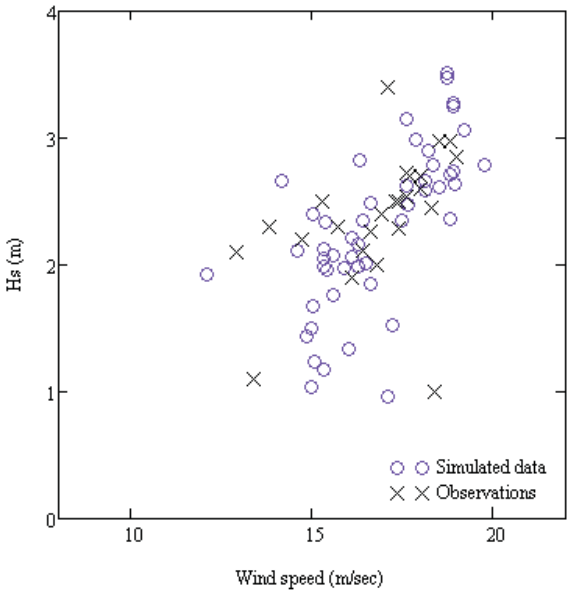

Figure 5.12. Simulated and observed values of the wind speed and significant wave height (Hs) for the Lake Erie site [Norouzi, 2012].

Similarly, the dependence between wave height and wave period is developed, as shown in Figure 5.13.

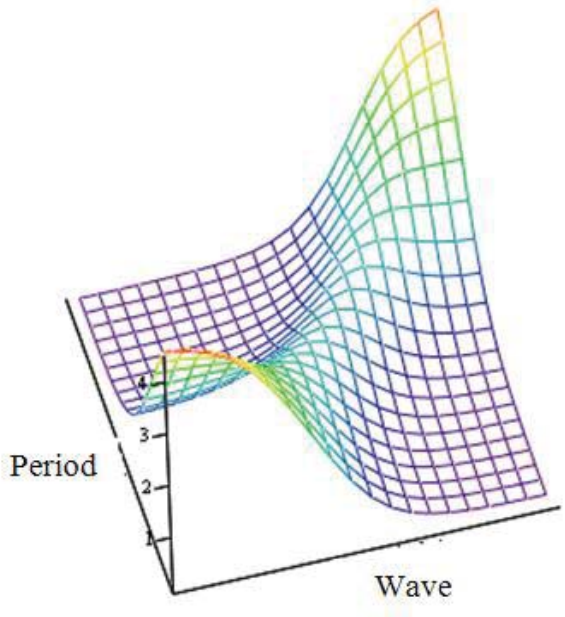

Figure 5.13. The PDF of significant wave height and period [Norouzi, 2012].

Again, a comparison of the simulated pairs of the wave period and the significant wave height with observations was used to validate the model's accuracy to predict measured data at the Lake Erie site Figure 5.14.

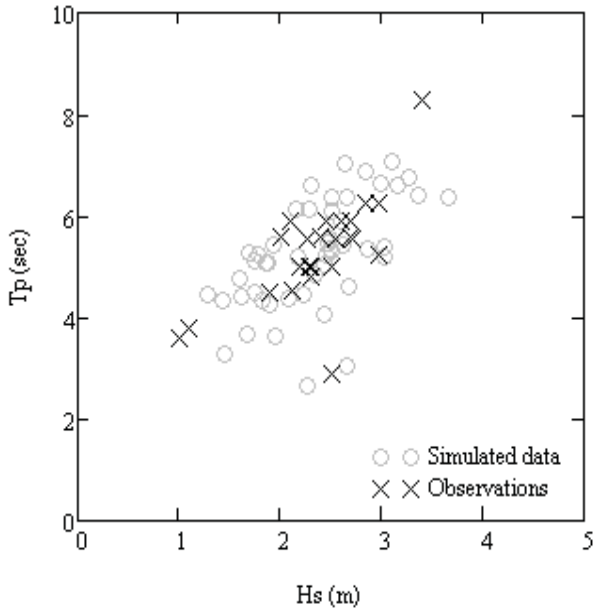

Figure 5.14. Simulated and observed values of the wave period (Tp) and significant wave height (Hs) for Lake Erie site [Norouzi, 2012].

Approach 2: Statistical Extrapolation for Extreme Events

Building the joint distribution of wind speed and significant wave height, as well as that of significant wave height and spectral period allows the extreme 1-year or 50-year wind and wave conditions with the desired confidence intervals be determined. Figure 5.15 shows 1,000 pairs of simulated data calculated using the copula models, and their comparison with the observations. Note that the wind speeds in Figure 5.15 are at the 5 m height.

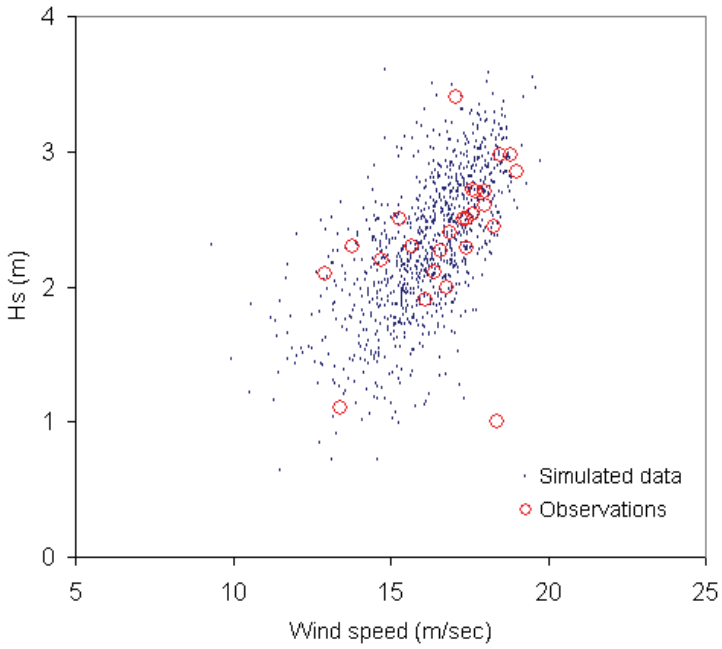

Figure 5.15. Observed data along with 1000 pair simulated data.

Using the 1,000 simulated pairs of the wind speed and significant wave height, the extreme 50-year conditions were calculated based on 95% confidence intervals. The following technique was used: 50 samples were drawn from 1,000 simulated pairs that were already generated using the copula models. The maxima were then selected from every sample. Samples were drawn until the desired confidence in results was obtained.

Table 5.3. Extreme 50-year wind and wave.

Wind speed	19.80 m/s
Significant wave height (Hs)	3.64 m

The wind speed in Table 5.3 is at 5 m height. The corresponding wind speed at the tower height of 90 m was calculated using the shear power law (Eq. 5.2). The shear coefficient at a typical offshore wind turbine site is 0.14 while the extreme shear coefficient reported by Marschall et al., [2009] is 0.09. Estimated wind speeds using both shear factors are presented in Table 5.4. The estimated values are based on the shear factor of 0.14 were used in this work to be on the safe side.

Table 5.4. Extreme 50-year wind at hub height considering shear factor.

	Wind speed
Wind shear 0.14	29.68 m/s
Wind shear 0.09	25.68 m/s

The spectral period of the dominant waves are shown in Table 5.5.

Table 5.5. Spectral period.

	Low 95% CI	Average	High 95% CI
Mean spectral period (s)	5.03	5.14	5.24

The selected values for all three quantities needed for the IEC design load cases are summarized in Table 5.6.

Table 5.6. Extreme 50-year wind, wave with associated spectral period.

Wind speed	Significant wave height	Spectral period
29.68 m/s	3.64 m	5.14 s

Second approach to calculate 50-year extreme wind and wave condition is based on fitting distributions independently to the wind and wave data. In this approach, it is assumed that the wind and wave are independent and the data are independent between different years. After fitting an appropriate distribution, the 50-year wind speed and significant wave height can be estimated by solving Eq. (5.8) for X_{50},

$$1 - P(x < X_{50})^{50} = \frac{1}{50} \tag{5.8}$$

Using the available data from the buoy 45005, the extreme 50-year wind speed and significant wave height were calculated as shown in Table 5.7.

Table 5.7. Extreme 50-year wind, wave with associated spectral period.

Wind speed	Significant wave height	Spectral period
31.71 m/s	3.74 m	5.14 s

Compared to the first approach, slightly larger values than those in Table 5.6 were estimated. This is because in the latter approach the wave and the wind are considered to be independent.

Approach 3: Combination of Confidence Interval, Statistical Extrapolation, and Standard

Third approach to estimate the 1-year extreme wind speed, V_{e1}, and the 1-year significant wave height, H_{s1}, is using the 95% confidence interval for the mean value of the maximum annual wind speeds during each of the considered period of years. This approach is applicable here since there are sufficient data to achieve the desired confidence. Also, the 50-year extreme wind speed, V_{e50}, and the 50-year significant wave height, H_{s50}, can be found using the statistical extrapolation.

Information from a total of 26 years from Figure 5.2 was used in order to construct probabilistic models of wind speed and wave height.

The 1-year extreme wind speed, V_{e1}, is specified using the 95% confidence interval for the mean value of the maximum annual wind speeds recorded during each of the above 26 years.

$$V_{e1} = \bar{V} + t_c \frac{\sigma}{\sqrt{n}} \tag{5.9}$$

In the above equation, $\bar{V}$ is the average value of the maximum annual speeds, t_c is the 95% percentile value of the Student distribution, σ is the estimated standard deviation of the maximum annual wind speed and n is the size of the population, which is 26.

In order to estimate the 50-year extreme wind speed V_{e50} several common probability density functions (PDF) were fitted to the maximum wind speeds data recorded each year from NOAA buoy 45005. These PDFs included Weibull, Lognormal and Gumbel distributions. Among the above PDFs, Weibull's distribution fitted the data best. Therefore, the cumulative distribution function (CDF) of the 50-year extreme wind speed V_{e50} can be calculated using Eq. (5.10).

$$F(V_{e50}) = 1 - e^{-\left(\frac{V_{e50}}{\lambda}\right)^k} \tag{5.10}$$

In the above equation $F(V_{e50})$ is the probability of not exceeding V_{e50}, λ is a scale parameter and k is a shape parameter. $F(V_{e50})$ indicates the probability of wind speed being less than V_{e50}. Assuming independence between consecutive years, one can estimate the extreme 50-year wind speed by solving equation for $F(V_{e50}) = 0.98$.

The NOAA buoy wind speed data were measured at a height of 5 m which corresponds to the top of the buoy. The power law of Eq. (5.2) [IEC 61400-1 (2005)] was used to estimate the wind speed at the turbine hub height. The 90 m hub height, z_r, and the 0.14 shear factor, α, are used for this approach.

The average 1-year maximum wind speed values is $\bar{V} = 16.92$, and the standard deviation is $\sigma = 1.68$. For a population size of n = 26, using Eq. (5.9), upper bound of 95 % confidence interval for the 1-year extreme wind speed at 5 m height, $V_{e1@5\mathrm{m}}$, would be 17.60 m/s. Using the power law, Eq. (5.2), the 1-year extreme wind speed at the hub height is estimated as $V_{e1@90\mathrm{m}}$ = 26.38 m/s, assuming the shear factor is α=0.14. It is reasonable to use the upper bound value in order to evaluate the safety of the design.

The Weibull distribution to the 26 years of annual maximum wind speeds has a scale parameter of $\lambda = 17.63$ and a shape parameter of $k = 13.28$. Using Eq. (5.10) V_{e50} is calculated as $V_{e50@5\mathrm{m}}$ = 19.54 m/s at a height of 5 m above the water level. Using the power law from Eq. (5.2), and a shear factor of α=0.14 the 50-year extreme wind speed at the 90 m height would be $V_{e50@90\mathrm{m}}$ = 29.29 m/s.

The 1-year extreme significant wave height H_{s1} was found using the 95% confidence interval of the maximum significant wave heights recorded in 26 years (Eq. (5.11))

$$H_{s1} = \bar{H} + t_c \frac{\sigma}{\sqrt{n}} \tag{5.11}$$

where, $\overline{H}$ is the mean value, t_c is the 95 percentile value of the Student distribution, σ is the standard deviation and n is the population size.

The 50-year extreme significant wave height H_{s50} is estimated by fitting the annual maximum significant wave height PDF to the wave data collected at NOAA buoy 45005 in 26 years. The 3-parameter Weibull distribution fits best to the annual maximum values of the significant wave height.

$$F(H_{s50}) = 1 - e^{-\left(\frac{H_{s50}-\delta}{\lambda}\right)^k} \tag{5.12}$$

where $F(H_{s50})$ is the probability of not exceeding H_{s50} , δ is the minimum value (threshold) of the significant wave height, and λ and k are scale and shape parameters.

The maximum, minimum and mean values of the wave period, T_p , corresponding to the significant wave height are found from Eq. (5.13) [IEC61400-3, 2009].

$$11.1\sqrt{H_s(V)/g} \leq T_p \leq 14.3\sqrt{H_s(V)/g} \tag{5.13}$$

where $H_s(V)$ is the significant wave height as a function of the wind speed V and g is acceleration of gravity.

The conditional significant wave heights H_s for each wind speed bin were found from the distribution of the significant wave height H_s estimated from buoy data. Interpolation is used to find H_s values at V_r and $V_r \pm$ 2 m/s. The same technique was used to estimate H_s for V_{hub} values of 21, 23 and 25 m/s because there is no recorded wind speed higher than 20 m/s.

The 1-year extreme significant wave height H_{s1} was found using the 95% confidence interval of the mean value of this height that was estimated from 26 annual maximum values measured from the NOAA buoy 45005. The average value of the 26 values is $\overline{H}$=2.76. The percentile value of the Student distribution is $t_c = 2.06$ for the 95% confidence interval because the size of the population is $n = 26$. The standard deviation is $\sigma = 0.44$. Using Eq. (5.11), the 1-year extreme significant wave height is estimated equal to 2.94 m.

The 50-year extreme significant wave height H_{s50} was estimated from the 3-parameter Weibull distribution that was obtained from the 26 annual maximum values of the significant wave heights. The cumulative distribution function $F(H_{s50})$ in Eq. (5.12) is set to $F(H_{s50})$ = 1-(1/50). The shape parameter k and the scale parameter λ are 1.543 and 0.7758, respectively. The threshold value is δ = 2.956. The 50-year extreme significant wave height H_{s50} was estimated as H_{s50} = 3.939 m by solving Eq. (5.12).

5.3.2 Ice Condition

Ice Coverage

Data from the National Oceanic and Atmospheric Administration (NOAA) suggests that the Great Lakes can freeze over quite often. More specifically, Lake Erie, due to its shallowness, can freeze over its entire surface during winter (Figure 5.16). This makes ice loads a serious concern for deployment of any offshore wind turbines into Lake Erie. During the coldest part of the winter in February, Lake Erie is covered with ice at least half the time.

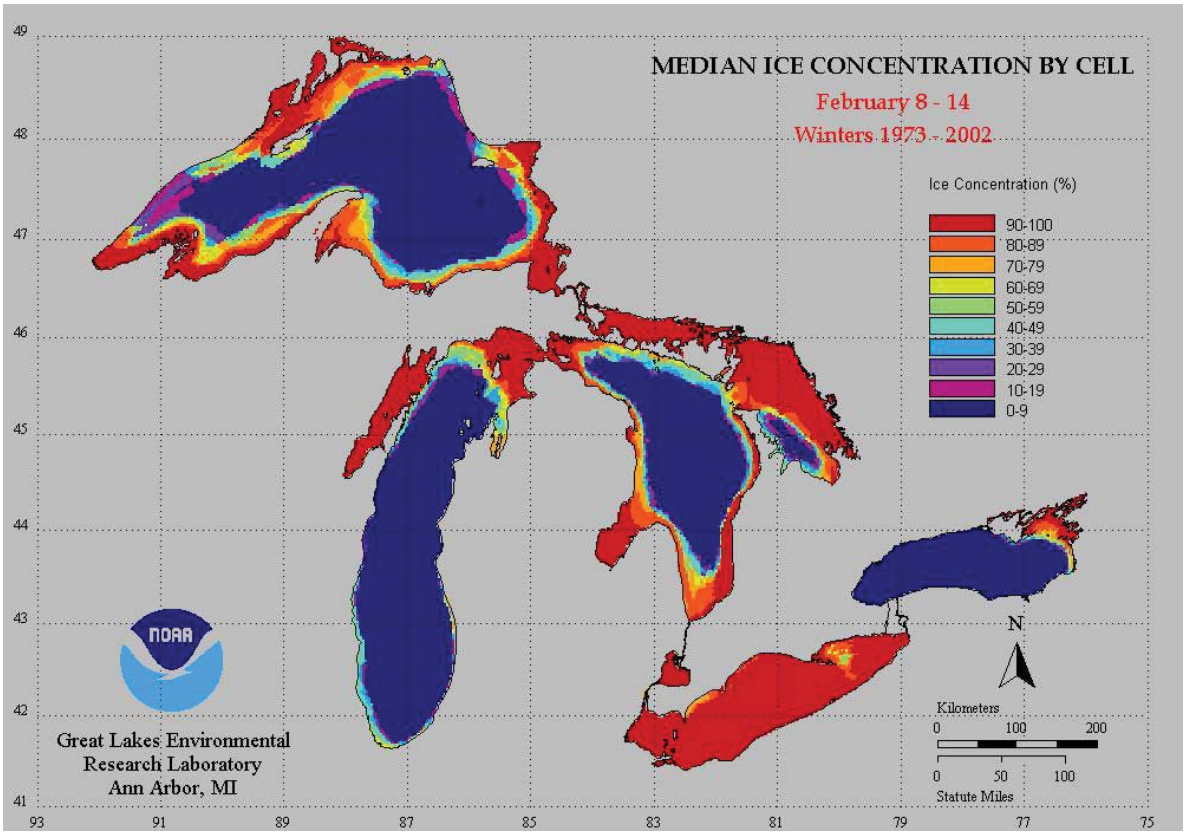

Figure 5.16. Ice coverage over winter in the Great Lakes.

Ice Floe Size

The NOAA data indicates that ice floes can be very large. NASA satellite imagery from Feb 22, 2011 reveals how big ice floes can get. In Figure 5.17, ice floe A is 35 km across, B is 15 km across, and C is 7 km across. If such a large moving chunk of ice hits an offshore structure, the ice chunk isn't going to stop moving. This means the structure of the offshore structure must be able to crush through the ice.

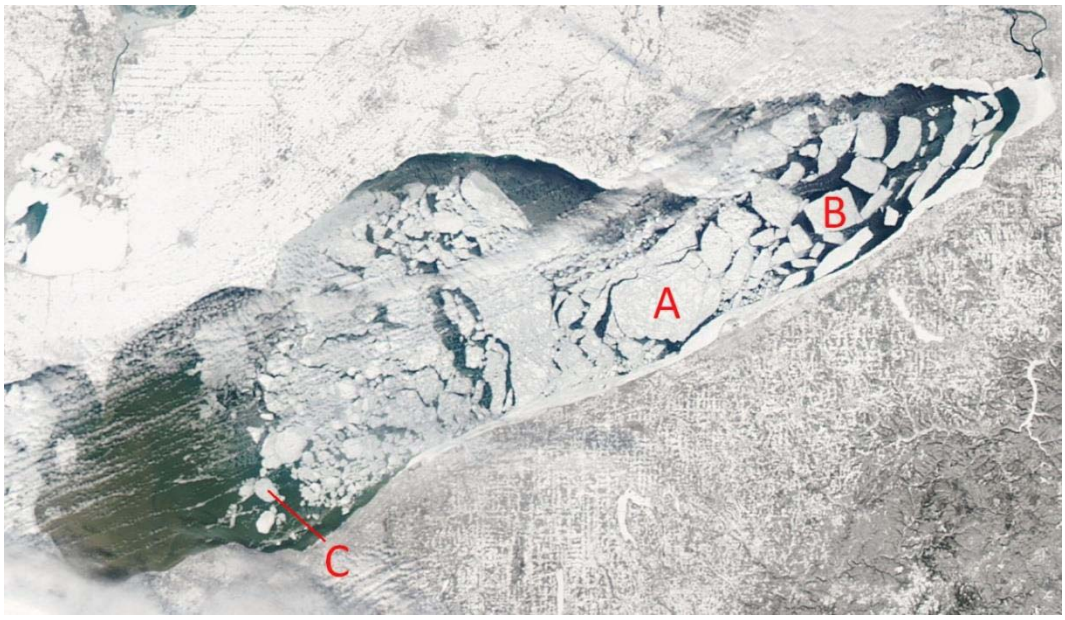

Figure 5.17. Ice floe in Lake Erie 2011 [Marschall et al., 2009].

Ice Ridges

When a flat ice sheet forms, it can buckle and crush together, refreezing into a thicker layer of ice accompanied by a mass of submerged ice rubble under the surface Figure 5.18. This formation is called an Ice Ridge, and the submerged rubble is called an Ice Keel. If an offshore structure encounters an ice ridge, it will be subjected to even greater loads than from a flat ice sheet, making ice ridges a significant concern for offshore structures.

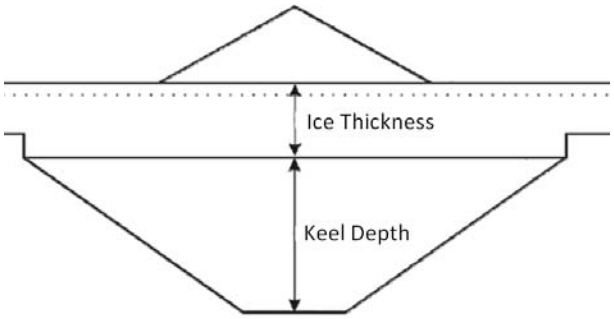

Figure 5.18. Ice ridge.

Ice Thickness

The NOAA ice thickness data for Lake Erie shows that the ice thickness can easily reach the range of 30-70 cm (1 to 2.4 ft). Also ice thicknesses up to120 cm (4 feet) have been observed Figure 5.19.

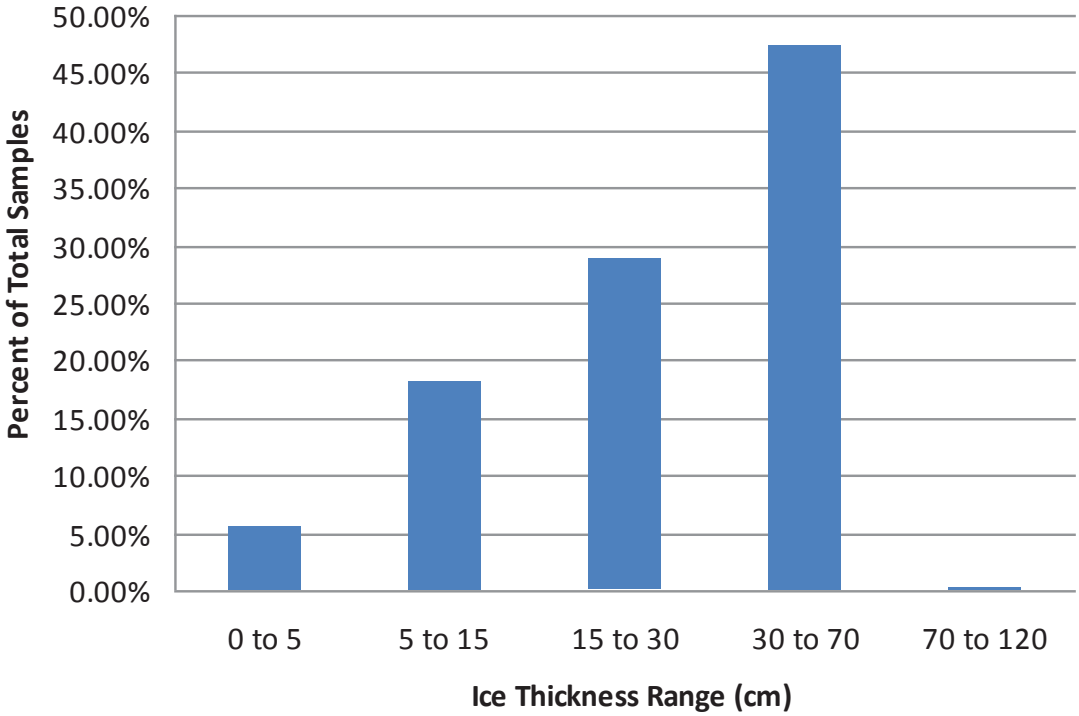

Figure 5.19. Ice thickness over Lake Erie [Wells, 2012].

Several sources have proposed an expression to estimate ice thickness as a function of cumulative freezing degree-days (FDD). The IEC standard 61400-3 [2009] proposes Eq. (5.14),

$$h_{\text{ice}} = 0.032\sqrt{0.9\text{FDD} - 50} \tag{5.14}$$

where, h_{ice} is the ice thickness in meters and FDD denotes accumulated freezing degree-days (in °C). Alternatively, the ice thickness can be estimated using the following equations according to [C-CORE, 2008] and White [2004], respectively.

$$h_{\text{ice}} = 1.308(\text{FDD})^{0.6} \tag{5.15}$$

$$h_{\text{ice}} = 0.8\sqrt{\text{FDD}} \tag{5.16}$$

The ice thickness is expressed in meters in the above three equations. Figure 5.20 compares the estimate of the ice thickness using Eqs. (5.14), (5.15) and (5.16) as a function of cumulative FDDs.

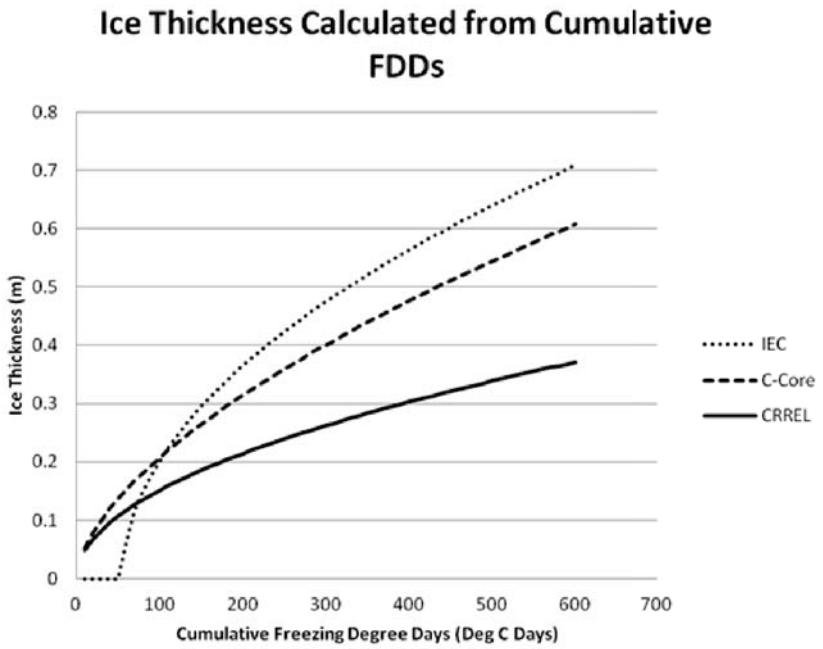

Figure 5.20: Predicted Ice Thicknesses from Cumulative Freezing Degree Days [Wells, 2012].

Figure 5.20. shows that the estimates of the ice thickness using the IEC standard returns the most conservative estimates of ice thickness values for the cumulative FDDs greater than about 100 degree C-days.

The temperature database from the National Data Buoy Center includes sufficient data for two locations from the extreme east and west ends of Lake Erie from 1983-2011. These locations are South Bass Island, Ohio (National Data Buoy Center SBIO1, 2012), and Dunkirk New York (National Data Buoy Center DBLN6, 2012). Other sites in Lake Erie had periods of record too short to be sufficient for statistical analysis. Figure 5.21 demonstrates maximum accumulated FDDs for different years from 1984 to 2011.

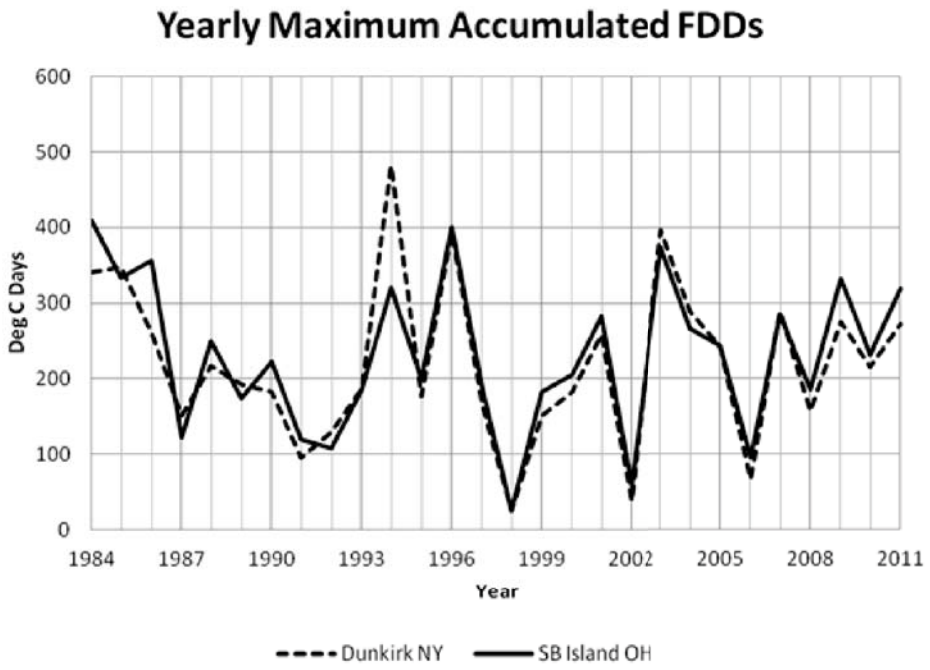

Figure 5.21. Maximum value of cumulative FDDs for winter seasons 1984-2011 for two Lake Erie sites [Wells, 2012].

Figure 5.21 shows that the conditions are quiet similar between these locations; therefore they should be representative of the condition over the entire lake. Using Eq. (5.14), the yearly maximum ice thicknesses as a function of FDD were estimated, as shown in Figure 5.22.

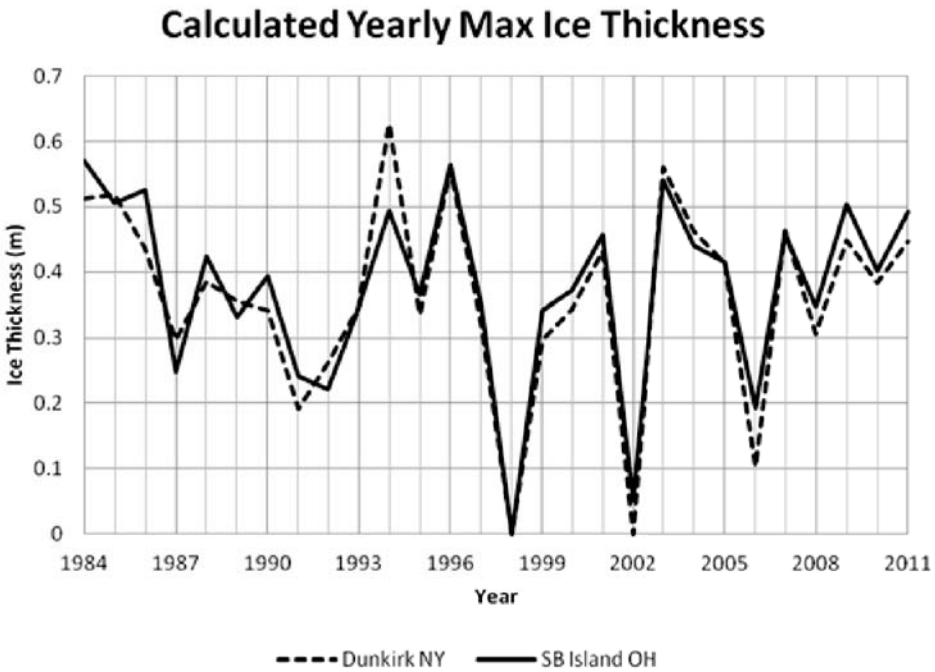

Figure 5.22. Calculated Ice Thickness from FDD data for winter seasons 1984-2011 for two Lake Erie sites [Wells, 2012].

The ice thickness values in Figure 5.22 represent the ice thickness by assuming that no ice ridges form. If the ice were to buckle and form ice ridges, a solid layer would refreeze in the middle of the ice ridges. The thickness of the consolidated layer would be about 1.5 times the level ice thickness [C-CORE, 2008].

50-year Return Period Ice Thickness

One of the IEC ice design load case requirements is estimation of 50-year return period ice thickness. Eq. (5.14) can be used to estimate 50-year return period ice thickness using the statistical data of one year. The 50-year return period thickness can be estimated from FDD data with the same return period. To do this, the Weibull distribution was found to fit well to the FDD data from the Dunkirk NY site, as shown in Figure 5.23. The conditions at this site are more severe than the South Bass Island site and thus a more conservative result is expected to using this site's data. From the Weibull distribution, the 50-year return period FDD is 469.3. Using this value and Eq. (5.14), the 50-year return period ice thickness is estimated 61.8 cm.

The above process was repeated using the Gumbel distribution and produced the 50-year return period FDD value for the Dunkirk site of 502.8 days and the ice thickness of 64 cm. This is consistent with the previously obtained value of 61.8 cm using the Weibull distribution.

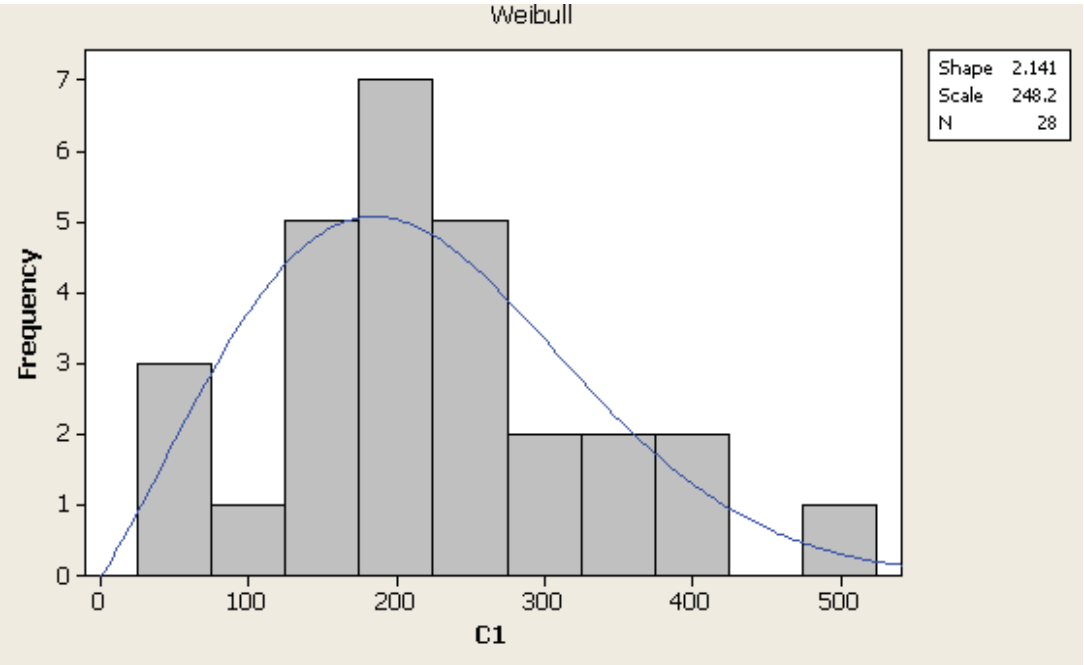

Figure 5.23. Weibull Distribution fit onto Cumulative FDD Data [Wells, 2012].

50-year Return Period Ice Ridge Keel Depth

From the ice scour data from [C-CORE, 2008] and [Lever, 2000], the 50-year return period ice ridge using Eq. (5.17) is 11.2 m.

$$h_{\text{keel}} = 1.954 \ln(T) + 3.501 \tag{5.17}$$

where h_{keel} is the depth of the ice keel in meters, and T is the desired return period in years.

5.3.3 Soil Condition

A thorough study of the soil condition at the exact location of installation is necessary prior to deployment of any offshore wind turbine. However, at the preliminary turbine design phase reviewing any soil data from the vicinity of the wind farm site should be sufficient. Hence, the soil data available from the Burke Airport Feasibility Study [Dames and Moore, 1974] were used.

Figure 5.24 displays the substrates 3-5 miles off Cuyahoga County shore line, inside Cleveland Bay.

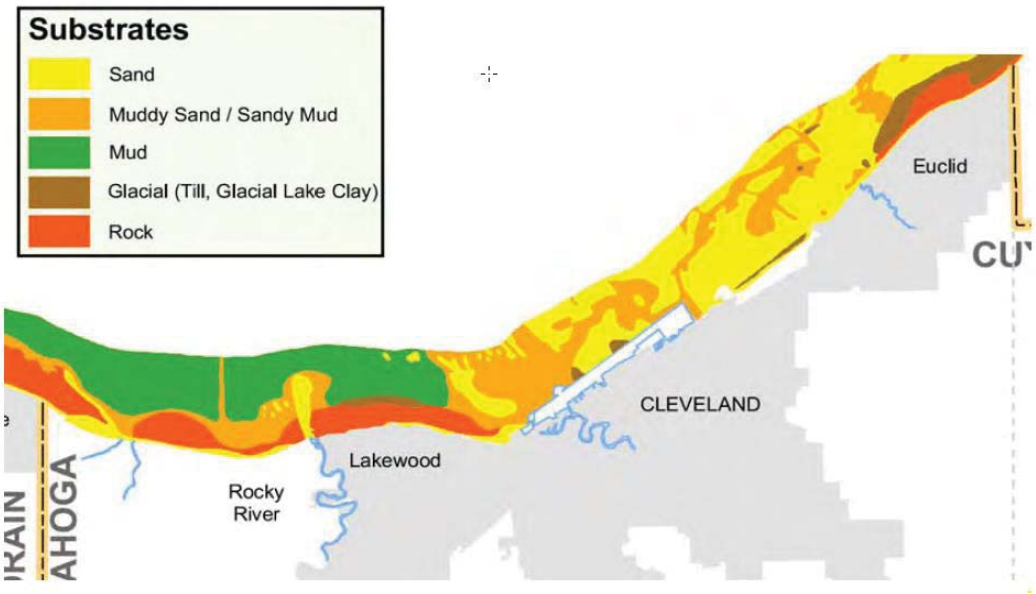

Figure 5.24. Substrates off the coast of Cleveland.

The Burke Airport Feasibility Study [1974] contains soil profiles derived from deep borings. These sections show some regularity in the soil layers as in Figure 5.25. The top layer consists of soft clay which is 5 to 10 m deep. This layer cannot support any foundation. The top layer thickness increases from West to East, but does not change from South to North. The mid- layer consist of stiff silt and very stiff silty clay, which is able to support foundations. The lowest layer is from bed rock, which is very hard and would significantly increase the cost of drilling.

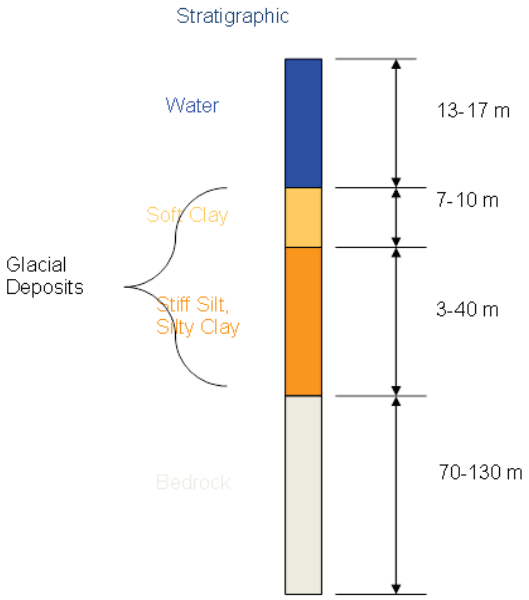

Figure 5.25. Soil condition at the site location.

In the Great Lakes Wind Energy Center Feasibility Study conducted by Marchall et. al., [2009] the soil condition for several sites have been reported. The thickness of soil strata are summarized in Table 5.8.

Table 5.8. Conservative estimation of the thickness of the soil strata available for load bearing at the different locations (extracted from Marchalls et al., 2009).

Site no.	Lake Bed (Desktop study) (ft)	Bedrock horizon (Desktop study) (ft)	Thickness of glacial deposits (ft)	Thickness of soft clay, estimations taken from Airport Feasibility study (ft^3)	Available pile length for load bearing, est. (ft)
1	510	400	110	20	90
2	525	380	145	20	125
3	510	430	80	20	60
4	500	450	50	20	30
5	510	400	110	20	90
6	500	410	90	20	70
6A	480	420	80	20	60
7	510	400	110	20	90
8	490	460	3	20	10

Available length for supporting the foundation would be soft clay thickness subtracted from glacial deposits. This length varies significantly with location based on Table 5.8.

5.4 Definition of IEC Design Load Cases

The offshore turbine loads analysis was based on IEC 61400-3 [2009] standard. Because this is a preliminary design study, a subset of the IEC design load cases (DLCs) is used to determine the loads and assess the safety of the turbine. These DLCs are listed in this section.

Table 5.9. Estimated wind and wave condition parameters.

V_{hub} (m/s)	V_{min} (m/s)	V_{max} (m/s)	H_s (m)	$T_{p\,\text{min}}$ (sec)	$T_{p\,\text{avg}}$ (sec)	$T_{p\,\text{max}}$ (sec)	Count
V_{in} = 3.00	2	4	0.211	1.630	1.865	2.100	32577
5.00	4	6	0.393	2.220	2.540	2.860	33283
7.00	6	8	0.662	2.884	3.300	3.716	23262
9.00	8	10	0.961	3.475	3.976	4.477	12450
$V_{r\,5\text{MW}}$-2 = 9.40	-	-	1.025	3.588	4.105	4.622	-
11.00	10	12	1.280	4.009	4.587	5.165	5310
$V_{r\,5\text{MW}}$ = 11.40	-	-	1.346	4.111	4.704	5.296	-
13.00	12	14	1.608	4.494	5.142	5.790	1916
$V_{r\,5\text{MW}}$+2 = 13.40	-	-	1.676	4.587	5.249	5.910	-
15.00	14	16	1.946	4.944	5.656	6.369	611
17.00	16	18	2.341	5.422	6.203	6.985	149
19.00	18	20	2.620	5.736	6.563	7.389	20
21.00	20	22	2.707	5.831	6.671	7.511	0
23.00	22	24	2.793	5.923	6.777	7.631	0
V_{out} = 25.00	24	26	2.880	6.014	6.881	7.748	0
V_{e1} = 26.38	-	-	H_{s1} = 2.94	6.077	6.953	7.828	-
V_{e50} = 39.36	-	-	H_{s50}= 4.1	7.176	8.210	9.245	-

To simulate wind turbine models under normal operating conditions, the hub height wind speed (V_{hub}) of 3 m/s (the cut-in speed, V_{in}) to 25 m/s (the cut-out speed, V_{out}) with a 2 m/s interval are used. Based on the desired power rating of the turbine, the rated wind speeds are determined. The rated wind speed, V_r, of the 5 MW wind turbines is 11.4 m/s. Wind speed increments of 2 m/s are selected to predict the wind turbine performance. The corresponding significant wave heights for the each wind speed are determined using conditional statistical extrapolation as explained in third approach of Section 5.3.1. The 1-year extreme wind speed V_{e1} = 26.38 m/s and the 1-year extreme significant wave height H_{s1} = 2.94 m estimated with third approach in Section 5.3.1 are used for this research. However, for the 50-year extreme wind speed and significant wave height, the 50-year extreme wind speed and significant wave height estimated in [Marschall et al., 2009] are used. Marschall et al., [2009] estimated that the 50-year wind speed is 38 m/s at 70 m height in the crib area. When this wind speed is converted to the wind speed at 90 m height, it becomes V_{e50} = 39.36 m/s which is largest 50-year extreme wind speed than any other methods dealt in Section 5.3.1. To be conservative, 39.36 m/s 50-year extreme wind speed is selected to be used in this research. Similar to the 50-year wind speed, Marschall et al., [2009] reported that the 50-year significant wave height is H_{s50} = 4.1 m which is higher than any other result values of methods in Section 5.3.1. This conservative value of 4.1 m is selected as the 50-year extreme significant wave height for this research. The maximum, minimum, and average wave periods are found according to Eq. (5.13) for each corresponding significant wave height.

The results for wind speeds, significant wave heights and wave periods used in this research are provided in Table 5.9. For each bin, the count column presents the number of recorded wind speeds contained in that bin among from the data recorded in 26 years.

A selected subset of the IEC design load cases in Table 5.10 is considered in this study. This subset is the same as that is used in reference [Jonkman et al., 2010]. The selected DLCs that are listed in Table 5.10 are based on the study by Jonkman et al., 2010. The IEC 61400-1 [2005] and IEC 61400-3 [2009] standards explain in detail the DLCs and their corresponding nomenclature.

Table 5.10. Selected subset DLCs wind conditions [Jonkman et al., 2010].

DLC	Winds Model	Winds Speed	Waves Model	Waves Height	Direction	Controls / Events	Load Factor
1) Power Production							
1.1	NTM	$V_{in}<V_{hub}<V_{out}$	NSS	$H_s=E[H_s\|V_{hub}]$	β=0°	Normal operation	1.50
1.2	NTM	$V_{in}<V_{hub}<V_{out}$	NSS	$H_s=E[H_s\|V_{hub}]$	β=0°	Normal operation, Fatigue	1.00
1.3	ETM	$V_{in}<V_{hub}<V_{out}$	NSS	$H_s=E[H_s\|V_{hub}]$	β=0°	Normal operation	1.35
1.4	ECD	$V_{hub}=V_r$, V_r±2m/s	NSS	$H_s=E[H_s\|V_{hub}]$	β=0°	Normal operation ±Δwind direction	1.35
1.5	EWS	$V_{in}<V_{hub}<V_{out}$	NSS	$H_s=E[H_s\|V_{hub}]$	β=0°	Normal operation ±Δvertical & horizontal wind shear	1.35
1.6a	NTM	$V_{in}<V_{hub}<V_{out}$	ESS	H_s=1.09×H_{s50}	β=0°	Normal operation	1.35
2) Power Production with Occurrence of Fault							
2.1	NTM	$V_{hub}=V_r$, V_{out}	NSS	$H_s=E[H_s\|V_{hub}]$	β=0°	Pitch runaway → Shutdown	1.35
2.3	EOG	$V_{hub}=V_r$, V_r±2m/s, V_{out}	NSS	$H_s=E[H_s\|V_{hub}]$	β=0°	Loss of load → Shutdown	1.10
6) Parked (Idling)							
6.1a	EWM	V_{hub}=0.95×V_{50}	ESS	H_s=1.09×H_{s50}	β=0°±30°	Yaw = 0°, ±8°	1.35
6.2a	EWM	V_{hub}=0.95×V_{50}	ESS	H_s=1.09×H_{s50}	β=0°±30°	Loss of grid → -180°<Yaw<180°	1.10
6.3a	EWM	V_{hub}=0.95×V_1	ESS	H_s=1.09×H_{s1}	β=0°±30°	Yaw = 0°, ±20°	1.35
7) Parked (Idling) and Fault							
7.1a	EWM	V_{hub}=0.95×V_1	ESS	H_s=1.09×H_{s1}	β=0°±30°	Seized blade: Yaw = 0°, ±8°	1.10

As described in [Jonkman et al., 2010], the DLC1.x series power production under normal operation is selected. The DLC2.x series power production with fault occurrences that will trigger a shutdown of the turbine is also included in the subset. The parked condition DLC6.x series and parked condition with fault occurrences DLC7.x series are considered with 50-year and 1-year extreme winds. Other DLCs such as startup (DLC3.x), normal shutdown (DLC4.x), emergency shutdown (DLC5.x), and transport, assembly maintenance and repair (DLC8.x) are not critical in the concept design stage and therefore are not considered here.

The load factors follow the IEC61400-1 standard. Specially, DLC1.1 uses load factor of 1.25×1.2 that is equal to 1.5. The extra factor of 1.2 is multiplied for the DLC1.1 with rule of thumb because IEC standard requires to use statistical extrapolation of the ultimate loads when the stochastic wind and wave conditions are used for the normal operating condition. The reference [Jonkman et al., 2007] includes details about the load factors for DLCs.

To account for the influence of wave and ice on the turbine loads, it was assumed that only the platform (the topmost part of the gravity base foundation) will experience the wave and ice loads. The rationale for this assumption is that the foundation is much stiffer than the tower and the rotor blades and thus this assumption is reasonable for a preliminary design study. Also, the wave heights are smaller than the height of the foundation. Therefore, the wave and ice loads

affect only the response of the foundation, and the wind loads affect only the wind turbine structure. The turbine loads are then transmitted to the foundation at the turbine-foundation interface. This quasi-static modeling approach allows simplifying the wind turbine-foundation interactions by treating the turbine-tower system as a structure supported by a rigid platform. As a result, the wave load conditions and DLC1.6a in Table 5.10 [Jonkman et al., 2010] are not considered in the wind turbine simulation. As explained in Jonkman et al., [2010], the stated design requirements are considered to be sufficient.

According to the IEC, six replications were performed for DLCs that involve stochastic winds (DLC1.1, 1.2 and 1.3). Different random seeds were used for each replication. Each replication has duration of 10-minute and 30 seconds. However, for DLC2.1 and 2.3, six replications of 2 minutes and 30 seconds were performed because a rotor shutdown procedure is included in these DLCs. The maximum loads occur after about 60 to 70 seconds from the beginning of the simulation, when the shutdown procedure is initiated. The rotor is parked after about 90 to 100 seconds. Thus, the part of the simulation after 150 seconds is omitted for fault conditions.

A single replication is performed for each DLC involving the deterministic wind. DLC1.4 and DLC1.5 are performed for 3 minutes and 30 seconds because the designed wind events occur at the 60th second. For all parking DLCs, simulations are performed for 2 minutes and 30 seconds. The length of this period is adequate because the turbine reaches the steady state conditions before the end of the simulation.

The IEC DLC2.1 includes situations of a control system fault or loss of electrical network. In this project, these situations were considered separately. The control system fault case corresponds to the failure of the pitch control system. This case represents the simulation of a shutdown situation when one of the blades is jammed at a pitch position. The loss of electrical network case is characterized by disabling the generator at a certain time during the simulation of wind turbine operation. The rotor is shutdown when the grid loss happens. DLC2.3 followed the same procedure of grid loss case of DLC2.1 with EOG wind condition. Both the pitch-to-feather brakes and a high-speed-shaft (HSS) brake are used for the shutdown procedures. Tip-brakes were used for the initial steps in the shutdown procedure for the turbine equipped with tip-brakes. The pitch-to-feather brakes are subsequently applied, when the rotor is stopped, to keep the rotor in the parked position.

Parked conditions (DLC6.x and DLC7.x) are implemented by applying pitch-to-feather brakes and a HSS brake. The initial rotor rotational speed is set to zero RPM. The yaw angles are set to various directions to simulate the misaligned cases. One of the blades is seized to zero degree pitch angle while other blades are set to the 90 degree parked position to simulate a situation where one blade seized for the DLC7.1a.

6 Design of 2-bladed Downwind Turbine

This chapter describes in six major sections the different aspects of the design parameters of a 2-bladed downwind turbine. The first Section 6.1 consists of an outline of the design approach for 2-bladed downwind turbine. An overview of rotor design is presented in Section 6.2. In Section 6.3 power control strategies are explained. Section 6.4 contains tower properties. Dynamic characteristics of tower and blade are discussed in Section 6.5. Finally, tower shadow effects are discussed in Section 6.6.

6.1 Design Approach

An overview of the preliminary design methodology of this project is presented in this section. Manwell et al., 2009, described a methodology consisting of eight steps. The steps were described earlier in section 3.1 and are also deliberated here to discuss the design of a 2-bladed downwind turbine, as outlined in Figure 6.1.

The NREL 5MW 3-bladed turbine was selected as a baseline design reference turbine. The rated power requirement is selected to be 5MW to match the power of the baseline turbine. A downwind rotor arrangement with two blades was selected. Similar to the reference turbine, a pitch controlled method was selected as the power control method. The blade geometry uses the series of airfoil profiles as the reference NREL turbine. Design tools developed by NREL were used to analyze the loads on the blade and to select the blade chord, thickness-to-chord ratio and twist distribution to optimize the concept blade design. The structural properties and the 3-bladed reference turbine blade lay-up were adopted for the 2-bladed concept turbine to allow a close comparison with the NREL 5 MW turbine. The blade internal structure was modeled based on the mass and stiffness distributions determined using NREL design tools (such as PreComp). The natural frequencies of the new blade were investigated using BModes for resonance. A teeter mechanism was considered for the concept 2-bladed turbine.

The IEC standards were used as guidance to select significant design load cases. For fatigue loads, normal operating conditions between cut-in and cut-out was selected. Loads at different location of major components of the turbine were analyzed using NREL tools. Blade deflections, tip to tower clearance, teeter limits and tower interference for critical design load cases were verified. Fatigue damage life is estimated using MLife code developed by NREL. A parametric study was conducted to select cone and tilt angle for optimum power production and enhanced fatigue life. Finally, a cost model is developed to minimize the cost of energy.

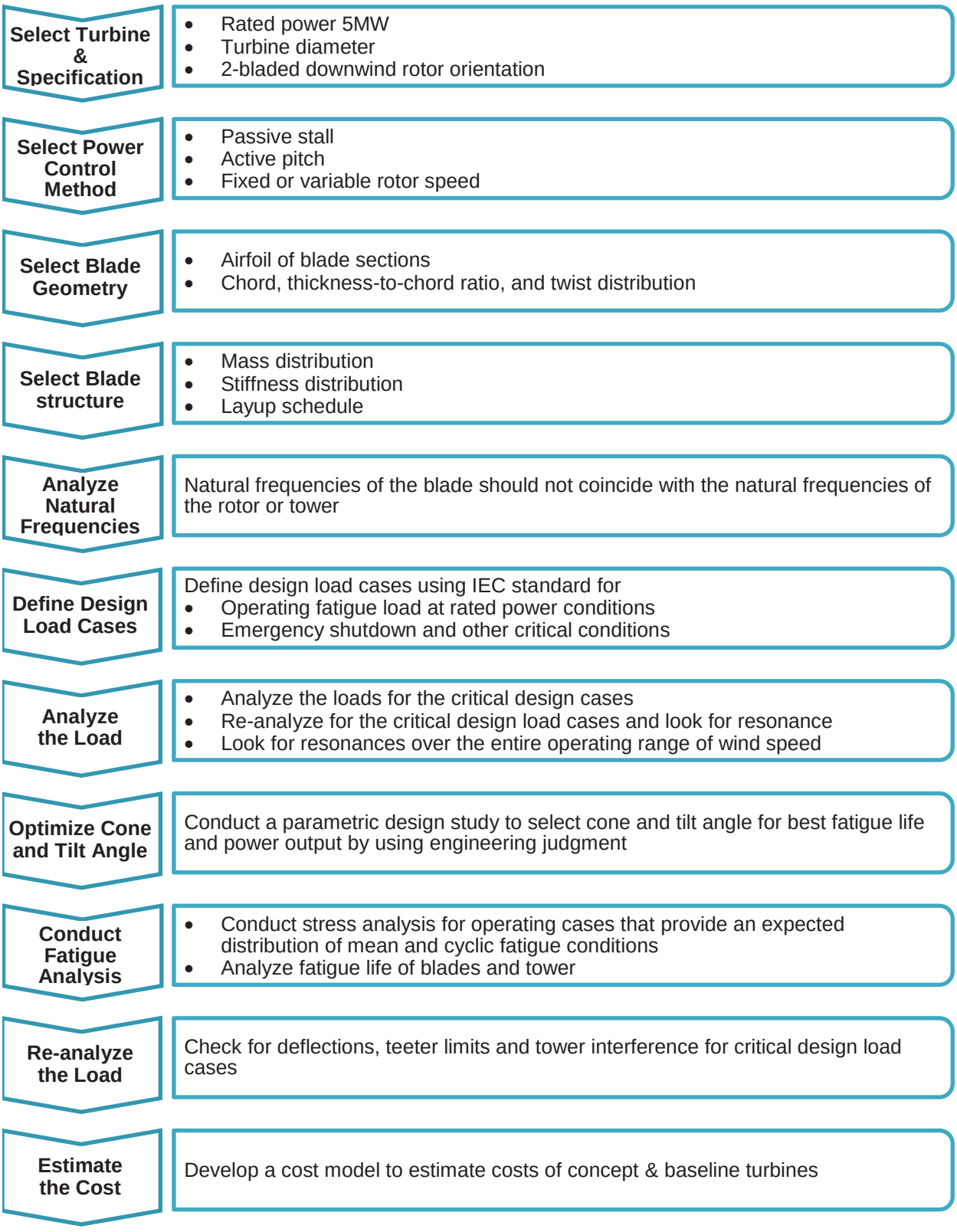

Figure 6.1. Flowchart for 2-bladed turbine design methodology.

6.2 Rotor Design

Removing one blade from the rotor is a simple concept. Realizing this simple concept is complicated. The work discussed here describes the designs changes made to transform the NREL 5MW 3-bladed rotor into a 2-bladed rotor. The blade twist angles were changed to accommodate a higher rotor rpm. The shaft tilt and blade cone angles were changed to take advantage of a downwind configuration. A teeter angle was added to alleviate blade loads. These changes are discussed further in this section.

6.2.1 Blade Aerodynamic Design

This analysis uses the NREL 5MW blade as a baseline blade for a 2-bladed rotor. The baseline was designed for a 3-bladed rotor. Airfoils, location of airfoil along the blade, and material properties were chosen for a three bladed rotor. This analysis adopts this design only to allow the use of the structural properties of NREL 5 MW turbine [Jonkman, et al., 2009] and thus enable a close comparative study of the 2-bladed turbine system with the reference NREL 5 MW system. Small changes to the chord and twist angles of the baseline blade were made only to construct the so-called 'optimized' blade in this report to better suit a 2-bladed rotor. It is noted that this blade geometry selection should not be regarded as an optimum design for the 2-bladed rotor and that ideal chord and twist distributions are only starting points for a larger design process that must incorporate the limitations of manufacturing and structural dynamics. For simplicity, engineering judgment was used to select the final twist distribution for the 'optimized' blade. The design steps described here therefore outline two designs: The University of Toledo (2BUT), and is the so-called optimized blade (2BOPT). The 2BOPT is used only in the Cost Analysis portion of this report to highlight the potential additional cost savings of the 2-bladed turbine concept.

Design Steps

The selection of values for the 2-bladed design were guided by optimum rotor theory, assuming Betz limit (axial induction=1/3) without wake effects. The following are the design steps used for the blades featured in this report.

- Used WT Perf [Buhl, 2004] to find the best Tip Speed Ratio (TSR) using the NREL baseline blade
- Once the TSR was found, the optimum rotor theory was used to find ideal chord length and twist angles
- Because the material properties would change if the chord length was changed, it was decided to keep the same chord length.
- It was assumed, due to manufacturing cost constraints, that the twist angles calculated by the ideal equations should not be used. A compromise was made to follow the twist angle slope of the NREL blade. This design is called the University of Toledo design or 2BUT. Note that the 2BUT design is not a blade designed optimally for a 2-bladed rotor.
- To obtain a more realistic optimal blade for a 2-balde rotor, a rule thumb was used, which considers that the performance difference between a 3 and 2-bladed rotor should be around 1-2%. Using the values from the ideal blade calculated earlier, the best TSR and performance was found at 9.5 TSR and 0.4792 Cp. This blade is called the Optimum Blade or 2BOPT.

Table 6.1. TSR and Cp of various wind turbine configurations.

	Tip-Speed Ratio	Coefficient of Power
NREL 3B original	7.5	0.4868
NREL 2B original	9.0	0.4670
NREL 2BUT	9.2	0.4728
NREL 2BOPT	9.5	0.4792

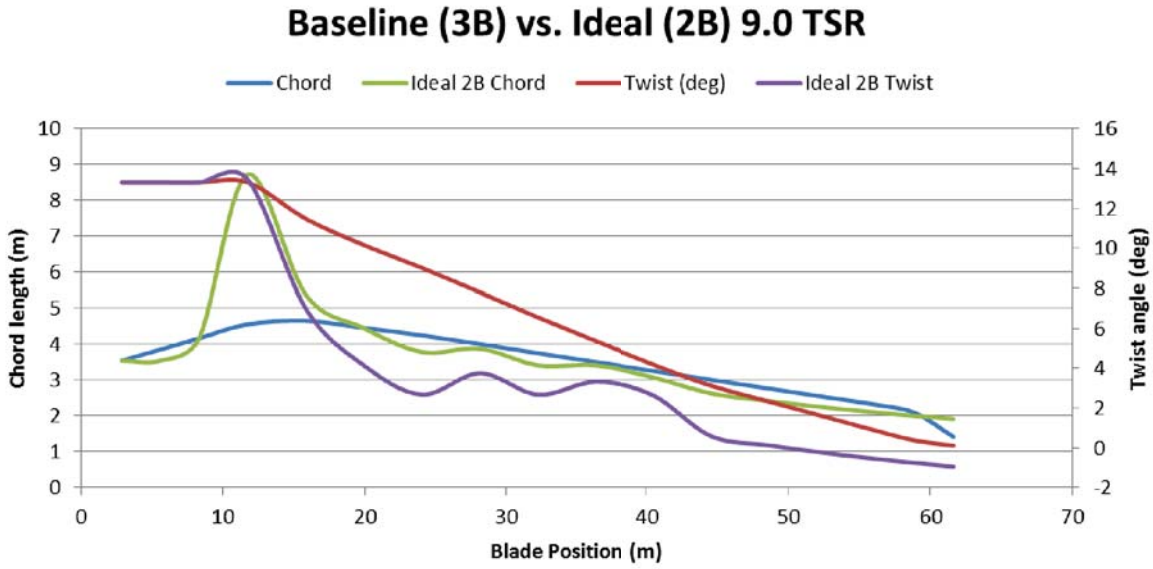

Figure 6.2. Chord length and twist distribution of baseline and 2BOPT blades.

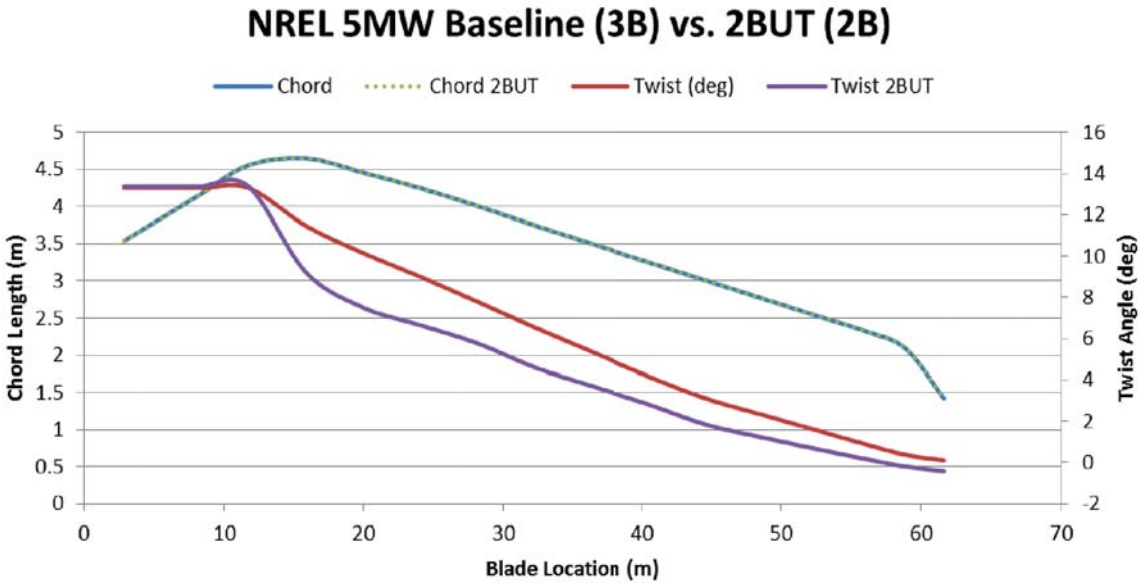

Figure 6.3. Chord length and twist distribution of baseline and 2BUT blades.

6.2.2 Blade Structural Design

The baseline blade design is developed using NREL 5MW wind turbine blade. Thus, the first step in the turbine blade design approach begins with a complete specification of the NREL 5 MW reference blade. This specification includes chord, twist, pitch axis, and airfoil profiles along the blade span. As stated earlier, the blade structural properties of the NREL 5MW reference offshore wind turbine model [Jonkman, et al., 2009] were selected for this research.

The released NREL 5MW reference offshore wind turbine model [Jonkman, et al., 2009] does not include detailed geometry information. This information, was obtained from [Lindenburg, 2002], [Kooijman, et al., 2003], and [Griffith, et al., 2011]. According to [Jonkman et al., 2009] the LMH64-5 blade of the DOWEC study [Lindenburg, 2002] is used to design the NREL 5MW reference wind turbine blade. The 1.1 m long end part of LMH64-5 blade is chopped to fit to the designed 63 m radius of the NREL 5MW reference wind turbine.

[Jonkman, et al., 2009] provides the chord lengths along the blade at 17 locations. In addition, 26 chord lengths at different locations are found from LMH64-5 blade paper [Lindenburg, 2002]. The last chord length at the tip side presented in [Lindenburg, 2002] was excluded because this chord is located beyond the NREL 5MW reference blade length. The chord length information from both sources was combined to determine a total of 42 chord lengths along the blade span.

The twist angles of the NREL 5MW reference blade are slightly different from the LMH64-5 blade. Thus, the twist angles only from the NREL 5MW reference blade were used.

Both [Jonkman et al., 2009] and the LMH64-5 blade [Lindenburg, 2002] did not include airfoil shape information; only the airfoil characteristics are provided in the references. However, the airfoil characteristics input file names used in both papers provide a hint to find the original airfoil shapes. The DOWEC 6 MW pre-design paper [Kooijman et al., 2003] has a table that links the airfoil characteristic input file names and airfoil shape names. Using the airfoil names, the normalized airfoil shape was found from the SNL100-00 blade paper [Griffith et al., 2011]. The SNL100-00 100m blade is made by scaling up the NREL 5MW reference blade. Thus, the airfoil shape, thickness-to-chord ratio, and pitch axis fractions of the SNL100-00 paper [Griffith et al., 2011] were used to define the geometry of NREL 5MW reference blade. Coordinates of the airfoil shapes are extracted from the graphical data provided in the SNL100-00 blade paper [Griffith et al., 2011]. The PreComp [Bir, 2005] airfoil input files were then generated using the airfoil coordinate information.

Using the collected data, the chord distribution of the NREL 5MW reference blade is shown in Figure 6.4 aligned along the pitch axis. The thickness-to-chord ratio distribution is plotted in Figure 6.5. The normalized airfoils are depicted in Figure 6.6 and Figure 6.7 using the airfoil coordinates extracted from SLN100-00 paper [Griffith et al., 2011]. The evolution of the shapes of the cross-sections from the circular airfoil to DU-99-W-405 airfoil is depicted in Figure 6.6. The assembled NREL 5MW reference blade geometry information is listed in Appendix 3.

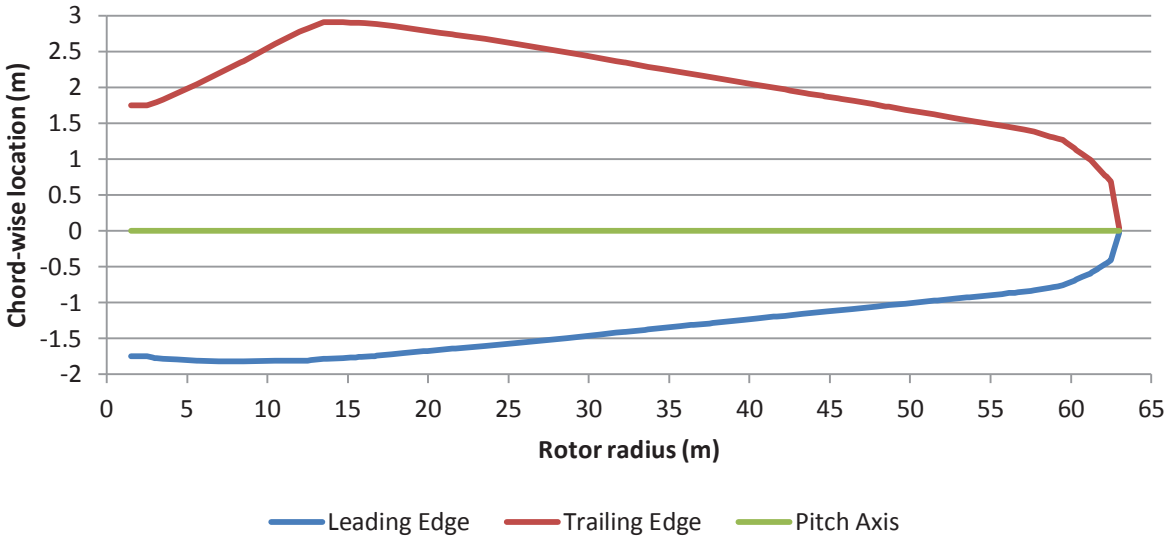

Figure 6.4. NREL 5MW reference blade chord distribution along pitch axis.

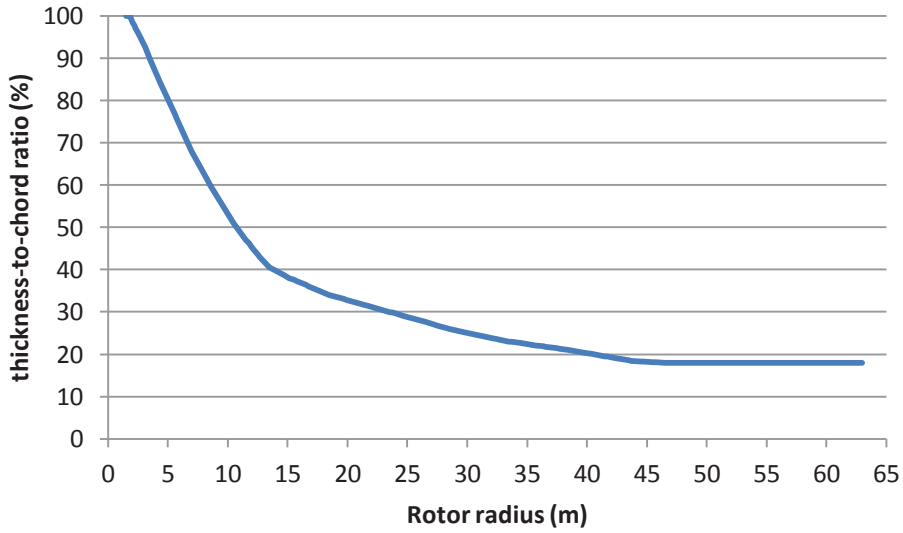

Figure 6.5. Thickness-to-chord ratio distribution of NREL 5MW reference blade.

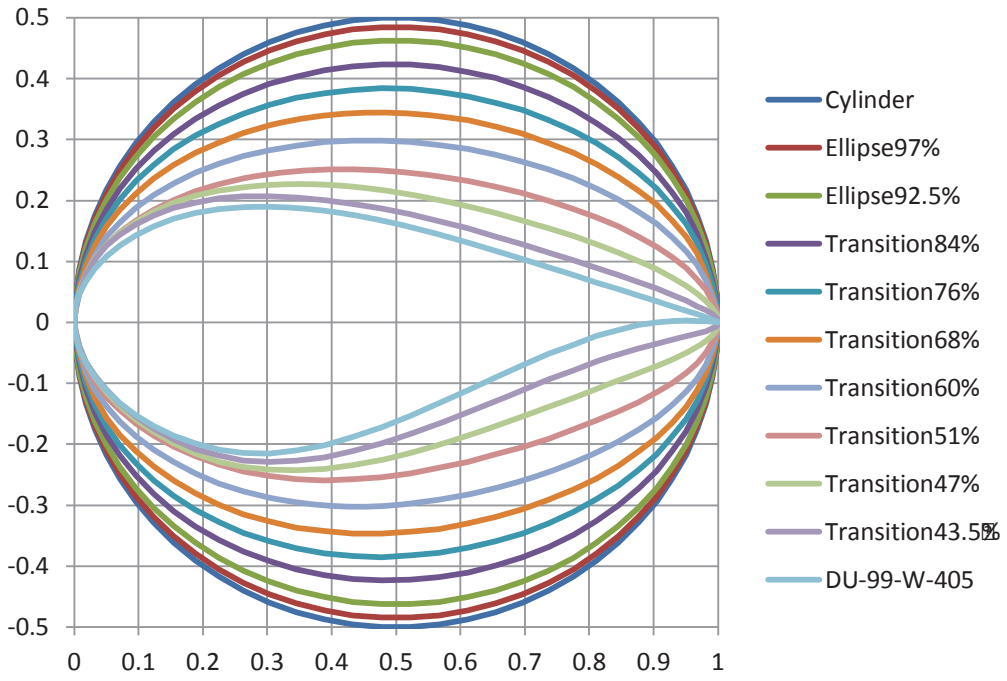

Figure 6.6. Normalized airfoil coordinates of NREL 5MW reference blade near root.
The "Transition" indicates the cross-sectional shape transitioning from an ellipse to DU-99-W-405 airfoil and the percentages are the percent thickness relative to cylindrical cross-section.

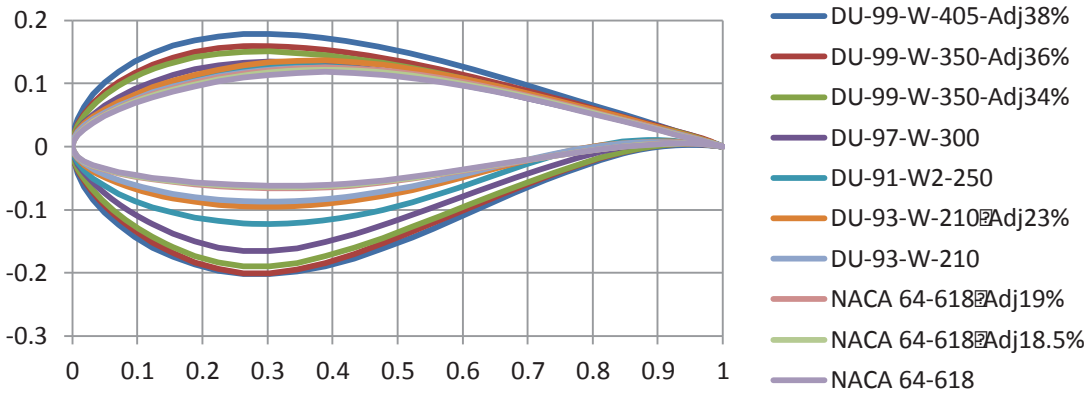

Figure 6.7. Normalized airfoil coordinates of NREL 5MW reference blade.

In addition to the baseline design, three other blade models were developed. One is the baseline blade with a tip-brake, and the other two models were constructed by optimizing the twist angle on the baseline blade for the 2-bladed machines, one with and the other without a tip-brake. The latter blade, the NREL 5 MW blade design with twist angles selected for a 2-bladed rotor configuration, is referred to as "BUT" in this report. Information about the twist distribution of BUT blade is described in section 6.2.1.

A tip-brake attached at the tip of each blade, with mass 77.8 kg, is considered based on the information in [Griffin, 1997]. The tip-brake is scaled up cubically for a 63 m radius rotor from a 6.4 kg tip-brake of a 27.4 m radius rotor. The 20 m^2 TBDrConD parameter of FAST primary input file, which is the product of area and drag coefficient (C_d), can effectively stop the rotor. The TBDrConD parameter is found from trial-error experiments. Here, it is assumed that tip-brakes are fully deployed in 1 second. In the FAST simulation, when the tip-brakes are deployed, they are modeled as forces that resist the rotation of the rotor at tip of the blades.

Using the above blade constructions, the blade mode shapes were found for the three new blade models. Modes 1 and 2 in flap-wise direction and mode 1 in edge-wise direction were calculated using the code BModes [Bir, 2005]. Using these data, the FAST blade input files were generated for the three additional blade designs.

6.2.3 Shaft Tilt and Cone Angles

In this section, the methodology to select proper tilt and cone angles to achieve the desired safety for a 2-bladed, downwind rotor configuration is presented in Figure 6.8.

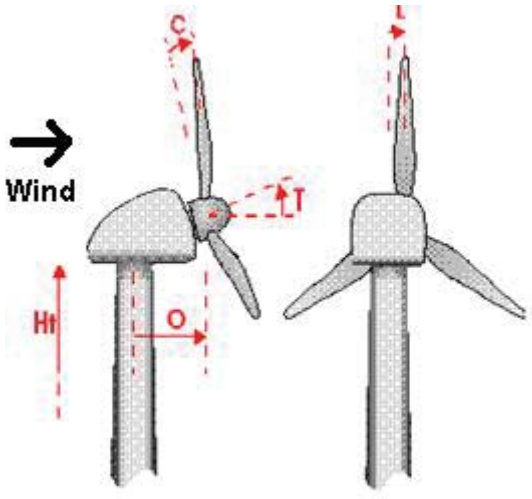

Figure 6.8. Illustration of tilt and cone angles (courtesy of GH Bladed).

The primary purpose of having tilt angles in upwind machines is to increase the clearance and reduce the risk of collision between the tower and the blades, but this is accomplished at the expense of reducing fatigue life, as it will be shown in Chapter 9 that a positive tilt angle can increase the fatigue damage inflicted on the blades. Moreover, in downwind machines tilt angle can introduce an extra yaw moment that is not desirable especially for free yaw machines. Therefore, whether or not a free yaw is used, small tilt angles should be used so long as they do not increase the risk of the tower and the blades collision.

Cone angles also reduce the risk of collision between the tower and the blades. As it will be shown in Chapter 9, although cone angles can decrease the mean stress of the cyclic loads at the blade root, they can result in power loss because the rotor swept area decreases with cone angle.

Based on simulation results, presented in Chapter 9, the risk of collision between the tower and the blades is highest under fault conditions. There are several fault conditions defined in the IEC 61400-1 standard. DLC 2.1 concerns with the occurrence of fault relating to control function or loss of electrical network connection when the wind turbine is operating normally. To model fault in the control mechanism, a scenario is considered in which pitch control in one blade fails and the system immediately triggers emergency shutdown. In another scenario, a case is considered in which the network is lost and the system immediately shuts down.

In DLC 2.2, rare events including faults relating to the protection functions or internal electrical systems should be considered as abnormal conditions. In DLC 2.3, Extreme Operating Gust (EOG) is combined with the loss of grid connection, and is considered as an abnormal event. In this case, the timing of these two events should be chosen to achieve the worst case loading. To model this case a Monte Carlo simulation with different timing was performed to find the worst timing condition.

Simulation studies conducted in this study show that the critical load case with highest likelihood of the blades hitting the tower occurs under DLC 2.1. In this fault condition, the power network is lost when the turbine is operating normally. The total probability of the blades hitting the tower under this fault condition would equal the probability of hitting the tower when the network is lost multiplied by the probability of losing the grid. This probability is calculated as follows,

$$P(C) = P(Grid_{Loss})P(C|Grid_{Loss}) \tag{6.1}$$

The designer's objective is to reduce the total probability represented on the left hand side of Eq. (6.1). A pair of large tilt and cone angles would decrease the second term on the right hand side and reduce the likelihood of this catastrophic failure. However, this is achieved at the expense of reduction in annual power production, because large tilt and cone angles would decrease the rotor swept area.

The value of the first term on the right hand side of Eq. (6.1) would depend on the quality of the grid connected to the wind turbine. This can vary throughout the country from one state to another state or even from one city to another city. To estimate the probability of the second term in Eq. (6.1) for a given tilt and cone angle a Monte Carlo simulation can be used. In this simulation, the combination of different wind speeds with different timing for the fault occurrence was considered.

As it will be shown in Chapter 9, the set of tilt and cone angles similar to the 3-bladed upwind turbine would be a conservative choice for the 2-bladed downwind configuration. Note that the total probability of failure was estimated by the product of the probability from Monte Carlo simulation with the probability of occurrence of losing the grid, which might be very low as well.

Using additional braking systems, such as tip brakes or generator brakes, can effectively reduce the probability of catastrophic failures, such as those described above. As shown in Chapter 9, a tilt angle equal to 2 degrees and cone equal to 0 degrees along with tip brake and teeter mechanism would be a good choice for the proposed concept design. However, a thorough

optimization analysis with considering all design factors, including alternative emergency shutdown strategies, should be performed in order to find optimum tilt and cone angles to maximize the annual power without sacrificing safety.

6.2.4 Teeter Mechanism Properties

The out-of-plane bending moments are transmitted to the LSS if the rotor is rigidly connected to the shaft. For 2-bladed rotors, the teeter mechanism as shown in Figure 6.9, can effectively mitigate the loads that are applied to the blades as well as to the LSS. Free teetering is permitted until the spring and damper make contact with the hub.

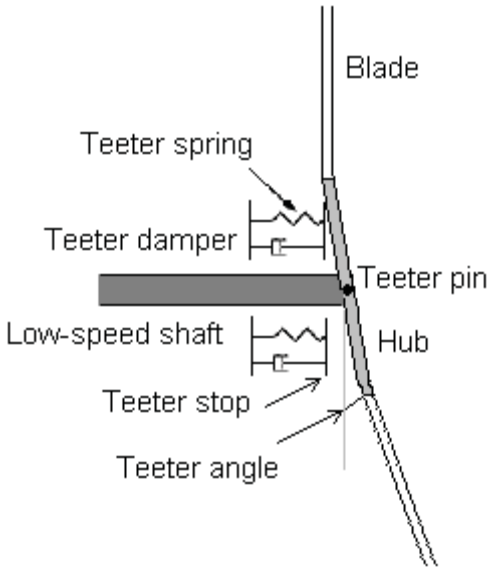

Figure 6.9. Schematic of a teetered rotor.

A standard model of a teeter restraint consists of a linear spring and a damper. The following parameters should be specified in order to model a linear teeter model using FAST.

- TeetMod: Enable teeter mechanism at value 1 and disable it at value 0
- TeetDmpP: Rotor-teeter damper position (degrees)
- TeetDmp: Rotor-teeter damping constant (N-m/(rad/s))
- TeetCDmp: Coulomb-friction damping moment resists teeter motion (N-m)
- TeetSStP: Rotor-teeter soft-stop position (degrees)
- TeetHStP: Rotor-teeter hard-stop position (degrees)
- TeetSSSp: Rotor-teeter soft-stop linear-spring constant (N-m/rad)
- TeetHSSp: Rotor-teeter hard-stop linear-spring constant (N-m/rad)

The spring rate in the teeter mechanism should be stiff enough to hold the rotor in its position under different loading conditions, including fault and park conditions, and soft enough to allow the rotor move in order to mitigate the loads on the blades and the LSS. The damping ratio should also be adjusted so that it dissipates the teetering motion appropriately.

Finding an appropriate damping ratio to model large scale structures is a complicated task. Parametric studies by considering different damping ratios and coefficients were conducted to study the effect of the teeter mechanism parameters in reducing the loads on the rotor and the blades.

Table 6.2. Different teeter parameters with constant stiffness.

Case	Rotor-teeter damping constant (N-m/(rad/s))	Rotor-teeter hard-stop linear-spring constant (N-m/rad)
1	7.50E+06	1.92E+08
2	1.29E+07	1.92E+08
3	2.00E+07	1.92E+08
4	3.00E+07	1.92E+08
5	5.00E+07	1.92E+08

Figure 6.10 demonstrates the free vibration of the rotor with an initial teeter equal to 3 degrees for different cases, as shown in Table 6.2. In this simulation all degrees of freedom other than the one related the teeter mechanism were disabled. Therefore, the energy dissipates only due to the damping in the teeter mechanism. In this situation the system behavior is represented by an 1-DOF system as shown in Figure 6.9 .

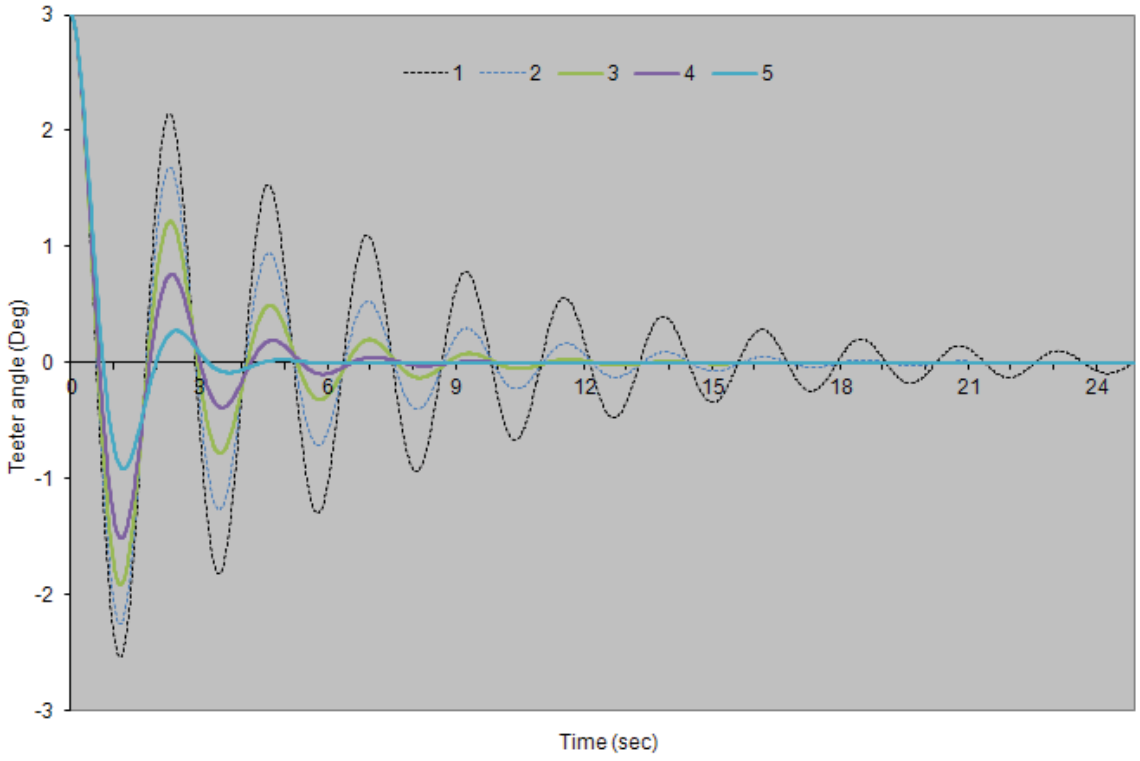

Figure 6.10. Free vibration of 2–bladed rotor with only teeter DOF enabled for different cases as shown in Table 6.2.

Using the value of the peaks in Figure 6.9 the damping ratios for cases in Table 6.2 are determines as summarized in Table 6.3.

Table 6.3. Damping ratios corresponding to Table 6.2.

Case	Damping ratio
1	0.06
2	0.10
3	0.15
4	0.23
5	0.38

If all degrees of freedom were enabled, the energy would dissipate not only due to the damping in the teeter mechanism, but also due to the structural damping in the blades, the tower and other structural components. The system response due to initial 3 degree teeter is shown in Figure 6.11.

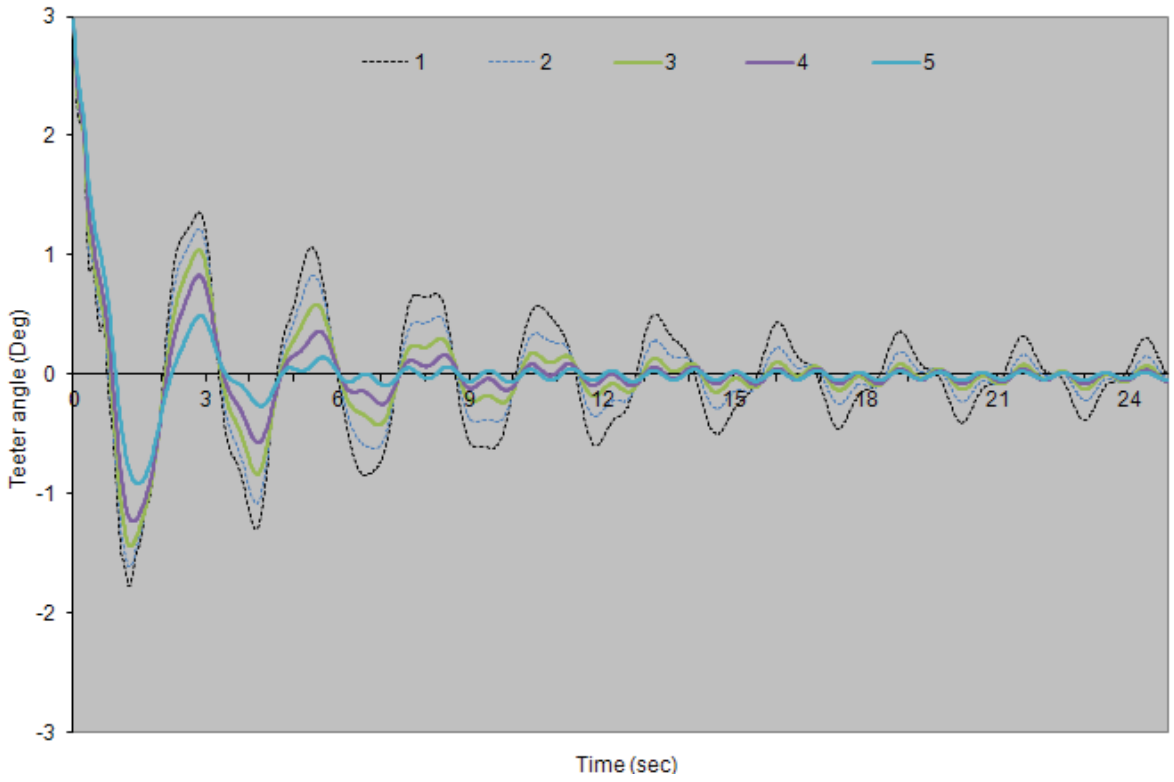

Figure 6.11. Free vibration of 2–bladed rotor with all DOFs enabled for different cases as shown in Table 6.2.

Note that since all cases considered in Table 6.2 have the same stiffness, all signals demonstared in Figure 6.10 and Figure 6.11 show the same period.

To study the teeter system, additional cases were considered by altering the spring rate as shown in Table 6.4 .

Table 6.4. Different teeter parameters with constant damping.

Case	Rotor-teeter damping constant (N-m/(rad/s))	Rotor-teeter hard-stop linear-spring constant (N-m/rad)
6	1.29E+07	9.00E+07
7	1.29E+07	1.40E+08
8	1.29E+07	1.92E+08
9	1.29E+07	2.50E+08
10	1.29E+07	3.00E+08

The counterpart of Figure 6.10 for teeter parameters given in Table 6.2 is shown in Figure 6.12 .

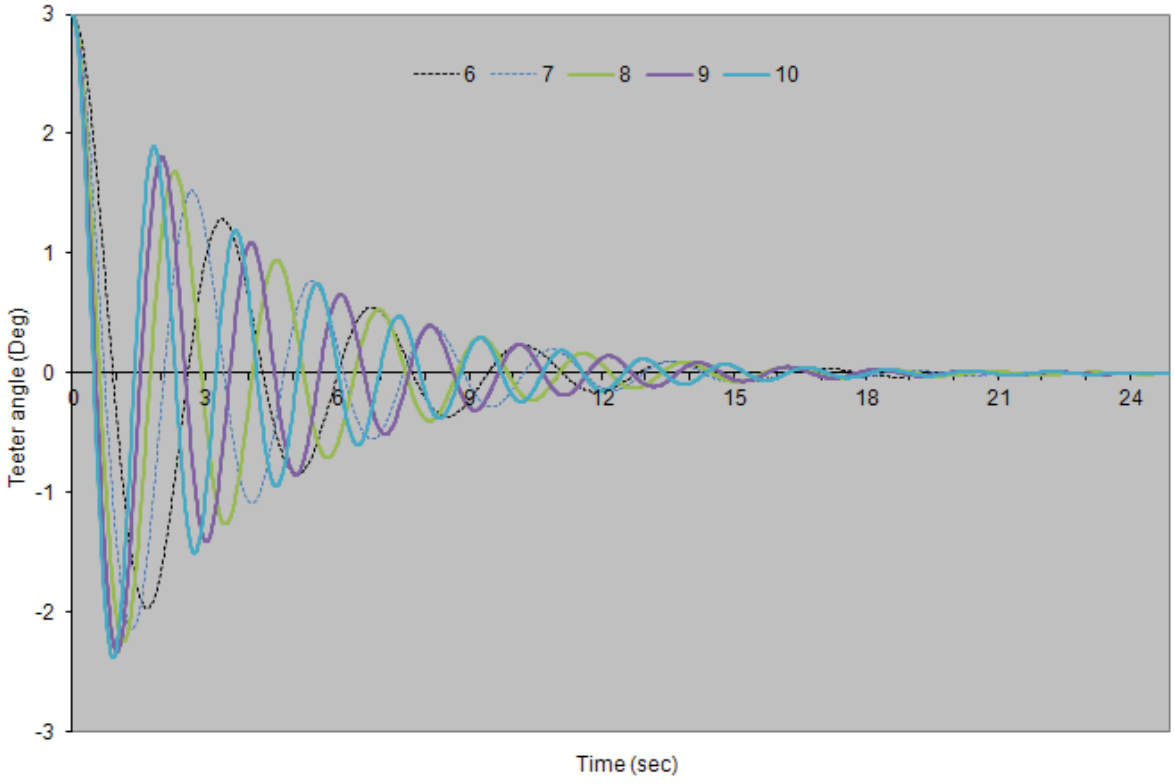

Figure 6.12. Free vibration of 2–bladed rotor with only teeter DOF enabled for different cases as shown in Table 6.4.

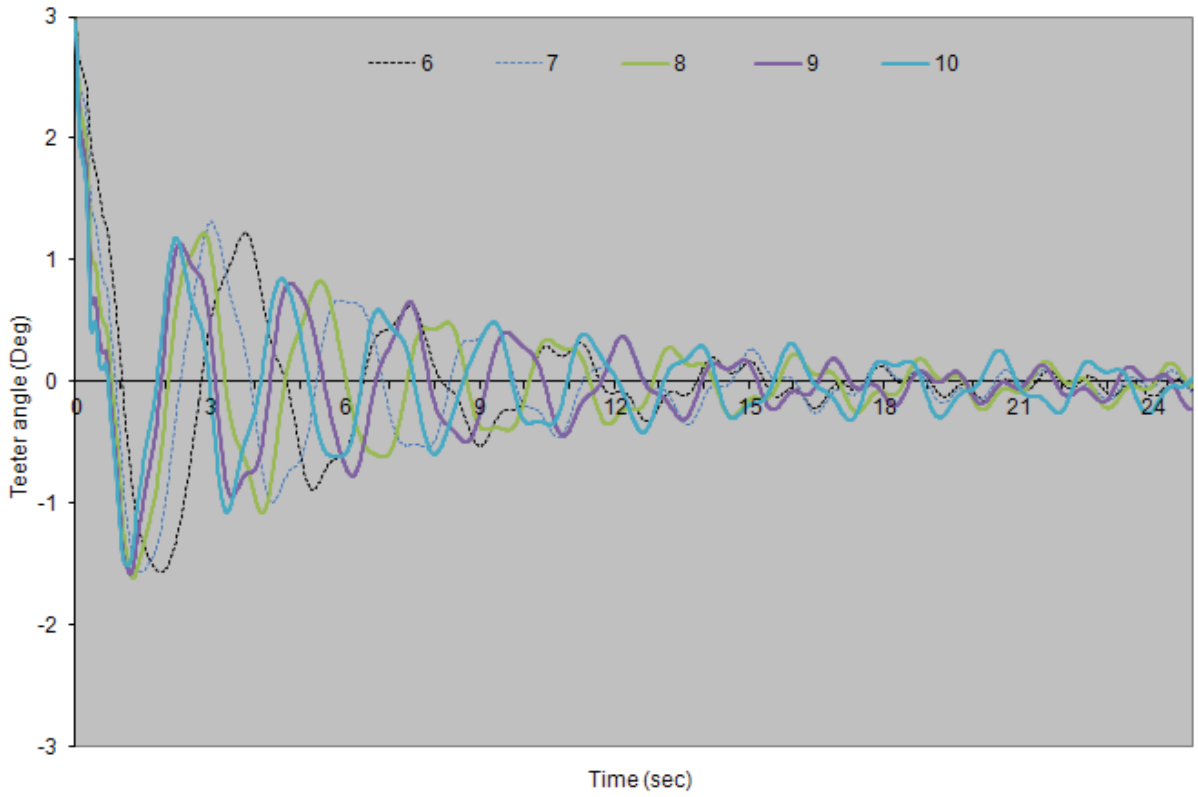

Figure 6.13. Free vibration of 2–bladed rotor with all DOFs enabled for different cases as shown in Table 6.4.

The damping ratios for cases in Table 6.4 are presented in Table 6.5.

Table 6.5. Damping ratio corresponding to Table 6.4.

Case	Damping ratio
6	0.08
7	0.08
8	0.10
9	0.11
10	0.14

The stiffness and damping coefficients of the teeter mechanism for the 2-bladed downwind machine were selected as 1.92E+05 kN-m/rad and 1.29E+04 kN-m/(rad/s), respectively. These values were arrived at by constraining the maximum teeter angle under normal conditions at approximately ±3 degrees. For other conditions, including fault conditions, the teeter angle was constrained to vary between ±6 degrees. It is assumed that the teeter stops are engaged from 0°, and the same stiffness applies for both the soft and the hard stops.

Figure 6.14 compares the out-of-plane bending moment at the root of the blade when the teeter mechanism is enabled and disabled. It can be seen that the teeter mechanism with the above setting effectively reduces the bending moment, especially close to the peaks. In Chapter 9, the

performance of the teeter mechanism in mitigating the loads applied to the blades are studied in detail.

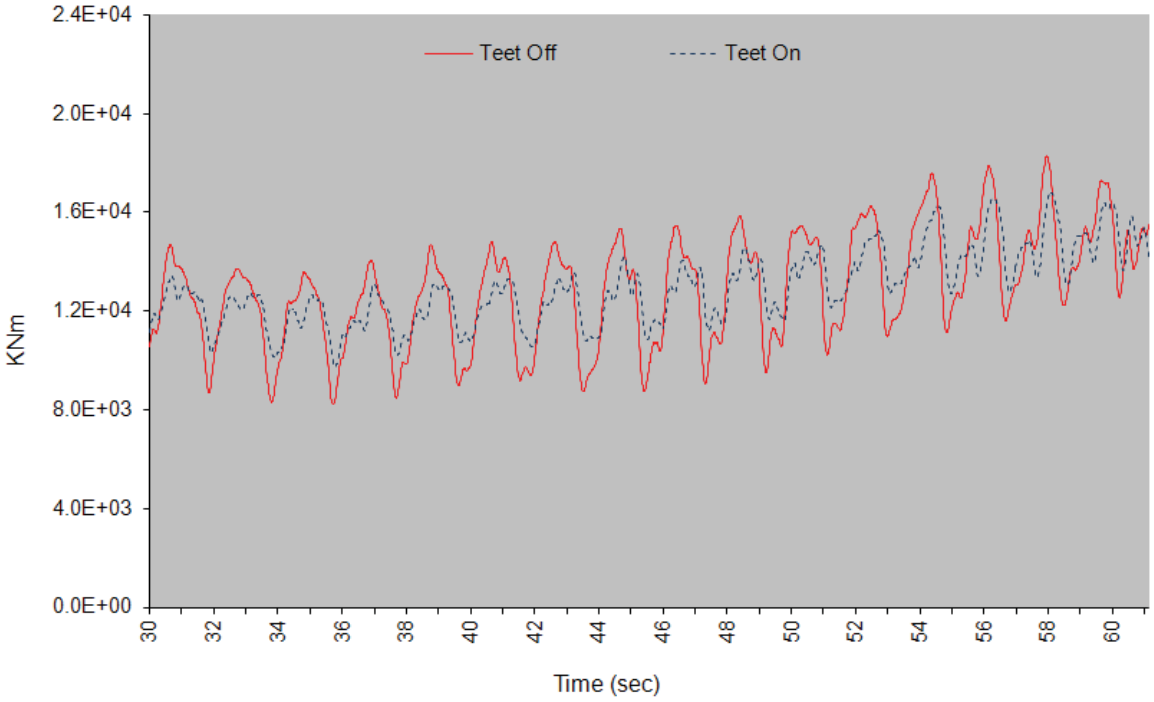

Figure 6.14. Out-of-plane bending moment at the root of the blade with teeter on/off.

Figure 6.15 demonstrates the hub height wind speed that was used to perform the above simulation.

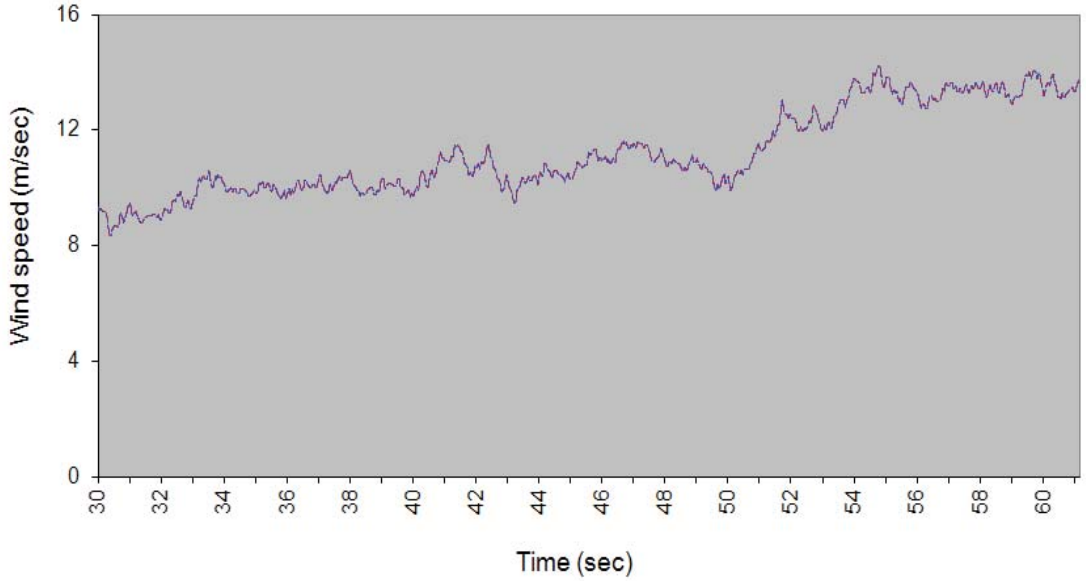

Figure 6.15. Hub-height wind speed.

The teeter parameters were selected so that the natural frequency of the teeter mechanism is far from the natural frequencies of excitation in order to avoid any resonance and cause catastrophic failure. However, finding optimum teeter parameters requires a thorough optimization analysis, considering all constraints and parameters. A more realistic model should include independent stiffness and damping rate for the soft and hard stops.

A series of teeter parameters was considered for a parametric study of teeter mechanism. These 7 different teeter parameter sets (teeter sets in short) were defined to compare the responses of load effects, tower-to-blade clearance, AEP, and teeter angles for each set. The teeter parameters of each set are defined in Table 6.6. The "TeeterNo" set was used to compare the wind turbine simulation responses of 2-bladed, teetered turbines with the corresponding turbine without a teeter mechanism. Also, the "TeeterNo" set is used for the 3-bladed machines because they do not have a teeter mechanism. The 6 teeter enabled sets are defined by scaling the hard teeter stop stiffness (TeetHSSp) to 10%, 25%, 30%, 50%, 75%, and 100% compared to the teeter set "Teeter1.0".The hard teeter stop stiffness and the damping constant of the teeter parameter set "Teeter1.0" were defined by scaling from a commercial wind turbine of different power rating. The damping constants (TeetDmp) of all 6 teeter enabled teeter sets were assumed to have the same damping ratio. The soft teeter stop stiffness (TeetSSSp) is set to 0 because only the hard teeter stop is considered for the teeter mechanism. Consequently, the soft teeter stop position (TeetSStP) is set to 0 as a default. The hard teeter stop position (TeetHStP) and the teeter damper position (TeetDmpP) are both set to 0 assuming that the teeter stop is engaged at all time. The Coulomb-friction damping (TeetCDmp) is set to 0 because it is ignored in the teeter mechanism model considered in this research.

Table 6.6. List of teeter parameter sets.

Teeter Sets		Teeter0.1	Teeter0.25	Teeter0.3	Teeter0.5	Teeter0.75	Teeter1.0	TeeterNo
Scale of TeetHSSp	(-)	0.1	0.25	0.3	0.5	0.75	1.0	No
TeetMod	(-)	1	1	1	1	1	1	0
TeetDmpP	(deg)	0	0	0	0	0	0	0
TeetDmp	(N-m/(rad/s))	7.431E6	1.175E7	1.287E7	1.662E7	2.035E7	2.350E7	0.0
TeetCDmp	(N-m)	0	0	0	0	0	0	0
TeetSStP	(deg)	0	0	0	0	0	0	0
TeetHStP	(deg)	0	0	0	0	0	0	0
TeetSSSp	(N-m/rad)	0	0	0	0	0	0	0
TeetHSSp	(N-m/rad)	6.400E7	1.600E8	1.920E8	3.200E8	4.800E8	6.400E8	0.0

From the results of the parametric study using FAST simulations under various DLCs considered in section 5.4, the teeter set 0.3 was selected for the 2-bladed turbines. In Figure 6.16, the teeter angle for different teeter models under normal, fault and parked conditions are shown from left to right. Under normal operating condition, the maximum teeter angle for the third model results teeter angles around 3 deg which meets the design target (3 deg). Under fault condition, the maximum teeter angle of the third design is less than the design target (6 deg). Under park condition all models perform safely.

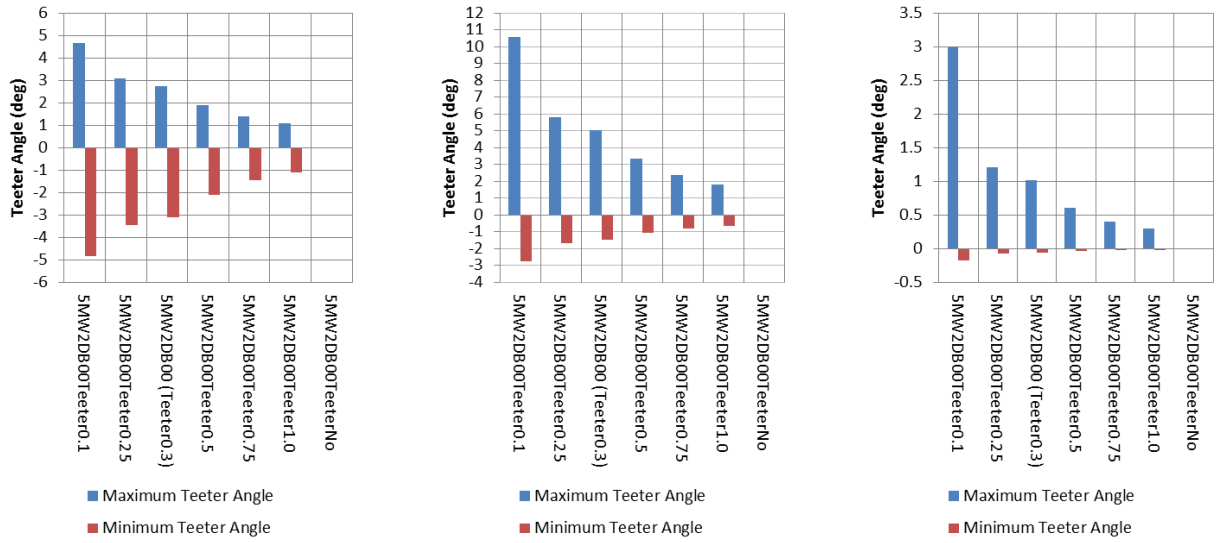

Figure 6.16. Teeter angle comparisons for various teeter parameters in normal operating condition, fault condition and parked condition.

The minimum tower to blade clearance is re-verified for these models with various teeter parameters. The minimum tower to blade clearances compared in Figure 6.17 are under normal operating, fault, and parked conditions. Under normal conditions, the clearance between the tower and the blades does not depend on the teeter parameters. This intuitively makes sense, because under normal operating condition the teeter mechanism does not engage and consequently does not affect the minimum clearance. However, under fault condition the teeter parameter with the least stiffness causes the second blade to collide with the tower. Considering minimum safe distance is 3.5 m, other cases are safe. As expected, as the teeter becomes stiffer, the response gets closer to those with a rigid hub rotor.

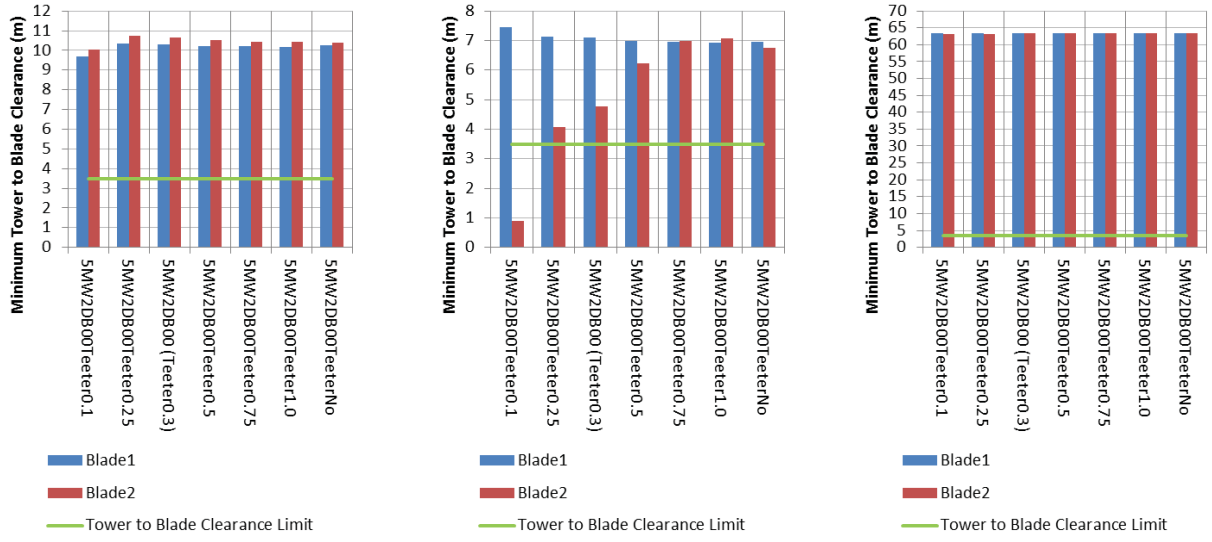

Figure 6.17. Minimum tower to blade clearance comparisons for various teeter parameters in normal operating condition and fault condition.

6.3 Power Control Method

The drivetrain performance controller is the brains of the wind turbine. It controls the power production of the wind turbine. There are other controllers used in a conventional wind turbine: yaw, start, stopping, safety and emergency controls. This section will focus on the operational or performance or power controller. The controller used is this analysis is a conventional variable-speed, pitch-to-feather controller. The information presented is the values of constants needed to build a dynamic link library used with FAST.

The drivetrain used in this analysis uses a conventional variable-speed, variable blade-pitch-to-feather control system. In English, this means the control system uses two controllers to regulate power production. One controller, generator-torque controller, is used in wind speeds below rated generator capacity. The purpose of this controller is to maximize power capture from the wind. Once the generator reaches its rated operational point, the second controller, blade-pitch controller, is used to maintain generator speed at the rated operational point. To maintain generator speed, it uses a gain-scheduled proportional integral (PI) control. Information in this section is based on research done for the NREL 5MW baseline offshore wind turbine [Jonkman et al., 2007, 2009].

Before continuing, it was found during the analysis that values for the coefficient of power (Cp) published in [Jonkman et al., 2009] were different than the ones found using the program WT_Perf. At this time, it is not known why the values do not match. One possible answer is the NREL baseline machine chose a rated rpm of 12.1 to keep the tip speed below 80 m/s. Keeping the tip-speed below 80 m/s is common practice to help eliminate noise in onland wind turbines. It may also be due to a difference in assumptions (air density of 1.225 kg/m^3, rotor radius 63 m, and rated power 5,296.610 kW).

In addition, to the discrepancy in Cp values, the 2-bladed controller used with the NREL blade uses a rotational speed of 16 rpm at rated wind speed. An ideal value for the rotational speed, at rated power is 15.85 rpm. At the time the controller was made it was thought the 15.85 value should be rounded up to 16 rpm.

Table 6.7. Tip-Speed-Ratio and Cp values.

	Tip-Speed Ratio (TSR)	Coefficient of Power (Cp)
NREL 3B published	7.55	0.4820
NREL 3B original (WT_Perf)	7.50	0.4868
NREL 2B original	9.00	0.4670
NREL 2B original (16 rpm)	9.50	0.4656
NREL 2BUT	9.20	0.4728

From this point forward in the description of the analysis done, the values for the tip-speed ratio and Coefficient of Power for the NREL baseline (3B) turbine were calculated by WT_Perf. All the values for the 2-bladed analysis are based on results from WT_Perf.

Table 6.8. Rated rpm and Rated Wind Speed.

	Rated (rpm)	Rated wind speed (m/s)
NREL 3B published	12.10	11.40
NREL 3B original (WT_Perf)	12.79	11.25
NREL 2B original	15.56	11.41
NREL 2B original (16 rpm)	16.45	11.42
NREL 2BUT	15.84	11.36

Typically, wind turbine control is based on the measurement of generator torque. The generator torque is a function of five different control regions: 1, 1 ½, 2, 2 ½, and 3. Region 1 is the region before the generator starts working. In this region the wind is used to start the rotor spinning. Region 1 ½ , is a transitional region to set a lower limit on when the wind turbine starts operation. Region 2 is a control region used to optimize power capture. In this region the generator torque is proportional to the square of the generator speed, to maintain a constant tip-speed ratio.

Table 6.9. Constant Inputs for .dll Controller.

	Generator Torque Constant (Nm/rpm^2)	Kp (Theata=0) (sec)	Ki (Theata=0)	Theata (rad)
NREL 3B published	0.0255764	0.0188268	0.0080686	0.1099965
NREL 2B original (16 rpm)	0.0146991	0.0087811	0.0037633	0.1073581
NREL 2BUT	0.0139320	0.0112085	0.0048036	0.0886778

Region 2 ½ is a linear transition between Region 2 and 3. Region 2 ½ is typically needed to limit tip speed that can cause noise at rated power. At above rated wind speed, region 3, the generator power is held constant (5 MW). In order to achieve constant generator power the blade pitch angles (angle of attack) are changed to produce the appropriate torque. This is done because at high wind speeds there is more power in the wind than the generator can convert into electricity. A gain-scheduled proportional integral (PI) control is used to maintain generator speed.

This section provided the constants, Generator Torque Constant, Proportional and Integral gain, needed to build a dynamic link library used with FAST to control performance.

6.4 Tower Properties

Because a gravity foundation is used for the turbine and the wind turbine configuration is changed from the NREL 5 MW, the tower properties of the NREL 5MW wind turbine tower design [Jonkman, 2006] had to be modified to fit the new system. In this section, the tower structural properties, top mass properties and mode shapes are presented.

The bottom part of the tower from the water level to the platform (11 m) elevation is assumed rigid. According to the platform design described in Chapter 7, the platform is placed sufficiently high above the water level so that the gravity foundation will support all wave and ice loads. The platform is assumed to be clamped to the bottom part. This assumption essentially decouples the transmission of wave and ice loads from the platform to the wind turbine. The tower rigid body height parameter (TwrRBHt) and platform model parameter (PtfmModel) of the FAST primary input file are set to 11 and 0, respectively, to account for these the design constraints.

Accordingly, the tower model in this work is a modification of the monopile tower in [Jonkman, 2006], and only the upper part, above the 11 m elevation, is used to represent the flexible part of tower. The calculated tower structural properties for the present tower model are presented in Table A2.1 in Appendix 2 and were applied from tower elevations of 11 m to 87.6 m. Therefore, only 76.6 m of tower length is considered flexible. The outer diameter of the tower at 11 m elevation is 5.973 m and at the top of the tower is 3.87 m. The thickness at 11 m elevation is 0.0269 m, and at top of the tower is 0.019 m. The tower is linearly tapered from bottom to top.

The mode shapes of the tower were calculated, accounting for the change in the structural properties and the top mass distribution. Only the flexible part of the tower was used for the mode shape calculations. A total of twelve different tower models were developed to account for changes in the top mass distribution. These six tower models were generated consisting of 3-bladed upwind, 2-bladed upwind, and 2-bladed downwind configurations, each with and without tip-brakes. Moreover, six 2-bladed downwind models with different shaft tilt, cone angles, and use of tip-brakes were developed. Depending on the number of blades, up and downwind configuration, use of tip-brake, shaft tilt angle, and cone angle, the tower top mass and moment of inertia were changed resulting in twelve different tower models being developed. The first and second mode shapes, fore-aft and side-to-side directions, were calculated using BModes and the polynomial coefficients were found by fitting to a sixth order polynomial.

To find the tower mode shapes, the tower top mass, center of mass (CM), and mass moment of inertia are required. The masses and CM information of the tower top components are listed in Table A2.2 in Appendix 1. Using the data from Table A2.2, the total tower top mass, center of mass locations, and mass moment of inertia were calculated as presented in Table A2.3. These data were used to estimate the mode shapes of the tower models using BModes. The tower structure input files for FAST simulation were generated using these structural properties and mode shapes for the various tower models.

6.5 Dynamic Characteristics of Tower and Blade

The natural frequencies of the tower and blades were computed using the BModes code in order to examine the dynamic characteristics of these structures. . The natural frequencies of the towers for different configurations are listed in Table 6.10. The natural frequencies of 3-bladed models and 2-bladed models have some differences. However, wind direction configuration, shaft tilt angle, conning angle, and application of tip-brake do not produce significant changes for natural frequencies except with mode 2, side-to-side natural frequencies. The percent differences of tower natural frequencies for different configurations are listed in Table 6.11.

Table 6.10. Tower natural frequencies.

Num. of Blade	Wind Direction	Tilt (deg)	Conning (deg)	Tip-brake	Mode1 Fore-Aft	Mode1 Side-to-Side	Mode2 Fore-Aft	Mode2 Side-to-Side
3	Up	5	2.5	No	0.3658	0.3665	3.3349	3.2125
3	Up	5	2.5	Yes	0.3657	0.3664	3.3335	3.2085
2	Up	5	2.5	No	0.3746	0.3752	3.4080	3.4218
2	Up	5	2.5	Yes	0.3745	0.3751	3.4071	3.4189
2	Down	5	2.5	No	0.3746	0.3752	3.4080	3.5138
2	Down	5	2.5	Yes	0.3745	0.3752	3.4071	3.5106
2	Down	5	0	No	0.3747	0.3752	3.4404	3.6343
2	Down	5	0	Yes	0.3746	0.3752	3.4399	3.6333
2	Down	0	2.5	No	0.3747	0.3753	3.4365	3.5027
2	Down	0	2.5	Yes	0.3746	0.3753	3.4356	3.4997
2	Down	0	0	No	0.3748	0.3753	3.4693	3.6189
2	Down	0	0	Yes	0.3747	0.3753	3.4688	3.6179

Table 6.11. Percent difference of tower natural frequencies.

Models Compared		% Difference			
% Difference of..	Relative to..	Mode1 Fore-Aft	Mode1 Side-to-Side	Mode2 Fore-Aft	Mode2 Side-to-Side
2-bladed Upwind	3-bladed Upwind	2.41	2.37	2.20	6.54
2-bladed Downwind	3-bladed Upwind	2.41	2.39	2.20	9.40
2-bladed Downwind	2-bladed Upwind	0.00	0.01	0.00	2.69
Shaft Tilt 0 deg	Shaft Tilt 5 deg	0.03	0.03	0.84	-0.37
Cone 0 deg	Cone 2.5 deg	0.03	0.00	0.96	3.40
With Tip-brake	Without Tip-brake	-0.03	-0.01	-0.02	-0.07

The blade natural frequencies for different blade models and configurations are listed in Table 6.12. Adding a tip-brake to a blade reduces its natural frequency by 4.45% on average for the mode shapes considered. Because the NREL 5MW baseline blade and BUT blade only differ in their twist angles, these blades have almost identical natural frequencies.

Table 6.12. Blade natural frequencies at 0 RPM.

Blade	Tip-brake	Mode1 Flap-wise	Mode1 Edge-wise	Mode2 Flap-wise	Mode2 Edge-wise
Baseline	No	0.6698	1.0791	1.9193	3.9493
Baseline	Yes	0.6401	1.0499	1.8090	3.7547
BUT	No	0.6683	1.0788	1.9177	3.9553
BUT	Yes	0.6401	1.0500	1.8089	3.7625

The Campbell diagrams for the following three different configurations are presented below: 3-bladed upwind, 2-bladed upwind, and 2-bladed downwind. Wind turbines with the same number of blades and wind direction, have very similar Campbell diagrams. Thus, only the Campbell diagrams for 3 models are listed here.

The excitation lines 1P, which are related to the rotation of the rotor, for all configurations do not cross any natural frequency under the rated rpm. However, the 3P or 2P lines, which are related to the blade passing rate, cross both the 1st natural frequency lines corresponding to the tower fore-aft and side-to-side modes around 7.4 rpm for 3-bladed turbines and 11.3 rpm for 2-bladed turbines. These rotational speeds need to be avoided during normal operation using a controller in order to avoid resonances. Other excitation lines will not affect significantly the tower and blade structure based on the information available at this point. These excitation lines may be considered at a later stage of the design.

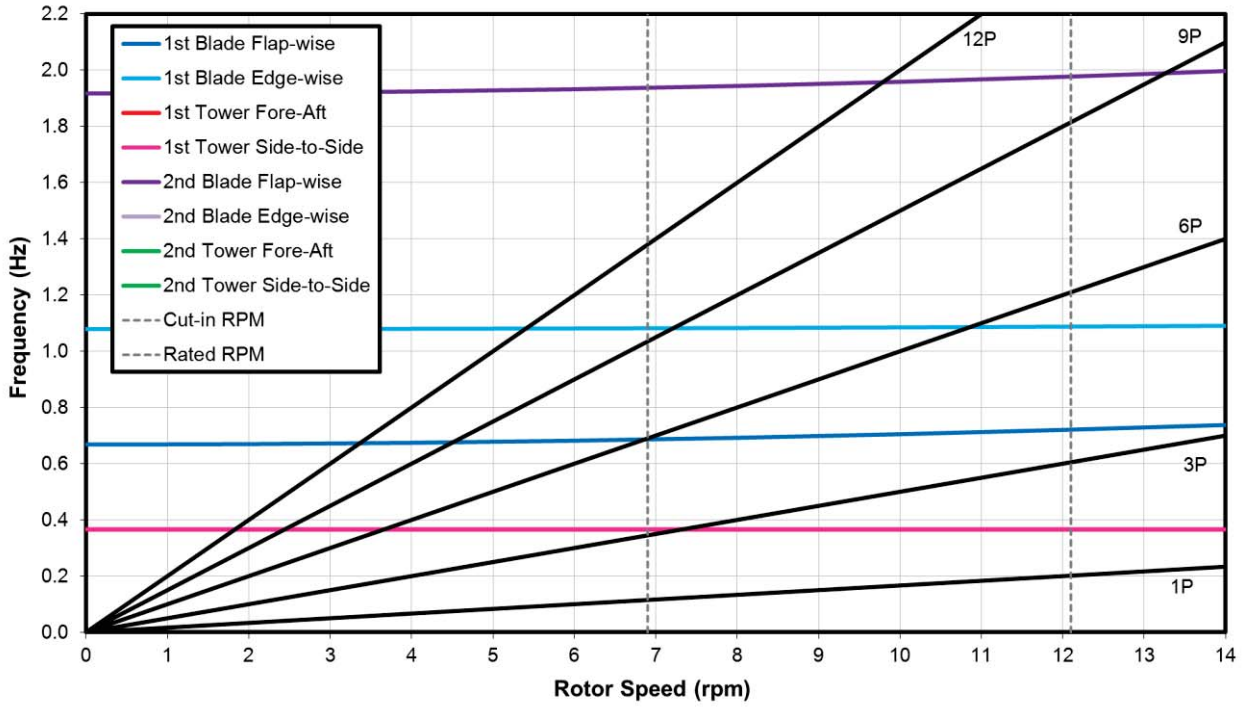

Figure 6.18. Campbell diagram of 3-bladed upwind turbine.

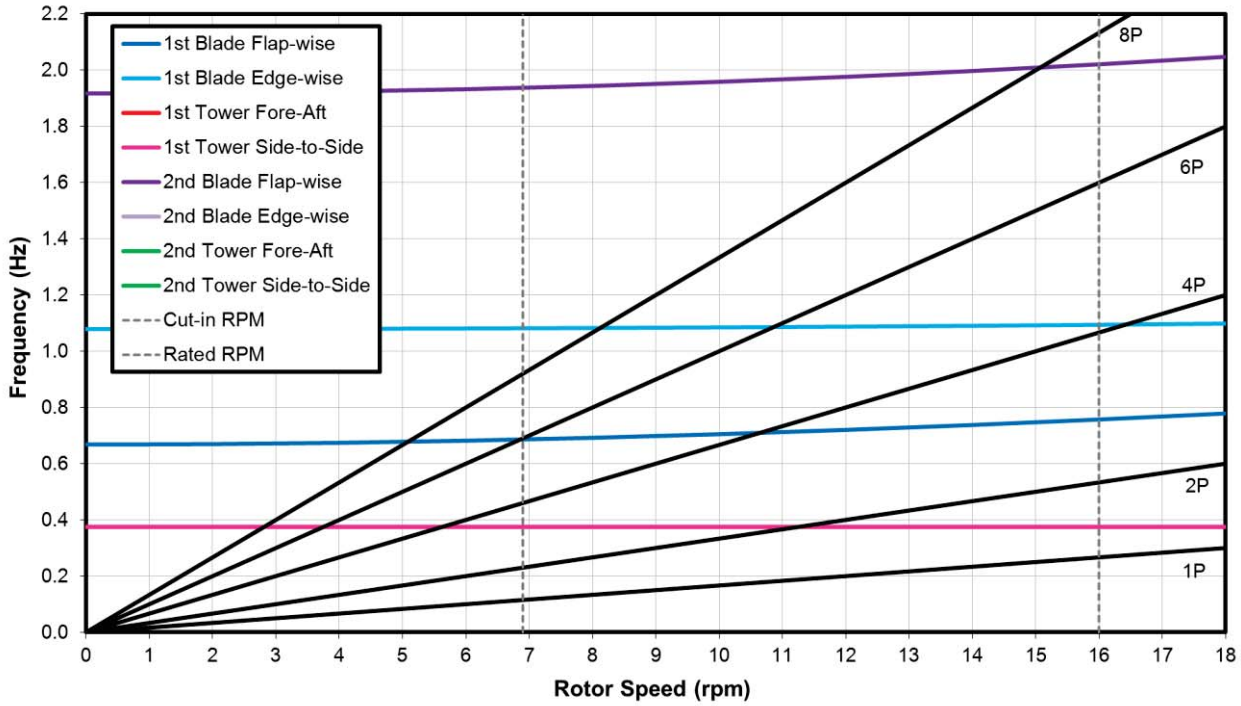

Figure 6.19. Campbell diagram of 2-bladed upwind turbine.

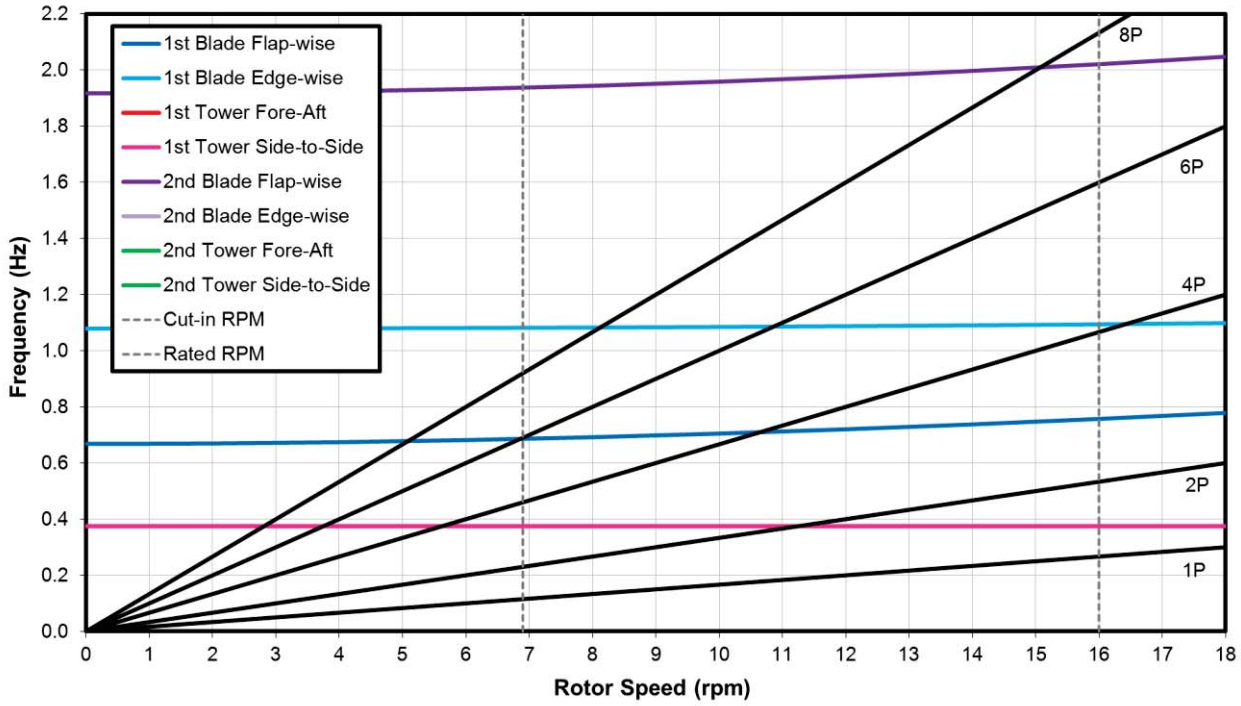

Figure 6.20. Campbell diagram of 2-bladed downwind turbine.

6.6 Modeling Tower Shadow Effects

Tower shadow is the distortion of the steady-state mean wind field due to the presence of the tower. For downwind configurations, the empirical model, which uses a cosine bell-shaped tower wake, can be used to model tower shadow effects. This model, which is based on the work of [Powles, 1983], is characterized using three parameters as follows:

- Maximum velocity deficit at the center of the wake
- Width of the tower shadow
- The reference downwind distance where the above parameters are defined.

The shadow width increases and the velocity deficit decreases with the square root of the distance from the tower. In this model, the wind speed perpendicular to the tower axis is calculated by Eq. (6.1),

$$V(x,y) = \left(1 - \Delta\cos^2\left(\frac{\pi y}{DW_{ts}}\right)\right) U_\infty \tag{6.1}$$

where Δ is the maximum velocity deficit as a fraction of the local wind speed, and W is the width of the tower shadow normalized by the tower diameter (D). The tower shadow width increases while velocity deficit decreases with the square root of the distance from the tower.

This model has been implemented in AeroDyn code [Laino & Hansen, 2002], which is used by FAST to calculate tower shadow effects. However, the required parameters should be estimated using a CFD analysis or experimental measurement. In this study an ANSYS FLUENT CFD simulation was carried out to estimate the required parameters to account for tower shadow effects with tower diameter equal to 1.88 m. Simulations were conducted using different wind speeds and for different reference distances from 2 m to 8 m behind the tower. The results are illustrated in Figure 6.21 to 6.25.

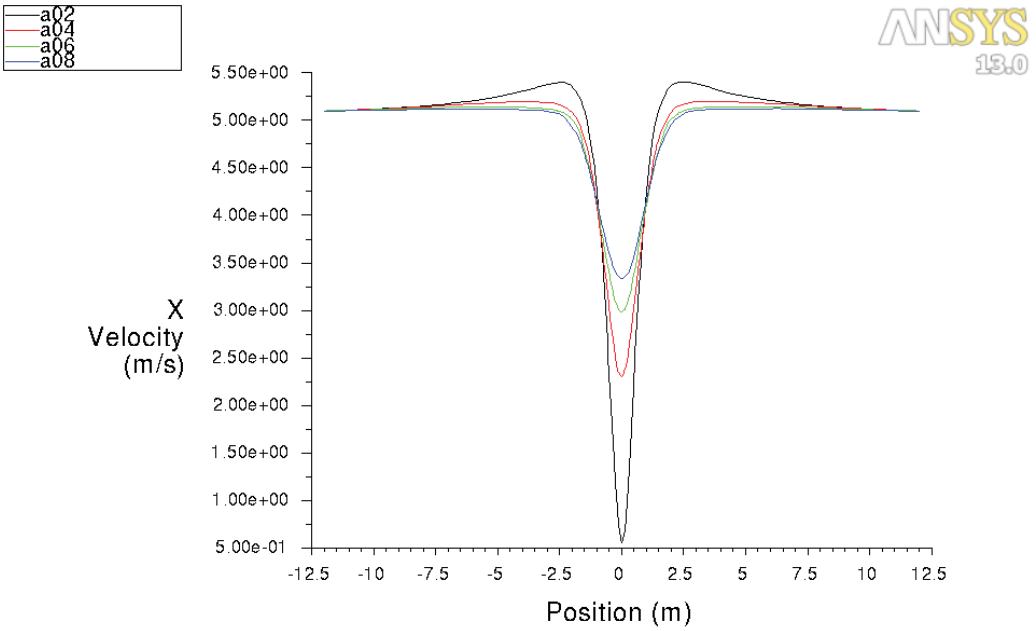

Figure 6.21. Velocity deficit for tower diameter of 1.88 m and wind speed equal to 5 m/s.

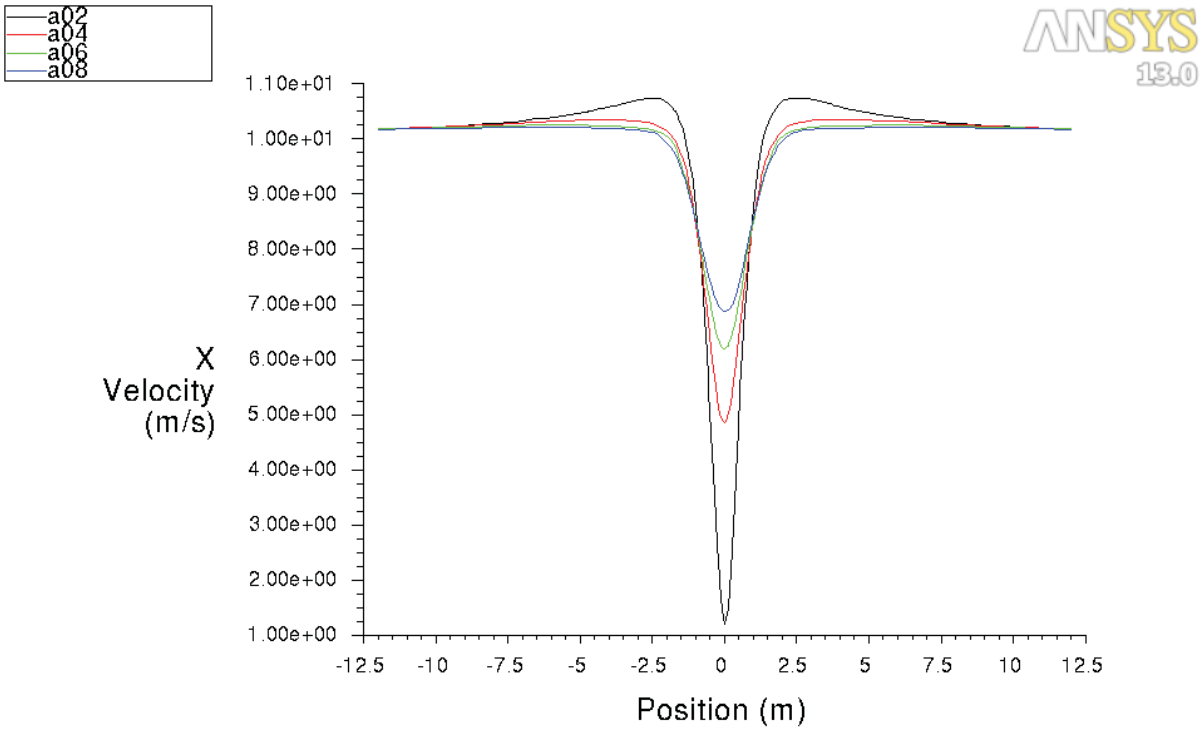

Figure 6.22. Velocity deficit for tower diameter 1.88 m and wind speed equal to 10 m/s.

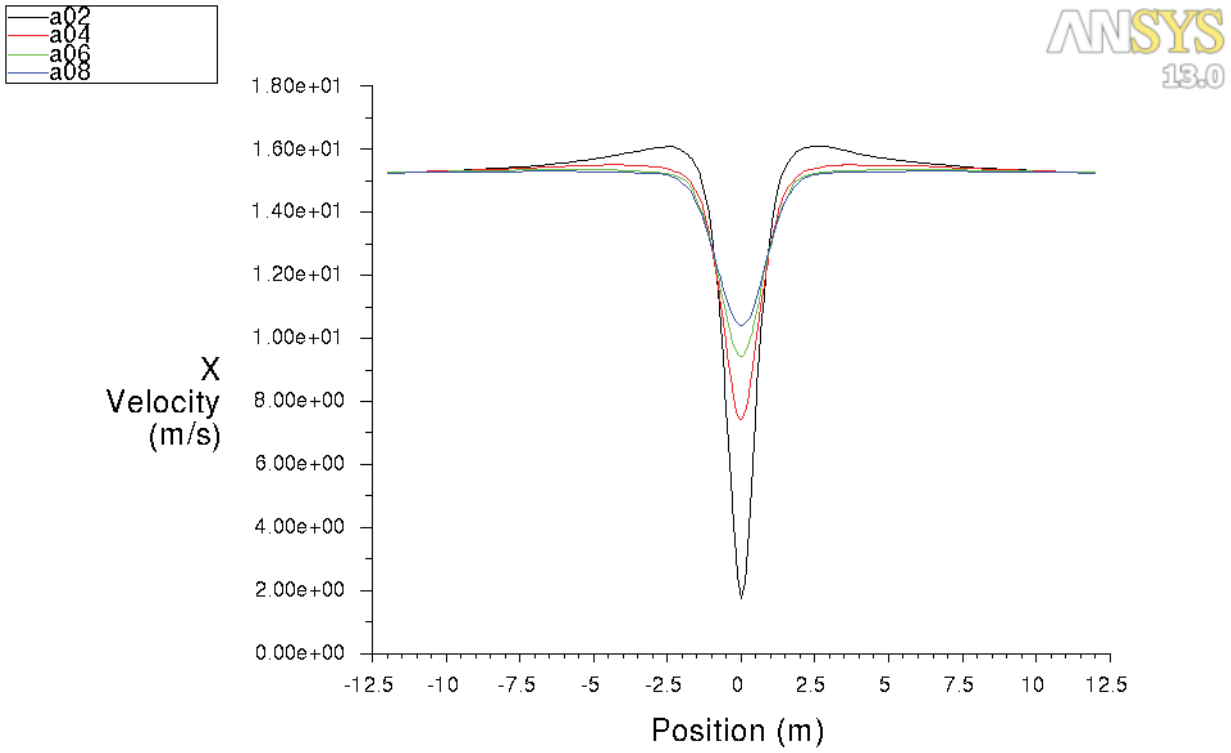

Figure 6.23. Velocity deficit for tower diameter 1.88 m and wind speed equal to 15 m/s.

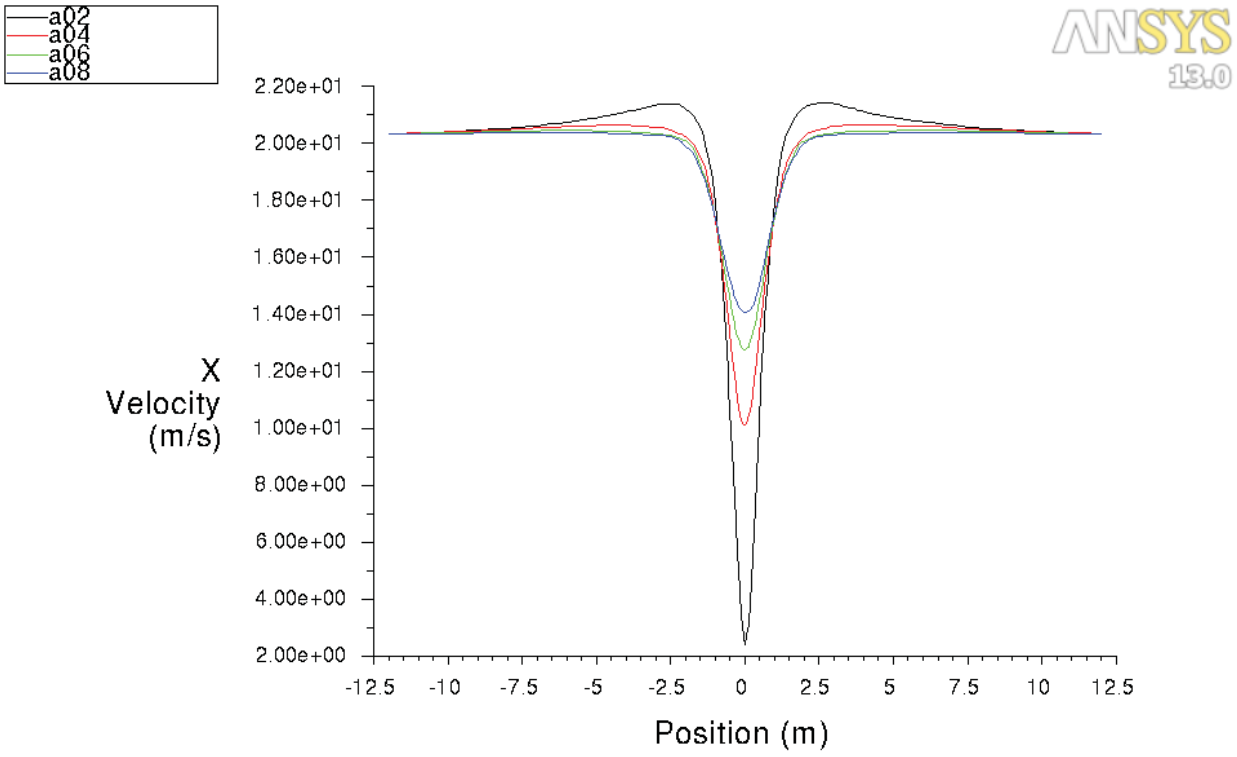

Figure 6.24. Velocity deficit for tower diameter 1.88 m and wind speed equal to 20 m/s.

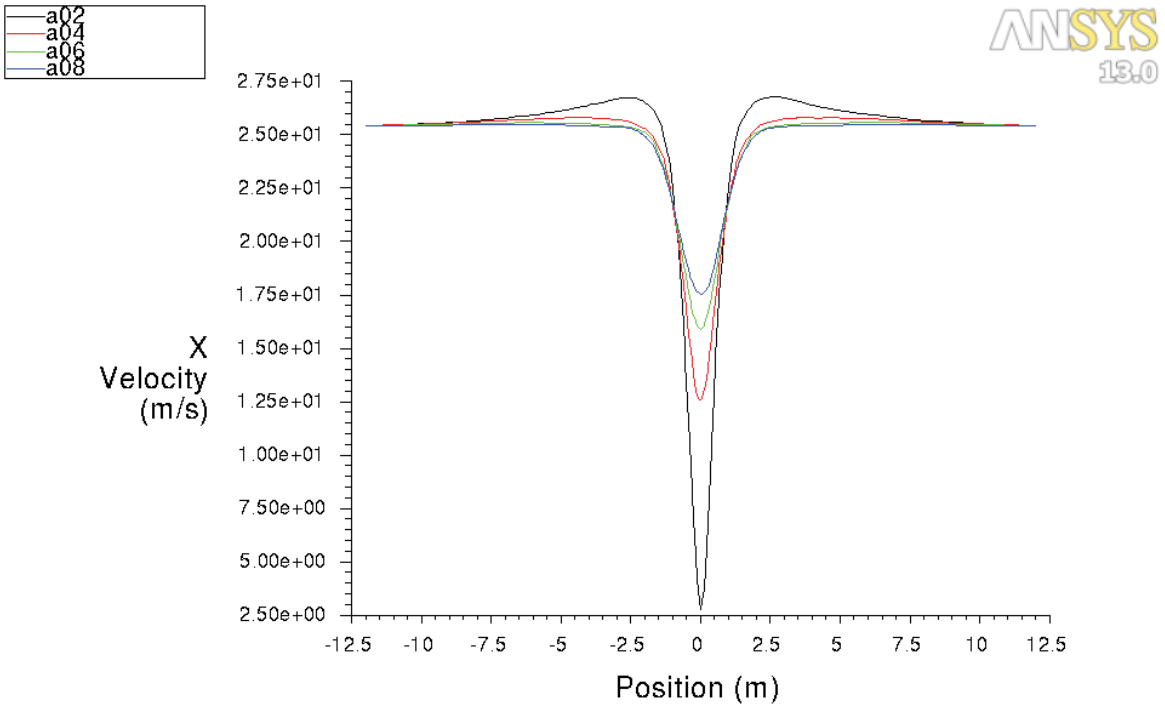

Figure 6.25. Velocity deficit for tower diameter 1.88 m and wind speed equal to 25 m/s.

The results of the CFD simulation at 4 m reference point for different wind speeds are summarized in Table 6.13. It is observed that at the reference point the width of the tower shadow remains almost constant as wind speed changes. The maximum velocity deficit is also approximately constant, as expected.

Table 6.13. Summary of the parameters to model tower shadow effects (ref distance 4 m).

U_∞	V/U_∞	W_{ts}/D
5	0.54	2.66
10	0.51	2.66
15	0.5	2.66
20	0.5	2.66
25	0.5	2.66

The above parameters were used to model the tower shadow effects in this study.

The tower shadow parameters are recalculated so that they can be applied to the proposed wind turbine designs. The tower shadow parameters are calculated at the 43.154 m tower height location. This is the location where a point on the blade at a distance of 75% of the rotor radius from its center is passing behind the tower for the wind turbine configuration with 5° shaft tilt angle and 2.5° pre-cone angle. Because the rated wind speeds are 11.4 m/s for the 5MW turbines, 0.51 value is selected for parameter TwrShad (V/U_∞) of the AeroDyn input file. The diameter at the 43.154m tower height location is 4.951 m. Thus, the ShadHWid ($W_{ts}/2$) parameter of

AeroDyn input file value is calculated to be 6.584 m. The T_Shad_Refpt parameter of AeroDyn input file is determined by linearly scaling the reference distance relative to the tower diameter. As a result, the value of parameter T_Shad_Refpt is estimated to be 10.533 m.

7 Foundation Design

The objective of this chapter is to describe the gravity base foundation (GBF) designed to support this project's downwind, 2-bladed wind turbine concept. Using engineering judgment reasoned in Section 7.1 a rigid connection was found to be adequate for operation of the wind turbine under normal conditions. However, for this preliminary study, the foundation-tower interaction was modeled as a rigid connection for all design load cases. This approach was reasonable since in Lake Erie wave and ice loads are dominant loads for the foundation design. Accordingly, the computed wind turbine loads determined using a rigid tower base were used to design the GBF. The design methodology was based on the ultimate wind turbine loads; the effects of wave and ice were limited to the foundation and not transmitted to the turbine

The subsections of this chapter are organized as follows. Section 7.1 is a stand-alone section included to demonstrate the limitations on the validity of the static coupling assumption between the foundation and turbine and how modeling of the turbine and foundation interaction affects estimating limit state loads. Section 7.2 summarizes the loads that are transmitted to the foundation due to the turbine operating under different design load cases. Section 7.3 explains the design process, and Section 7.4 describes the final design.

7.1 Importance of Modeling Tower and Foundation Interaction

To demonstrate aspects of decoupling the foundation and turbine that impact design considerations, a simple model is used in this section to show how the interaction of the foundation and turbine could affect structural integrity of a wind turbine under different loading conditions. The NREL 5 MW turbine was used for this purpose.

The simplest model of soil-structure interaction is characterized by a stiffness matrix only. In this model for every loading condition at the base of a tower, the elements of the stiffness matrix from soil mechanics need to be specified. Using this model (Figure 7.1), three steps are involved. In the first step, by assuming a clamped base, FAST is run for a given load case, and the loads are calculated at the tower base. In the second step, using the loads estimated from the first step, a soil mechanics software is used to calculate the displacements for a virtual beam inside the soil. Lastly, in the third step, the elements of the stiffness matrix for the virtual beam are calculated using the displacements obtained in the second step.

The stiffness matrix obtained from the above process would be load case dependent. As was mentioned earlier this model is the simplest way to model the soil-tower interaction. In reality, the soil behavior is complex and nonlinear, dependent on the magnitude of the loads.

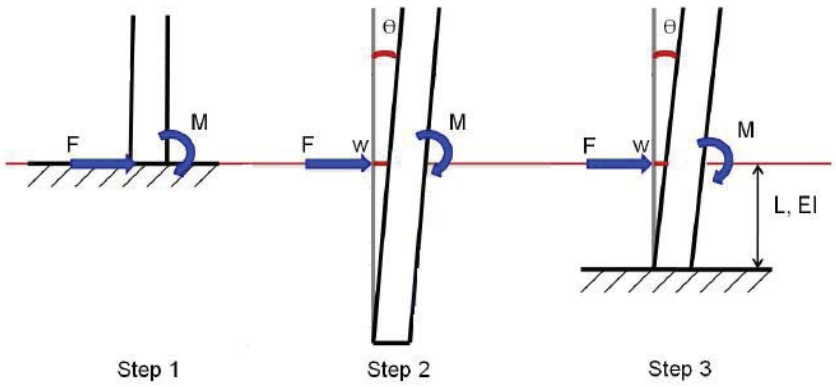

Figure 7.1. Steps to characterize soil-tower stiffness matrix [Bush, 2009].

For a cantilever beam under a shear load and a bending moment, the deflection is calculated using Eq. (7.1),

$$\begin{bmatrix}\delta\\ \theta\end{bmatrix} = \begin{bmatrix}\frac{L^3}{3EI} & \frac{L^2}{2EI}\\ \frac{L^2}{2EI} & \frac{L}{EI}\end{bmatrix}\begin{bmatrix}F\\ M\end{bmatrix} \tag{7.1}$$

Then the stiffness matrix would be as follows,

$$K = \begin{bmatrix}\frac{12EI}{L^3} & \frac{-6EI}{L^2}\\ \frac{-6EI}{L^2} & \frac{4EI}{L}\end{bmatrix} \tag{7.2}$$

Figure 7.1. and Eq. (7.1) correspond to a two-dimensional model. The three dimensinal counter part of Eq. (7.2) would have 6×6 elements.

Using the mass properties of the NREL 5 MW machine, the following stiffness matrix was found to be representative of the model based on DNV-OS-J101 standard.

$$K = \begin{bmatrix} 1.6GN/m & 0 & 0 & 0 & -5.49GN/m & 0\\ 0 & 1.6GN/m & 0 & 5.49GN/rad & 0 & 0\\ 0 & 0 & 2.5GN/m & 0 & 0 & 0\\ 0 & 5.49GN/rad & 0 & 25GNm/rad & 0 & 0\\ -5.49GN/m & 0 & 0 & 0 & 25GN/rad & 0\\ 0 & 0 & 0 & 0 & 0 & 25GNm/rad \end{bmatrix} \tag{7.3}$$

First, using simple calculations the range of defelections are estimated for a normal operating condition. Consider the following loads to estimate the deflections.

Largest horizontal shear load	: 2160 kN
Largest Lateral	: 853 kN
Largest vertical load	: 5581 kN
Mx	: 65840 kNm
My	: 188900 kNm
Mz	: 5118 kNm

Assume that the above loads are applied statically and individually to the structure. The corresponding deflections would be as follows,

Surge = 0.14 cm
Sway = 0.05 cm
Heave = 0.2 cm
Roll = 0.15°, this translates into approximately 0.25 m displacement at the top of the tower
Pitch = 0.43°, this means that the displacement at the top of the tower would be approximately 0.75 m
Yaw = 0.0002 rad

This means that as intuitively expected the pitch and roll DOFs should be the most critical.

FAST was recompiled to include flexibility as shown in Eq. (7.3). Figure 7.2, Figure 7.3 and Figure 7.4 demonstrate a simulation with wind speed 20 m/sec and normal turbulence when the grid is lost at 60 seconds and the turbine is shut down immediately. Figure 7.2 shows the tower top displacement in the fore-aft direction.

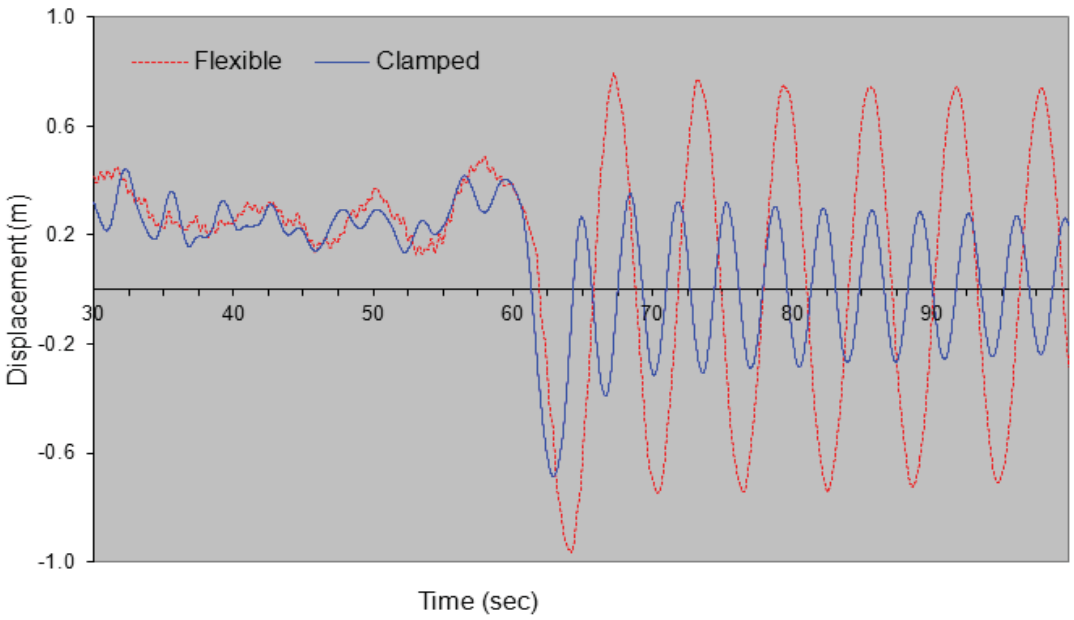

Figure 7.2. Tower top displacement in fore-aft direction under fault and normal condition.

Figure 7.3 illustrates the fore-aft bending moment at the base of tower, and Figure 7.4. demonstrates the side-to-side displacement at the tower top.

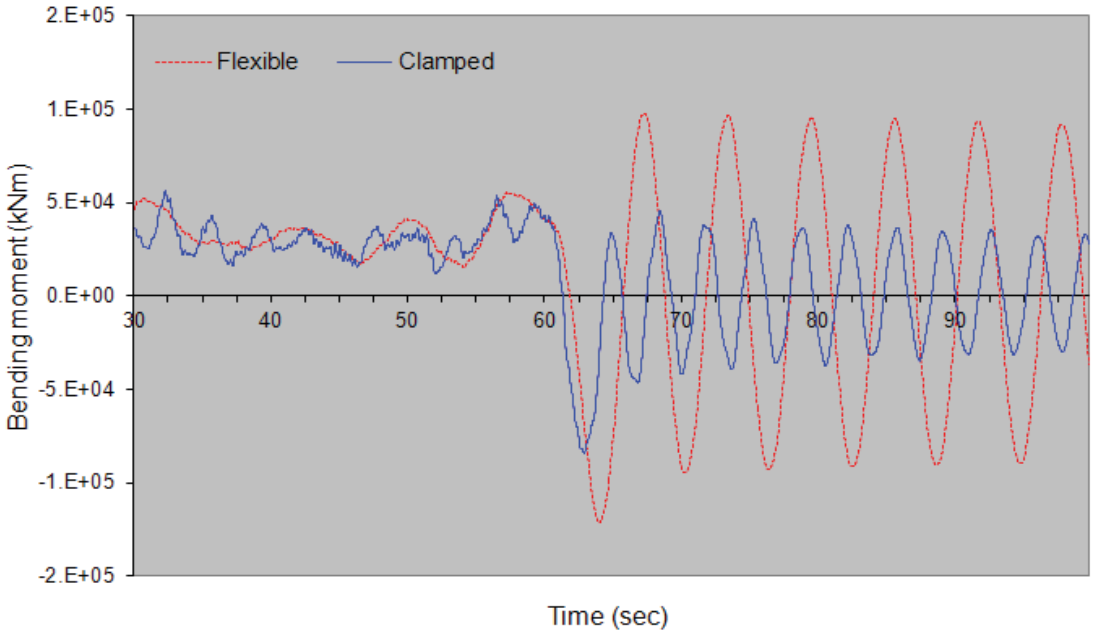

Figure 7.3. Fore-aft bending moment at the base of tower under fault and normal condition.

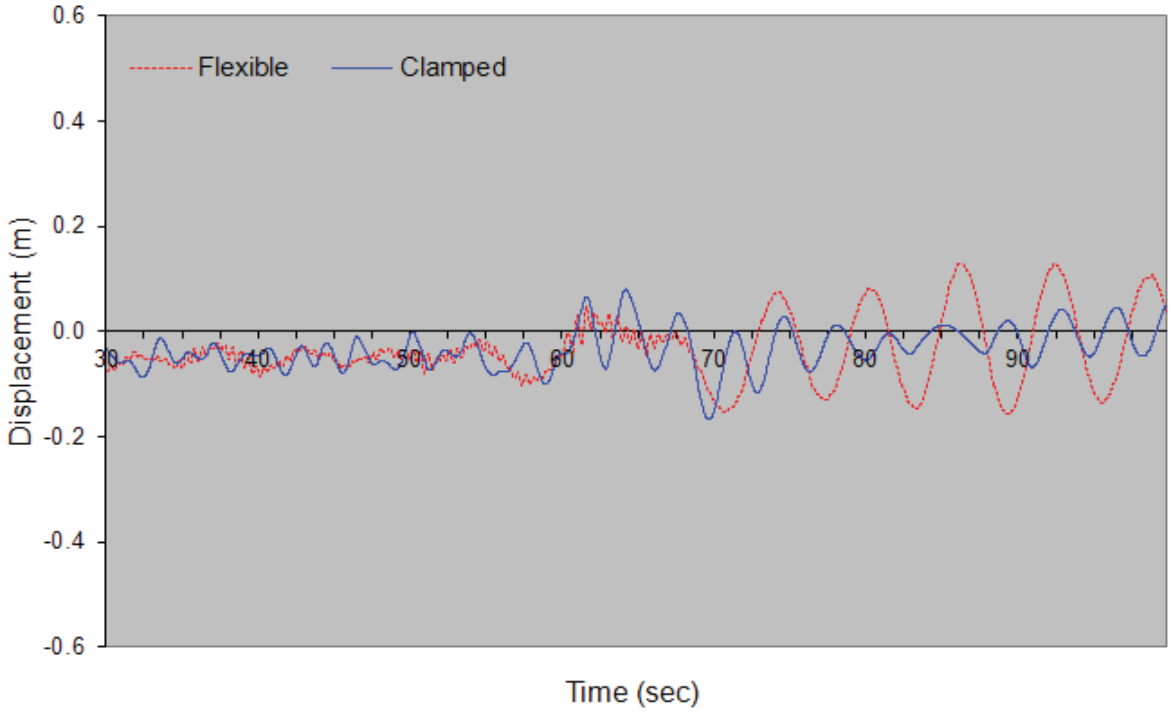

Figure 7.4. Tower top side-to-side displacement under fault and normal condition.

This test case demonstrates that for normal operating conditions, there is not a significant difference between the clamped model and the flexible foundation, but for fault conditions, the difference can be significant. This means that to design the wind turbine for fatigue loads using a clamped model or using a simple model as described above could be sufficient, but to estimate the loads due to ultimate loads for fault conditions accurate modeling of tower and soil interaction is necessary.

7.2 Loads Transmitted From Monopole to Foundation

In order to design a GBF, one needs to estimate the loads applied to the foundation at the tower and foundation interface due to the wind turbine operation under different conditions. For the foundation concept that is considered in this study Figure 7.5, the wave and ice loads are applied to the gravity foundation, as the tower is installed on the top of foundation above the sea level.

Figure 7.5. Gravity base foundation.

The load cases that were used in this study are similar to those used by Jonkman & Buhl [2007] to estimate the loads applied to the top of the foundation due to the operation of a wind turbine.

The load cases used here are identical to those listed in Table 5.10. The metrological conditions described in Chapters 5 were used to determine the environmental loads for these design load cases.

Table 7.1 summerizes the maximum loads that are calculated at the base of the tower corresponding to the load cases in Table 5.10. In Chapter 9 more details on the calculation of these loads are presented. Refer to Appendix 4 for the definitions of nomenclatures used in Table 7.1.

Table 7.1. Summary of turbine loads at the base of the tower.

Normal Operation									
		When F_{xyt} is		When M_{xyt} is		When F_{zt} is		When M_{zt} is	
Loads	Units	Max	Min	Max	Min	Max	Min	Max	Min
F_{xyt}	(kN)	**1270**	**0**	1267	18	353	327	301	250
F_{zt}	(kN)	-5513	-5550	-5513	-5550	**-5420**	**-5690**	-5662	-5426
M_{xyt}	(kN-m)	101517	2347	**101533**	**13**	30190	27549	28844	24238
M_{zt}	(kN-m)	1215	-113	1362	-15	-9598	5959	**7155**	**-10240**
Fault Conditions									
		When F_{xyt} is		When M_{xyt} is		When F_{zt} is		When M_{zt} is	
Loads	Units	Max	Min	Max	Min	Max	Min	Max	Min
F_{xyt}	(kN)	**1289**	**0**	1226	6	281	228	310	385
F_{zt}	(kN)	-5643	-5561	-5481	-5561	**-5289**	**-5839**	-5780	-5321
M_{xyt}	(kN-m)	96830	497	**97635**	**32**	22557	19752	25417	29382
M_{zt}	(kN-m)	-32	-60	117	-69	-13248	10533	**11969**	**-14647**
Parked Conditions									
		When F_{xyt} is		When M_{xyt} is		When F_{zt} is		When M_{zt} is	
Loads	Units	Max	Min	Max	Min	Max	Min	Max	Min
F_{xyt}	(kN)	**602**	**0**	601	5	134	21	580	522
F_{zt}	(kN)	-5530	-5605	-5533	-5552	**-5517**	**-5670**	-5545	-5543
M_{xyt}	(kN-m)	45719	863	**45842**	**2**	9057	3113	44823	40672
M_{zt}	(kN-m)	1216	-11	1408	-1	-542	30	**1760**	**-1640**

In the calculation of the above loads no wave or ice loads were applied to the wind turbine tower, because the foundation design extends about 11.5 m above the sea level. This height was selected so that waves and ice would be limited to the foundation and not reach the tower.

7.3 Foundation Design

In order to develop the GBF, the DNV-OS-J101 standard was used to estimate Ultimate Limit State loads, assuming that the design of the GBF will primarily be determined by ultimate loads [Marrone et al., 2013]. In this preliminary study Fatigue Limit State and Serviceability Limit States were not considered; however, these loads are important concerns and should be taken into account in the detailed design stage. Furthermore, the transportation and installation loads were also neglected at this preliminary stage.

Wave conditions are defined based on the IEC-61400-3 [2009] standard. Wave load cases are either deterministic or random. Figure 7.6 lists the parameters that are required to define regular or irregular wave conditions.

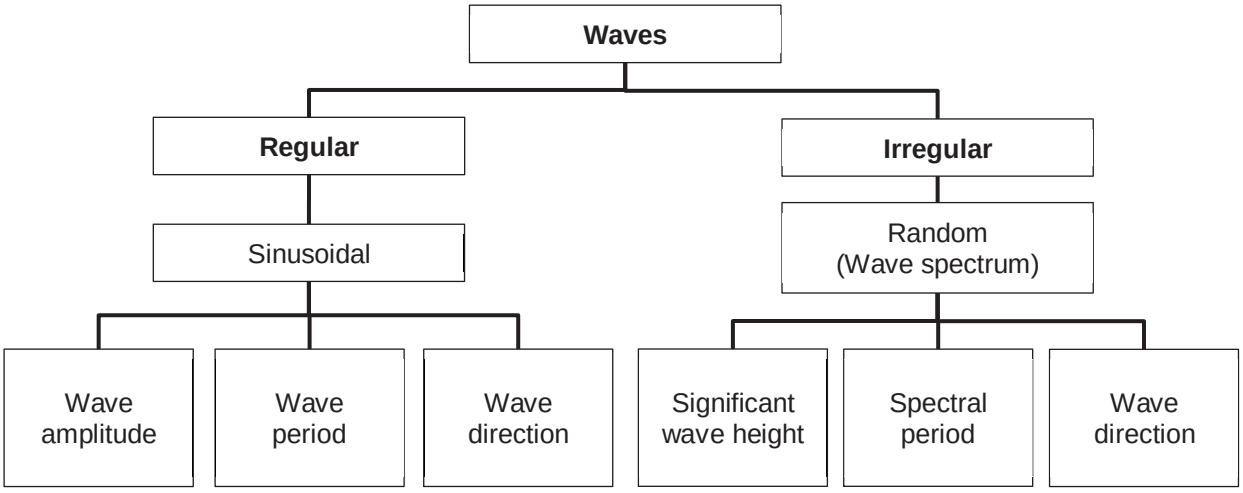

Figure 7.6. Wave conditions based on IEC 61400-3 standard.

For the deterministic waves the amplitude, the period, and the direction of approach of the waves should be specified.

Pierson-Moskowitz and JONSWAP spectra should be used in order to generate wave load cases to analyze loads on an offshore wind turbine according to the IEC standards. The two-parameter Pierson-Moskowitz spectrum is characterized by significant wave height and peak spectral period. The first parameter specifies the energy content of the waves and the latter specifies the frequency of the waves. Random waves are specified by selecting an appropriate wave spectrum, the probability distribution of wave direction and spectral period based on the environmental condition of a potential wind turbine site.

Below is a list of the load cases for each type of waves to consider based on the IEC standards for an offshore wind turbine:

1) Deterministic waves
    a. Normal wave height (NWH)
    b. Severe wave height (SWH)
    c. Extreme wave height (EWH)
    d. Reduced wave height (RWH)

2) Irregular waves
    a. Normal sea state (NSS)
    b. Severe sea state (SSS)
    c. Extreme sea state (ESS)
    d. Breaking wave

Depending on the location of an offshore wind turbine and the environment conditions, an appropriate wave theory should be used to model the hydrodynamic forces. IEC standard 61400–3 ed. 1 (2009) provides guidance on the selection of a suitable wave theory based on the environmental conditions at a given site (Figure 7.7). In this figure, H, L, T, d, and g denote the wave height, wave length, wave period, water depth, and gravitational acceleration, respectively. For more information regarding the wave theories and their ranges of application, refer to ISO19901-1 standard.

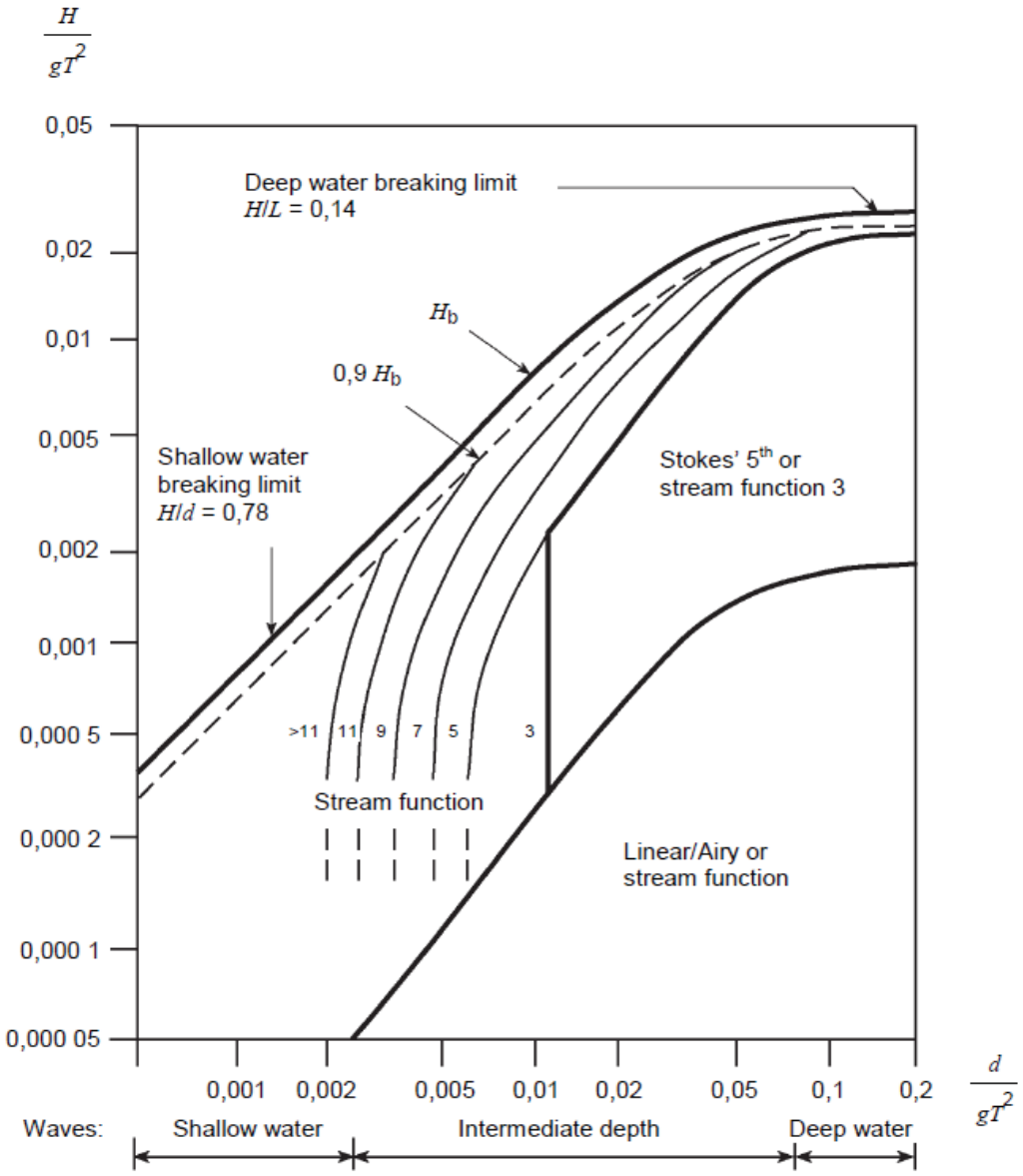

Figure 7.7. Selecting suitable wave kinematic model based on water depth and wave height [IEC 61400-3, 2009].

DNV-OS-J101 is the primary standard for wind turbine foundation design. This standard is a stand-alone document that covers design, construction, installation and inspection of offshore wind turbine structures.

For the foundation design in this study, the water level is listed in Table 7.2.

Table 7.2. Design Water Levels.

Water depth (chart datum)	17.0 m
50 year water level variation (surge)	± 2.4 m
1 year water level variation	± 1.0 m

The US Army Corps of Engineers (USACE) collects data at multiple Wave Information Study (WIS) stations in Lake Erie[1] as shown in Figure 7.8.

Figure 7.8. Location of hindcast data stations [Marone et al., 2013].

The metrological data that are available through NOAA buoy 45005 were reviewed and the 50-year return period significant wave height was determined to be 4.1 m. Table 7.3 summarizes the water depth and the 50-year return period wave heights from different hindcast locations and compares them with the data from buoy 45005.

Table 7.3. Water depth and design wave heights [Marrone et al., 2013].

Station	Water Depth (m)	H 50-year (m)
WIS 92105	8	2.6
WIS 92092	12	4.0
WIS 92134	11	3.5
NDBC 45005	12	4.1
WIS 92082	14	4.4
WIS 92070	16	5.1
WIS 92053	20	6.0

Using the hindcast data is advantageous over using those from the buoy because it includes data from winter time when the buoy is not operational. To be more conservative, the 50-year return

[1] http://wis.usace.army.mil/hindcasts.shtml

period wave was estimated from WIS 92070 station, which is 1 m higher (5.1 m) than that from the buoy 45005. It is noted that WIS 92070 is closer to the site of study than the buoy.

Based on the DNV standard and the wind turbine simulation results from Table 7.1, the load cases and the corresponding loads that were used for the design purpose are summarized in Table 7.4.

Table 7.4. Load Cases and corresponding results that are used to design the GBF [Marrone et al., 2013].

Operating Conditions	Normal		Fault		
Equivalent DNV load case	DLC 1.6	DLC 1.6	DLC 2.1	DLC 2.3	DLC 7.1
Horizontal Load (kN)	1270	301	1289	385	602
Overturning Moment (kNm)	101533	2884	97635	29382	45842
Torsional Moment (kNm)	1362	10240	117	14647	1760
Weight of Turbine + Tower (kN)	5416	5416	5416	5416	5416
Wave Condition	SSS Hs,50yr =5.1 m Tp = 7.2 s	SSS Hs,50yr =5.1 m Tp = 7.2s	NSS Hs=E[Hs|U10,hub] = 2.5 m Tp = 6.5 s	NSS Hs=E[Hs|U10,hub] = 2.5 m Tp = 6.5 s	ESS Hs,1yr = 3.5 m Tp = 6 s
Still Water Level	1 year water level = +1.0m	1 year water level = +1.0m	Mean water level = 0.0 m	Mean water level = 0.0 m	1 year water level =+1.0m
Load Factor	1.35	1.35	1.35	1.1	1.1

The main assumptions made to calculate the hydrodynamic loads are as follows [Marrone et al., 2013]:

- Stream function wave theory and Morison's equation [Ochi, 2005] were used to calculate hydrodynamic loads. Wave loads consist of two components, one is due to drag force which depends on the velocity of water particles and an inertia, which is a function of acceleration.
- The design wave height (Hmax) was considered to be 1.86 times the significant wave height (Hs) according to DNV-OS-J101. This is similar to the IEC 61400-3 [2009] standard.
- The friction coefficient was selected for a structure with a rough surface due to marine growth. Marine growth was assumed to be 40 mm thick over the full height of the foundation structure above the mudline.
- The effect of breaking waves was not considered because the maximum wave height is less than the depth-limited wave height (approximately 0.78 times water depth [DNV-OS-J101, section 308].
- Current forces acting on the foundation were assumed negligible.
- The interface elevation is assumed +11.5 m above the sea level to avoid waves slamming onto the service platform.

Ice forces on structures can be very significant in offshore wind farms. Ice force calculation is dependent on ice mechanical properties, structural characteristics of the ice and calculation methods. Ice strength characteristics vary based on temperature, salt content, density and other parameters.

Table 7.5 shows the ice parameters used for the concept design work.

Table 7.5. Ice properties [Marrone et. al., 2013].

Property	Value (SI)	Source
Density (kg/cu.m)	999.8 (Horz./Vert. Force) / 916 (Ridge Force)	
Ice-concrete dynamic frictional coefficient	0.15	IEC 61400-3, 2009
Compressive strength (MPa)	4.4	C-CORE, 2008
Flexural strength (MPa)	1.76	Timco, G.W. and O'Brien, S. 1994
Level of ice thickness (m)	0.618	IEC 61400-3, 2009 NDBC Station DBLN6
Consolidated ice layer thickness (m)	0.927	C-CORE, 2008
Sail thickness (m)	N/A	
Keel thickness (m)	11.2	C-CORE, 2008

Ice loads can occur due to a number of mechanisms as discussed in Chapter 5 and in [Wells, 2012]. In the Great Lakes, loads from both sheet ice and ridge ice should be considered.

Sheet ice loading is well documented in a number of design standards, including DNV-OS-J101 and IEC 61400-3. However, ice ridges are not well understood with significant uncertainty in theoretical approaches and experimental data, as mentioned in Chapter 5. There are several design methods to determine ridge ice loads, but in this preliminary design stage the method proposed by Brown & Seify [2005] was selected. The Brown & Seify [2005] method is based on an empirical formula derived from full scale field measurements on a structure with an upward breaking ice cone. Because an upward breaking ice cone was also incorporated in the GBF, this method was appropriate for the concept design.

Table 7.6 summarizes the results of the ice load calculations.

Table 7.6. Summary of ice loads [Marrone et al., 2013].

Ice Force	Value (MN)	Value (kips)	Reference
Horizontal sheet ice force	1.6	359.7	DNV-OS-J101
Vertical sheet ice force	0.7	157.4	DNV-OS-J101
Horizontal ridge ice force	3.0	374.4	Brown T.G. and Seify, M. El., 2005

Prior to finalizing the foundation design, however, site-specific ice research should be conducted to better understand ice loads. This could include scale model testing to confirm the Brown & Seify [2005] model.

Given the anticipated design ice parameters, a preliminary sensitivity analysis of the ice cone size and angle was conducted (Figure 7.9). Assuming a constant column diameter, the outer diameter of the ice cone grows as the angle increases. This growth is necessary to maintain a constant height of the ice cone, so the ice will contact the cone in the range of site water levels. As the ice cone angle increases (reference: 0 degrees being horizontal and 90 degrees being vertical, or the absence of an ice cone), a number of effects are observed, wave load decreases, ridge ice force decreases, sheet ice forces increase.

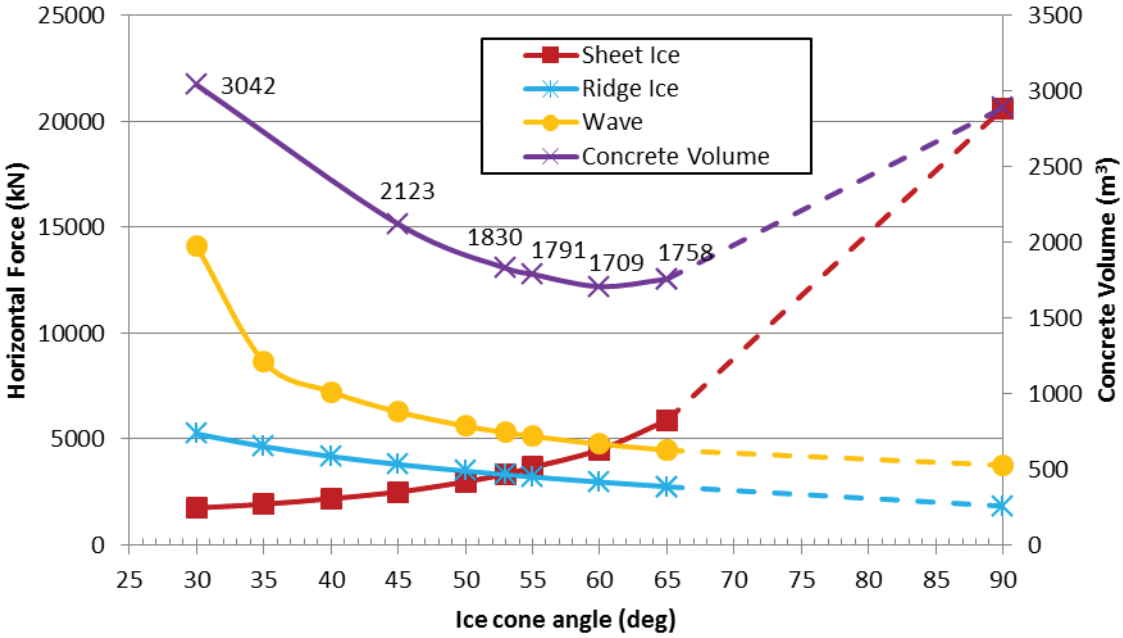

Figure 7.9. Variation of horizontal forces and concrete volumes with ice cone angle [Marone et al., 2013].

Note that as the ice cone angle decreases to improve the performance against the sheet ice, the wave and ridge ice effect is greater on the larger structure because of its larger cross section. A 53 degree ice cone angle provides a reasonable overall structure weight while maintaining a factor of safety appropriate for the concept level design and assumptions [Marone et al., 2013]. Lower foundation weight is anticipated to result in a lower foundation fabrication cost, which will ultimately result in an overall lower cost of energy.

Here, the effects of wave and ice loads on a monopile platform are compared with those on a GBF. Based on Morison's equation for a cylinder, the fluid force per unit length can be written as follows [Ochi, 2005],

$$F(t) = C_D \rho \frac{D}{2} v(t)^2 + C_M \rho \pi \frac{D^2}{4} a(t) \tag{7.4}$$

The first term in the above equation is the drag force, and the second term represents inertia force. The inertia force is the force exerted by the fluid while it accelerates and decelerates as it passes the structure. The drag force is a function of velocity (v) while the inertia force depends on acceleration (a). In Eq. (7.4), the diameter of the cylinder is denoted by D, and density, drag and inertia coefficients are denoted by ρ, C_D and C_M, respectively.

Inertia and drag coefficients are functions of the Reynolds number, surface roughness, and Keulegan-Carpenter number [Ochi, 2005]. Both velocity and acceleration of the incident waves vary with time, and their maxima do not occur at the same instant, because there is a phase difference between them.

The diameter for the monopile platform developed by the NREL is approximately 6 m, while the diameter of the GBF would be in the range of 12 m, as shown in the next section. Therefore, based on Eq. (7.4), the drag force for the gravity foundation should be 2 times that for the monopile, and the inertia force would be 4 times of that for the monopile. However, the maximum drag force does not occur when maximum inertia force occurs. Still, the maximum difference would be significant.

For ice loads, a gravity foundation design using an upward ice cone reduces the loads dramatically. However, the large diameter of the column increases the wave loads significantly compared with a monopile design. In the monopile concept, wave loads are smaller but ice loads without ice cones would be extremely high.

7.4 Description of Foundation

The GBF designed to support the downwind, 2-bladed rotor wind turbine for this project is a semi-floating type. The semi-floating GBF consists of, from bottom to top: a base plate, a buoyancy chamber, a taper zone, a column (with ice cone), and a service platform. The semi-floating GBF was selected primarily due to regional logistical constraints to install the GBF with locally available construction equipment.

Weights and Dimensions

As shown in Figure 7.10, the overall GBF height is 36.1 m. The base plate is 1 m thick by 25 m in diameter and forms the floor of the buoyancy chamber. The buoyancy chamber is 6 m tall. The main column is 7 m in diameter. The GBF will be filled with ballast sand to 5 m from the interface elevation.

The unballasted reinforced concrete GBF weighs approximately 4400 tonnes. Transporting and maneuvering a fully-fabricated, 4400 tonne GBF require specialized equipment and vessels. The floating-type structure weighs considerably less once the buoyancy chambers are floated, allowing transportation and placement with available vessels and equipment in the region. Ballast accounts for an additional 4990 tonnes when filled at the site. For further information on construction and installation methods, refer to Marrone, et al. [2013].

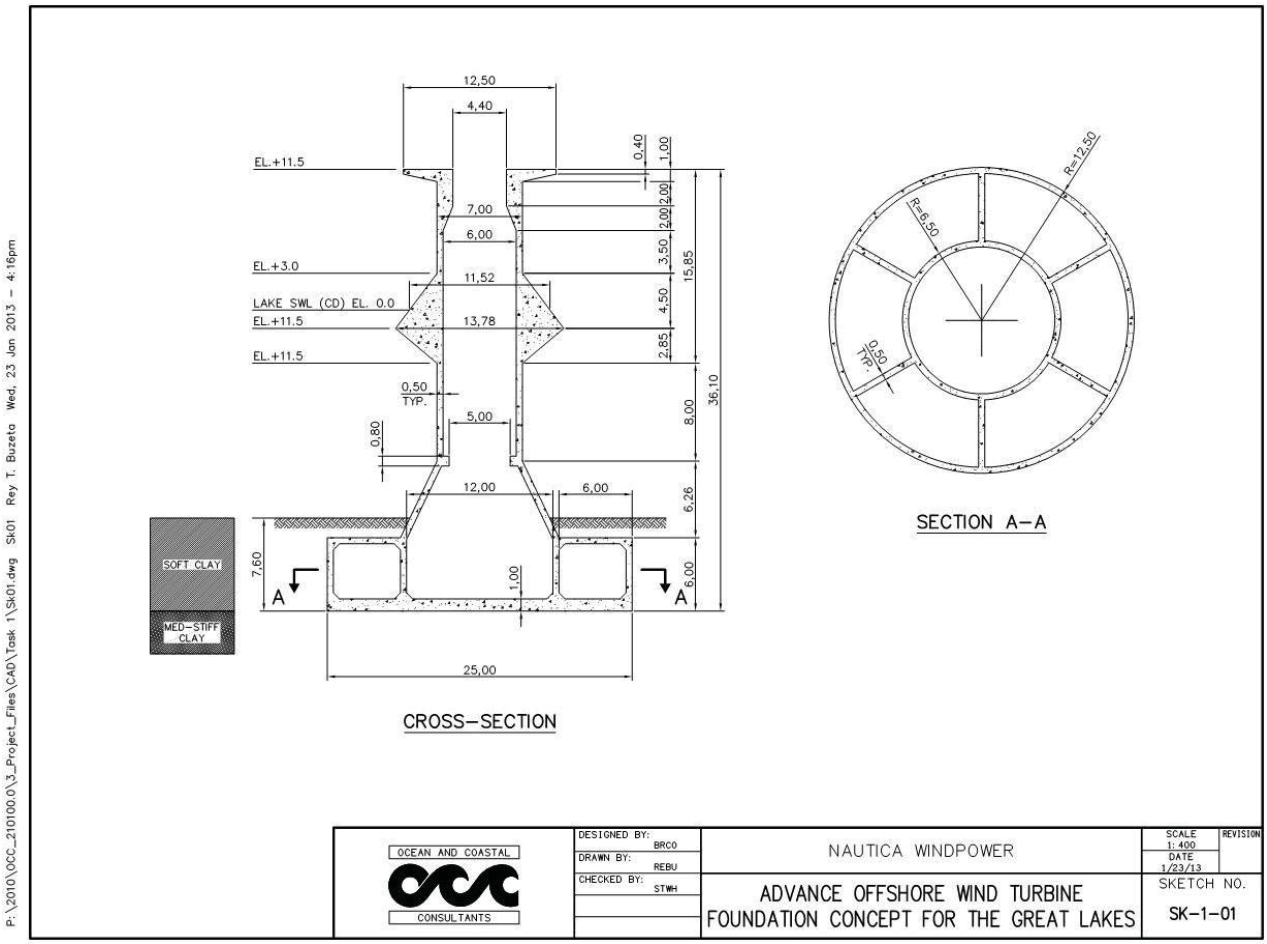

Figure 7.10. GBF dimensions [Marone et al., 2013].

8 Cost Model

This chapter presents the cost analysis conducted to assess potential economic advantages of the downwind, 2-bladed wind turbine design concept. This analysis is necessary in order to draw credible conclusions on the designs since, although reducing the number of blades from 3 to 2 (i.e., the idea of removing one blade for the rotor) is simple conceptually, the effects cascade throughout the system. The complexity of these changes to components such as the gearbox, generator and tower were not examined rigorously in this work, but they have an impact on the cost offshore wind energy.

This chapter discusses the methods and the rationale used to estimate the cost of energy of three wind turbine designs, the description of models considered and cost analysis. The three turbine models considered were:

1. A Baseline 3-bladed wind turbine, based on the NREL Offshore 5MW wind turbine (3B)
2. The University of Toledo 2-bladed rotor design (2BUT), based on the design studies presented throughout this report
3. An optimized 2-bladed wind turbine that takes into account further improvements expected when a 2-bladed rotor is used, but not rigorously analyzed in this work

The analysis is grouped into two main areas:

1. Foundations
2. System Availability

The foundation cost is the largest single component of the total cost for an offshore wind turbine. The drivetrain has the largest capital cost, but is comprised of 11 components. The foundation is the second most expensive component behind the drivetrain, but is comprised of only one component. In addition, the foundation has its own installation cost. Its installation is only slightly less costly than that of the entire wind turbine. Even small decreases in the foundation cost, can have a large effect on the overall cost of the wind turbine system.

System availability increases using a 2-bladed rotor. As a rule of thumb, there is a 1-2 percent energy production difference between a 3- and 2- bladed wind turbine rotor. This percent difference is only based on the rotor aerodynamic energy production. It does not account for system losses, or down-time due to failures or maintenance of the system. When the failure rates and days down due to failure are taken into account the difference between the energy productions from 3- and 2-bladed is reduced.

8.1 Model Descriptions

This section briefly describes the three models used in the cost analysis.

8.1.1 Baseline 3-Bladed Design (3B)

8.1.1.1 Basic Characteristics

The Baseline wind turbine used in this model is created using the NREL 5MW Offshore Wind Turbine [Jonkman, et al., 2009]. As the exact location of the wind turbine has not been chosen, "best judgment" values for the principal parameters were selected. The published value of Coefficient of Power (Cp) is 0.482. For this study, a Cp of 0.4867 was used. This value was obtained from the program WT_Perf, which was used to determine the Cp values for the blades used in the 2-bladed rotor wind turbines. The increased Cp value for the Baseline was used to maintain consistency.

Table 8.1. Baseline (3B) NREL 5 MW wind turbine.

Baseline 3B		
Rotor Radius (m)	-	63
Hub Height (m)	-	100
System Life (years)	-	20
Foundation	-	NREL estimate Monopole
Distance to Shore (m)	-	15
Anemometer Average Wind Speed (m/s)	-	7.2
Anemometer Height (m)	-	50
Wind Shear Factor	-	0.14
Average Wind Speed at Hub (m/s)	-	7.93
Control	-	Pitch-to-Feather
Generator	-	High-Speed

8.1.1.2 Balance of System (BOS)

Balance of System includes everything that is needed to operate a wind turbine, other than the wind turbine. This includes: hardware needed to connect the turbine to the grid, transportation, installation and other requirements such as permits, and decommissioning.

Hardware

Cost estimates for the BOS hardware were based on information in the NREL cost scaling study [Fingersh et al., 2006].

Transportation

Transportation costs were estimated based on the delivery of the components to the port staging and assembly area. There is transportation cost associated with getting the components to the offshore installation site. The cost of offshore transportation is calculated in the installation estimate. For simplicity, it was assumed that the turbine would be transported in 8 sections: 3 blades, 1 hub, 1 nacelle, 3 tower sections.

Installation

The installation estimate used in this analysis is based on the engineering approach in the "Offshore Wind Energy Installation and Decommissioning Cost Estimation in the U.S. Outer

Continental Shelf" report. The estimate is broken into two parts, foundation and turbine installation. An estimate for cable laying is currently not included, but that cost is the same regardless of the turbine design and does not influence the comparative cost of energy. The values for foundation and turbine installation are added together to provide an estimated cost for turbine installation. Values chosen for the analysis were:

Table 8.2. Baseline (3B) installation inputs.

Installation Values (3B)		
Main Installation Vessel Type	-	Self-Transport Jack-up Barge
Number of Tugs	-	2
Number of Barge	-	0
Number of Crew	-	3
Installation Time Foundation (hrs)	-	96
Vessel Capacity (turbines)	-	2
Installation Time Turbine (hrs)	-	120
Number of Lifts for Turbine Installation	-	4

Other

Cost estimates for the BOS were based on information in the NREL cost scaling study.

8.1.1.3 Repair and Maintenance

The repair and maintenance cost of the analysis is divided into 6 different parts:

1. General Scheduled Maintenance – This includes visual inspection of major components and joints, inspection/test of electrical connections, lubrication services, and operating tests including emergency shutdown. To estimate the cost of these actions, the number of days the turbine is "down" or not operational is estimated. Then the day rate of a support/engineering vessel needed for the action is multiplied by the number of days down to determine a cost.

2. Bottom Lease – Based on annual energy production

3. Plant Operation – Based on annual energy production

4-5. Unscheduled Turbine Maintenance and BOS Maintenance – Uses a logic similar to the General Maintenance. However, unlike the General Maintenance, which occurs at a scheduled time, values of the Annual Fail Rate from UpWind and Faulstich reports were used to determine the maintenance frequency. Like the General Maintenance cost the number of days down is used to estimate a cost based on vessel day rates. Unlike General Maintenance, the cost of the component multiplied by a "repair costs factor" was used to determine the amount of money spent on labor instead of replacing the component.

6. Administrative and Support – Based on annual energy production

8.1.1.4 Levelized Replacement Cost

Levelized Replacement/Overhaul Cost calculates the cost of major component replacements or overhauls over the lifetime of the turbine. For this analysis, three components were used to calculate replacement costs in the future: blades, gearbox, and generator. For this analysis, the method outlined in the United States Department of Energy FOA 0000415 (Appendix E) was used for calculating the Levelized Cost of Energy (LCOE).

The time for replacement was chosen using values from Faulstich's paper. These values were chosen as 8 years for blades, gearbox, and generator. Also included in the cost of replacement is the number of days the turbine is unavailable. This affects both the upfront capital expense and the availability of the wind turbine.

8.1.2 UT Design (2BUT)

8.1.2.1 Basic Characteristics University of Toledo Design (2BUT)

For the purpose of the cost analysis, the simple design changes of removing one blade and changing the orientation from upwind to downwind was considered for the UT Design (2BUT).

The design changes to the baseline wind turbine performed by the University of Toledo (UT) are listed below:

Table 8.3. University of Toledo design (2BUT).

2BUT		Scaling Logic
Blades (Total All)	-	Removed one Blade
Pitch mechanism & bearings	-	Removed one Pitching mechanism

Completed but not included this analysis:

- Added Teeter Mechanism
- Reduced Shaft Tilt
- Added Tip-Brakes

Removal of One Blade

Removal of one blade also means the removal of one pitch control mechanism. The blade used in this cost analysis is representative of the blade used in the engineering design (2BUT). The NREL 5 MW blade was designed for a 3-bladed rotor. When a blade designed for a 3-bladed rotor is used in a 2-bladed rotor the efficiency decreases. Blade design is complicated and dependent not just on aerodynamics and structural mechanics, but also the limitations of materials and construction. Use of the 2BUT blade is the first step towards improving efficiency of the NREL 5MW blade for a 2-bladed rotor. For the 2BUT blade the twist angle was changed to somewhere between the existing NREL blade twist and a more optimal twist angle for a 2-bladed rotor. As mentioned earlier, the Cp for the 2BUT blade was found equal to 0.4728, using

WT_Perf. The NREL blade has a published Cp value of 0.4820. It was found during analysis, using WT_Perf in the same way as was done for the 2BUT blade, that the NREL blade has a Cp value of 0.4867. This discrepancy should be taken into account when assessing the results.

8.1.2.2 Balance of System (BOS) University of Toledo Design (2BUT)

Transportation

Transportation costs were reduced by the scaling factor of 7/8. By removing one blade, one-less component needs to be transported. This is a conservative estimate. Transporting blades is complicated. Indeed, unlike other components, blade size limits the routes and types of vehicles or vessels and personnel needed for transportation.

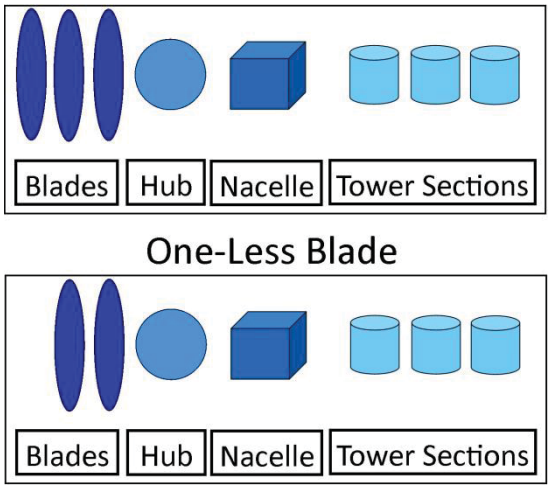

Figure 8.1. Transportation assumption 3 and 2 blades.

Installation

Installation costs were estimated similarly as the baseline with two changes:

Vessel capacity was increased by 12.5%, because if one less blade was needed for the rotor, there would be two extra blades left on the vessel after installation of the turbine.

Installation time was decreased by 25%, because of having to preform one-less lift to install the turbine. See Figure 8.2.

Table 8.4. University of Toledo design (2BUT) installation inputs.

Installation Values (2BUT)		
Vessel Capacity (turbines)	-	2.25
Installation Time Turbine (hrs)	-	90
Number of Lifts for Turbine Installation	-	3

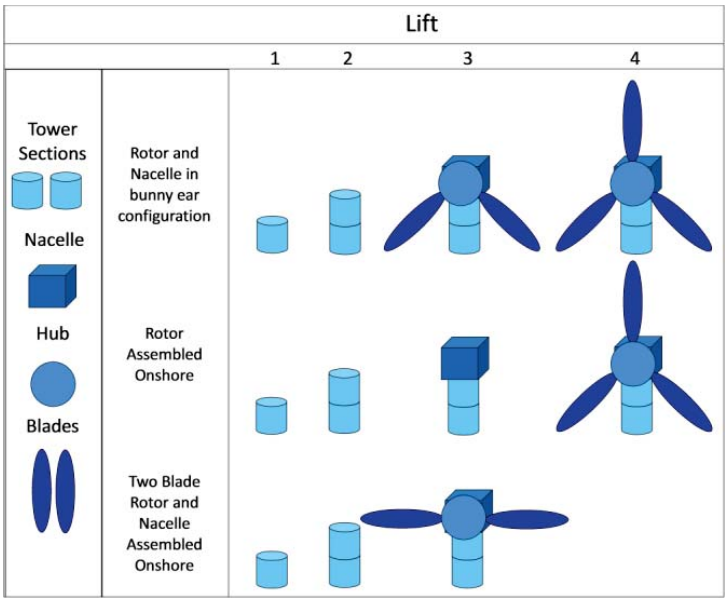

Figure 8.2. Installation assumption.

8.1.2.3 Repair and Maintenance University of Toledo Design (2BUT)

The repair and maintenance estimate changed the annual failure rates of two component; blades and pitch mechanism. The other 5 parts of the operation and maintenance cost estimates remained the same as those of the baseline.

It was assumed that with one-less blade the annual failure rate would decrease by a third.

Table 8.5. University of Toledo design (2BUT) repair and maintenance assumptions.

2BUT		Unscheduled Scaling Factor
Blades	-	One-Less Blade reduces annual failure rate by one third
Pitch	-	One-Less Blade reduces annual failure rate by one third

8.1.2.4 Levelized Replacement Cost University of Toledo Design (2BUT)

The levelized replacement costs for the gearbox and generator remained the same as the baseline (3B). The blade replacement time was increased from 8 years to 12.

8.1.3 Optimized Design (2BOPT)

8.1.3.1 Basic Characteristics Optimized Design (2BOPT)

For this analysis, the model builds on the changes of the UT design that removed one blade and pitch mechanism. In addition, blade efficiency was raised and changes to other components were made.

Table 8.6. Optimized design (2BOPT).

2BOPT		Scaling Logic
Blades (Total All)	-	Removed one Blade
Pitch mechanism & bearings	-	Removed one Pitching mechanism
Low speed shaft	-	Reduced by Ratio of Rotor Costs
Bearings	-	Reduced by Ratio of Rotor Costs
Gearbox	-	Reduced based on lower Torque - Cost reduced based on Ratio of Gearbox Mass
Yaw drive & bearing	-	Reduced 20% Teeter alleviates Yaw Moment
Main frame	-	Reduced by Ratio of Rotor Costs
Marinization	-	(10.00% of Turbine and Tower System)

Increased Blade Efficiency

In addition to removing one blade from the rotor, the blade's efficiency was increased from a Cp of 0.4728 to 0.4791. The changes to efficiency of the rotor were based on improving the chord and twist distributions using blade momentum theory. Changes to the other components on top of the turbine were based on the reduction of mass of the rotor, or the increase of rotor speed reducing torque delivered to drivetrain, and the use of a teeter mechanism (in the case of the yaw control mechanism).

8.1.3.2 Balance of System (BOS) Optimized Design (2BOPT)

Transportation

Remained the same as that of the UT Design (2BUT).

Installation

Remained the same as that of the UT Design (2BUT).

8.1.3.3 Repair and Maintenance Optimized Design (2BOPT)

In addition to the changes to the annual failure rates for the blade and pitch mechanism for the 2BUT design, the following changes were made for the 2BOPT design:

Table 8.7. Optimized design (2BOPT) repair and maintenance.

2BOPT		Unscheduled Scaling Factor
Blades	-	One-Less Blade reduces annual failure rate by one third
Gearbox	-	Higher RPM lowers torque and gear ratio Improving System Life; reduced 20%
Drivetrain	-	Higher RPM lowers torque; one less blade reduces mass of rotor; reduced 20%
Mainframe & Nacelle Cover	-	Reduced based on capital cost of Mainframe
Yaw system	-	Yaw Moment decreased with addition of teeter mechanism; reduced 20%
Pitch	-	One-Less Blade reduces annual failure rate by one third

8.1.3.4 Levelized Replacement Cost Optimized Design (2BOPT)

The Levelized replacement cost added increased the gearbox life similarly to the changes of the 2BUT design. The gearbox replacement time increased from 8 years to 10. This reduced the number of times the gearbox needed to be replaced from 2 to 1.

8.2 Summary

As will be shown in Chapter 9, using cost of energy as the suitable measure of merit, this report shows that there is a 9.9% decrease in Levelized Cost of Energy (LCOE) by simply removing one blade from the rotor. Additional cost benefits are possible with other improvements. These decreases in cost form a strong case to consider using two blades in an offshore environment.

9 Results and Discussion

The objectives of this chapter are to assess the safety, annual energy production and cost of 2-bladed upwind and downwind turbine designs and compare them with those of the baseline 5MW 3-bladed turbine. For this purpose, the responses of the baseline and the proposed 2-bladed designs to the environmental loads prescribed by IEC, and the annual energy production were calculated using the computational tools and methods presented in Chapter 4. Finally, the cost of energy for the above three basic design configurations was calculated in order to assess the economic viability of the proposed 2-bladed downwind design.

Chapter 9 consists of four sections. The performance of the wind turbines in this study is presented in Section 9.1. This includes analyses and comparisons of maximum forces and moments, fatigue life, tower-to-blade clearance and teeter angle of 16 wind turbine models in Figure 9.1 and Table 9.1. In addition, the effect of changes in the number of blades, rotor position relative to the tower (upwind and downwind), teeter parameters, rotor brake, shaft tilt and cone angles, and changes in the blade designs are discussed. Section 9.2 presents the forces and moments applied to the foundation for the three configurations in this project. Section 9.3 presents and compares the annual energy production and cost. Based on the results, a final 2-bladed downwind design is proposed. Finally, Section 9.4 summarizes the main observations.

9.1 Analysis of Turbine Designs

This section analyses the performance of the three alternative basic turbine designs in this project along with parametric studies used to select the final design. The results include maximum forces and moments, fatigue life, tower-to-blade clearance and teeter angle.

A series of FAST simulations were performed for the wind turbine models for the selected design load cases (DLCs). The FAST_SM code, which is introduced in Section 4.1, was used to manage all FAST simulations. The DLC for normal operation, fault, and parked conditions were explained in Section 5.4. The wind turbine designs used in the simulations were explained in detail in Chapter 6. Because of the large number of simulations, only important results are presented. The complete set of results is in Appendix 8.

Wind Turbine Configuration Models

Using the three basic wind turbine configurations (3-bladed upwind, 2-bladed upwind and 2-bladed downwind), various wind turbine models are made by considering different combinations of the following attributes:

- Number of blades
- Upwind/downwind position of the rotor
- Blade design (baseline and BUT blades)
- Shaft tilt angle
- Conning angle
- Teeter parameters
- Use of tip-brake

Figure 9.1 defines the wind turbine configurations considered in this study. A total of 16 different wind turbine models were compared in this section in order to investigate the effects of the above design attributes on the performance and safety. Table 9.1 describes the wind turbine models employed in this investigation. The effects of the design parameters of the wind turbine models in Table 9.1 were studied by changing these parameters and calculating the resulting changes in the forces and moments, fatigue life, tower-to-blade clearance, and teeter angle. However, the effect of different types of brakes on fatigue life was not investigated because this effect is small. The 3-bladed upwind turbine model (5MW3UB00) is the baseline model. The responses of the alternative models are compared with the baseline. Appendix 1 provides details about the design attributes of all 16 wind turbine models in this study.

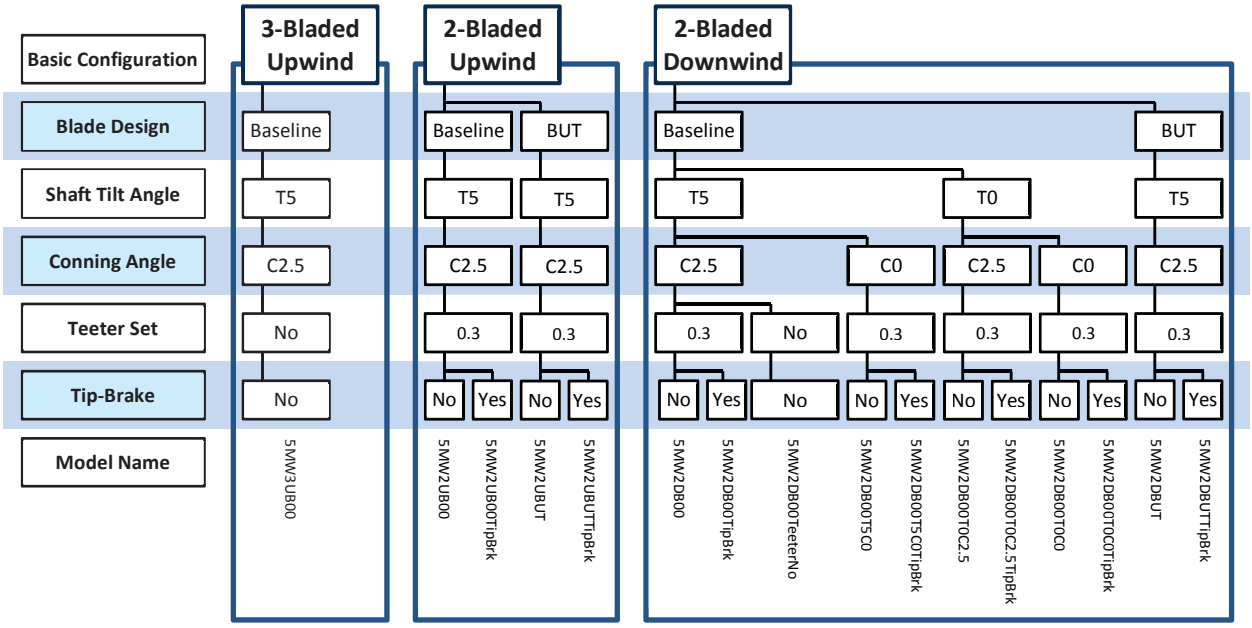

Figure 9.1. Variations of wind turbine configuration models.

Table 9.1. List of wind turbine models.

#	Model	Rating	Num. of Blades	Wind Direction	Blade Model	Tilt (deg)	Cone (deg)	Teeter Set	Tip Brake	Tower Shadow
1	5MW3UB00	5MW	3	Up	Baseline	5	2.5	No	No	No
2	5MW2UB00	5MW	2	Up	Baseline	5	2.5	0.3	No	No
3	5MW2UB00TipBrk	5MW	2	Up	Baseline	5	2.5	0.3	Yes	No
4	5MW2UBUT	5MW	2	Up	BUT	5	2.5	0.3	No	No
5	5MW2UBUTTipBrk	5MW	2	Up	BUT	5	2.5	0.3	Yes	No
6	5MW2DB00	5MW	2	Down	Baseline	5	2.5	0.3	No	Yes
7	5MW2DB00TipBrk	5MW	2	Down	Baseline	5	2.5	0.3	Yes	Yes
8	5MW2DBUT	5MW	2	Down	BUT	5	2.5	0.3	No	Yes
9	5MW2DBUTTipBrk	5MW	2	Down	BUT	5	2.5	0.3	Yes	Yes
10	5MW2DB00T5C0	5MW	2	Down	Baseline	5	0	0.3	No	Yes
11	5MW2DB00T5C0TipBrk	5MW	2	Down	Baseline	5	0	0.3	Yes	Yes
12	5MW2DB00T0C2.5	5MW	2	Down	Baseline	0	2.5	0.3	No	Yes
13	5MW2DB00T0C2.5TipBrk	5MW	2	Down	Baseline	0	2.5	0.3	Yes	Yes
14	5MW2DB00T0C0	5MW	2	Down	Baseline	0	0	0.3	No	Yes
15	5MW2DB00T0C0TipBrk	5MW	2	Down	Baseline	0	0	0.3	Yes	Yes
16	5MW2DB00TeeterNo	5MW	2	Down	Baseline	5	2.5	No	No	Yes

Design Load Cases

Twelve DLCs are considered in this study as defined in Section 5.4. These are organized into three groups:

1) **Normal operating conditions**:
   DLC1.1, DLC1.3, DLC1.4, DLC1.5H (horizontal wind shear), and DLC1.5V (vertical wind shear)
2) **Fault conditions**:
   DLC2.1G (grid fault), DLC2.1P (pitch controller fault of one blade), and DLC2.3
3) **Parked conditions**:
   DLC6.1a, DLC6.2a, DLC6.3a, and DLC7.1a

Locations of Interest

There are six locations of interest:

- Tower base
- Tower top
- Blade roots (Blade 1 and Blade 2)
- Shafts
  - Low-speed shaft (LSS)
  - High-speed shaft (HSS)
  - Generator

Forces and moments are computed at the four different locations of interest; tower base, tower top, blade roots, and LSS. The tower base is located 11m above the water surface, which is co-located with the top of the foundation. Torque values at the LSS and HSS, and generator are recorded. The terms "LSS torsional moment" and "LSS torque (rotor torque)" refer to the same quantity and are used interchangeably in this report.

DLC2.1 and DLC7.1a include failure of the pitch controller of one blade, and require checking the loads on both blades. Therefore, simulation results for two blades are collected because the load effect at the roots in all blades of a turbine are considered together by selecting the maxima and the minima between the two blades. This is because the structural design of rotor blades is assumed identical and a blade can be at any azimuth position.

Definition of Load Effects

In a FAST simulation, the tower, blades and shafts are modeled as beams. Three forces and three moments are calculated at each location along a beam at the tower base, tower top, blade roots, and LSS. In this research, these six internal loads are converted into four *load effects* (Appendix 4). The term *load effect* refers collectively to the following four types of internal loads in this report:

- Shear forces
- Bending moments
- Axial forces
- Torsional moments

These load effects are calculated at the tower base, tower top, blade roots, and LSS. The root mean squared (RMS) values are used for shear forces and bending moments to combine shear forces or bending moments in two different directions. This calculation is valid because the cross-sections at the locations of interest are circular and the structural properties are homogeneous. Although composite materials are used in the blades, the structural properties are assumed homogeneous at the blade root. The complete definitions of the load effects are described in Appendix 4.

A total of 18 different load effects and torques are collected from the FAST simulations. These are the axial and shear forces, and the bending and torsional moments at the four locations of interest, and the torques at the HSS and generator. These 18 load effects are compared to the ultimate load to assess the structural safety of the turbine. In fatigue life estimation, the same load effects are considered except for the torques.

In many parametric studies, shear and axial forces, and bending and torsional moments change in the same direction. In these cases, we only discuss the collective effect of this change on these all of these load effects.

Ultimate Load Effects and Torques

Maximum load effect and torque data are placed for the 16 models in Table 9.1. These results were used to examine the extreme load effect on the wind turbine structure under various conditions. The most vulnerable state of a wind turbine model can be found by analyzing these quantities. The FAST results were sorted using the DLC post-processor code, which was

introduced in Section 4.2. Maximum, minimum, maximum of average values and minimum of average values were sorted from the FAST simulation results. A total of 13,824 maximum, minimum, maximum of average, and minimum of average values were obtained from 18 different load effects and torques, 16 models, and 12 DLCs (4×18×16×12 = 13,824).

The maximum and the minimum load effects are the maximum and minimum load effect values in a time marching output of a FAST simulation. If there are multiple *replications* for a particular *simulation condition*, the corresponding maximum and the minimum values are averaged. A *simulation condition* is defined by a set of a wind condition, a wave condition, and wind turbine settings within a DLC as described in Figure 4.1 in Section 4.1. A simulation condition can have one or multiple *replications*. The only difference among the different replications of a simulation condition is in the random seeds that are used for generating time histories of the wind and wave inputs. Also, the average load effect is estimated from a time marching output of a FAST simulation. Similar to the maximum and minimum load effects, if there are multiple replications for a simulation condition, the average loads are averaged within a simulation condition. Within a DLC, the maximum and the minimum load effects, and the maximum and the minimum average load effect are sorted. Again, among the sorted load effects in a DLC, the four types of load effects are sorted for the normal operating, fault, and parked conditions groups respectively. Because the maximum and the minimum load effects are sorted using data from various simulation conditions, the average load effects also have ranges for each average load effect for the various DLCs. All of these processes are completed using the DLC post-process code using the outputs from FAST_SM code (Sections 4. 1 and 4.2). These maximum, minimum, maximum of average, and minimum of average load effects are used for the ultimate load effect analyses.

Fatigue Life

To perform the fatigue life estimation analysis load effect data from 9 wind turbine models were used. These include models 1, 2, 4, 6, 8, 10, 12, 14, and 16 in Table 9.1. In the fatigue analysis the time marching data from the FAST simulations corresponding to the DLC2.1 only were considered. Time marching data of 4 types of load effects at 5 locations of interest were input into MLife to estimate the fatigue life of the selected wind turbine models. The effect of torsional moment is neglected in the fatigue life estimation.

Minimum Tower-to-Blade Clearance and Maximum and Minimum Teeter Angles

The minimum tower-to-blade clearance and maximum and minimum teeter angles in all 12 DLCs were computed from the selected 16 different wind turbine models. These are the same as the models used for the ultimate load effect analyses. The results were prepared with the DLC post-processor code of Section 4.2 using the FAST simulation time marching outputs. The DLC post-processor code was used to process data for minimum tower-to-blade clearances and the maximum and minimum teeter angles.

Data Presentation

Weighted percent difference graphs are employed in this report in order to easily compare the aggregate change in the load effects for different designs. This type of graphs shows the trends of load effects at the locations of interest in a given condition. Appendix 7 explains in detail the weighted percent difference graphs. Load effect graphs are also used for the cases where detailed load effect results need to be presented. The load effect graph shows the range of maximum and

minimum, and the average load effects. It also shows the *safe limit*, which denotes the maximum load effect for the baseline design scaled by the corresponding load factor. The details of the derivation of the safe limit and the construction of this type of graphs are described in Appendices 5 and 6, respectively.

Figure 9.2 and Figure 9.3 show the weighted percent difference for the load effects. Figure 9.2 is for the maximum and minimum average load effects (average load effects in short expression), and Figure 9.3 is for the maximum and minimum load effects (maximum load effects in short expression). Each figure depicts data for three different conditions; normal operating, fault, and parked conditions. Using these graphs, the difference in load effects and trends for the various design changes will be illustrated and discussed in the following subsections.

Figure 9.4 and Figure 9.5 show torques at the HSS and generator respectively. The generator torque under parked conditions is zero because the generator is off in this condition.

Figure 9.6 shows the minimum tower-to-blade clearance. The green horizontal line of the minimum tower-to-blade clearance in these graphs is the minimum required clearance, which is 3.5 *m*. If the minimum tower-to-blade clearance becomes less than 3.5*m*, then the blade is considered very likely to crash into the tower. The maximum and minimum teeter angles of various models are presented in Figure 9.7. The effect on fatigue life will be discussed in a separate subsection for the various wind turbine models.

The comparison studies are presented throughout Sections 9.1.1 to 9.1.6. Each Section discusses and compares the average load effects, maximum load effects, torques, minimum tower-to-blade clearance, and maximum and minimum teeter angles. For each response, normal operating, fault, and parked conditions are considered and discussed in Figure 9.2 to Figure 9.7. When average load effects and maximum load effects are discussed, the load effects at the tower base, tower top, blade roots, and LSS are presented sequentially within a condition. Moreover, in each section, the torques of HSS, and generator are discussed.

Finally, the tabulated simulation results on load effects, tower-to-blade clearance, and teeter angle are listed in Section 9.1.7. The tabulated values exactly match the magnitude of either maximum or minimum, and maximum of average or minimum of average values of the load effect graphs. Also the tables in Section 9.1.7 include percent differences relative to the baseline model results. Moreover, detailed results that include the corresponding DLC and wind speed information are listed in Appendix 8.

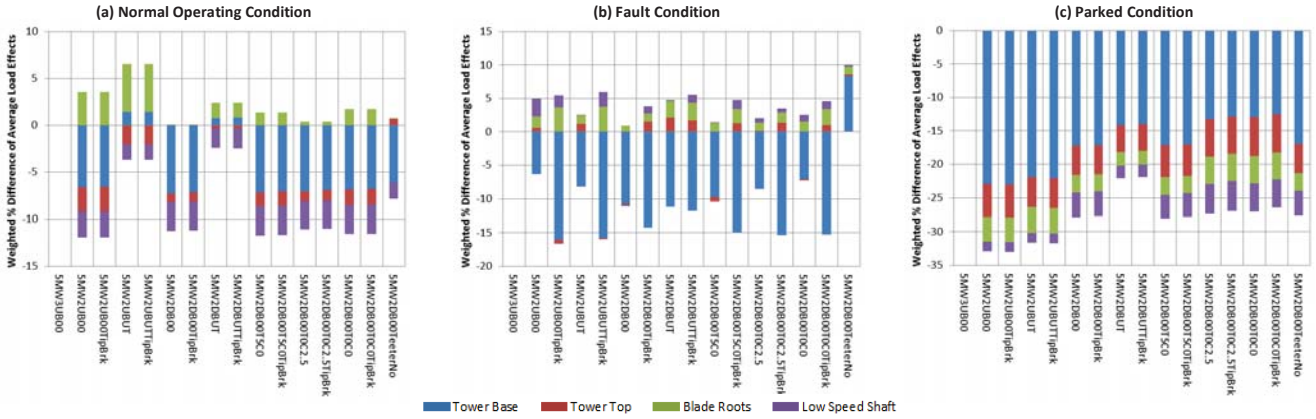

Figure 9.2. Weighted % difference of average load effects under normal operating, fault, and parked conditions.

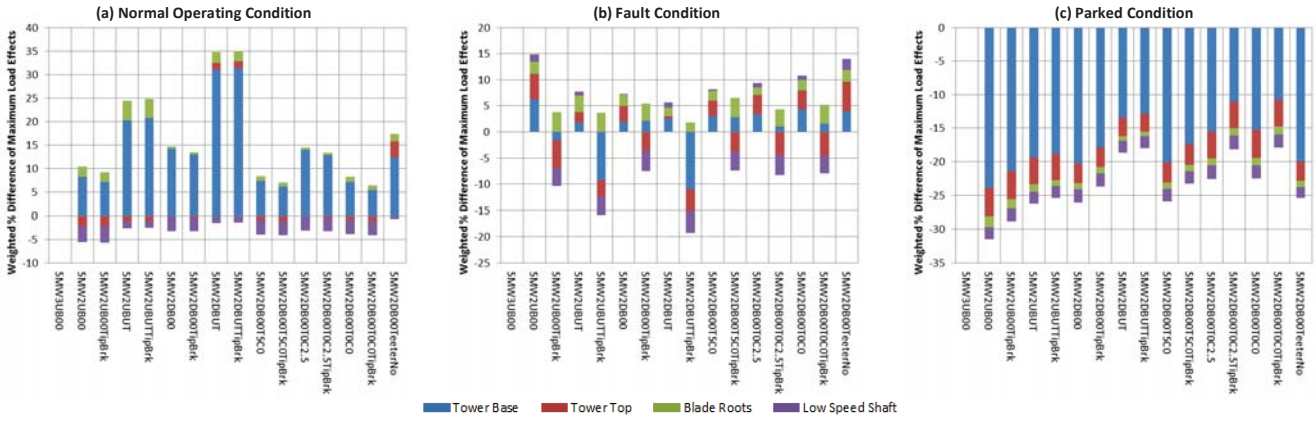

Figure 9.3. Weighted % difference of maximum load effects under normal operating, fault, and parked conditions.

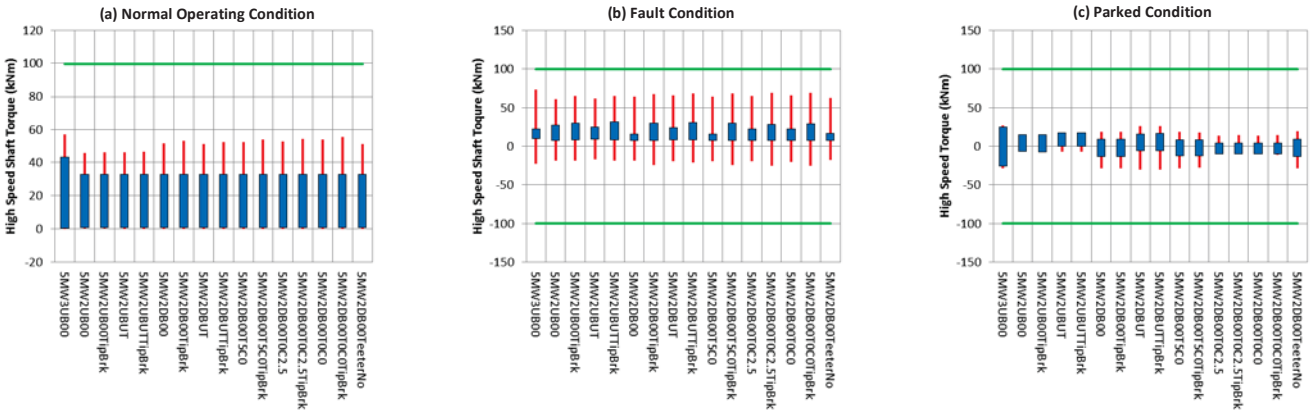

Figure 9.4. Torques in HSS under normal operating, fault, and parked conditions.

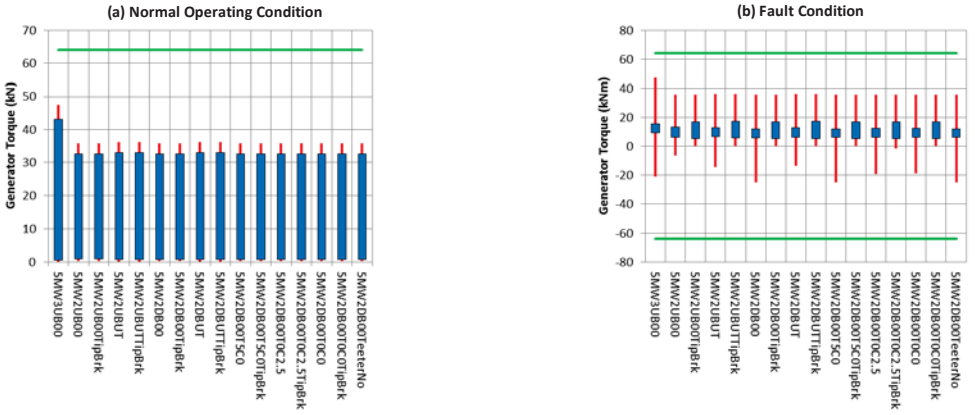

Figure 9.5. Torques of generator under normal operating, and fault conditions.

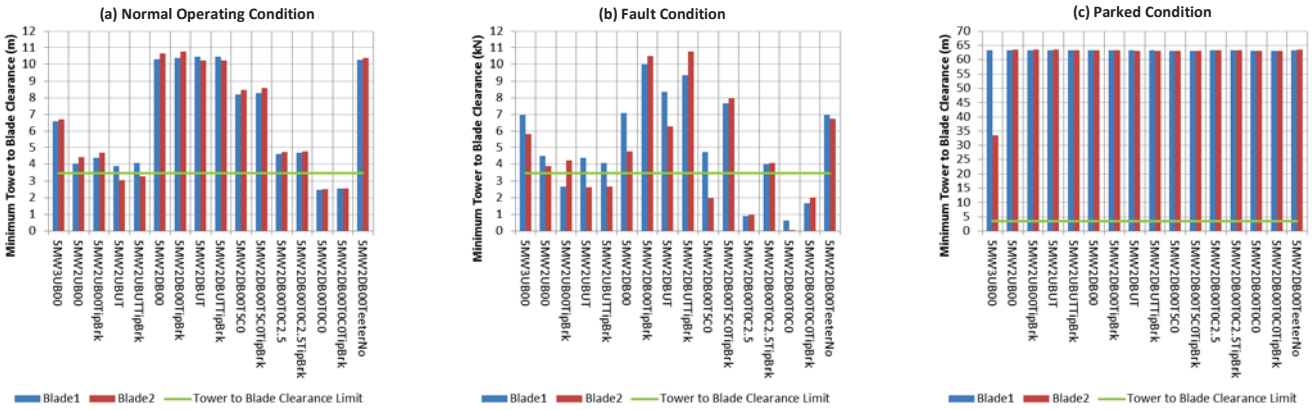

Figure 9.6. Minimum tower-to-blade clearances under normal operating, fault, and parked conditions.

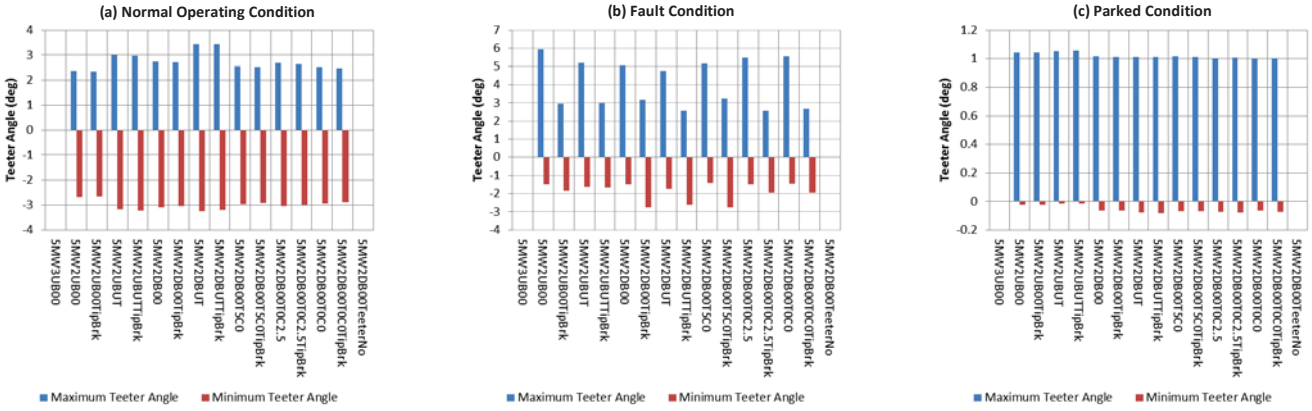

Figure 9.7. Maximum and minimum teeter angles under normal operating, fault, and parked conditions.

9.1.1 Number of Blades

This section investigates the effects of the number of blades on the structural integrity of a turbine. For this purpose, the responses of the 3-bladed baseline model and the 2-bladed wind turbine models are studied. The average load effects, maximum load effects, torques, minimum tower-to-blade clearance, and maximum and minimum teeter angles in normal operating, fault, and parked conditions are presented and compared below.

Average Load Effects

The weighted percent difference of the average load effects in Figure 9.2 (a) shows the effect of changes in the turbine configuration under normal operating conditions. The average load effects at the tower base of 2-bladed machines with baseline blades are lower than those of the 3-bladed baseline model. Under normal operating conditions, all 2-bladed wind turbine models, other than the one with disabled teeter mechanism, have lower average load effects at the tower top than the baseline model. At the blade roots, on the other hand, when only the upwind machines are compared, 2-bladed machines have larger average load effects than the 3-bladed baseline machine. The average load effects at the LSS of all 2-bladed machines are lower under normal operating conditions than the corresponding load effects of the 3-bladed baseline machine. This is because the shaft is rotating faster in the former machines.

Figure 9.2 (b) shows the weighted percent differences of the average load effects under fault conditions. Most of the average load effects at the tower base of the 2-bladed machines are lower than those in the baseline model. If only the 2-bladed upwind model without tip-brake (5MW2UB00) is compared with the baseline model (5MW3UB00), the 5MW2UB00 model has larger average load effects at the tower top under fault conditions. The average load effects at the blade roots of the 2-bladed machines under fault conditions exceed those in the baseline model. This is expected because the rotor spins faster. Overall, the average load effects at the LSS of the 2-bladed machines under fault conditions exceed the load effects of the baseline model.

The weighted percent differences of the average and maximum load effects under parked conditions are shown in Figure 9.2 (c). All 2-bladed machines have lower average load effects for all locations of interest under parked conditions.

Maximum Load Effects

The weighted percent differences of maximum load effects under normal operating conditions are shown in Figure 9.3 (a). In contrast to the average load effects at the tower base, the maximum load effects at the tower base of the 2-bladed machines exceed those in the baseline model. The maximum load effects at the tower top of the 2-bladed models under normal operating conditions are usually lower than those in the baseline model. The maximum load effects at the blade roots for all 2-bladed machines under normal operating conditions exceed those of the baseline model with 3 blades.

As shown in Figure 9.8, all maximum axial forces (vertical red lines) at the blade roots of the 2-bladed machines exceed the safe limit marked by the green line. This is because the rotor of the 2-bladed machines rotates faster than the rotor of 3-bladed machines. The blade should be reinforced so that it can sustain the maximum axial force at its root. Moreover, the maximum and minimum torsional moments in many designs exceed or are close to the safe limit at the blade

roots for the 2-bladed machines as shown in Figure 9.8. The blade root of the 2-bladed models need be reinforced in order to sustain the higher torsional moments of the 2-bladed machines. On the other hand, the maximum load effects for all 2-bladed models are lower at the LSS compared to the baseline model.

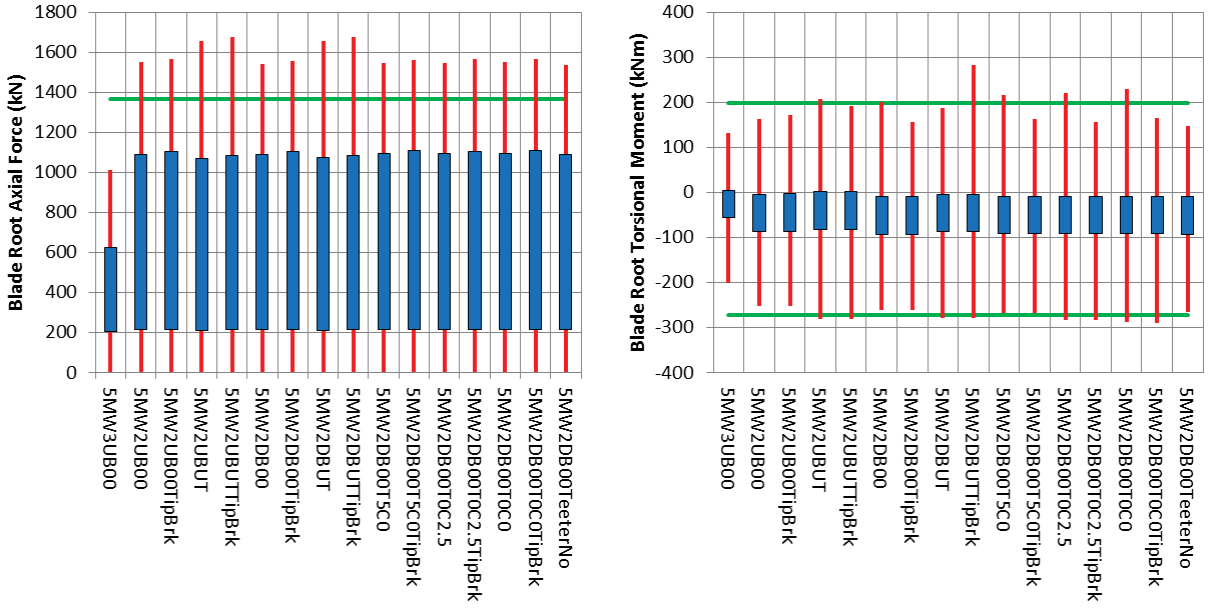

Figure 9.8. Axial forces and torsional moments at blade root of the 5MW wind turbines under normal operating conditions.

The maximum load effects of various models under fault conditions are shown in Figure 9.3 (b). Without tip-brakes, the 2-bladed models have larger maximum load effects at both the tower base and top under fault conditions. However, use of tip-brakes reduces the load effects at the tower top so that these effects become lower for the 2-bladed models than their 3-bladed counterparts. The maximum load effects at the blade roots increase for all models under fault conditions for the 2-bladed machines compared to the baseline model with three blades.

All maximum axial forces, and maximum or minimum torsional moments in the blades of the 2-bladed machines exceed the safe limits as shown in Figure 9.9. On the other hand, all load effects at the LSS are within the safe limits.

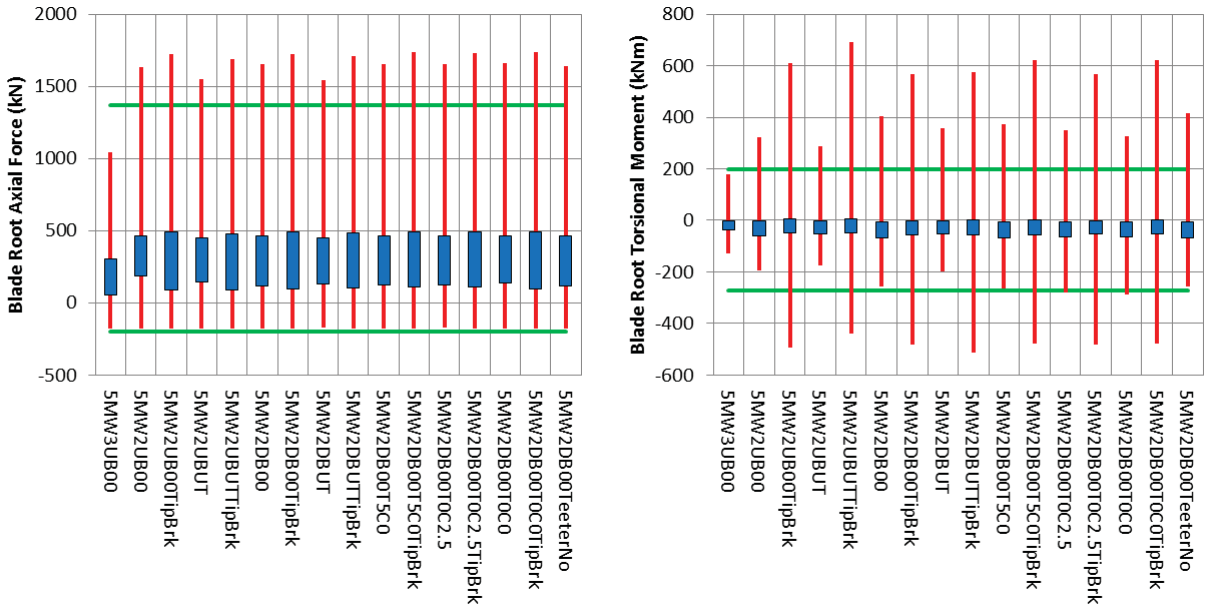

Figure 9.9. Axial forces and torsional moments at blade roots of the 5MW wind turbines under fault conditions.

The weighted percent differences of the maximum load effects under parked conditions are shown in Figure 9.3 (c). Similar to the average load effects, all 2-bladed machines have less maximum load effects at all locations of interest.

Torques

The results in Figure 9.4 show that the average torques of the HSSs of all 2-bladed machines are almost equal under normal operating conditions. The 2-bladed machines have less HSS torque than the 3-bladed baseline machine under normal operating conditions. The maximum torque values of 2-bladed machines are also lower than those of the 3-bladed baseline machine under normal operating conditions. However, under fault conditions, the maximum average torques values of most 2-bladed machines exceed those of the 3-bladed machine. The range of maximum and minimum torque values of 2-bladed machines without tip-brakes are smaller than those of the 3-bladed machine in most of cases under fault conditions. All average torque values of 2-bladed machines are within the range of their counterparts of the 3-bladed baseline machines under parked conditions. Except for the 2-bladed downwind machines with shaft tilt angle equal to 5 degrees, the maximum and minimum torques under parked conditions are comparable to the maximum torques of the 3-bladed baseline machine.

The generator torque values are shown in Figure 9.5. The average generator torque values are almost equal and depend on the number of blades under normal operating conditions. The same is true for the maximum values. The 2-bladed upwind machines have lower average and maximum generator torques under fault conditions than the 3-bladed upwind machine.

Minimum Tower-to-Blade Clearance

The 2-bladed upwind machines have significantly less minimum tower-to-blade clearances than the 3-bladed upwind machine under both normal operating and fault conditions (Figure 9.6). Under parked conditions, because the rotors of the 2-bladed machines are parked at 90° azimuth position, the tower-to-blade clearance of both blades is very large and the risk of impact is practically zero. The same is true for the 3-bladed machine. These are parked at 0° azimuth angle. Blade 2 of 3-bladed machines has clearance approximately equal to half of the rotor radius because the second blade of the 3-bladed machines is located at 120° azimuth angle.

Maximum and Minimum Teeter Angle

The 3-bladed machine has a zero teeter angle because it does not have a teeter mechanism. On the other hand, 2-bladed machines with the teeter mechanism have teeter angles as shown in Figure 9.7. Because the teeter parameters are selected according to the criteria discussed in Section 6.2.5, the teeter angle of 2-bladed machines varies approximately from -3° to 3° under the normal operating conditions, and from -3° to 6° angle under the fault conditions. Also under parked conditions the maximum teeter angle is approximately 1° for the models with teeter mechanism.

9.1.2 Upwind/Downwind Configuration

Upwind machines are compared with their downwind counterparts in this section. Turbines with and without a tip brake are considered (Table 9.2). The average and maximum load effects, minimum tower-to-blade clearance, and maximum and minimum teeter angles are examined and compared for these configurations.

Table 9.2. Wind turbine models used for upwind/downwind comparison.

Upwind Turbines	Downwind Turbines
5MW2UB00	5MW2DB00
5MW2UB00TipBrk	5MW2DB00TipBrk
5MW2UBUT	5MW2DBUT
5MW2UBUTTipBrk	5MW2DBUTTipBrk

Average Load Effects

The weighted percent difference of average load effects are presented in Figure 9.2 (a) for normal operating conditions. The downwind configuration has lower load effects at the tower base than the upwind configuration. On the other hand, the upwind machines have lower load effects at the tower top than the downwind machines. Figure 9.2 (a) shows that the 2-bladed upwind machines are experiencing the highest average load effects at the blade roots. The load effects at the blade root of the 2-bladed downwind turbines with the baseline blade (5MW2DB00) are almost equal to those of the baseline model. However, this should be interpreted carefully. As shown in Figure 9.10, the maximum average shear force and the maximum average bending moment at blade root, which are indicated by the blue bars, decrease compared to the baseline model for the 2-bladed downwind models. However, the maximum average axial force and the minimum average torsional moments are higher and they cancel the reduction of weighted

percent difference from the shear force and the bending moment. For the 2-bladed machines, the load effects at the LSS of the downwind machines decrease more than the corresponding load effects of the upwind machines.

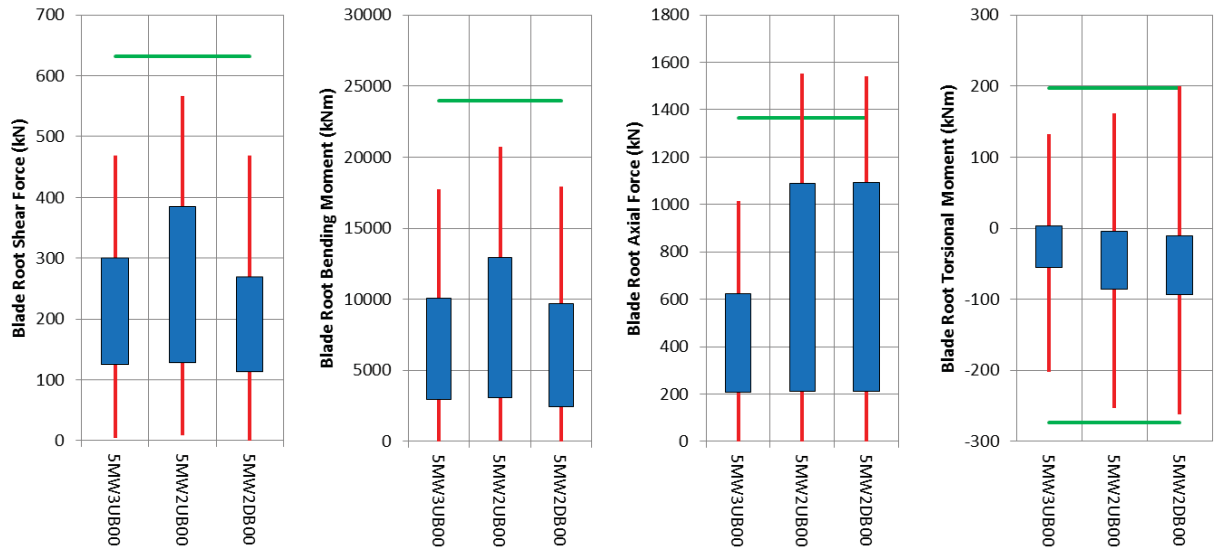

Figure 9.10. Comparison of the load effects at the blade roots of 3-bladed upwind, 2-bladed upwind and downwind turbines under normal operating conditions.

Figure 9.2 (b) shows weighted percent differences of the average load effects under fault conditions. The 2-bladed downwind machines without the tip-brakes have less average load effects at the tower base than the 2-bladed upwind machines without the tip-brakes. The 2-bladed upwind machines without the tip-brakes have higher average load effects at the tower top relative to the baseline model. On the other hand, the 2-bladed downwind machines without the tip-brakes have lower average load effects at the tower top compared to the baseline model. Usually the 2-bladed downwind machines have less average load effects at the blade roots than the 2-bladed upwind machines. The 2-bladed upwind machines usually have larger average load effects at the LSS than the 2-bladed downwind machines.

Figure 9.2 (c) shows that the average load effects of the 2-bladed upwind machines are reduced more than those of the 2-bladed downwind machines under parked conditions.

Maximum Load Effects

The weighted percent differences of maximum load effects under normal operating conditions are shown in Figure 9.3 (a). The load effects at the tower base of the downwind configuration models exceed those of the upwind configuration models. The 2-bladed upwind machines have lower maximum load effects at the tower top than the 2-bladed downwind machines. At the blade roots, the 2-bladed upwind turbines have larger maximum load effects than the 2-bladed downwind turbines. The 2-bladed upwind machines have lower maximum load effects at the LSS compared to the 2-bladed downwind machines.

The maximum load effects under fault conditions of various models are shown in Figure 9.3 (b). In general, the maximum load effects at all locations of interest of 2-bladed downwind machines are lower than those in 2-bladed upwind machines.

As shown in Figure 9.3 (c), the maximum load effects of 2-bladed upwind machines decrease more than those of 2-bladed downwind machines under parked conditions.

Torques

Figure 9.4 shows that the maximum HSS torque of the 2-bladed downwind machines are higher than those of the 2-bladed upwind machines under normal operating conditions. Under fault conditions, if the 5MW2UB00 and 5MW2DB00 models are compared, then the downwind turbine has smaller average HSS torque than its upwind counterpart. However, the maximum HSS torque values of these two models are comparable. Overall, the average HSS torque values of 2-bladed downwind turbines are slightly smaller than those of the 2-bladed upwind turbines under parked conditions. Also the range of the maximum and minimum HSS torque of 2-bladed downwind machines is wider than that of their upwind counterparts.

The generator torque of upwind and downwind machines under both normal operating and fault conditions are comparable (Figure 9.5). The only remarkable difference is in the minimum generator torque of 5MW2UB00 and 5MW2DB00 models under normal conditions, where torque of the former is much higher than that of the later.

Minimum Tower-to-Blade Clearance

There are dramatic differences in the minimum tower-to-blade clearance of 2-bladed upwind and downwind machines as shown in Figure 9.6. In general, downwind turbines have higher clearance than upwind ones. Under normal operating conditions, the 2-bladed downwind machines have more than twice larger tower-to-blade clearance than the 2-bladed upwind machines. Moreover, the 2-bladed downwind machines have much larger tower-to-blade clearance than the 3-bladed baseline machine under normal operating conditions. Under fault conditions, the tower-to-blade clearance of 2-bladed downwind machines is larger than that of the 2-bladed upwind machines. However, the differences are smaller than in those under normal operating conditions.

Maximum and Minimum Teeter Angle

As shown in Figure 9.7, the 2-bladed downwind machines have larger maximum and minimum teeter angles than the 2-bladed upwind machines under normal operating conditions. However, the order is reversed under fault conditions.

9.1.3 Blade Design

Wind turbine models with the baseline blades are compared with their counterparts with the BUT blades, in this subsection. The effects of these two different blades on the average and maximum load effects, minimum tower-to-blade clearance, and maximum and minimum teeter angles of the wind turbine models are studied.

Table 9.3. Wind turbine models used for effect of blade design comparison.

Models with Baseline Blades	Models with BUT Blades
5MW2UB00	5MW2UBUT
5MW2UB00TipBrk	5MW2UBUTTipBrk
5MW2DB00	5MW2DBUT
5MW2DB00TipBrk	5MW2DBUTTipBrk

Average Load Effects

The weighted percent difference of average load effects under normal operating conditions is shown in Figure 9.2 (a). Overall, for 2-bladed machines, replacing the baseline blades with BUT blades increases the load effects. Turbine designs with BUT blades have higher load effects both at the base and top of the tower than with baseline blades. Use of the BUT blades increases the average load effects at the blade roots for both upwind and downwind machines. The wind turbines with the baseline blades have lower load effects at the LSS than the wind turbines with the BUT blades.

Figure 9.2 (b) shows the weighted percent difference of the average load effects under fault conditions. In general, the average load effects at tower top, blade roots, and LSS increased when the BUT blades are used compared to the load effects when the baseline blades are used. The average tower base load effects for models without tip-brakes are lower for models with BUT blades than for models with baseline blades. However, if tip-brakes are used, the tower base load effects are higher for the models with BUT blades than their counterparts with baseline blades.

The weighted percent difference of the average load effects under parked conditions of wind turbine models are shown in Figure 9.2 (c). The wind turbines with the baseline blades have lower average load effects than the wind turbines with the BUT blade.

Maximum Load Effects

The weighted percent differences of maximum load effects under normal operating conditions are shown in Figure 9.3 (a). It is observed that designs with BUT blades have higher load effects than their counterparts with baseline blades. According to Figure 9.11, to Figure 9.13, the maximum shear forces and the maximum bending moments at the tower base and the top, and the blade roots of the models with the BUT blades exceeded the safe limit. Moreover, the minimum torsional moments at the tower base and the top, and the blade roots of the 2-bladed downwind models with the BUT blades are very close to the safe limit. Thus, these maximum load effects at the tower base must be carefully investigated in the detailed design for these models.

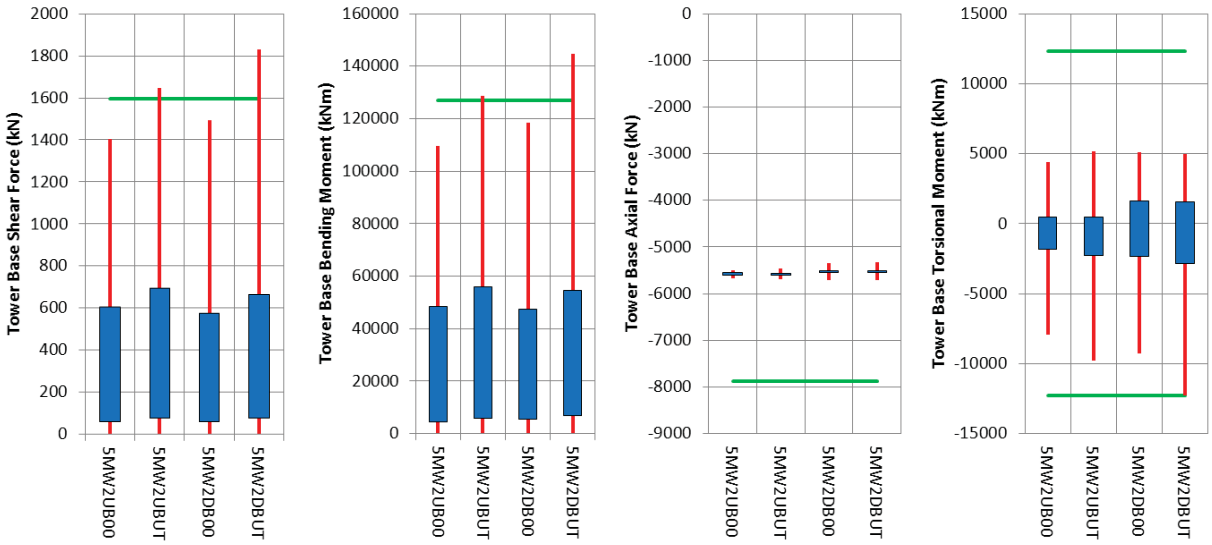

Figure 9.11. Comparisons of load effects at the tower base for different blade designs under normal operating conditions.

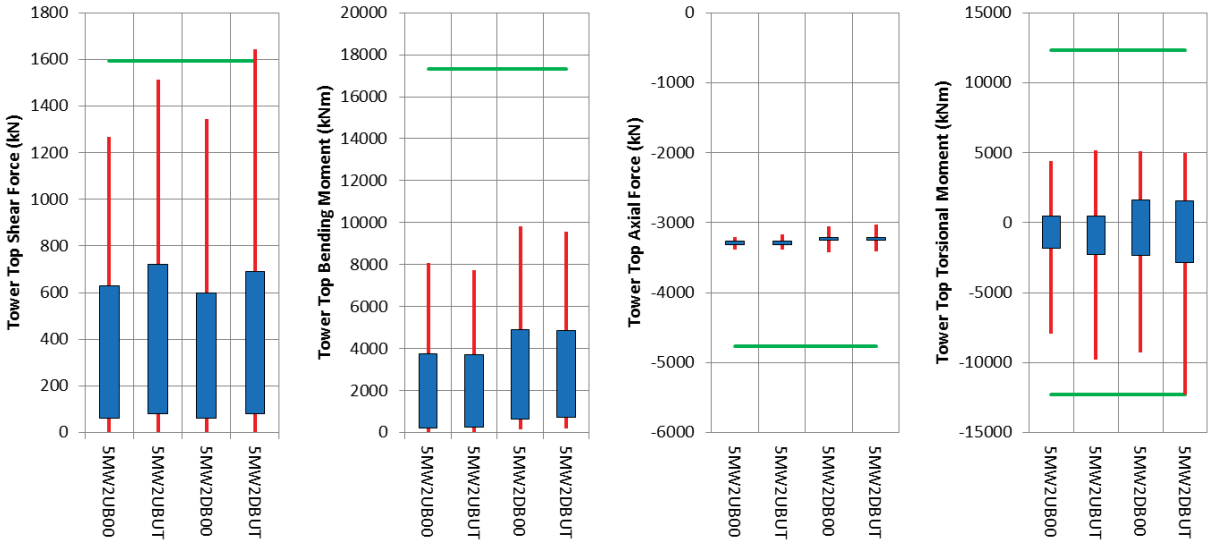

Figure 9.12. Comparisons of load effects at the tower top for different blade designs under normal operating conditions.

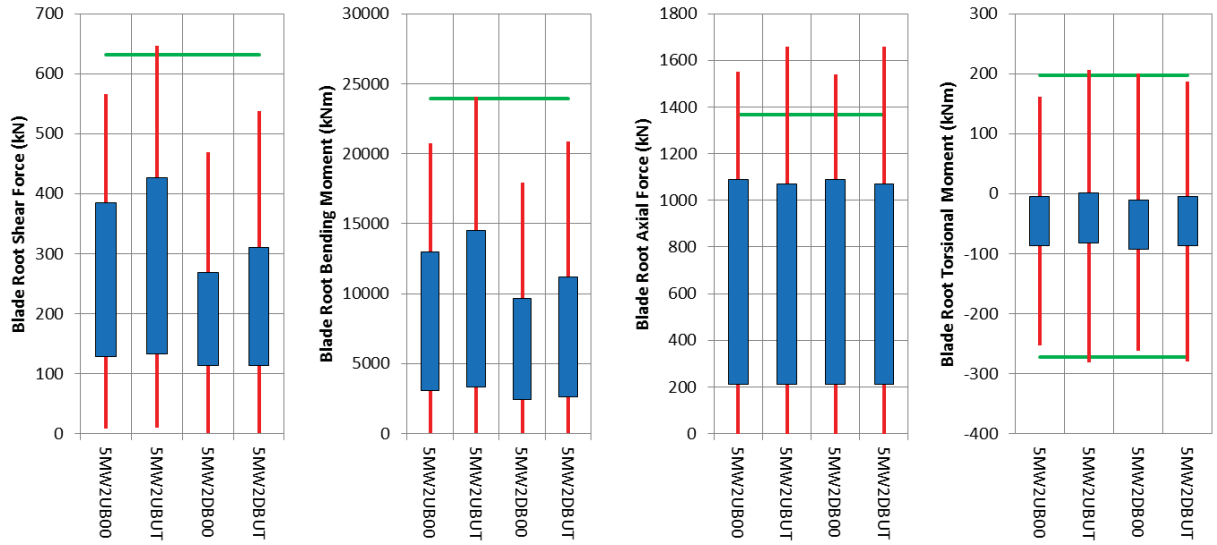

Figure 9.13. Comparisons of load effects at the blade roots for different blade designs under normal operating conditions.

The maximum load effects under fault conditions for various models are shown in Figure 9.3 (b). In general, the BUT blades decrease the load effects of wind turbines compared to the baseline blades. Figure 9.3 (c) presents the same information under parked conditions. In general, maximum load effects are larger with the BUT blades than with the baseline blades under both fault and parked conditions.

Torques

In general, the design of blades does not have a significant effect on torque on the HSS under normal operating and fault conditions as shown in Figure 9.4. Under parked conditions, the models with the BUT blades have higher average torque on the HSS. Moreover, the difference between the maximum and minimum HSS torque increases under parked conditions when the BUT blades are used.

Overall, as shown in Figure 9.5, the torque of the generator under both normal and fault conditions is insensitive to the design of the blades. The only remarkable observation is that the minimum generator torque of the models with the BUT blades have similar generator torques for both upwind and downwind configurations under fault conditions. On the other hand, the models with the baseline blades have different torques.

Minimum Tower-to-Blade Clearance

The use of BUT blades reduces the minimum tower-to-blade clearance as shown in Figure 9.6. The minimum tower-to-blade clearance of the 2-bladed upwind turbine with the BUT blades is less than the minimum required clearance under normal operating and fault conditions. Use of the BUT blades reduces the minimum tower-to-blade clearance more for the 2-bladed upwind machine than for the 2-bladed downwind machine under normal operating conditions. However, the trend under fault conditions is not consistent. When the BUT blades are used for the 2-bladed upwind machine without the tip-brakes, the minimum tower-to-blade clearance is reduced.

However, the minimum tower-to-blade clearance increases when the BUT blades are used for the 2-bladed downwind machine without the tip-brake model under fault conditions.

Maximum and Minimum Teeter Angle

Figure 9.7 shows that use of the BUT blades increases the maximum and minimum teeter angles of the 2-bladed machines under normal operating conditions. However, under fault conditions, 2-bladed wind turbines without tip-brakes, and with the BUT blades have lower maximum and minimum teeter angles than their counterparts with the baseline blades.

9.1.4 Shaft Tilt and Conning Angles

The following cases are considered to examine the combined effects of the shaft tilt and conning angles on 2-bladed downwind turbine models.

Table 9.4. Wind turbine models used for effects of shaft tilt and conning angle comparison.

Shaft Tilt Angle (deg)	Conning Angle (deg)	Wind Turbine Models	
5	2.5	5MW2DB00,	5MW2DB00TipBrk
5	0	5MW2DB00T5C0,	5MW2DB00T5C0TipBrk
0	2.5	5MW2DB00T0C2.5,	5MW2DB00T0C2.5TipBrk
0	0	5MW2DB00T0C0,	5MW2DB00T0C0TipBrk

The average and maximum load effects, torques, minimum tower-to-blade clearance, and maximum and minimum teeter angles for the above models are compared under normal operating, fault, and parked conditions.

Average Load Effects

Figure 9.2 (a) shows that average load effects under normal operating conditions depend on the wind turbine configuration. In general, the average load effects at the tower base and the tower top are insensitive to the shaft tilt and conning angle. The only considerable observation is that the bending moment at the tower top is lower when the conning angle is zero as tabulated in Table 9.9. The change of the shaft tilt and the conning angle to zero increase the average load effects at the blade roots and the LSS. The effect of the conning angle is larger than the effect of the shaft tilt angle for the average load effects at the blade roots and the LSS. Shear forces and bending moments contribute the most to this effect as shown in Table 9.12 and Table 9.15.

Figure 9.2 (b) shows the weighted percent difference of the average load effects under fault conditions. When the tip-brakes are not used, the average load effects at the tower base increase as shaft tilt and conning angles change to zero. The average load effects at the tower top increase as the shaft tilt changes to zero when the tip-brakes are not used. The opposite happens when the conning angle changes to zero. On the other hand, when the tip-brakes are used, the average load effects at the tower base and the top become insensitive to the change of shaft tilt and conning angles. If the shaft tilt or conning angles are set to zero, the average load effects at the blade roots and the LSS increase.

Overall, when the shaft tilt angle or the conning angles are changed to zero, the load effects increase as shown in Figure 9.2 (c).

Maximum Load Effects

The weighted percent differences of the maximum load effects under normal operating conditions are shown in Figure 9.3 (a). When the conning angle becomes zero the maximum load effects at the tower base and top decrease. Maximum load effects at the tower base and the top are insensitive to changes in the shaft tilt angle. On the other hand, changing both the conning and the shaft tilt angles to the zero increases the maximum load effects at the blade roots. This increase is primarily due to the change in the conning angle. Although changing the shaft tilt and the conning angle to the zero angles reduces the maximum load effects at the LSS, this change is small.

The maximum load effects under fault conditions for various models are shown in Figure 9.3 (b). The changes of conning angle and shaft tilt angle to zero increase the maximum load effects at all locations of interest if there are no tip-brakes. If the tip-brakes are used, the maximum load effects at the tower base, blade roots, and LSS increase when the conning angle is changed to zero. However, when the shaft tilt angle is changed to zero, the maximum load effects at the tower base and the blade roots decrease when the tip-brakes are used.

The weighted percent difference of the maximum load effects under parked conditions are shown in Figure 9.3 (c). Overall similar to the average load effects when the shaft tilt angle or the conning angles become zero the maximum load effects increase.

Torques

As shown in Figure 9.4, a change of the shaft tilt or conning angle to zero increases maximum HSS torque slightly under normal operating conditions. The maximum HSS torques for different shaft tilt and conning angles are comparable under fault conditions. The maximum of the average HSS torque for zero shaft tilt angle exceeds that for 5° shaft tilt angle under fault conditions when the tip-brakes are not applied. The change in the shaft tilt angle to zero degrees reduces the range of the HSS torque more than for the 5° shaft tilt angle under parked conditions. However, the change of the conning angle has almost no effect on the HSS torque under parked conditions.

The average generator torques are similar for different shaft tilt and conning angle cases as shown in Figure 9.5 under normal operating and fault conditions. However, the zero degree shaft tilt angle reduces the range of minimum generator torque under fault conditions. Changing the conning angle makes insignificant changes on generator torque.

Minimum Tower-to-Blade Clearance

Figure 9.6 shows that as the shaft tilt and conning angles approach zero, the tower-to-blade clearance decreases under normal operating conditions. The models with both zero shaft tilt and conning angles crash into the tower. Thus, the wind turbine should have the proper shaft tilt or conning angles to prevent collision of the blades with the tower. As suggested in Section 9.3.1, setting the shaft tilt angle to 2° and the conning angle to 0° is a good configuration to produce more AEP safely for the 5MW 2-bladed downwind turbine. As the tilt and cone angles approach zero degree, the tower-to-blade clearance reduces significantly under the fault conditions.

Maximum and Minimum Teeter Angle

As shown in Figure 9.7, as the shaft tilt or conning angles are changed to zero, this reduces the maximum and minimum teeter angles. The reduction is larger when the conning angle is changed under normal operating conditions. However, under fault conditions, the range of teeter angle increases as the shaft tilt or conning angle is set to 0°. The effect of a change in the shaft tilt angle is larger than that of the conning angle under fault conditions.

9.1.5 Teeter

In this section, the effect of teeter mechanism on the responses of the 2-bladed downwind turbine to is studied. The average and maximum load effects, torques, minimum tower-to-blade clearance, and maximum and minimum teeter angles are compared between the 5MW2DB00 and 5MW2DB00TeeterNo wind turbine models.

Average Load Effects

The weighted percent difference of average load effects in Figure 9.2 (a) shows that the average load effects at the tower base, blade roots, and LSS decrease when teeter mechanism is used for the 2-bladed downwind machine under normal operating conditions. Moreover, Figure 9.2 (b) shows that the average load effects under fault conditions of all locations of interest decrease when the teeter mechanism is used. In parked conditions, the use of teeter mechanism does not change significantly the average load effects as shown in Figure 9.2 (c).

Maximum Load Effects

The weighted percent differences of maximum load effects under normal operating conditions are shown in Figure 9.3 (a). Except the tower base, the maximum load effects at all locations of interest decrease when the teeter mechanism is used under normal operating conditions. As shown in Figure 9.14, the minimum torsional moment of 2-bladed downwind machine without teeter mechanism exceeds the safe limit. Thus, the 2-bladed machine requires having proper teeter parameter setting to operate safely. When the teeter mechanism is not used, the maximum load effects at the tower top increases considerably while the case without the teeter mechanism reduces the load effects at the tower base. As shown in Figure 9.15, the minimum torsional moment at the tower top of the 2-bladed downwind machine without teeter exceeds the safe limit.

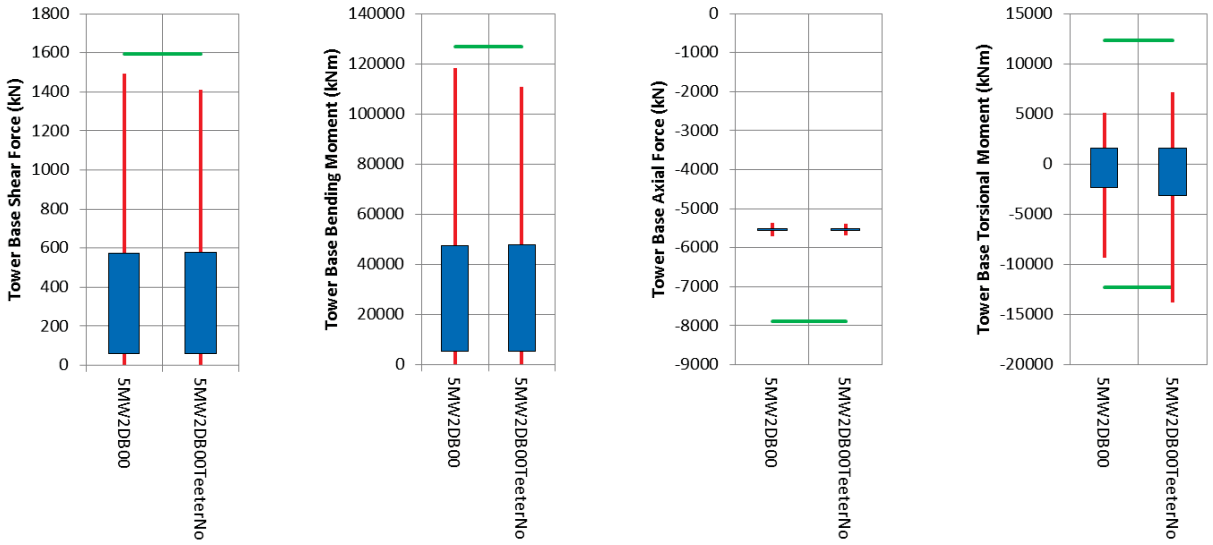

Figure 9.14. Tower base load effect comparisons for application of teeter mechanism under normal operating conditions.

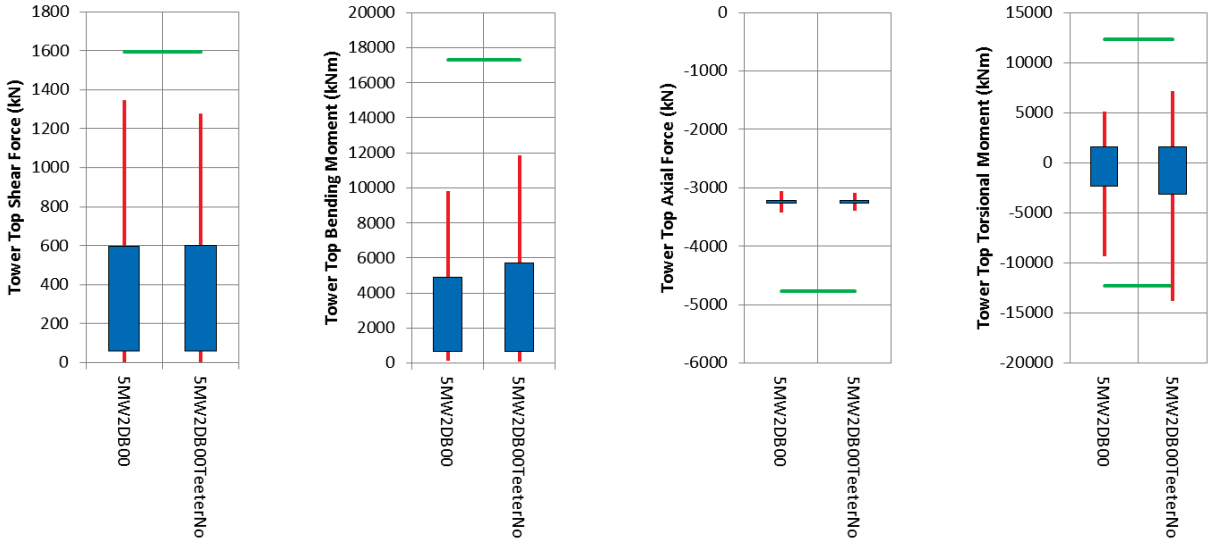

Figure 9.15. Tower top load effect comparisons for application of teeter mechanism under normal operating conditions.

Under fault conditions, maximum load effects at all locations interest are reduced when the teeter mechanism is applied as shown in Figure 9.3 (b). The maximum torsional moments at the tower base are larger for the wind turbines without tip-brakes as shown in Figure 9.16. The maximum load effects at the tower top increase significantly when the teeter mechanism is not used. As shown in Figure 9.17, the maximum bending moment at the tower top of the 2-bladed downwind model without teeter mechanism model is very close to the safe limit.

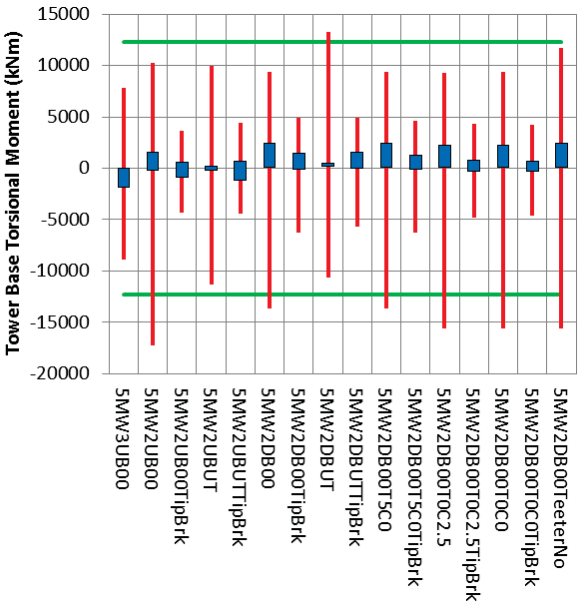

Figure 9.16. Torsional moments at tower base under fault conditions.

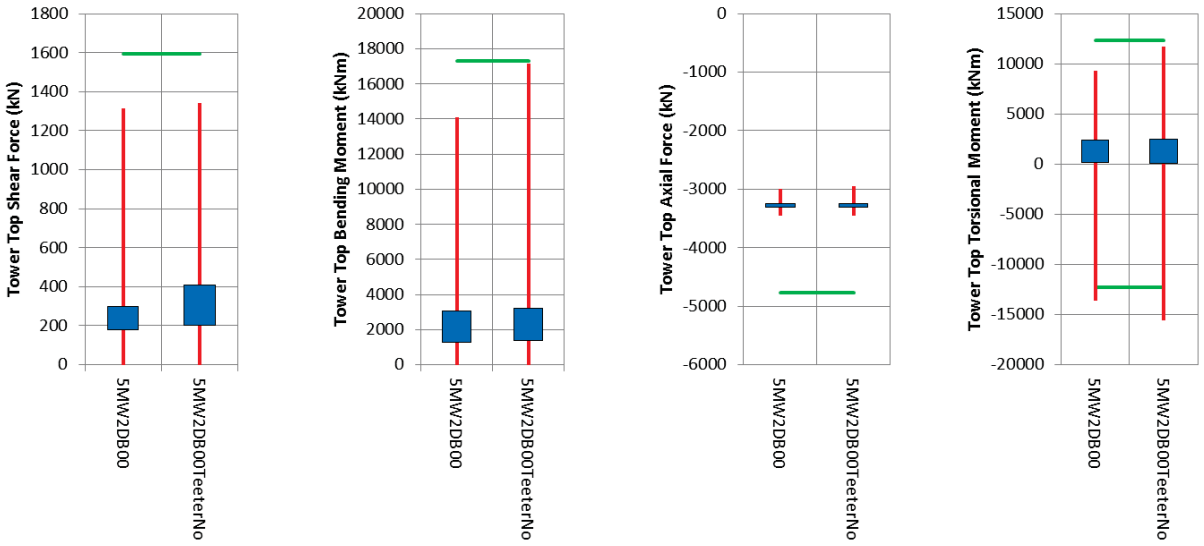

Figure 9.17. Tower top load effect comparisons for application of teeter mechanism under fault conditions.

The model without the teeter mechanism has slightly larger maximum load effects under parked conditions. However the effect is small as shown in Figure 9.3 (c).

Torques

The maximum HSS torque of the model with teeter mechanism is slightly higher than that of the model without teeter mechanism under both normal operating and fault conditions as shown in Figure 9.4. However, the opposite happens opposite under parked conditions. There is almost no difference in the average HSS torques for the models with different teeter mechanisms under all conditions.

As shown in Figure 9.5, the generator torques are almost equal under both normal operating and fault conditions for different teeter cases.

Minimum Tower-to-Blade Clearance

The 2-bladed downwind model without teeter mechanism has slightly less minimum tower-to-blade clearance than the model with teeter mechanism, under normal operating conditions (Figure 9.6). Under fault conditions, the minimum tower-to-blade clearance drops much more for the case with teeter mechanism then the case without teeter mechanism.

Maximum and Minimum Teeter Angle

The model without teeter mechanism does not have teeter angle as shown in Figure 9.7, while other case have.

9.1.6 Brakes

This section covers responses of 2-bladed wind turbine models using tip-brakes. The details of the tip-brake are explained in Section 6.2.3. The wind turbine models without tip-brakes use the pitch-to-feather method to shut down the turbine. The differences of turbine responses to different shutdown procedures using different brakes under fault conditions are examined in this section. Moreover, the additional mass at the tip of the blades representing the tip-brakes are compared under normal operating and parked conditions. The models are compared with and without tip-brakes cases.

Table 9.5. Wind turbine models used for effect of brakes comparison.

Models without Tip-brakes	Models with Tip-brakes
5MW2UB00	5MW2UB00TipBrk
5MW2UBUT	5MW2UBUTTipBrk
5MW2DB00	5MW2DB00TipBrk
5MW2DBUT	5MW2DBUTTipBrk
5MW2DB00T5C0	5MW2DB00T5C0TipBrk
5MW2DB00T0C2.5	5MW2DB00T0C2.5TipBrk
5MW2DB00T0C0	5MW2DB00T0C0TipBrk

Average Load Effects

The weighted percent differences of the average load effects under normal operating conditions are shown in Figure 9.2 (a). The use of tip-brakes did not cause significant changes to the average load effects at any location of interest under normal operating conditions.

Figure 9.2 (b) shows weighted percent difference of the average load effects under fault conditions. Using tip-brakes significantly reduced the average load effects at the tower base for all turbine configurations. In general, the tip-brakes reduce the average load effects at the tower top, except for the 2-bladed downwind turbine with the baseline blade model. However, the average load effects at the blade roots are larger when tip-brakes are used. In most of cases, the tip-brakes increase average load effects at the LSS under fault conditions.

As shown in Figure 9.2 (c) the tip-brakes do not affect the average load effects considerably under parked conditions.

Maximum Load Effects

The weighted percent differences of the maximum load effects under normal operating conditions are shown in Figure 9.3 (a). The tip-brakes help to reduce the maximum load effects at the tower base under normal operating conditions except for the wind turbines with the BUT blades. The tip-brakes make a considerable difference for the maximum load effects at the tower top under normal operating conditions. The tip-brakes help to reduce the maximum load effects at the blade roots, but their effects very small. The wind turbine models with tip-brakes have slightly larger maximum load effects at the LSS.

The maximum load effects under fault conditions for various models are shown in Figure 9.3 (b). This graph shows the advantages of using tip-brakes. Overall, the maximum load effects decrease when the tip-brakes are used under fault conditions. The maximum torsional moments at the tower base and the tower top exceed the safe limit for models having no the tip-brakes, as shown in Figure 9.16 and Figure 9.18. The maximum load effects at the blade roots increase more when the tip-brakes are used. As shown in Figure 9.19, the maximum shear forces at the blade roots for most of wind turbines with the tip-brakes exceed or come close to the safe limit.

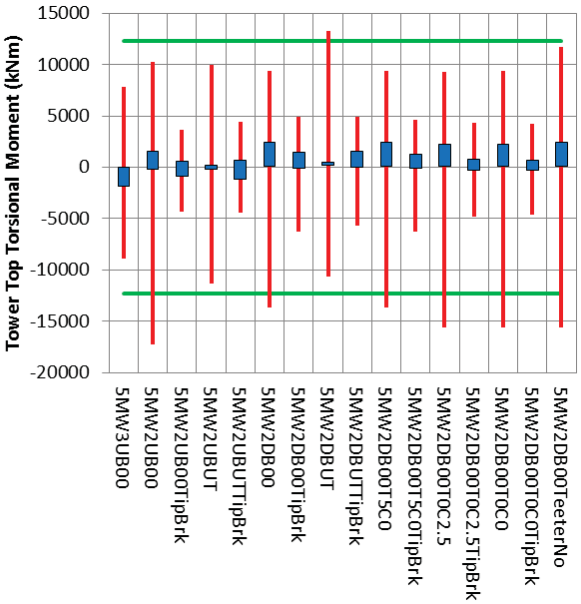

Figure 9.18. Torsional moments at tower top under fault conditions.

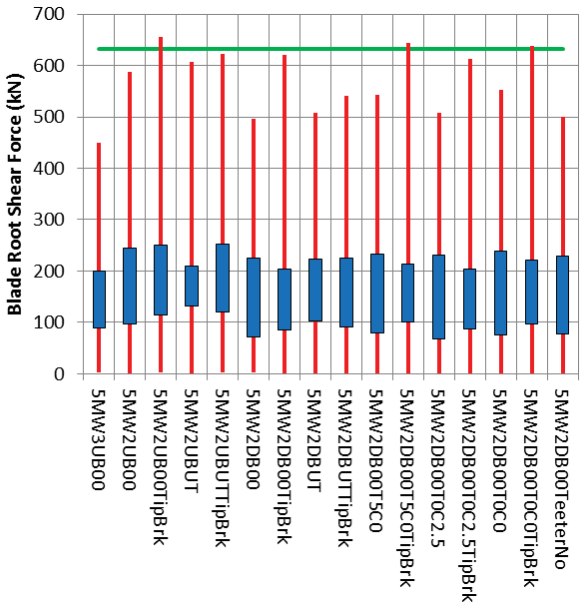

Figure 9.19. Shear forces at blade roots under fault conditions.

As shown in Figure 9.3 (c), the maximum load effects under parked conditions increase when tip-brakes are used.

Torques

In Figure 9.4, the models with the tip-brakes have a slightly higher maximum HSS torque than the models without tip-brakes for 2-bladed downwind machines under normal operating conditions, while 2-bladed upwind machines show almost no difference. However, under fault conditions, the ranges of maximum and average HSS torque for all 2-bladed machines with the tip-brake are larger than those of models without the tip-brakes. Virtually no differences were observed between the models with and without the tip-brakes under parked conditions.

As shown in Figure 9.5, the range of the average generator torque of turbine models with the tip-brakes is larger than that in the models without tip-brakes under fault conditions. However, tip brakes have the opposite effect on the ranges of the maximum and minimum generator torque.

Minimum Tower-to-Blade Clearance

Figure 9.6 shows that the tip-brakes do not affect significantly the minimum tower-to-blade clearance under normal operating conditions. However, the tip-brakes increase the clearance significantly for the 2-bladed downwind machines under fault conditions. However, the tip-brakes are ineffective for the 2-bladed upwind turbines.

Maximum and Minimum Teeter Angle

As shown in Figure 9.7, maximum and minimum teeter angles are unaffected when using tip-brakes under normal operating conditions. However, the application of the tip-brakes reduces the maximum teeter angle significantly under fault conditions. On the other hand, the the minimum teeter angles for 2-bladed downwind machines increase but stays within a range from -3° to 3°.

9.1.7 Summary of Simulation Results

The load effects at the tower base, tower top, blade roots, and LSS are presented in Table 9.6 to Table 9.17. The percent differences with the baseline design are also listed. Except for the axial force, only the magnitude of shear force, bending moment, and torsional moment are listed, because signs are not meaningful for these quantities. However, the signs of axial forces are shown to distinguish between tension and compression. The largest magnitude of torque results at LSS, HSS and generator are presented in Table 9.18 to Table 9.20. The minimum tower-to-blade clearance and maximum and minimum teeter angle are listed in Table 9.21 and Table 9.22 respectively. Refer to Appendix 8 for the DLC and wind speed information corresponding to the results.

Table 9.6. Load effects at tower base under normal operating conditions.

	Shear Force				Bending Moment				Axial Force				Torsional Moment			
	Maximum		Average		Maximum		Average		Maximum		Average		Maximum		Average	
Model	Value (kN)	%diff (%)	Value (kN)	%diff (%)	Value (kN m)	%diff (%)	Value (kN m)	%diff (%)	Value (kN)	%diff (%)	Value (kN)	%diff (%)	Value (kN m)	%diff (%)	Value (kN m)	%diff (%)
5MW3UB00	1181	0.0	685	0.0	93942	0.0	53934	0.0	-5836	0.0	-5788	0.0	9119	0.0	2625	0.0
5MW2UB00	1405	18.9	606	-11.6	109496	16.6	48577	-9.9	-5679	-2.7	-5608	-3.1	7922	-13.1	1802	-31.3
5MW2UB00TipBrk	1379	16.7	607	-11.4	107410	14.3	48674	-9.8	-5681	-2.7	-5610	-3.1	7951	-12.8	1771	-32.5
5MW2UBUT	1645	39.3	696	1.5	128540	36.8	55820	3.5	-5684	-2.6	-5615	-3.0	9773	7.2	2262	-13.8
5MW2UBUTTipBrk	1664	40.8	696	1.6	129283	37.6	55852	3.6	-5684	-2.6	-5616	-3.0	9729	6.7	2261	-13.9
5MW2DB00	1495	26.5	576	-16.0	118349	26.0	47465	-12.0	-5718	-2.0	-5551	-4.1	9307	2.1	2354	-10.3
5MW2DB00TipBrk	1469	24.4	578	-15.7	116337	23.8	47619	-11.7	-5720	-2.0	-5552	-4.1	9308	2.1	2321	-11.6
5MW2DBUT	1831	55.0	663	-3.2	144619	53.9	54675	1.4	-5710	-2.2	-5550	-4.1	12250	34.3	2861	9.0
5MW2DBUTTipBrk	1836	55.4	664	-3.1	145193	54.6	54761	1.5	-5716	-2.1	-5552	-4.1	12250	34.3	2847	8.5
5MW2DB00T5C0	1400	18.5	584	-14.8	106981	13.9	47828	-11.3	-5724	-1.9	-5549	-4.1	8816	-3.3	2126	-19.0
5MW2DB00T5C0TipBrk	1371	16.1	585	-14.6	104812	11.6	47954	-11.1	-5727	-1.9	-5551	-4.1	8790	-3.6	2100	-20.0
5MW2DB00T0C2.5	1492	26.3	580	-15.4	117768	25.4	47584	-11.8	-5714	-2.1	-5568	-3.8	9493	4.1	2449	-6.7
5MW2DB00T0C2.5TipBrk	1467	24.1	582	-15.1	115986	23.5	47736	-11.5	-5716	-2.1	-5569	-3.8	9459	3.7	2417	-7.9
5MW2DB00T0C0	1399	18.4	588	-14.2	106416	13.3	47974	-11.1	-5720	-2.0	-5568	-3.8	8972	-1.6	2199	-16.2
5MW2DB00T0C0TipBrk	1365	15.5	590	-14.0	103507	10.2	48105	-10.8	-5725	-1.9	-5570	-3.8	8869	-2.7	2173	-17.2
5MW2DB00TeeterNo	1412	19.5	577	-15.9	110809	18.0	47891	-11.2	-5686	-2.6	-5552	-4.1	13790	51.2	3114	18.6

Table 9.7. Load effects at tower base under fault conditions.

	Shear Force				Bending Moment				Axial Force				Torsional Moment			
	Maximum		Average		Maximum		Average		Maximum		Average		Maximum		Average	
Model	Value (kN)	%diff (%)	Value (kN)	%diff (%)	Value (kN m)	%diff (%)	Value (kN m)	%diff (%)	Value (kN)	%diff (%)	Value (kN)	%diff (%)	Value (kN m)	%diff (%)	Value (kN m)	%diff (%)
5MW3UB00	1386	0.0	392	0.0	111495	0.0	30759	0.0	-5828	0.0	-5737	0.0	8876	0.0	1868	0.0
5MW2UB00	1498	8.1	347	-11.6	115128	3.3	27228	-11.5	-5750	-1.3	-5596	-2.5	17278	94.7	1576	-15.6
5MW2UB00TipBrk	1443	4.1	284	-27.7	112975	1.3	22503	-26.8	-5686	-2.4	-5583	-2.7	4323	-51.3	878	-53.0
5MW2UBUT	1451	4.7	332	-15.3	112531	0.9	26145	-15.0	-5761	-1.2	-5571	-2.9	11310	27.4	207	-88.9
5MW2UBUTTipBrk	1179	-14.9	281	-28.4	93868	-15.8	22415	-27.1	-5693	-2.3	-5584	-2.7	4462	-49.7	1129	-39.5
5MW2DB00	1380	-0.4	309	-21.3	110466	-0.9	24630	-19.9	-5745	-1.4	-5610	-2.2	13638	53.7	2431	30.1
5MW2DB00TipBrk	1466	5.8	262	-33.2	118227	6.0	22606	-26.5	-5718	-1.9	-5570	-2.9	6259	-29.5	1446	-22.6
5MW2DBUT	1517	9.4	301	-23.1	116346	4.4	24412	-20.6	-5812	-0.3	-5585	-2.7	13267	49.5	489	-73.8
5MW2DBUTTipBrk	1178	-15.0	295	-24.8	93647	-16.0	24059	-21.8	-5717	-1.9	-5570	-2.9	5721	-35.5	1539	-17.6
5MW2DB00T5C0	1405	1.3	318	-19.0	112574	1.0	25220	-18.0	-5744	-1.4	-5609	-2.2	13635	53.6	2456	31.5
5MW2DB00T5C0TipBrk	1488	7.4	259	-33.9	119434	7.1	22240	-27.7	-5720	-1.9	-5570	-2.9	6266	-29.4	1310	-29.9
5MW2DB00T0C2.5	1416	2.2	326	-16.9	111228	-0.2	25890	-15.8	-5742	-1.5	-5606	-2.3	15583	75.6	2194	17.5
5MW2DB00T0C2.5TipBrk	1491	7.6	258	-34.3	117709	5.6	21970	-28.6	-5691	-2.4	-5573	-2.9	4795	-46.0	795	-57.4
5MW2DB00T0C0	1438	3.8	338	-13.7	113130	1.5	26757	-13.0	-5742	-1.5	-5606	-2.3	15555	75.3	2225	19.1
5MW2DB00T0C0TipBrk	1509	8.9	260	-33.8	118812	6.6	22030	-28.4	-5694	-2.3	-5570	-2.9	4614	-48.0	658	-64.7
5MW2DB00TeeterNo	1407	1.5	449	14.3	112319	0.7	35761	16.3	-5751	-1.3	-5610	-2.2	15572	75.4	2464	31.9

Table 9.8. Load effects at tower base under parked conditions.

	Shear Force				Bending Moment				Axial Force				Torsional Moment			
	Maximum		Average		Maximum		Average		Maximum		Average		Maximum		Average	
Model	Value (kN)	%diff (%)	Value (kN)	%diff (%)	Value (kN m)	%diff (%)	Value (kN m)	%diff (%)	Value (kN)	%diff (%)	Value (kN)	%diff (%)	Value (kN m)	%diff (%)	Value (kN m)	%diff (%)
5MW3UB00	877	0.0	342	0.0	67766	0.0	28359	0.0	-5758	0.0	-5756	0.0	4250	0.0	3800	0.0
5MW2UB00	539	-38.6	181	-47.2	41614	-38.6	13970	-50.7	-5583	-3.0	-5568	-3.3	3354	-21.1	3265	-14.1
5MW2UB00TipBrk	581	-33.7	179	-47.7	44334	-34.6	13886	-51.0	-5584	-3.0	-5569	-3.3	3352	-21.1	3262	-14.1
5MW2UBUT	611	-30.4	189	-44.7	46547	-31.3	14629	-48.4	-5585	-3.0	-5560	-3.4	3368	-20.8	3274	-13.8
5MW2UBUTTipBrk	619	-29.4	187	-45.3	47130	-30.5	14537	-48.7	-5587	-3.0	-5561	-3.4	3368	-20.8	3274	-13.8
5MW2DB00	596	-32.0	228	-33.4	45467	-32.9	17594	-38.0	-5671	-1.5	-5669	-1.5	3565	-16.1	3280	-13.7
5MW2DB00TipBrk	637	-27.3	228	-33.3	48102	-29.0	17644	-37.8	-5672	-1.5	-5671	-1.5	3542	-16.7	3278	-13.7
5MW2DBUT	704	-19.7	255	-25.6	53004	-21.8	19632	-30.8	-5678	-1.4	-5676	-1.4	3579	-15.8	3292	-13.4
5MW2DBUTTipBrk	714	-18.6	255	-25.4	53672	-20.8	19728	-30.4	-5680	-1.4	-5679	-1.3	3579	-15.8	3290	-13.4
5MW2DB00T5C0	594	-32.2	229	-33.1	45672	-32.6	17664	-37.7	-5673	-1.5	-5672	-1.5	3532	-16.9	3252	-14.4
5MW2DB00T5C0TipBrk	640	-27.1	230	-32.9	48636	-28.2	17751	-37.4	-5675	-1.4	-5673	-1.4	3506	-17.5	3250	-14.5
5MW2DB00T0C2.5	668	-23.9	264	-23.0	50814	-25.0	20312	-28.4	-5586	-3.0	-5585	-3.0	3411	-19.7	3310	-12.9
5MW2DB00T0C2.5TipBrk	746	-15.0	267	-22.2	55724	-17.8	20533	-27.6	-5588	-3.0	-5588	-2.9	3419	-19.6	3311	-12.9
5MW2DB00T0C0	665	-24.2	266	-22.2	51096	-24.6	20507	-27.7	-5587	-3.0	-5585	-3.0	3370	-20.7	3283	-13.6
5MW2DB00T0C0TipBrk	740	-15.6	270	-21.2	56083	-17.2	20790	-26.7	-5589	-2.9	-5588	-2.9	3377	-20.5	3284	-13.6
5MW2DB00TeeterNo	602	-31.3	231	-32.6	45857	-32.3	17786	-37.3	-5670	-1.5	-5669	-1.5	3749	-11.8	3262	-14.2

Table 9.9. Load effects at tower top under normal operating conditions.

	Shear Force				Bending Moment				Axial Force				Torsional Moment			
	Maximum		Average		Maximum		Average		Maximum		Average		Maximum		Average	
Model	Value (kN)	%diff (%)	Value (kN)	%diff (%)	Value (kN m)	%diff (%)	Value (kN m)	%diff (%)	Value (kN)	%diff (%)	Value (kN)	%diff (%)	Value (kN m)	%diff (%)	Value (kN m)	%diff (%)
5MW3UB00	1181	0.0	712	0.0	10492	0.0	5180	0.0	-3531	0.0	-3489	0.0	9119	0.0	2625	0.0
5MW2UB00	1269	7.4	629	-11.6	8068	-23.1	3768	-27.3	-3381	-4.2	-3311	-5.1	7922	-13.1	1802	-31.3
5MW2UB00TipBrk	1246	5.4	630	-11.5	7952	-24.2	3750	-27.6	-3384	-4.2	-3312	-5.1	7951	-12.8	1771	-32.5
5MW2UBUT	1513	28.1	722	1.5	7718	-26.4	3725	-28.1	-3383	-4.2	-3316	-4.9	9773	7.2	2262	-13.8
5MW2UBUTTipBrk	1528	29.3	723	1.6	7811	-25.6	3720	-28.2	-3385	-4.1	-3318	-4.9	9729	6.7	2261	-13.9
5MW2DB00	1344	13.8	598	-15.9	9830	-6.3	4881	-5.8	-3424	-3.0	-3255	-6.7	9307	2.1	2354	-10.3
5MW2DB00TipBrk	1323	12.0	600	-15.7	9572	-8.8	4860	-6.2	-3426	-3.0	-3257	-6.6	9307	2.1	2321	-11.6
5MW2DBUT	1644	39.1	689	-3.1	9570	-8.8	4870	-6.0	-3416	-3.3	-3255	-6.7	12250	34.3	2861	9.0
5MW2DBUTTipBrk	1651	39.7	690	-3.0	9609	-8.4	4864	-6.1	-3421	-3.1	-3257	-6.7	12250	34.3	2847	8.5
5MW2DB00T5C0	1295	9.7	606	-14.8	9182	-12.5	4587	-11.5	-3430	-2.9	-3254	-6.7	8816	-3.3	2126	-19.0
5MW2DB00T5C0TipBrk	1272	7.7	608	-14.6	9018	-14.0	4567	-11.8	-3433	-2.8	-3255	-6.7	8790	-3.6	2100	-20.0
5MW2DB00T0C2.5	1344	13.7	603	-15.3	9828	-6.3	4672	-9.8	-3418	-3.2	-3272	-6.2	9493	4.1	2449	-6.7
5MW2DB00T0C2.5TipBrk	1323	12.0	605	-15.0	9434	-10.1	4653	-10.2	-3422	-3.1	-3273	-6.2	9459	3.7	2417	-7.9
5MW2DB00T0C0	1281	8.4	611	-14.1	9170	-12.6	4375	-15.5	-3426	-3.0	-3273	-6.2	8972	-1.6	2199	-16.2
5MW2DB00T0C0TipBrk	1249	5.7	613	-13.9	8827	-15.9	4355	-15.9	-3431	-2.8	-3274	-6.2	8869	-2.7	2173	-17.2
5MW2DB00TeeterNo	1277	8.1	600	-15.7	11831	12.8	5696	10.0	-3391	-4.0	-3256	-6.7	13790	51.2	3114	18.6

Table 9.10. Load effects at tower top under fault conditions.

	Shear Force				Bending Moment				Axial Force				Torsional Moment			
	Maximum		Average		Maximum		Average		Maximum		Average		Maximum		Average	
Model	Value (kN)	%diff (%)	Value (kN)	%diff (%)	Value (kN m)	%diff (%)	Value (kN m)	%diff (%)	Value (kN)	%diff (%)	Value (kN)	%diff (%)	Value (kN m)	%diff (%)	Value (kN m)	%diff (%)
5MW3UB00	1318	0.0	363	0.0	12821	0.0	2974	0.0	-3525	0.0	-3442	0.0	8876	0.0	1868	0.0
5MW2UB00	1414	7.3	331	-8.8	13935	8.7	3507	17.9	-3454	-2.0	-3301	-4.1	17278	94.7	1576	-15.6
5MW2UB00TipBrk	1434	8.8	283	-22.1	7162	-44.1	3878	30.4	-3388	-3.9	-3289	-4.5	4323	-51.3	878	-53.0
5MW2UBUT	1367	3.7	306	-15.5	14300	11.5	3887	30.7	-3467	-1.7	-3275	-4.9	11310	27.4	208	-88.9
5MW2UBUTTipBrk	1207	-8.4	287	-20.8	7100	-44.6	3864	29.9	-3399	-3.6	-3290	-4.4	4462	-49.7	1129	-39.5
5MW2DB00	1313	-0.4	298	-17.8	14113	10.1	3066	3.1	-3451	-2.1	-3315	-3.7	13638	53.7	2431	30.1
5MW2DB00TipBrk	1460	10.7	257	-29.1	8339	-35.0	4142	39.3	-3424	-2.9	-3275	-4.9	6259	-29.5	1446	-22.6
5MW2DBUT	1398	6.0	301	-17.0	13616	6.2	4432	49.0	-3517	-0.2	-3290	-4.4	13267	49.5	489	-73.8
5MW2DBUTTipBrk	1185	-10.1	299	-17.5	8156	-36.4	4195	41.1	-3423	-2.9	-3276	-4.8	5721	-35.5	1539	-17.6
5MW2DB00T5C0	1336	1.4	306	-15.7	13949	8.8	2763	-7.1	-3449	-2.2	-3314	-3.7	13637	53.6	2456	31.5
5MW2DB00T5C0TipBrk	1476	11.9	257	-29.2	8151	-36.4	3978	33.8	-3425	-2.8	-3275	-4.9	6265	-29.4	1310	-29.9
5MW2DB00T0C2.5	1343	1.8	313	-13.7	13370	4.3	3270	10.0	-3447	-2.2	-3312	-3.8	15583	75.6	2195	17.5
5MW2DB00T0C2.5TipBrk	1472	11.7	259	-28.6	8226	-35.8	4066	36.7	-3395	-3.7	-3278	-4.8	4795	-46.0	795	-57.4
5MW2DB00T0C0	1363	3.4	324	-10.7	13312	3.8	3065	3.1	-3446	-2.3	-3311	-3.8	15555	75.3	2225	19.1
5MW2DB00T0C0TipBrk	1486	12.7	264	-27.2	8246	-35.7	3823	28.6	-3398	-3.6	-3275	-4.9	4614	-48.0	659	-64.7
5MW2DB00TeeterNo	1344	1.9	409	12.9	17167	33.9	3212	8.0	-3455	-2.0	-3315	-3.7	15572	75.4	2464	31.9

Table 9.11. Load effects at tower top under parked conditions.

	Shear Force				Bending Moment				Axial Force				Torsional Moment			
	Maximum		Average		Maximum		Average		Maximum		Average		Maximum		Average	
Model	Value (kN)	%diff (%)	Value (kN)	%diff (%)	Value (kN m)	%diff (%)	Value (kN m)	%diff (%)	Value (kN)	%diff (%)	Value (kN)	%diff (%)	Value (kN m)	%diff (%)	Value (kN m)	%diff (%)
5MW3UB00	748	0.0	355	0.0	6040	0.0	4036	0.0	-3464	0.0	-3464	0.0	4250	0.0	3800	0.0
5MW2UB00	474	-36.7	160	-55.1	1787	-70.4	1708	-57.7	-3287	-5.1	-3274	-5.5	3354	-21.1	3265	-14.1
5MW2UB00TipBrk	480	-35.8	160	-55.1	1830	-69.7	1722	-57.3	-3287	-5.1	-3276	-5.4	3352	-21.1	3262	-14.1
5MW2UBUT	503	-32.8	167	-53.0	2067	-65.8	1972	-51.1	-3288	-5.1	-3265	-5.7	3368	-20.8	3274	-13.8
5MW2UBUTTipBrk	507	-32.2	167	-52.9	2060	-65.9	1971	-51.2	-3290	-5.0	-3267	-5.7	3368	-20.8	3274	-13.8
5MW2DB00	520	-30.5	201	-43.3	3105	-48.6	1921	-52.4	-3377	-2.5	-3376	-2.5	3565	-16.1	3280	-13.7
5MW2DB00TipBrk	529	-29.3	203	-42.8	3107	-48.6	1931	-52.2	-3378	-2.5	-3376	-2.5	3542	-16.7	3278	-13.7
5MW2DBUT	578	-22.8	224	-36.8	3237	-46.4	2079	-48.5	-3384	-2.3	-3383	-2.3	3579	-15.8	3292	-13.4
5MW2DBUTTipBrk	584	-22.0	227	-36.1	3255	-46.1	2062	-48.9	-3386	-2.3	-3384	-2.3	3579	-15.8	3290	-13.4
5MW2DB00T5C0	522	-30.2	202	-43.1	3041	-49.7	1675	-58.5	-3380	-2.4	-3378	-2.5	3532	-16.9	3252	-14.4
5MW2DB00T5C0TipBrk	533	-28.8	204	-42.6	2974	-50.8	1677	-58.4	-3381	-2.4	-3380	-2.4	3506	-17.5	3250	-14.5
5MW2DB00T0C2.5	603	-19.5	232	-34.6	1906	-68.4	1070	-73.5	-3292	-5.0	-3292	-5.0	3411	-19.7	3310	-12.9
5MW2DB00T0C2.5TipBrk	612	-18.2	235	-33.7	1890	-68.7	1093	-72.9	-3294	-4.9	-3293	-4.9	3419	-19.6	3311	-12.9
5MW2DB00T0C0	606	-19.0	234	-34.0	1699	-71.9	981	-75.7	-3293	-4.9	-3292	-5.0	3370	-20.7	3283	-13.6
5MW2DB00T0C0TipBrk	619	-17.3	238	-33.0	1863	-69.1	1011	-75.0	-3295	-4.9	-3294	-4.9	3377	-20.5	3284	-13.6
5MW2DB00TeeterNo	525	-29.9	204	-42.7	3137	-48.1	1944	-51.8	-3376	-2.5	-3376	-2.5	3749	-11.8	3262	-14.2

Table 9.12. Load effects at blade roots under normal operating conditions.

	Shear Force				Bending Moment				Axial Force				Torsional Moment			
	Maximum		Average		Maximum		Average		Maximum		Average		Maximum		Average	
Model	Value (kN)	%diff (%)	Value (kN)	%diff (%)	Value (kN m)	%diff (%)	Value (kN m)	%diff (%)	Value (kN)	%diff (%)	Value (kN)	%diff (%)	Value (kN m)	%diff (%)	Value (kN m)	%diff (%)
5MW3UB00	468	0.0	300	0.0	17734	0.0	10101	0.0	1013	0.0	624	0.0	202	0.0	56	0.0
5MW2UB00	566	20.9	385	28.6	20723	16.9	12963	28.3	1552	53.2	1090	74.6	253	25.1	86	55.1
5MW2UB00TipBrk	569	21.6	387	29.1	20672	16.6	12978	28.5	1567	54.7	1104	76.8	254	25.5	86	55.1
5MW2UBUT	646	38.1	427	42.5	24036	35.5	14479	43.3	1658	63.6	1070	71.4	281	39.1	82	47.3
5MW2UBUTTipBrk	644	37.7	428	42.8	23987	35.3	14460	43.2	1674	65.2	1084	73.6	281	39.0	82	47.3
5MW2DB00	469	0.2	269	-10.4	17953	1.2	9672	-4.2	1540	52.0	1091	74.7	262	29.4	93	67.1
5MW2DB00TipBrk	473	1.0	269	-10.3	17827	0.5	9638	-4.6	1556	53.6	1105	76.9	262	29.4	93	67.4
5MW2DBUT	538	14.9	310	3.3	20880	17.7	11207	11.0	1658	63.7	1071	71.6	280	38.7	87	57.1
5MW2DBUTTipBrk	534	14.0	310	3.4	20700	16.7	11147	10.4	1674	65.2	1085	73.8	282	39.6	88	57.3
5MW2DB00T5C0	514	9.7	308	2.9	18891	6.5	10913	8.0	1545	52.6	1093	75.1	267	32.2	92	65.4
5MW2DB00T5C0TipBrk	518	10.6	309	3.2	18763	5.8	10899	7.9	1561	54.1	1107	77.3	269	32.9	92	65.8
5MW2DB00T0C2.5	481	2.7	283	-5.7	18030	1.7	9979	-1.2	1548	52.8	1092	74.8	284	40.5	92	64.8
5MW2DB00T0C2.5TipBrk	484	3.4	283	-5.6	17912	1.0	9947	-1.5	1563	54.3	1105	77.0	284	40.6	92	65.1
5MW2DB00T0C0	526	12.3	323	7.9	18940	6.8	11236	11.2	1552	53.2	1093	75.1	289	43.1	91	62.8
5MW2DB00T0C0TipBrk	530	13.1	324	8.2	18850	6.3	11227	11.1	1568	54.8	1107	77.3	291	44.0	91	63.2
5MW2DB00TeeterNo	508	8.4	268	-10.5	19770	11.5	9675	-4.2	1534	51.4	1091	74.7	266	31.5	93	67.8

Table 9.13. Load effects at blade roots under fault conditions.

	Shear Force				Bending Moment				Axial Force				Torsional Moment			
	Maximum		Average		Maximum		Average		Maximum		Average		Maximum		Average	
Model	Value (kN)	%diff (%)	Value (kN)	%diff (%)	Value (kN m)	%diff (%)	Value (kN m)	%diff (%)	Value (kN)	%diff (%)	Value (kN)	%diff (%)	Value (kN m)	%diff (%)	Value (kN m)	%diff (%)
5MW3UB00	450	0.0	200	0.0	15045	0.0	5084	0.0	1042	0.0	304	0.0	178	0.0	38	0.0
5MW2UB00	588	30.7	245	22.7	18580	23.5	5862	15.3	1636	57.0	462	51.9	323	81.8	59	53.2
5MW2UB00TipBrk	655	45.7	249	24.8	20930	39.1	6997	37.6	1723	65.4	489	60.8	609	242.1	49	29.4
5MW2UBUT	607	34.9	210	4.9	20435	35.8	5667	11.5	1551	48.8	450	48.1	287	61.4	52	37.0
5MW2UBUTTipBrk	622	38.3	251	25.8	20842	38.5	7066	39.0	1692	62.4	479	57.4	692	288.7	50	30.0
5MW2DB00	497	10.5	226	12.8	18397	22.3	5427	6.7	1651	58.4	463	52.1	404	126.9	69	81.4
5MW2DB00TipBrk	621	38.0	205	2.4	20249	34.6	5586	9.9	1724	65.5	489	60.9	566	218.1	58	51.2
5MW2DBUT	508	12.9	223	11.7	17522	16.5	6349	24.9	1541	47.9	452	48.5	358	101.3	55	42.6
5MW2DBUTTipBrk	540	20.1	224	12.2	17291	14.9	6443	26.7	1710	64.1	486	59.8	577	224.2	57	50.2
5MW2DB00T5C0	542	20.5	232	16.2	17727	17.8	5665	11.4	1657	59.0	464	52.5	374	110.2	69	81.0
5MW2DB00T5C0TipBrk	644	43.2	213	6.3	21083	40.1	6143	20.8	1734	66.4	490	61.1	622	249.4	57	49.3
5MW2DB00T0C2.5	508	12.9	232	15.8	17114	13.8	5540	9.0	1655	58.8	464	52.4	349	96.2	66	72.0
5MW2DB00T0C2.5TipBrk	613	36.3	203	1.5	19989	32.9	5743	13.0	1730	66.0	492	61.9	566	218.0	54	40.7
5MW2DB00T0C0	554	23.1	239	19.7	17892	18.9	5746	13.0	1661	59.4	464	52.6	326	83.0	66	71.7
5MW2DB00T0C0TipBrk	637	41.7	221	10.5	20831	38.5	6290	23.7	1739	66.9	493	62.0	622	249.6	53	39.8
5MW2DB00TeeterNo	500	11.2	229	14.3	18744	24.6	5521	8.6	1638	57.2	462	52.0	415	133.5	69	81.4

Table 9.14. Load effects at blade roots under parked conditions.

	Shear Force				Bending Moment				Axial Force				Torsional Moment			
	Maximum		Average		Maximum		Average		Maximum		Average		Maximum		Average	
Model	Value (kN)	%diff (%)	Value (kN)	%diff (%)	Value (kN m)	%diff (%)	Value (kN m)	%diff (%)	Value (kN)	%diff (%)	Value (kN)	%diff (%)	Value (kN m)	%diff (%)	Value (kN m)	%diff (%)
5MW3UB00	288	0.0	282	0.0	7696	0.0	7514	0.0	-183	0.0	-183	0.0	202	0.0	194	0.0
5MW2UB00	233	-19.0	232	-17.6	6204	-19.4	5329	-29.1	-10	-94.8	-4	-97.7	185	-8.5	147	-24.5
5MW2UB00TipBrk	234	-18.6	233	-17.2	6390	-17.0	5377	-28.4	-9	-95.1	-3	-98.1	188	-7.0	146	-24.7
5MW2UBUT	230	-19.9	229	-18.6	6711	-12.8	5266	-29.9	-8	-95.8	-3	-98.6	178	-11.9	135	-30.7
5MW2UBUTTipBrk	234	-18.5	230	-18.4	7011	-8.9	5303	-29.4	-9	-95.3	-2	-98.7	182	-9.9	134	-30.8
5MW2DB00	268	-6.9	265	-5.8	6868	-10.8	5957	-20.7	-10	-94.7	-5	-97.1	178	-11.6	148	-23.9
5MW2DB00TipBrk	267	-7.3	266	-5.5	6832	-11.2	6006	-20.1	-10	-94.6	-5	-97.1	182	-10.1	148	-24.1
5MW2DBUT	273	-5.2	247	-12.4	7149	-7.1	6382	-15.1	-19	-89.8	-10	-94.6	173	-14.5	135	-30.3
5MW2DBUTTipBrk	272	-5.4	247	-12.2	7177	-6.8	6432	-14.4	-19	-89.5	-10	-94.5	177	-12.4	135	-30.3
5MW2DB00T5C0	266	-7.4	266	-5.6	6804	-11.6	5994	-20.2	-9	-95.2	-5	-97.5	178	-11.7	148	-23.8
5MW2DB00T5C0TipBrk	267	-7.0	267	-5.3	6806	-11.6	6044	-19.6	-9	-95.0	-5	-97.5	182	-9.9	148	-23.9
5MW2DB00T0C2.5	234	-18.7	222	-21.1	6630	-13.9	5102	-32.1	6	-103.5	-2	-98.8	188	-7.0	110	-43.4
5MW2DB00T0C2.5TipBrk	228	-20.6	223	-20.9	6610	-14.1	5139	-31.6	6	-103.3	-3	-98.6	194	-3.8	110	-43.5
5MW2DB00T0C0	235	-18.2	222	-21.1	6651	-13.6	5103	-32.1	-6	-97.0	-2	-98.8	186	-8.1	110	-43.2
5MW2DB00T0C0TipBrk	229	-20.5	223	-20.9	6597	-14.3	5141	-31.6	-6	-96.7	-3	-98.6	194	-4.0	110	-43.3
5MW2DB00TeeterNo	267	-7.2	265	-5.8	6855	-10.9	5957	-20.7	-10	-94.7	-5	-97.2	180	-11.0	148	-24.0

Table 9.15. Load effects at LSS under normal operating conditions.

	Shear Force				Bending Moment				Axial Force				Torsional Moment			
	Maximum		Average		Maximum		Average		Maximum		Average		Maximum		Average	
Model	Value (kN)	%diff (%)	Value (kN)	%diff (%)	Value (kN m)	%diff (%)	Value (kN m)	%diff (%)	Value (kN)	%diff (%)	Value (kN)	%diff (%)	Value (kN m)	%diff (%)	Value (kN m)	%diff (%)
5MW3UB00	1128	0.0	1085	0.0	13417	0.0	4924	0.0	1091	0.0	790	0.0	5549	0.0	4189	0.0
5MW2UB00	1005	-10.9	914	-15.7	8572	-36.1	3537	-28.2	1023	-6.3	693	-12.3	4458	-19.7	3168	-24.4
5MW2UB00TipBrk	1007	-10.8	916	-15.6	8581	-36.0	3508	-28.7	1028	-5.8	694	-12.1	4471	-19.4	3168	-24.4
5MW2UBUT	1001	-11.3	914	-15.8	11852	-11.7	4496	-8.7	1114	2.1	784	-0.7	4489	-19.1	3198	-23.6
5MW2UBUTTipBrk	1004	-11.0	915	-15.6	11988	-10.7	4477	-9.1	1117	2.4	785	-0.7	4519	-18.6	3198	-23.6
5MW2DB00	1081	-4.2	922	-14.9	9083	-32.3	3472	-29.5	842	-22.8	504	-36.2	5005	-9.8	3167	-24.4
5MW2DB00TipBrk	1080	-4.3	924	-14.8	9052	-32.5	3432	-30.3	847	-22.4	506	-36.0	5145	-7.3	3167	-24.4
5MW2DBUT	1074	-4.8	922	-15.0	11532	-14.0	4237	-13.9	935	-14.3	593	-25.0	4983	-10.2	3199	-23.6
5MW2DBUTTipBrk	1081	-4.2	924	-14.8	11526	-14.1	4220	-14.3	938	-14.1	594	-24.9	5089	-8.3	3199	-23.6
5MW2DB00T5C0	1086	-3.7	921	-15.1	8742	-34.8	3360	-31.8	856	-21.6	512	-35.2	5091	-8.2	3167	-24.4
5MW2DB00T5C0TipBrk	1086	-3.7	922	-15.0	8710	-35.1	3328	-32.4	861	-21.1	513	-35.0	5228	-5.8	3167	-24.4
5MW2DB00T0C2.5	1064	-5.7	920	-15.2	8839	-34.1	3420	-30.5	925	-15.2	586	-25.9	5106	-8.0	3167	-24.4
5MW2DB00T0C2.5TipBrk	1063	-5.8	921	-15.1	8857	-34.0	3381	-31.3	930	-14.7	587	-25.6	5269	-5.0	3167	-24.4
5MW2DB00T0C0	1069	-5.2	921	-15.1	8590	-36.0	3308	-32.8	937	-14.2	594	-24.8	5235	-5.6	3167	-24.4
5MW2DB00T0C0TipBrk	1072	-5.0	922	-15.0	8602	-35.9	3278	-33.4	942	-13.7	596	-24.6	5391	-2.8	3167	-24.4
5MW2DB00TeeterNo	1073	-4.9	924	-14.8	13073	-2.6	4674	-5.1	847	-22.4	505	-36.1	4956	-10.7	3167	-24.4

Table 9.16. Load effects at LSS under fault conditions.

	Shear Force				Bending Moment				Axial Force				Torsional Moment			
	Maximum		Average		Maximum		Average		Maximum		Average		Maximum		Average	
Model	Value (kN)	%diff (%)	Value (kN)	%diff (%)	Value (kN m)	%diff (%)	Value (kN m)	%diff (%)	Value (kN)	%diff (%)	Value (kN)	%diff (%)	Value (kN m)	%diff (%)	Value (kN m)	%diff (%)
5MW3UB00	1153	0.0	1070	0.0	13018	0.0	2581	0.0	1219	0.0	278	0.0	7142	0.0	2149	0.0
5MW2UB00	1103	-4.4	933	-12.8	17106	31.4	3786	46.7	1066	-12.6	267	-4.2	5924	-17.1	2639	22.8
5MW2UB00TipBrk	1009	-12.5	915	-14.4	7310	-43.8	3034	17.5	1266	3.9	318	14.3	6337	-11.3	2880	34.0
5MW2UBUT	1100	-4.6	900	-15.8	15613	19.9	2556	-1.0	1161	-4.8	297	6.8	6009	-15.9	2384	11.0
5MW2UBUTTipBrk	1028	-10.8	916	-14.4	7194	-44.7	3085	19.5	1187	-2.6	350	25.8	6357	-11.0	3022	40.7
5MW2DB00	1117	-3.2	974	-8.9	14296	9.8	3331	29.0	-974	-179.9	100	-64.0	6214	-13.0	1553	-27.7
5MW2DB00TipBrk	1073	-6.9	937	-12.4	6349	-51.2	2708	4.9	1100	-9.8	154	-44.6	6584	-7.8	2922	36.0
5MW2DBUT	1175	1.9	941	-12.1	15931	22.4	2786	7.9	966	-20.7	129	-53.6	6365	-10.9	2331	8.5
5MW2DBUTTipBrk	1079	-6.4	937	-12.4	5884	-54.8	2662	3.1	995	-18.4	184	-33.8	6644	-7.0	2973	38.4
5MW2DB00T5C0	1115	-3.3	974	-9.0	14530	11.6	3510	36.0	-986	-180.9	102	-63.2	6269	-12.2	1550	-27.9
5MW2DB00T5C0TipBrk	1074	-6.8	936	-12.5	6495	-50.1	2913	12.9	1121	-8.0	156	-44.0	6641	-7.0	2882	34.1
5MW2DB00T0C2.5	1097	-4.8	960	-10.2	15661	20.3	3223	24.9	989	-18.9	180	-35.3	6307	-11.7	2134	-0.7
5MW2DB00T0C2.5TipBrk	1044	-9.5	926	-13.4	6151	-52.8	2562	-0.7	1191	-2.3	234	-15.9	6698	-6.2	2750	28.0
5MW2DB00T0C0	1097	-4.9	960	-10.3	15851	21.8	3407	32.0	1004	-17.6	182	-34.6	6433	-9.9	2144	-0.2
5MW2DB00T0C0TipBrk	1048	-9.2	924	-13.7	6888	-47.1	2799	8.4	1211	-0.7	236	-15.3	6742	-5.6	2803	30.5
5MW2DB00TeeterNo	1128	-2.2	974	-8.9	18026	38.5	3608	39.8	-971	-179.6	101	-63.9	6101	-14.6	1557	-27.5

Table 9.17. Load effects at LSS under parked conditions.

	Shear Force				Bending Moment				Axial Force				Torsional Moment			
	Maximum		Average		Maximum		Average		Maximum		Average		Maximum		Average	
Model	Value (kN)	%diff (%)	Value (kN)	%diff (%)	Value (kN m)	%diff (%)	Value (kN m)	%diff (%)	Value (kN)	%diff (%)	Value (kN)	%diff (%)	Value (kN m)	%diff (%)	Value (kN m)	%diff (%)
5MW3UB00	1147	0.0	1140	0.0	5723	0.0	4671	0.0	450	0.0	222	0.0	2840	0.0	2508	0.0
5MW2UB00	945	-17.6	912	-20.0	4036	-29.5	3952	-15.4	308	-31.4	199	-10.7	1455	-48.8	1409	-43.8
5MW2UB00TipBrk	950	-17.2	914	-19.8	4039	-29.4	3955	-15.3	278	-38.1	199	-10.6	1477	-48.0	1423	-43.2
5MW2UBUT	951	-17.1	911	-20.1	4040	-29.4	3952	-15.4	302	-33.0	197	-11.4	1734	-38.9	1675	-33.2
5MW2UBUTTipBrk	952	-17.0	913	-19.9	4044	-29.3	3955	-15.3	319	-29.0	197	-11.3	1728	-39.2	1674	-33.2
5MW2DB00	1023	-10.8	1021	-10.4	3655	-36.1	3554	-23.9	-391	-187.0	-107	-148.1	2826	-0.5	1300	-48.2
5MW2DB00TipBrk	1024	-10.7	1022	-10.3	3684	-35.6	3553	-23.9	-342	-176.1	-107	-148.2	2826	-0.5	1320	-47.3
5MW2DBUT	1030	-10.2	1028	-9.8	3661	-36.0	3518	-24.7	-392	-187.1	-107	-147.9	2972	4.6	1546	-38.3
5MW2DBUTTipBrk	1031	-10.1	1030	-9.7	3663	-36.0	3516	-24.7	-397	-188.3	-107	-147.9	2975	4.8	1579	-37.0
5MW2DB00T5C0	1025	-10.6	1024	-10.2	3837	-33.0	3738	-20.0	-394	-187.5	-107	-148.2	2813	-1.0	1216	-51.5
5MW2DB00T5C0TipBrk	1027	-10.4	1025	-10.0	3828	-33.1	3738	-20.0	-343	-176.2	-107	-148.3	2745	-3.3	1236	-50.7
5MW2DB00T0C2.5	939	-18.1	938	-17.7	3625	-36.7	3536	-24.3	-364	-180.9	116	-47.7	1291	-54.5	971	-61.3
5MW2DB00T0C2.5TipBrk	942	-17.9	939	-17.6	3631	-36.6	3535	-24.3	-318	-170.8	116	-47.7	1429	-49.7	992	-60.4
5MW2DB00T0C0	940	-18.0	938	-17.7	3774	-34.1	3698	-20.8	-365	-181.1	117	-47.4	1327	-53.3	975	-61.1
5MW2DB00T0C0TipBrk	942	-17.9	940	-17.5	3780	-33.9	3699	-20.8	-320	-171.2	117	-47.4	1416	-50.1	1004	-60.0
5MW2DB00TeeterNo	1022	-10.9	1021	-10.4	4004	-30.0	3548	-24.0	-394	-187.7	-107	-148.1	2845	0.2	1300	-48.2

Table 9.18. Torques under normal operating conditions.

	LSS				HSS				Generator			
	Maximum		Average		Maximum		Average		Maximum		Average	
Model	Value (kN m)	%diff (%)	Value (kN m)	%diff (%)	Value (kN m)	%diff (%)	Value (kN m)	%diff (%)	Value (kN m)	%diff (%)	Value (kN m)	%diff (%)
5MW3UB00	5549	0.0	4189	0.0	57	0.0	43	0.0	47	0.0	43	0.0
5MW2UB00	4458	-19.7	3168	-24.4	46	-19.7	33	-24.4	36	-24.4	33	-24.4
5MW2UB00TipBrk	4471	-19.4	3168	-24.4	46	-19.4	33	-24.4	36	-24.4	33	-24.4
5MW2UBUT	4489	-19.1	3198	-23.6	46	-19.1	33	-23.6	36	-23.6	33	-23.6
5MW2UBUTTipBrk	4519	-18.6	3198	-23.6	47	-18.6	33	-23.6	36	-23.6	33	-23.6
5MW2DB00	5005	-9.8	3167	-24.4	52	-9.8	33	-24.4	36	-24.4	33	-24.4
5MW2DB00TipBrk	5145	-7.3	3167	-24.4	53	-7.3	33	-24.4	36	-24.4	33	-24.4
5MW2DBUT	4983	-10.2	3199	-23.6	51	-10.2	33	-23.6	36	-23.6	33	-23.6
5MW2DBUTTipBrk	5089	-8.3	3199	-23.6	52	-8.3	33	-23.6	36	-23.6	33	-23.6
5MW2DB00T5C0	5091	-8.2	3167	-24.4	52	-8.3	33	-24.4	36	-24.4	33	-24.4
5MW2DB00T5C0TipBrk	5228	-5.8	3167	-24.4	54	-5.8	33	-24.4	36	-24.4	33	-24.4
5MW2DB00T0C2.5	5106	-8.0	3167	-24.4	53	-8.0	33	-24.4	36	-24.4	33	-24.4
5MW2DB00T0C2.5TipBrk	5269	-5.0	3167	-24.4	54	-5.0	33	-24.4	36	-24.4	33	-24.4
5MW2DB00T0C0	5235	-5.6	3167	-24.4	54	-5.6	33	-24.4	36	-24.4	33	-24.4
5MW2DB00T0C0TipBrk	5391	-2.8	3167	-24.4	56	-2.8	33	-24.4	36	-24.4	33	-24.4
5MW2DB00TeeterNo	4956	-10.7	3167	-24.4	51	-10.7	33	-24.4	36	-24.4	33	-24.4

Table 9.19. Torques under fault conditions.

	LSS				HSS				Generator			
	Maximum		Average		Maximum		Average		Maximum		Average	
Model	Value (kN m)	%diff (%)	Value (kN m)	%diff (%)	Value (kN m)	%diff (%)	Value (kN m)	%diff (%)	Value (kN m)	%diff (%)	Value (kN m)	%diff (%)
5MW3UB00	7142	0.0	2149	0.0	74	0.0	22	0.0	47	0.0	15	0.0
5MW2UB00	5924	-17.1	2639	22.8	61	-17.1	27	22.8	36	-24.4	13	-12.8
5MW2UB00TipBrk	6337	-11.3	2880	34.0	65	-11.3	30	34.0	36	-24.4	17	9.5
5MW2UBUT	6009	-15.9	2384	11.0	62	-15.9	25	11.0	36	-23.6	13	-16.8
5MW2UBUTTipBrk	6357	-11.0	3022	40.7	66	-11.0	31	40.7	36	-23.6	17	10.6
5MW2DB00	6214	-13.0	1553	-27.7	64	-13.0	16	-27.7	36	-24.4	12	-23.8
5MW2DB00TipBrk	6584	-7.8	2922	36.0	68	-7.8	30	36.0	36	-24.4	17	9.5
5MW2DBUT	6365	-10.9	2331	8.5	66	-10.9	24	8.5	36	-23.6	13	-16.2
5MW2DBUTTipBrk	6644	-7.0	2973	38.4	68	-7.0	31	38.3	36	-23.6	17	10.6
5MW2DB00T5C0	6269	-12.2	1550	-27.9	65	-12.2	16	-27.9	36	-24.4	12	-23.8
5MW2DB00T5C0TipBrk	6641	-7.0	2882	34.1	68	-7.0	30	34.1	36	-24.4	17	9.5
5MW2DB00T0C2.5	6307	-11.7	2134	-0.7	65	-11.7	22	-0.7	36	-24.4	12	-20.3
5MW2DB00T0C2.5TipBrk	6698	-6.2	2750	28.0	69	-6.2	28	28.0	36	-24.4	17	9.5
5MW2DB00T0C0	6433	-9.9	2144	-0.2	66	-9.9	22	-0.2	36	-24.4	12	-20.0
5MW2DB00T0C0TipBrk	6742	-5.6	2803	30.5	70	-5.6	29	30.5	36	-24.4	17	9.5
5MW2DB00TeeterNo	6101	-14.6	1557	-27.5	63	-14.6	16	-27.5	36	-24.4	12	-23.5

Table 9.20. Torques under parked conditions.

	LSS				HSS			
	Maximum		Average		Maximum		Average	
Model	Value (kN m)	%diff (%)	Value (kN m)	%diff (%)	Value (kN m)	%diff (%)	Value (kN m)	%diff (%)
5MW3UB00	2840	0.0	2508	0.0	29	0.0	26	0.0
5MW2UB00	1455	-48.8	1409	-43.8	15	-48.8	15	-43.8
5MW2UB00TipBrk	1477	-48.0	1423	-43.2	15	-48.0	15	-43.2
5MW2UBUT	1734	-38.9	1675	-33.2	18	-38.9	17	-33.2
5MW2UBUTTipBrk	1728	-39.2	1674	-33.2	18	-39.2	17	-33.2
5MW2DB00	2826	-0.5	1300	-48.2	29	-0.5	13	-48.2
5MW2DB00TipBrk	2826	-0.5	1320	-47.3	29	-0.5	14	-47.3
5MW2DBUT	2972	4.6	1546	-38.3	31	4.6	16	-38.3
5MW2DBUTTipBrk	2975	4.8	1579	-37.0	31	4.7	16	-37.0
5MW2DB00T5C0	2813	-1.0	1216	-51.5	29	-1.0	13	-51.5
5MW2DB00T5C0TipBrk	2745	-3.3	1236	-50.7	28	-3.3	13	-50.7
5MW2DB00T0C2.5	1291	-54.5	971	-61.3	13	-54.5	10	-61.3
5MW2DB00T0C2.5TipBrk	1429	-49.7	992	-60.4	15	-49.7	10	-60.5
5MW2DB00T0C0	1327	-53.3	975	-61.1	14	-53.3	10	-61.1
5MW2DB00T0C0TipBrk	1416	-50.1	1004	-60.0	15	-50.1	10	-60.0
5MW2DB00TeeterNo	2845	0.2	1300	-48.2	29	0.2	13	-48.2

Table 9.21. Minimum tower-to-blade clearance.

Condition	Normal operating		Fault		Parked	
Model	Value (m)	%diff (%)	Value (m)	%diff (%)	Value (m)	%diff (%)
5MW3UB00	6.59	0.0	5.82	0.0	33.47	0.0
5MW2UB00	4.04	-38.7	3.89	-33.0	63.21	-0.2
5MW2UB00TipBrk	4.36	-33.8	2.66	-61.9	63.21	-0.2
5MW2UBUT	3.08	-54.1	2.65	-54.4	63.21	-0.2
5MW2UBUTTipBrk	3.29	-50.9	2.66	-54.2	63.21	-0.2
5MW2DB00	10.30	56.3	4.76	-18.2	63.29	89.1
5MW2DB00TipBrk	10.37	57.3	10.01	43.5	63.29	89.1
5MW2DBUT	10.24	52.7	6.28	8.0	63.12	88.6
5MW2DBUTTipBrk	10.24	52.7	9.38	34.6	63.10	88.5
5MW2DB00T5C0	8.19	24.3	2.00	-65.7	63.06	88.4
5MW2DB00T5C0TipBrk	8.28	25.6	7.65	9.8	63.06	88.4
5MW2DB00T0C2.5	4.62	-29.9	0.88	-87.4	63.31	0.0
5MW2DB00T0C2.5TipBrk	4.69	-28.9	3.99	-42.8	63.29	0.0
5MW2DB00T0C0	2.48	-62.4	0.02	-99.7	63.09	-0.3
5MW2DB00T0C0TipBrk	2.54	-61.4	1.67	-76.1	63.08	-0.4
5MW2DB00TeeterNo	10.26	55.6	6.75	16.1	63.33	0.0

Table 9.22. Maximum and minimum teeter angle.

Condition	Normal operating		Fault		Parked	
Model	Max (deg)	Min (deg)	Max (deg)	Min (deg)	Max (deg)	Min (deg)
5MW3UB00	0.00	0.00	0.00	0.00	0.00	0.00
5MW2UB00	2.38	-2.69	5.94	-1.49	1.04	-0.02
5MW2UB00TipBrk	2.36	-2.65	2.97	-1.82	1.04	-0.02
5MW2UBUT	2.99	-3.17	5.20	-1.63	1.05	-0.02
5MW2UBUTTipBrk	2.97	-3.22	3.00	-1.65	1.05	-0.02
5MW2DB00	2.74	-3.09	5.05	-1.49	1.01	-0.06
5MW2DB00TipBrk	2.71	-3.04	3.19	-2.75	1.01	-0.06
5MW2DBUT	3.44	-3.24	4.77	-1.71	1.01	-0.08
5MW2DBUTTipBrk	3.44	-3.19	2.58	-2.62	1.01	-0.08
5MW2DB00T5C0	2.57	-2.96	5.14	-1.41	1.02	-0.07
5MW2DB00T5C0TipBrk	2.54	-2.91	3.26	-2.77	1.01	-0.07
5MW2DB00T0C2.5	2.68	-3.04	5.47	-1.48	1.00	-0.07
5MW2DB00T0C2.5TipBrk	2.64	-2.99	2.58	-1.95	1.01	-0.08
5MW2DB00T0C0	2.52	-2.93	5.55	-1.45	1.00	-0.07
5MW2DB00T0C0TipBrk	2.48	-2.89	2.67	-1.93	1.00	-0.07
5MW2DB00TeeterNo	0.00	0.00	0.00	0.00	0.00	0.00

9.1.8 Fatigue Life Estimation

Cumulative fatigue damage values at four critical wind turbine locations are calculated for different turbine designs using the NREL MLife code. Wind turbine responses to external forces are determined by the FAST code. The output files of load time histories generated by FAST are used as input files in MLife in order to extrapolate fatigue damage over the turbine lifetime. Six 10-minute FAST simulations were run at each mean wind speed to generate load time histories at normal operating conditions. Simulations were run for 12 different mean wind speeds of 3, 5, 7, 9, 11, 13, 15, 17, 19, 21, 23 and 25 m/s. See Section 4.4 for the methodology used for estimating the fatigue damage.

As mentioned earlier in Section 9.1, fatigue damaged is investigated at four critical turbine locations the blade root, tower base, tower top and LSS. Four types of load effects used for this purpose include shear forces, bending moments, axial forces, and torsional moments. Damage values that these four load effects cause were calculated at all four locations. The results are then compared with those of the baseline 5MW 3-bladed upwind turbine. Descriptions of various turbine models are in Appendix 1.

The analysis of the results show that the 2-bladed downwind turbine has average fatigue damage values considerably less than one in all four critical locations under study. A value of damage equal to one indicates failure. Also, damage accumulation at critical locations of the 2-bladed downwind turbine is comparable to the damage accumulation of the baseline 3-bladed upwind turbine.

In Figure 9.20 the average fatigue damage accumulation due to the most critical loads, such as the blade root shear force and bending moment, tower base shear force and bending moment, and tower top shear force are compared across the three turbine designs. While all of the turbine designs considered here have average damage less than 0.15, 5MW2UBUT and 5MW2DBUT designs incur more damage than the other designs due to the bending moment and the shear forces at the blade root.

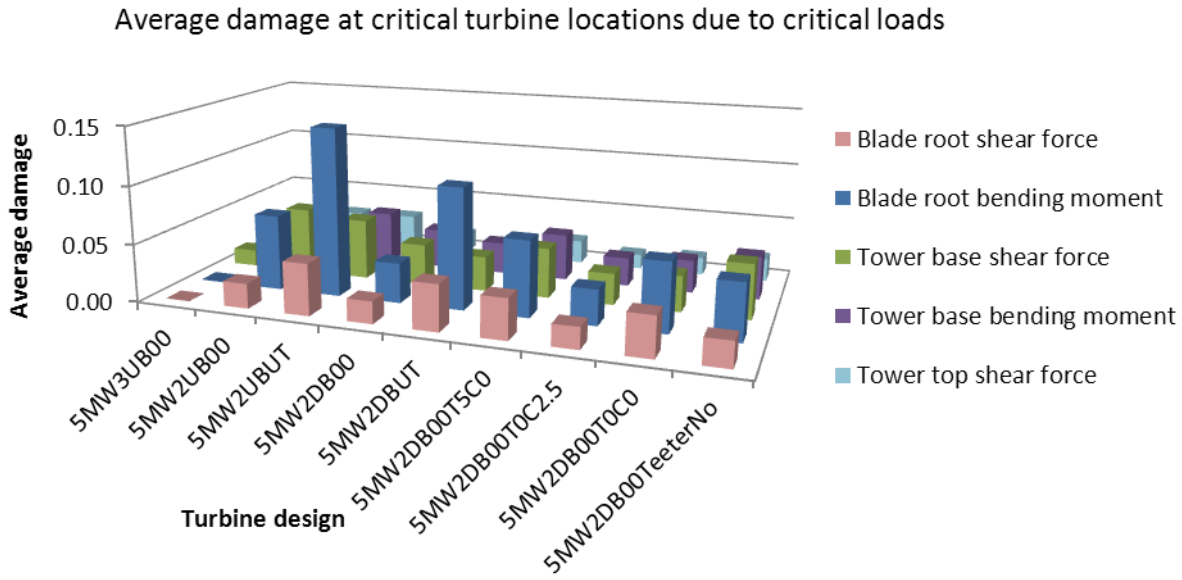

Figure 9.20. Average damage accumulation at critical turbine location.

Figure 9.21 compares the relative damage due to the most critical loads for the turbine designs. The design with most damage was considered to have relative damage of one and the rest of the designs were ranked accordingly. For example, from Figure 9.21, it is observed that design 5MW3UB00 experiences the least damage caused by the blade root bending moment among all other designs. Likewise, 5MW2DB00 turbine experiences relatively lower damage due to blade root bending moment than the other designs. 5MW2DB00 turbine experiences the most damage caused by the tower base bending moment. Tower top shear force causes most damage in 5MW2DBUT turbine.

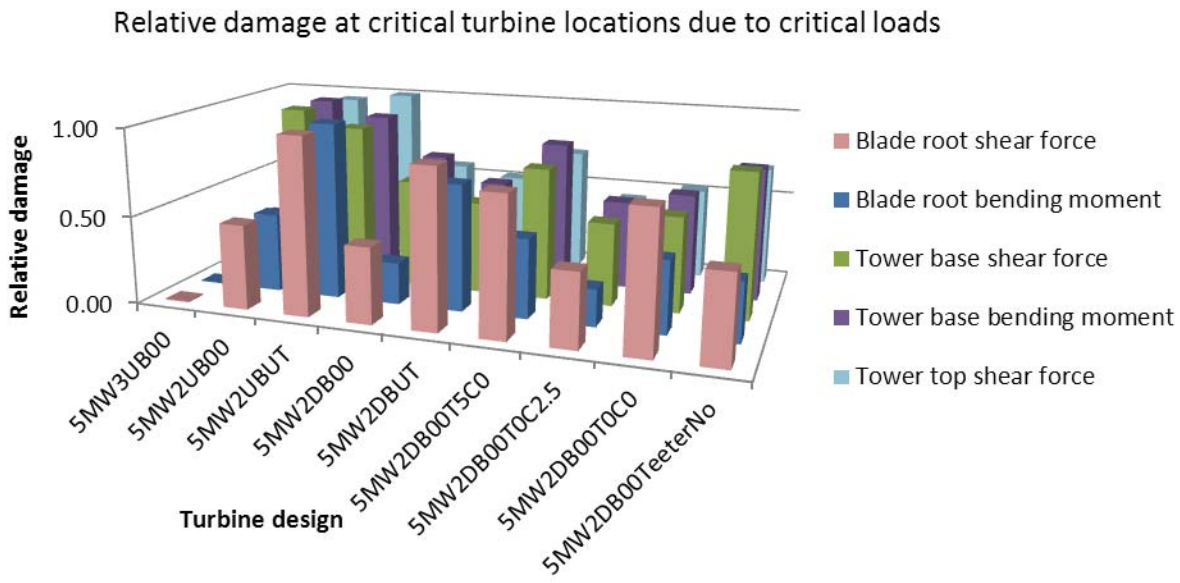

Figure 9.21. Relative damage accumulation at the critical turbine location of each turbine.

The relative damage at each location is discussed below:

Damage at Tower Base and Tower Top

Figure 9.22 to Figure 9.25 illustrate the damage at the tower base and the tower top. Shear forces and bending moments dominate at the tower base in terms of damage accumulation. Adding a teeter mechanism reduces significantly the fatigue loading due to the bending moment at the tower top, whereas this effect is insignificant at the tower base where thrust loads dominate the moments. In relative comparison, the 2-bladed downwind turbine with baseline blades having zero tilt angle and 2.5° coning angle incurs less damage at the tower base than other two bladed turbines. The 2-bladed upwind turbine with baseline blades experiences most damage due to shear force and bending moment. The average damage accumulation at the tower base and tower top due to different load effects is listed in Table 9.23 and Table 9.24, respectively. Figure 9.24 and Figure 9.25 depict the same results for the tower top.

Table 9.23. Lifetime damage at tower base.

Turbine design	Shear force	Bending moment	Axial force	Torsional moment
5MW3UB00	1.4277E-02	1.2199E-02	6.3623E-25	3.0116E-12
5MW2UB00	5.7550E-02	4.9290E-02	1.6840E-23	1.6244E-11
5MW2UBUT	5.2446E-02	4.5283E-02	1.8498E-23	1.5223E-11
5MW2DB00	3.5496E-02	3.4299E-02	1.4951E-21	1.3957E-10
5MW2DBUT	3.0143E-02	2.7582E-02	4.4547E-21	3.7905E-10
5MW2DB00T5C0	4.3164E-02	4.0436E-02	1.2337E-21	1.0677E-10
5MW2DB00T0C2.5	2.7140E-02	2.4956E-02	1.5365E-21	4.9833E-11
5MW2DB00T0C0	3.1286E-02	2.8473E-02	4.3420E-22	4.1915E-11
5MW2DB00TeeterNo	4.7185E-02	3.7426E-02	1.7048E-22	3.0414E-09

Table 9.24. Lifetime damage at tower top.

Turbine design	Shear force	Bending moment	Axial force	Torsional moment
5MW3UB00	7.9408E-03	4.0846E-10	5.6596E-23	3.0132E-12
5MW2UB00	2.7979E-02	5.0298E-10	2.0364E-21	1.6242E-11
5MW2UBUT	2.9275E-02	7.7331E-10	1.9557E-21	1.5223E-11
5MW2DB00	1.6597E-02	9.6986E-08	2.5073E-19	1.3965E-10
5MW2DBUT	1.5124E-02	1.8128E-07	7.3457E-19	3.7902E-10
5MW2DB00T5C0	2.0464E-02	5.3171E-08	2.1331E-19	1.0679E-10
5MW2DB00T0C2.5	1.2764E-02	8.5464E-08	2.5074E-19	4.9859E-11
5MW2DB00T0C0	1.5257E-02	6.1773E-08	7.0512E-20	4.1931E-11
5MW2DB00TeeterNo	1.9935E-02	5.3762E-05	3.0132E-20	3.0415E-09

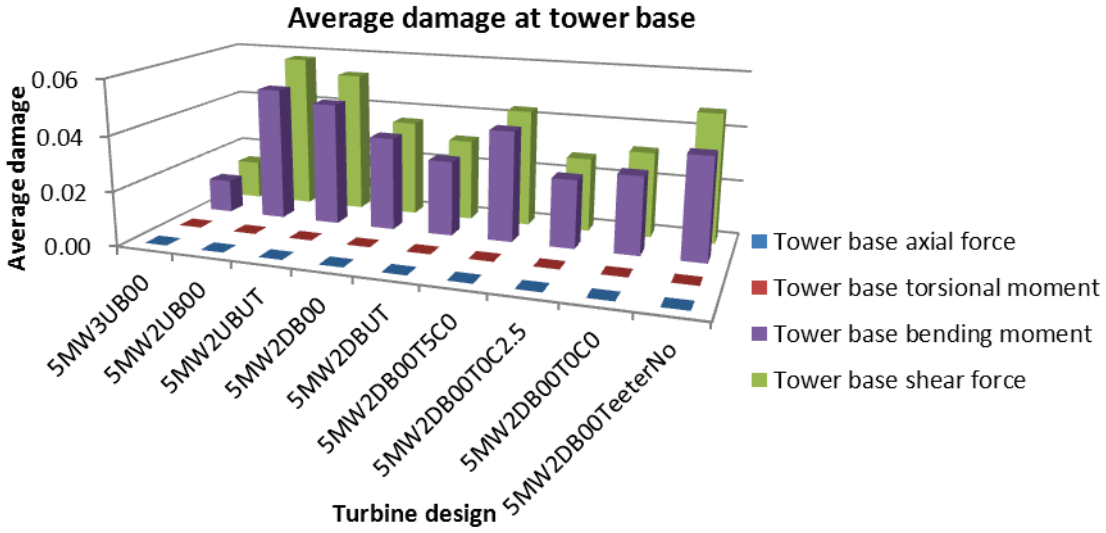

Figure 9.22. Average damage at tower base.

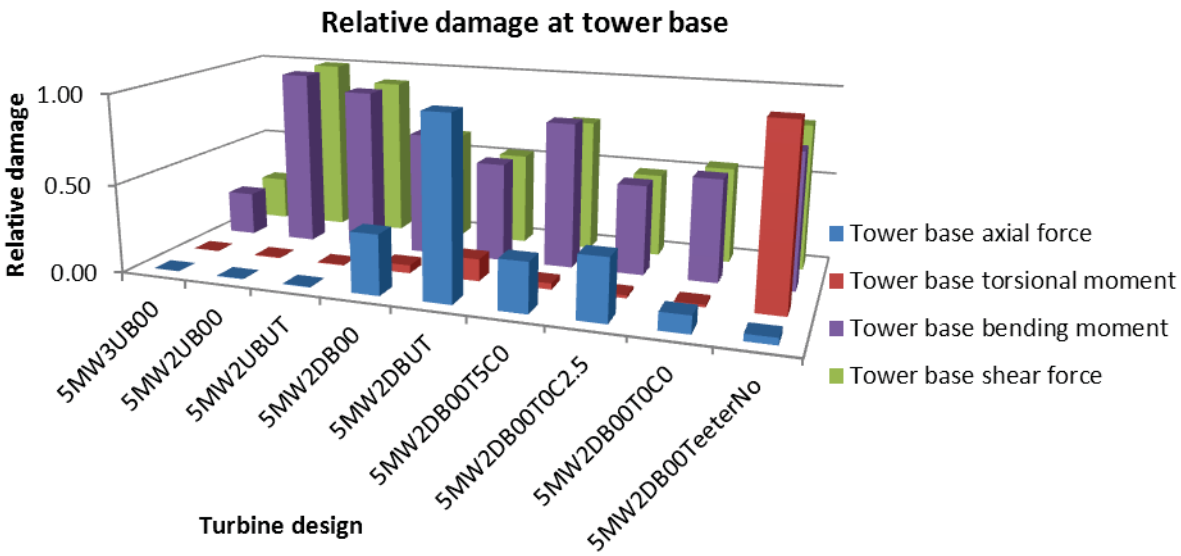

Figure 9.23. Relative damage at tower base.

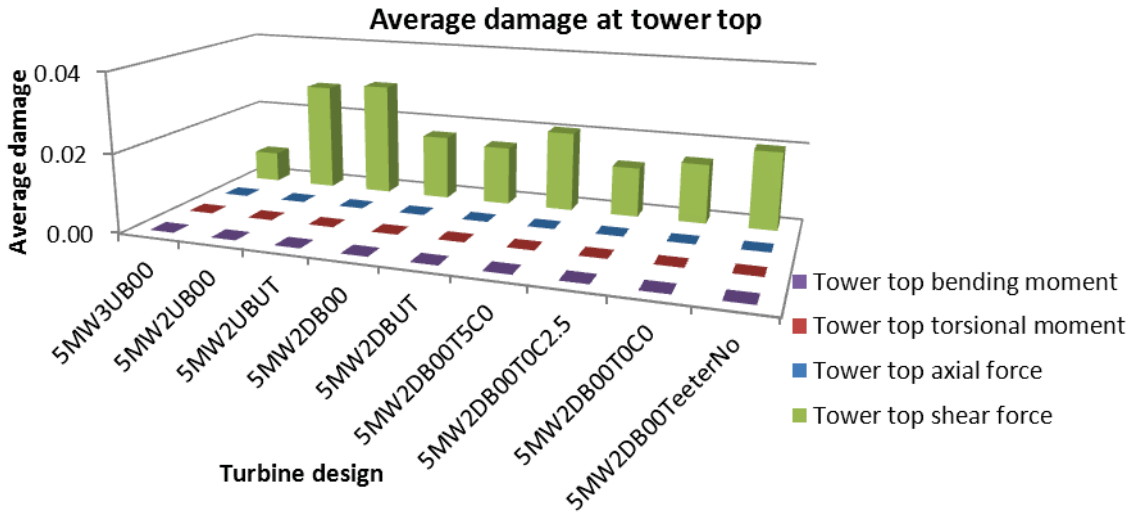

Figure 9.24. Average damage at tower top.

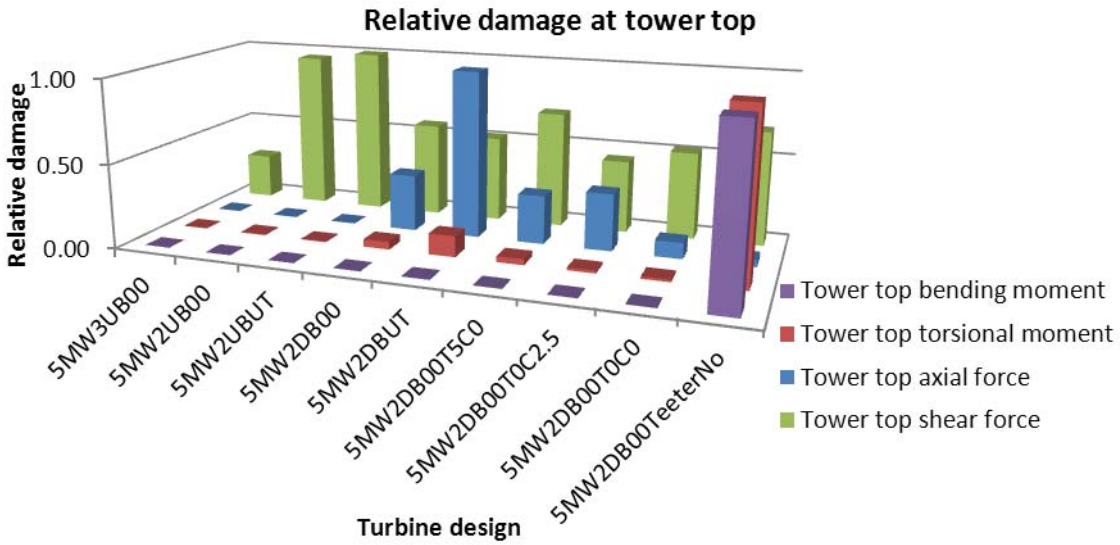

Figure 9.25. Relative damage at tower top.

Damage at Blade Root

Table 9.25 compares the damage at the blade root across all the turbine designs. The 2-bladed upwind and downwind blade designs with the BUT blade are the most vulnerable to fatigue failure. The 2-bladed downwind turbine with baseline blades is safe having comparable fatigue damage to the baseline reference 3-bladed upwind turbine at the blade root.

These results in Figure 9.26 suggest that the blade root is more vulnerable to fatigue due to the bending moment than other turbine components.

Table 9.25. Lifetime damage at blade root.

Turbine design	Shear force	Bending moment	Axial force	Torsional moment
5MW3UB00	2.9347E-04	8.1039E-04	3.4951E-06	4.4155E-08
5MW2UB00	2.1350E-02	6.5222E-02	9.7910E-05	1.7440E-06
5MW2UBUT	4.4421E-02	1.4524E-01	4.2582E-04	3.3670E-06
5MW2DB00	1.9088E-02	3.4523E-02	1.1141E-04	6.7553E-07
5MW2DBUT	3.9693E-02	1.0416E-01	3.9767E-04	3.0143E-06
5MW2DB00T5C0	3.4721E-02	6.5354E-02	1.0144E-04	1.5607E-06
5MW2DB00T0C2.5	1.8456E-02	3.0595E-02	1.1077E-04	1.2343E-06
5MW2DB00T0C0	3.4433E-02	5.9418E-02	9.2329E-05	3.1834E-06
5MW2DB00TeeterNo	2.1916E-02	4.8876E-02	8.7312E-05	7.5430E-07

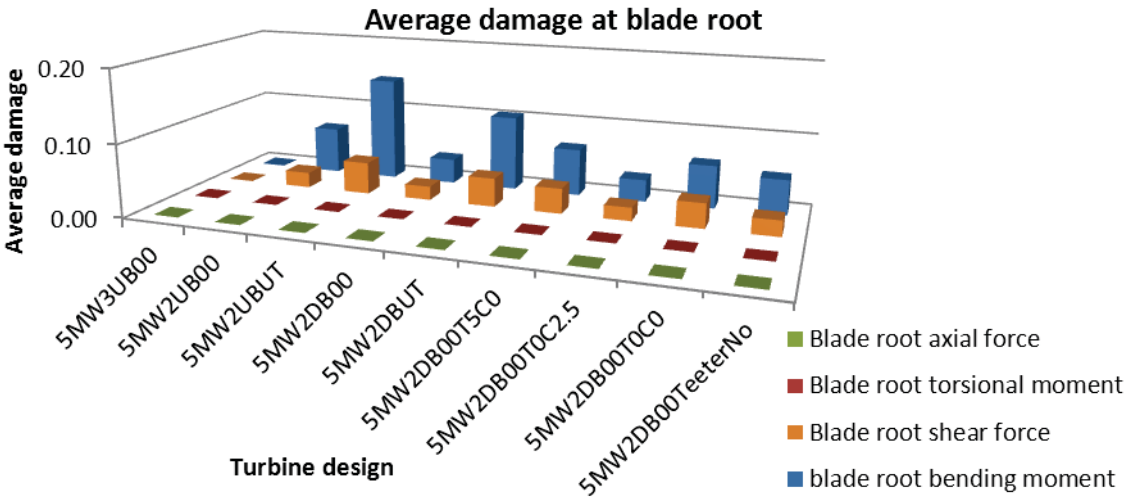

Figure 9.26. Average damage at blade root.

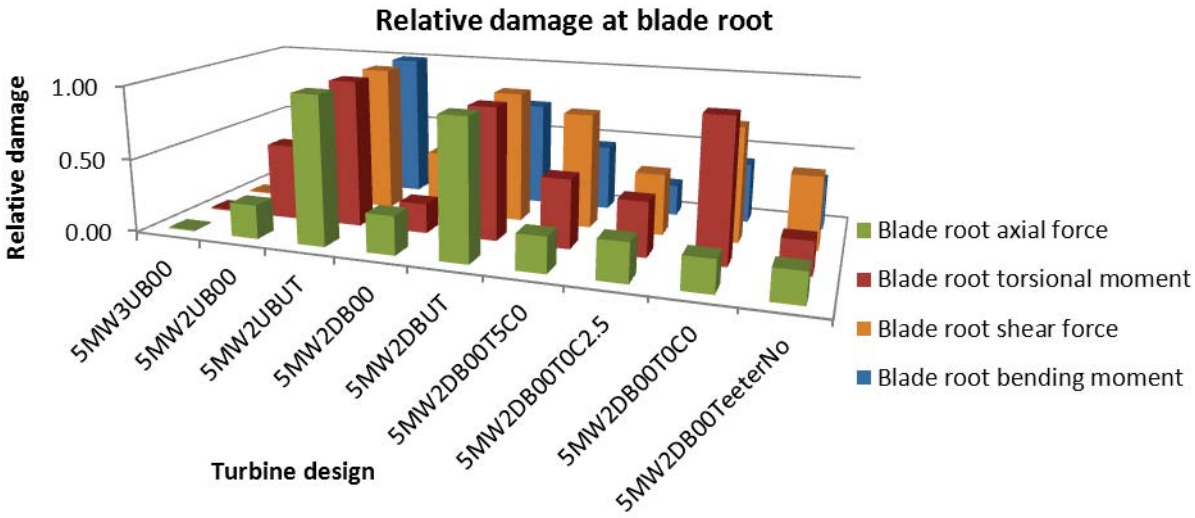

Figure 9.27. Relative damage at blade root.

Figure 9.27 shows that, among all turbine designs considered in this study, 5MW2UBUT design accumulates more damage at the blade root than any other design. It is also observed that increasing the coning angle from 0 to 2.5° reduces the torsional moment, shear force as well as bending moment. However, damage caused by axial force is minimum for the turbine with zero conning angle. Reducing tilt angle from 5 to 0° increases the damage due to the torsional moment.

Damage at Low Speed Shaft

Introducing a teeter mechanism reduces the LSS bending moments significantly as shown in Figure 9.28. The relative damage comparison in Figure 9.29 shows that increasing the tilt angle from zero degrees to five degrees considerably reduces the damage inflicted to the LSS by torsional moment. Also, increasing coning angle from zero degrees to 2.5 degrees has the similar effect on the design.

The lifetime cumulative damage inflicted to the LSS due to different load effects is listed in Table 9.26.

Table 9.26. Lifetime damage at LSS.

Turbine design	Shear force	Bending moment	Axial force	Torsional moment
5MW3UB00	1.5453E-18	1.3805E-07	1.0231E-04	1.0886E-08
5MW2UB00	8.1575E-17	8.3091E-07	2.0157E-04	1.8108E-09
5MW2UBUT	7.6770E-17	1.1795E-06	3.2269E-04	1.8571E-09
5MW2DB00	2.7042E-14	1.0142E-05	9.6315E-05	5.8518E-08
5MW2DBUT	7.7535E-14	1.1017E-05	1.5381E-04	4.2132E-08
5MW2DB00T5C0	2.1046E-14	1.0868E-05	1.2291E-04	1.0179E-07
5MW2DB00T0C2.5	3.0401E-14	3.9987E-06	1.1719E-04	1.1194E-07
5MW2DB00T0C0	9.2225E-15	4.9234E-06	1.5460E-04	2.2945E-07
5MW2DB00TeeterNo	7.0115E-15	7.8443E-03	1.1258E-04	5.6861E-08

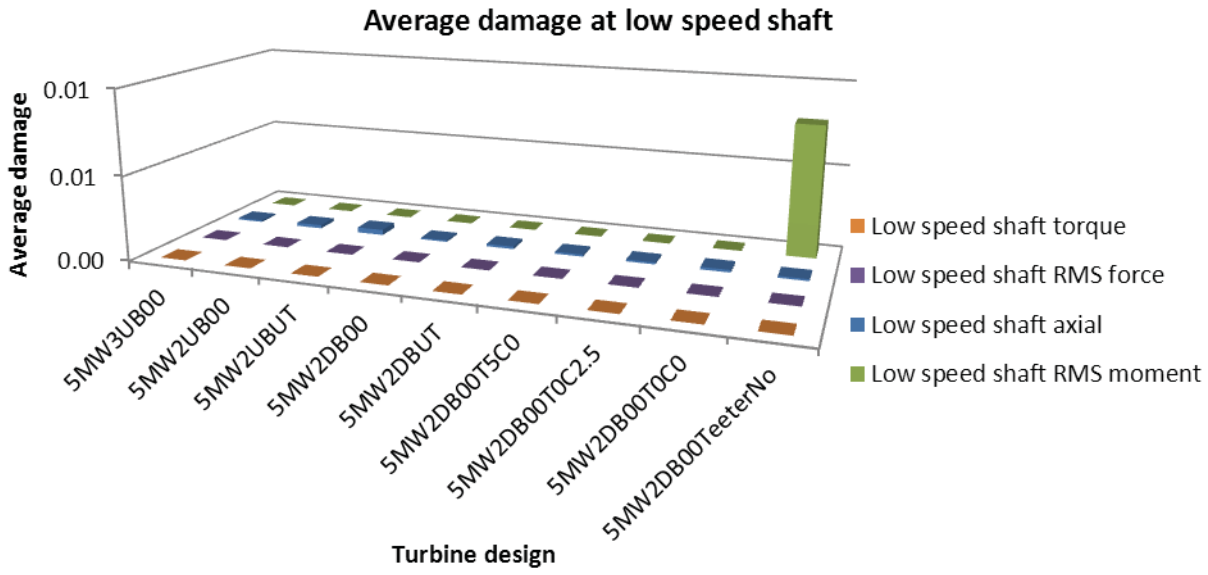

Figure 9.28. Average damage at LSS

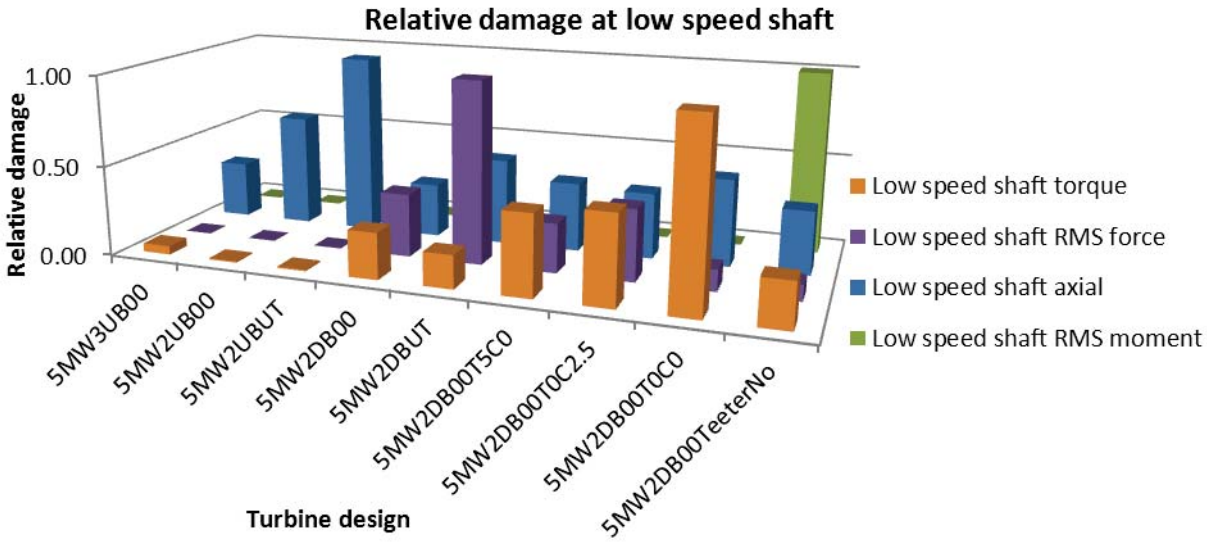

Figure 9.29. Relative damage at LSS.

The average damage accumulation at critical turbine locations caused by bending moment, shear force, axial force and torsional moment are summarized for different turbine designs in Figure 9.30 to Figure 9.33.

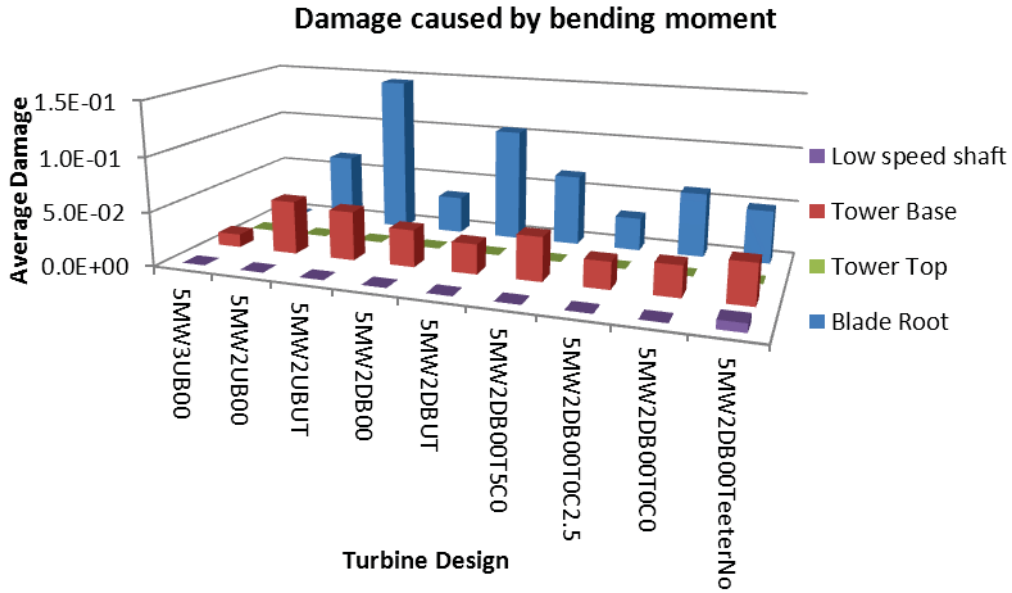

Figure 9.30. Average damage due to bending moment at tower base, tower top, blade root, and LSS.

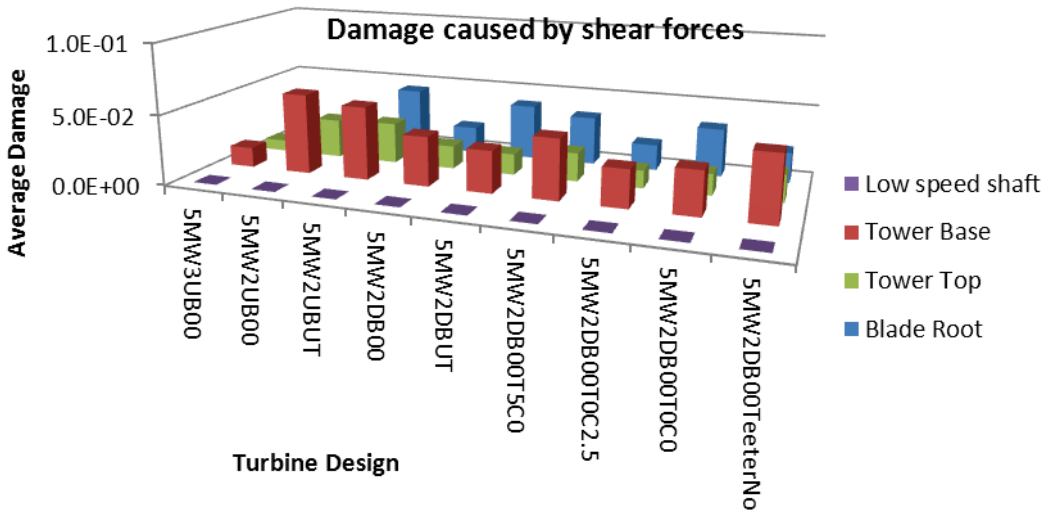

Figure 9.31. Average damage due to shear force at LSS, tower base, tower top, and blade root.

Figure 9.31 shows that blade shear force inflicts more damage at the tower base than at other locations.

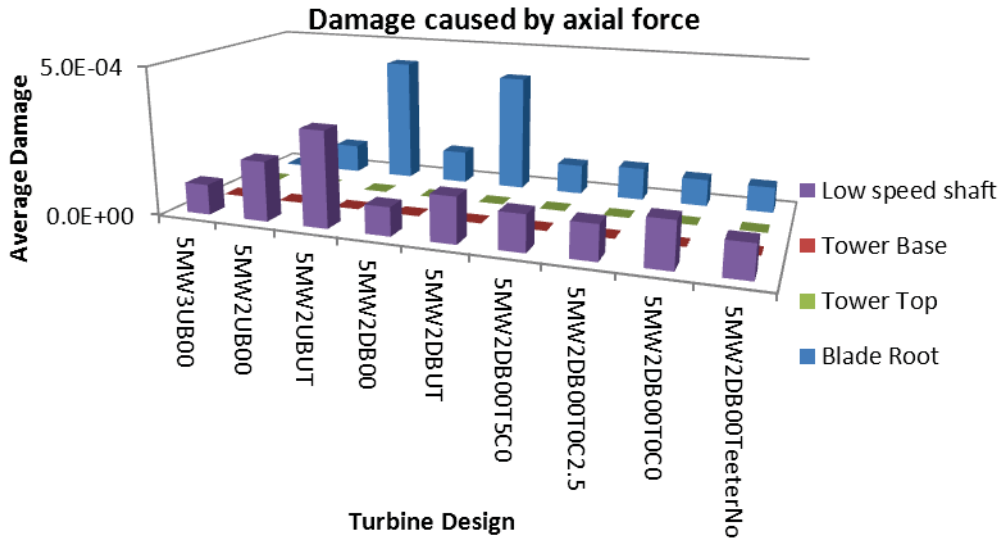

Figure 9.32. Average damage due to axial force at LSS, tower base, tower top, and blade root.

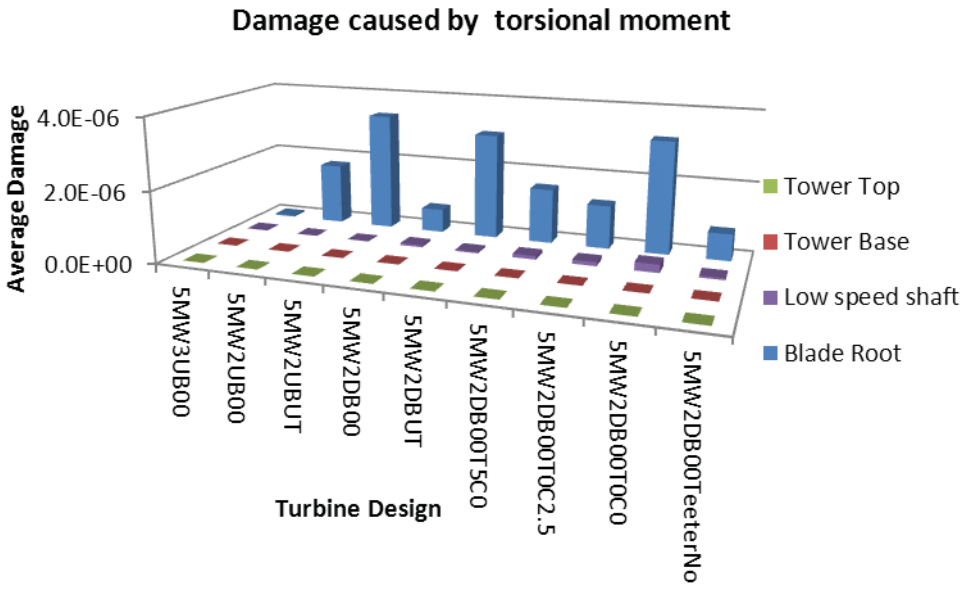

Figure 9.33. Average damage due to torsional moment at tower base, tower top, blade root, and LSS.

Conclusions

The results of fatigue analysis suggest that the 3-bladed baseline NREL turbine has relatively less damage at the four critical locations than the 2-bladed upwind and downwind turbine designs in this study. The 2-bladed upwind and downwind turbines with the BUT blade are the most vulnerable to fatigue failure. In addition, the results indicate that the damage due to bending moment on the blade root often dominates. Utilization of a teeter mechanism in a turbine system can effectively decrease the fatigue damage. Increasing the coning angle also decreases damage caused by bending moments, shear forces and torsional moments at a blade root. Increasing the tilt angle reduces the damage associated with torsional moment at the blade root and damage caused by the LSS torsional moment.

9.2 Loads Applied to the Foundation

In this section, the loads that are transferred from the turbine to the foundation for different configurations are compared. For this purpose, 3- and 2-bladed upwind and 2-bladed downwind configurations were considered. It should be noted that the wave and ice loads are driving the foundation design as it was shown in Chapter 7. Although the loads due to the operation of the turbine are not dominating the foundation design, the comparison of these loads would be beneficial and is presented here.

Table 9.27 compares the load effects at the base of the tower under normal operating conditions for different configurations.

In general, 2-bladed designs are subjected to higher shear forces and bending moments than the 3-bladed design. The largest maximum shear force is observed for the 2-bladed downwind

configuration, but it is almost equal to the shear force for the 2-bladed upwind configuration. The same trend is observed for the bending moments. As expected, the axial forces for the 2-bladed configurations are slightly smaller than those of the design with three blades. The torsional moment at the base of the tower for 2-bladed downwind configuration is comparable with that for the 3-bladed one. However, the torsional moment for the 2-bladed upwind configuration is considerably smaller than that for the other two concepts.

Different trends are observed for average load effects. The 3-bladed concept has the maximum average shear force. This could be because average thrust load is larger for this concept. For the same reason, the average bending moments are smaller for the 2-bladed downwind configuration. Average axial force is smaller for the 2-bladed concepts as the turbine weight is smaller. However, the torsional moment for the 2-bladed downwind configuration is the largest among the three concepts.

Table 9.27. Result data at tower base under normal operating conditions.

Load Effects		Shear Force			Bending Moment			Axial Force			Torsional Moment		
		Value (kN)	DLC (-)	Vs (m/s)	Value (kN m)	DLC (-)	Vs (m/s)	Value (kN)	DLC (-)	Vs (m/s)	Value (kN m)	DLC (-)	Vs (m/s)
Model		5MW3UB00											
Maximums	Max	1181	DLC1.3	15.0	93942	DLC1.3	15.0	-5654	DLC1.3	25.0	5090	DLC1.4	13.4
	Min	1	DLC1.3	21.0	100	DLC1.3	25.0	-5836	DLC1.3	17.0	-9119	DLC1.4	11.4
Averages	Max	685	DLC1.5H	11.0	53934	DLC1.5V	11.0	-5730	DLC1.5H	25.0	827	DLC1.4	13.4
	Min	77	DLC1.3	3.0	4816	DLC1.3	3.0	-5788	DLC1.5V	11.0	-2625	DLC1.4	9.4
Model		5MW2UB00											
Maximums	Max	1405	DLC1.4	9.4	109496	DLC1.4	9.4	-5498	DLC1.3	25.0	4418	DLC1.4	13.4
	Min	1	DLC1.3	21.0	95	DLC1.3	25.0	-5679	DLC1.3	25.0	-7922	DLC1.4	11.4
Averages	Max	606	DLC1.5H	11.0	48577	DLC1.5V	11.0	-5556	DLC1.3	3.0	453	DLC1.4	13.4
	Min	61	DLC1.3	3.0	4595	DLC1.3	3.0	-5608	DLC1.3	11.0	-1802	DLC1.4	9.4
Model		5MW2DB00											
Maximums	Max	1495	DLC1.4	9.4	118349	DLC1.4	9.4	-5353	DLC1.4	9.4	5079	DLC1.3	25.0
	Min	1	DLC1.3	25.0	84	DLC1.3	21.0	-5718	DLC1.3	25.0	-9307	DLC1.4	11.4
Averages	Max	576	DLC1.5V	11.0	47465	DLC1.5V	11.0	-5514	DLC1.5H	11.0	1588	DLC1.3	25.0
	Min	59	DLC1.3	3.0	5374	DLC1.5H	3.0	-5551	DLC1.3	25.0	-2354	DLC1.4	9.4

Table 9.28 is the counterpart of Table 9.27 for fault conditions.

Maximum shear forces are largest for the 2-bladed upwind configuration. The shear force for 3-bladed design and the 2-bladed downwind configuration are lower. The maximum bending moments of the three configurations are almost equal but the one for the 2-bladed upwind design is slightly larger than the other two. For axial forces, similar to normal operating conditions the loads are smaller for 2-bladed concepts. Torsional moments under fault conditions are considerably larger than those under normal operating conditions. The torsional moments are larger for 2-bladed configurations. The smaller of the two is for the downwind configuration. Similar to maximum loads, the average shear force is the smallest for 2-bladed downwind configuration. The maximum average bending moments are smallest for the 2-bladed downwind configuration. For average axial forces, similar trends to normal operating conditions are observed under fault conditions. Average torsional moments are largest for the 2-bladed downwind configuration among the three concepts.

Table 9.28. Result data at tower base under fault conditions.

Load Effects		Shear Force			Bending Moment			Axial Force			Torsional Moment		
		Value (kN)	DLC (-)	Vs (m/s)	Value (kN m)	DLC (-)	Vs (m/s)	Value (kN)	DLC (-)	Vs (m/s)	Value (kN m)	DLC (-)	Vs (m/s)
Model		5MW3UB00											
Maximums	Max	1386	DLC2.3	25.0	111495	DLC2.3	25.0	-5526	DLC2.1P	25.0	7782	DLC2.1P	11.4
	Min	0	DLC2.3	11.4	38	DLC2.3	9.4	-5828	DLC2.3	11.4	-8876	DLC2.1P	25.0
Averages	Max	392	DLC2.3	25.0	30759	DLC2.3	25.0	-5671	DLC2.1P	25.0	27	DLC2.1G	11.4
	Min	222	DLC2.1P	11.4	17788	DLC2.1P	11.4	-5737	DLC2.1P	11.4	-1868	DLC2.1P	25.0
Model		5MW2UB00											
Maximums	Max	1498	DLC2.3	25.0	115128	DLC2.3	25.0	-5211	DLC2.1P	25.0	10261	DLC2.1P	11.4
	Min	0	DLC2.3	11.4	40	DLC2.3	25.0	-5750	DLC2.1P	25.0	-17278	DLC2.1P	25.0
Averages	Max	347	DLC2.3	13.4	27228	DLC2.3	13.4	-5552	DLC2.1G	25.0	1576	DLC2.1P	25.0
	Min	192	DLC2.1G	11.4	15465	DLC2.1G	11.4	-5596	DLC2.1P	25.0	-238	DLC2.3	25.0
Model		5MW2DB00											
Maximums	Max	1380	DLC2.3	25.0	110466	DLC2.3	25.0	-5291	DLC2.1P	25.0	9330	DLC2.1P	11.4
	Min	1	DLC2.3	13.4	37	DLC2.3	13.4	-5745	DLC2.1P	25.0	-13638	DLC2.1P	25.0
Averages	Max	309	DLC2.3	13.4	24630	DLC2.3	13.4	-5544	DLC2.3	11.4	2431	DLC2.1P	25.0
	Min	177	DLC2.3	9.4	14527	DLC2.3	9.4	-5610	DLC2.1P	25.0	142	DLC2.3	9.4

Table 9.29 demonstrates the load effects that are applied to the foundation under parked conditions.

The shear forces applied to the base are the largest for the 3-bladed design. This intuitively makes sense as the drag loads for three blades would be larger than that for two blades. Similar trends are observed for average shear forces. For the same reason the bending moments that are observed for the 3-bladed design are the largest among the three concepts. The differences that are observed between the results of 2-bladed downwind and upwind are mostly due to the different tilt and coning angles.

The axial forces, similar to normal operating and fault conditions are smaller for 2-bladed concepts. Maximum and average torsional moments are smaller for the 2-bladed concepts. They are slightly smaller for 2-bladed upwind case. This could be due to different tilt and cone angle settings.

Table 9.29. Result data at tower base under parked conditions.

Load Effects		Shear Force			Bending Moment			Axial Force			Torsional Moment		
		Value (kN)	DLC (-)	Vs (m/s)	Value (kN m)	DLC (-)	Vs (m/s)	Value (kN)	DLC (-)	Vs (m/s)	Value (kN m)	DLC (-)	Vs (m/s)
Model		5MW3UB00											
Maximums	Max	877	DLC6.2a	37.4	67766	DLC6.2a	37.4	-5636	DLC6.1a	37.4	3901	DLC7.1a	25.0
	Min	0	DLC6.2a	37.4	41	DLC6.2a	37.4	-5758	DLC6.2a	37.4	-4250	DLC6.2a	37.4
Averages	Max	342	DLC6.2a	37.4	28359	DLC6.2a	37.4	-5636	DLC6.1a	37.4	3800	DLC7.1a	25.0
	Min	24	DLC6.3a	25.0	959	DLC6.3a	25.0	-5756	DLC7.1a	25.0	-1989	DLC6.2a	37.4
Model		5MW2UB00											
Maximums	Max	539	DLC6.2a	37.4	41614	DLC6.2a	37.4	-5429	DLC6.2a	37.4	3354	DLC7.1a	25.0
	Min	0	DLC6.2a	37.4	6	DLC6.2a	37.4	-5583	DLC6.2a	37.4	-186	DLC6.2a	37.4
Averages	Max	181	DLC6.2a	37.4	13970	DLC6.2a	37.4	-5431	DLC6.2a	37.4	3265	DLC7.1a	25.0
	Min	8	DLC6.2a	37.4	658	DLC6.2a	37.4	-5568	DLC7.1a	25.0	-51	DLC6.2a	37.4
Model		5MW2DB00											
Maximums	Max	596	DLC6.2a	37.4	45467	DLC6.2a	37.4	-5519	DLC6.2a	37.4	3565	DLC7.1a	25.0
	Min	0	DLC6.2a	37.4	2	DLC6.2a	37.4	-5671	DLC6.2a	37.4	-153	DLC6.2a	37.4
Averages	Max	228	DLC6.2a	37.4	17594	DLC6.2a	37.4	-5544	DLC6.2a	37.4	3280	DLC7.1a	25.0
	Min	4	DLC6.2a	37.4	462	DLC6.2a	37.4	-5669	DLC6.2a	37.4	-118	DLC6.1a	37.4

Overall, the load effects applied to the foundation are larger for the 2-bladed concepts. The torsional moments under fault conditions increase by 97% and 54% for 2-bladed upwind and downwind configurations, respectively. However, as it was mentioned in Chapter 7, these loads are not significant compared to the wave and ice loads that are applied to the foundation. Therefore, they would not dominate the foundation design.

9.3 Analysis of System Performance and Cost

In this section, a comparison of the annual power production, and cost of the wind turbine designs in this project is presented. Recommendations for increasing power production are provided. Moreover, a final 2-bladed downwind design is proposed.

9.3.1 Annual Energy Production in Lake Erie Environment

The predicted AEP results for wind turbine models considered in this project are listed in Table 9.30, and are compared in Figure 9.34. These AEP results are calculated according to the simulation based annual energy production estimation method of Section 4.6. These AEP values include the efficiency of the drivetrain.

Overall, 2-bladed upwind and downwind turbines produce slightly less AEP than their 3-bladed upwind counterparts. Compared to 5MW 3-bladed turbines, the 5MW 2-bladed upwind turbines with the baseline blade produce about 4.3% less AEP, and 2-bladed downwind machines produce 6.8% less AEP. On the other hand, these differences are reduced by about 2.7% and 3%, respectively, for the upwind and downwind machines by using BUT blades.

To quantify how the tower shadow affects AEP, the AEP of two 5MW 2-bladed downwind models with and without tower shadow effect are compared. The model without the tower shadow effect produces 2.26% more AEP than the model that accounts for it. From this comparison, it can be concluded that about 70% of the AEP loss in the downwind configuration is due to the tower shadow effect.

As the shaft tilt and conning angles approach zero degrees, the AEP increases. Comparing the model having a 5° shaft tilt angle and zero degree conning angle, with the model having zero degree shaft tilt angle and 2.5° conning angle, reducing the conning angle to zero degrees is more effective than reducing the shaft tilt angle to zero in order to increase AEP. For example, a 2.5° decrease in conning angle improved the AEP by approximately 0.51%, whereas a 5° shaft tilt angle change increased the AEP by only 0.15% (for the models without tip-brakes).

The stiffness of the teeter also affects the AEP. Generally, as the teeter stiffness decreases so does the AEP. Thus, using stiffer teeter stop is more beneficial as long as they do not increase the load on the wind turbine structure.

Tip-brakes reduce the natural frequency of the blades because of their mass. The natural frequency results listed in Section 6.5 show that attaching a tip-brake reduces the natural frequencies of the tower and the blades. The attachment of the tip-brake changes the mode shapes, and the corresponding mode shape data are used for the FAST simulation for the cases with and without tip-brakes. Because adding a tip brake reduces the natural frequency, blades

with a tip brake may vibrate more smoothly than without. Rotor blades may produce higher AEP but detailed investigations are necessary to determine whether tip-brakes help to harvest more AEP than the turbines that do not use tip-brakes. One suggested concept to improve AEP can be a merged winglet type tip-brake. Installing tip-brakes to reduce load effects and increase minimum tower-to-blade clearance in emergency shutdown procedure under fault conditions can potentially help increase AEP. In conclusion, to maximize AEP for the 2-bladed downwind machine, the following design changes are recommended in the order of their effectiveness:

- Choose appropriate blade length for the desired rating considering the wind resource at the installation site.
- Optimize the twist distribution for the 2-bladed machine.
- Minimize the tower shadow effect.
- Use stiffer teeter as long as it does not increase the loads considerably on the wind turbine structure.
- Use zero degree conning angle first and then adjust the shaft tilt angle to near zero degree while maintaining an acceptable minimum tower-to-blade clearance.
- Use tip-brakes. Although this change is listed last, attaching a tip-brake to the blade is recommended because of its other advantages, such as larger tower-to-blade clearance during an emergency shutdown procedure.

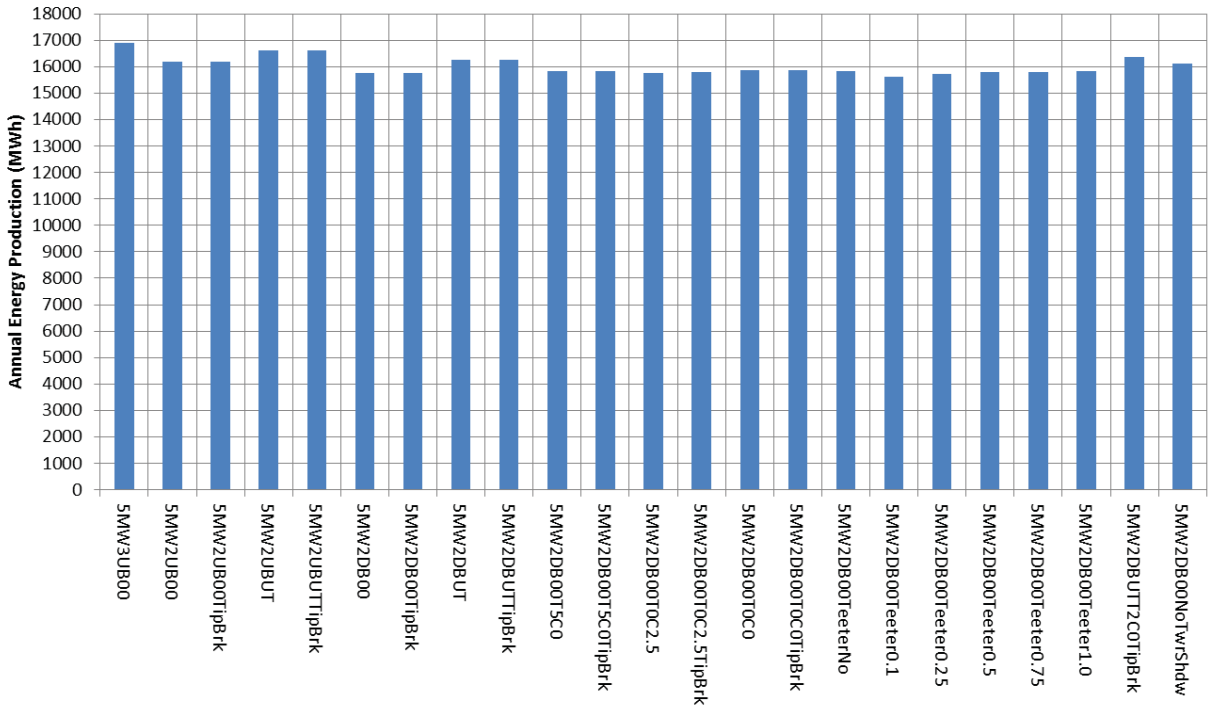

Figure 9.34. AEP comparisons of wind turbine models.

Table 9.30. AEP comparisons of wind turbine models.

#	Model	AEP (MWh)	%Difference
1	5MW3UB00	16912	0.00
2	5MW2UB00	16180	-4.33
3	5MW2UB00TipBrk	16193	-4.25
4	5MW2UBUT	16627	-1.69
5	5MW2UBUTTipBrk	16630	-1.67
6	5MW2DB00	15755	-6.84
7	5MW2DB00TipBrk	15768	-6.76
8	5MW2DBUT	16242	-3.96
9	5MW2DBUTTipBrk	16245	-3.94
10	5MW2DB00T5C0	15835	-6.37
11	5MW2DB00T5C0TipBrk	15844	-6.31
12	5MW2DB00T0C2.5	15778	-6.70
13	5MW2DB00T0C2.5TipBrk	15789	-6.64
14	5MW2DB00T0C0	15872	-6.15
15	5MW2DB00T0C0TipBrk	15883	-6.09
16	5MW2DB00TeeterNo	15847	-6.30
17	5MW2DB00Teeter0.1	15622	-7.63
18	5MW2DB00Teeter0.25	15739	-6.94
19	5MW2DB00Teeter0.5	15793	-6.61
20	5MW2DB00Teeter0.75	15812	-6.51
21	5MW2DB00Teeter1.0	15821	-6.45
22	5MW2DB00NoTwrShadow	16111	-4.74

9.3.2 Cost Model Results and Discussion

The following results are for the three models (Baseline NREL Design 3B, University of Toledo Design 2BUT, and an Optimized 2BOPT Design) outlined in Chapter 8.

9.3.2.1 Initial Capital Costs Turbine – Results

This section looks at the Mass and Cost estimates of the wind turbine and foundation. Combined with the next subsection, Balance of System Results, the two make up the upfront capital needed to install the wind turbine. The following subsections cover the operating, maintenance and replacement cost during the wind turbine's system life.

Table 9.31. Levelized cost of energy (LCOE) $/kWhr.

$/kWhr	3B	2BUT	2BOPT
Turbine Capital Costs	0.0511	0.0493	0.0469
BOS Capital Costs	0.0387	0.0362	0.0359
Repair & Maintenance	0.0209	0.0204	0.0194
Levelized Replacement	0.0346	0.0249	0.0149
Total	0.1453	0.1308	0.1170
Difference		9.9%	19.5%

The following section presents the results of all 3 models. With each model, components were removed or mass reduced. The UT Design removed the blade. The Optimized Design reduced the mass of the drivetrain, tower, and foundation.

9.3.2.2 Mass per Rated Power (kg/kW) – Results

The mass of the different models reduced with each iteration. Removing one blade reduced the mass by 1.1%. Reducing the mass of other components based on one less blade, 2BOPT, generated an additional 0.92% in mass savings over the baseline.

Table 9.32. Mass comparison (kg/kW).

Mass Estimate (kg/kW)	3B	2BUT	2BOPT
Rotor	15.70	12.09	12.09
Drivetrain (including generator, etc.)	44.75	44.75	41.72
Tower	67.54	67.54	67.54
Foundation	200.00	200.00	200.00
Control, Safety System, and Condition Monitoring	0.00	0.00	0.00
Marinization (10.00% of Turbine and Tower System)	0.10	0.10	0.10
Total Turbine Mass (kg/kW)	328.08	324.47	321.44
Mass Difference (kg/kW)		3.61	6.64
Mass Difference (%)		1.10%	2.02%
Total Turbine Mass (metric ton)	1640.42	1622.37	1607.22

The graphs Total Mass and Rotor and Total Mass and Drivetrain, show the incremental mass reductions.

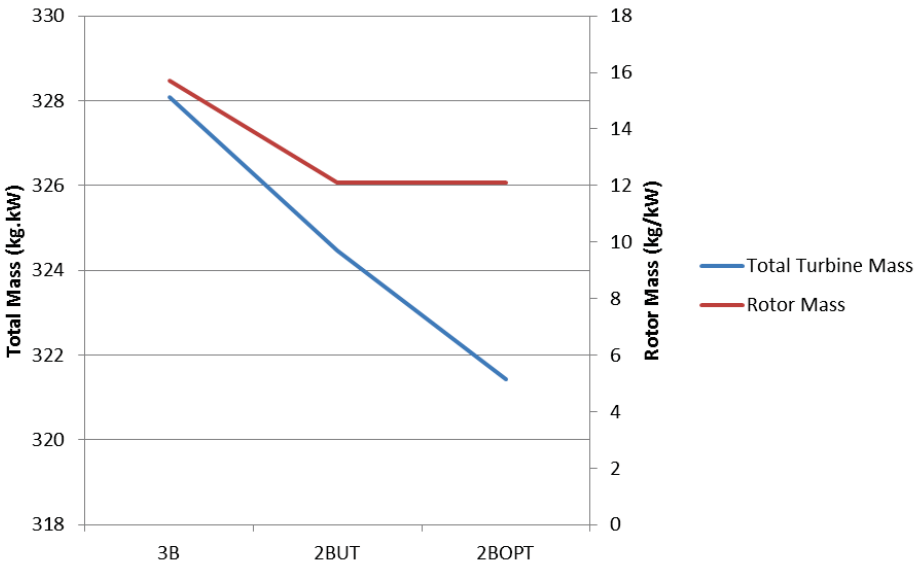

Figure 9.35. Total mass to rotor.

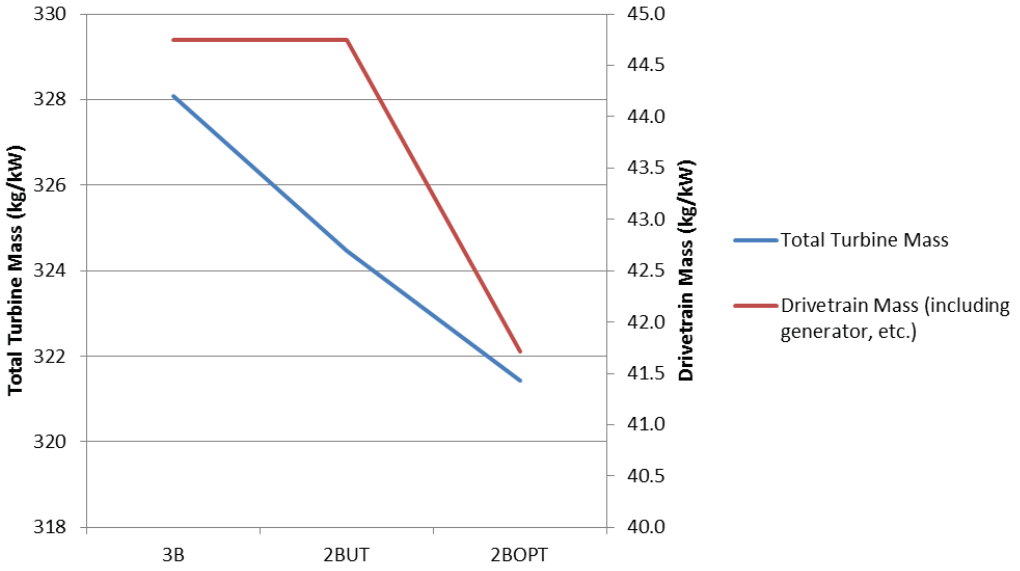

Figure 9.36. Total mass to drivetrain.

9.3.2.3 Cost per Rated Power ($/kW) – Results

With each iteration, the total cost of the different models was reduced. Cost savings closely followed the mass reductions. The largest factor to the reduction of cost was the removal of one blade from the rotor.

Table 9.33. Cost comparison ($/kW).

Cost ($/kW)	3B	2BUT	2BOPT
Rotor	276.79	196.67	196.67
Drivetrain (including generator, etc.)	715.22	715.22	648.47
Tower	174.35	174.35	174.35
Foundation	504.90	504.90	504.90
Control, Safety System, and Condition Monitoring	18.93	18.93	18.93
Marinization (10.00% of Turbine and Tower System)	169.02	161.01	154.33
Total Turbine Cost ($/kW)	1859.21	1771.07	1697.65
Mass Difference ($/kW)		88.14	161.56
Mass Difference (%)		4.74%	8.69%
Total Turbine Cost ($)	$9.30	$8.86	$8.49

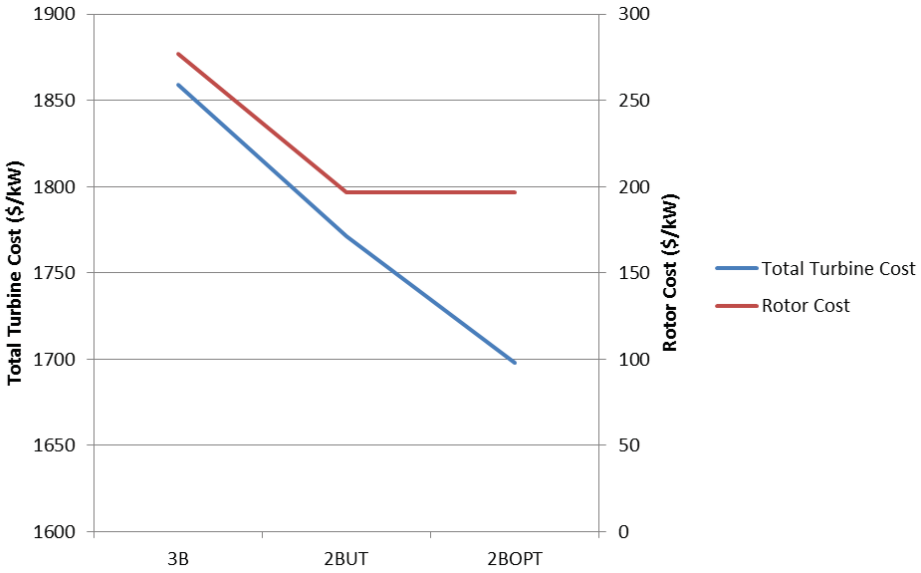

Figure 9.37. Total cost to rotor.

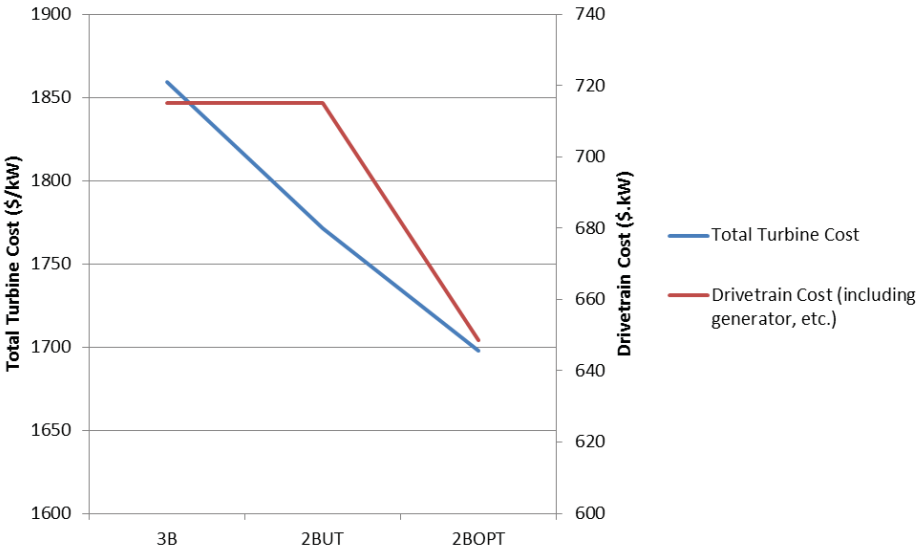

Figure 9.38. Total cost to foundation.

9.3.2.4 Balance of System Cost per Rated Power ($/kW) – Results

The Balance of System cost fell moderately (around 8%) when using the current, static foundation installation methods. This may seem small but amounts to 113.25 $/kW for the Optimized Design.

Table 9.34. Balance of system (BOS) cost comparison ($/kW).

Cost ($/kW)	3B	2BUT	2BOPT
BOS Hardware	161.74	161.74	161.74
Transportation	336.36	302.29	302.29
Installation	640.45	572.81	572.81
Other	270.22	264.52	262.32
Total BOS Costs ($/kW)	1408.78	1301.36	1299.16
Total BOS Costs ($ in thousands)	$7,043.88	$6,506.80	$6,495.79

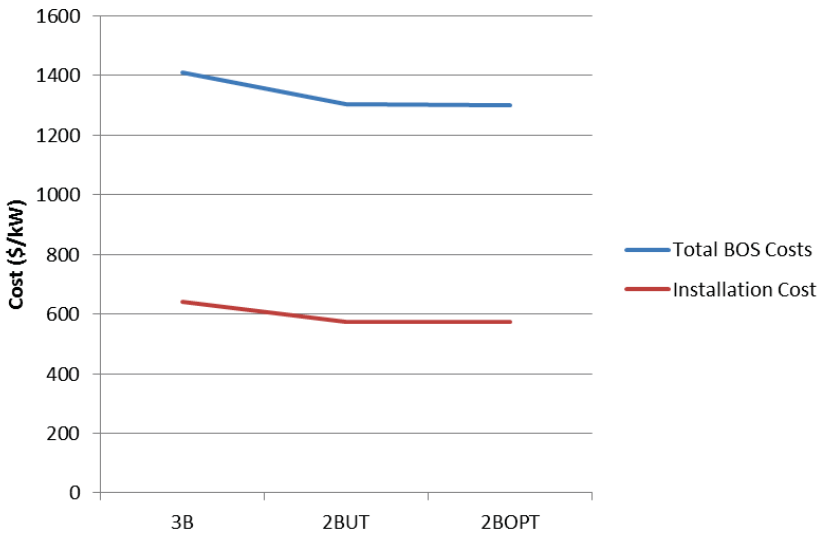

Figure 9.39. Total BOS cost to installation cost.

9.3.2.5 Repair and Maintenance Cost per Rated Power ($/kW) – Results

All changes to Operations and Maintenance cost were due to better performing components, with less annual failure. This is largely due to the removal of one blade. In addition, the removal of one blade increased gearbox and yaw control reliability and decreased unscheduled maintenance.

Table 9.35. Repair and maintenance cost comparison ($/kW).

Operations and Maintenance	3B	2BUT	2BOPT
General Scheduled Maintenance	5.70	5.70	5.70
Bottom Lease	3.18	3.14	3.16
Plant Operations Cost	2.06	2.03	2.05
Unscheduled Turbine Maintenance	39.12	37.14	34.63
Unscheduled BOS Maintenance	9.84	9.84	9.84
Administration and Support	0.88	0.87	0.88
Total O&M Cost	60.78	58.72	56.27

9.3.2.6 Levelized Replacement Cost per Rated Power ($/kW) – Results

The decrease in Replacement costs for the Optimized Design came from the expected system life increase of the gearbox running at less torque. The NREL drivetrain report [H. Link, W. LaCava, 2011] qualitatively states that system life should improve with lower torque transferred to the gearbox.

Table 9.36. Levelized replacement cost comparison ($/kW).

Cost ($/kW)	3B	2BUT	2BOPT
Blades	36.14	6.81	6.81
Gearbox	38.09	38.09	9.55
Generator	26.71	26.71	26.71
Total	100.93	71.60	43.07

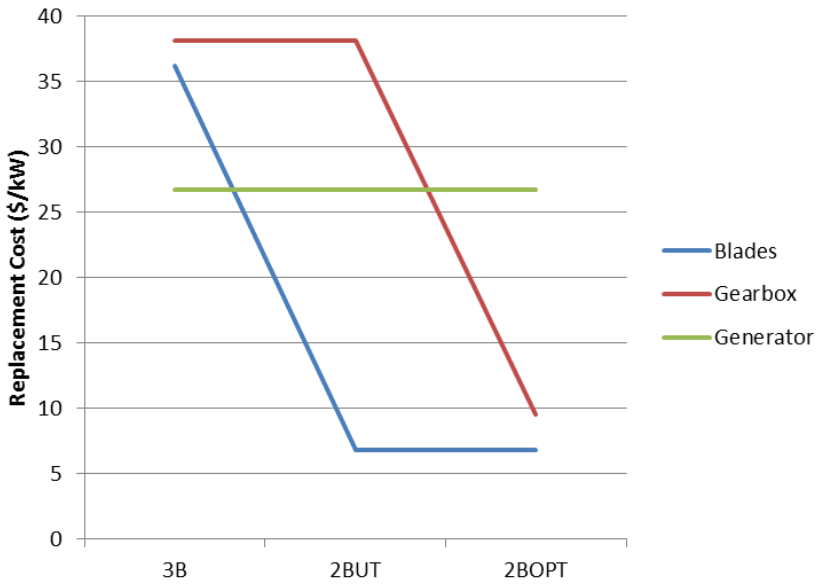

Figure 9.40. Replacement costs blade, gearbox, and generator.

9.3.2.7 Annual Energy Production (AEP) – Results

There is a decrease in gross annual energy production from the three- to two-bladed rotors. In addition, system availability increases with each iteration of the two bladed models. This is significant because system availability is more important for an offshore wind farm, when repairs must be made offshore, than in wind turbines on land.

Table 9.37. Annual energy production (AEP) comparison.

	3B	2BUT	2BOPT
AEP Gross (MWh)	18,887	18,619	18,741
Total Losses	0.20	0.20	0.20
System Availability	0.9663	0.9674	0.9691
AEP Net (MWh)	14,565	14,374	14,494
Capacity Factor	0.3325	0.3282	0.3309
Total Days Down (days)	12.32	11.92	11.28

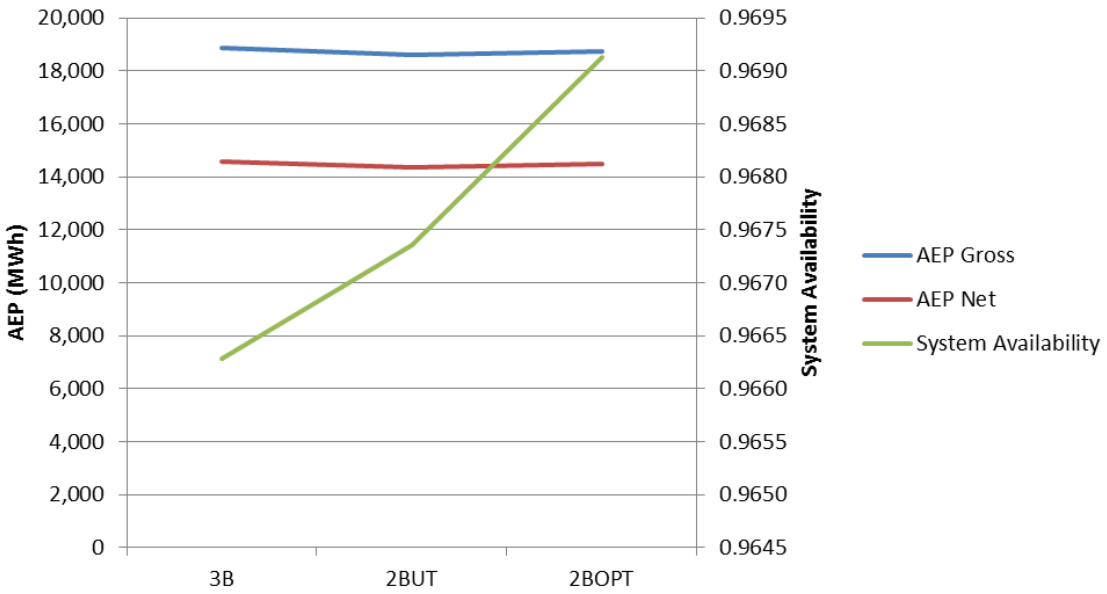

Figure 9.41. Annual energy production and system availability.

9.3.2.8 Levelized Cost of Energy (LCOE)– Results

For this analysis, the method outlined in the United States Department of Energy FOA 0000415 (Appendix E) was used for calculating the Levelized Cost of Energy (LCOE). This method divides the wind energy system into four cost sections: Turbine Capital, Balance of System Capital, Operations and Maintenance, and Replacement Costs.

Table 9.38. Levelized cost of energy (LCOE) $/kWhr.

$/kWhr	3B	2BUT	2BOPT
Turbine Capital Costs	0.0511	0.0493	0.0469
BOS Capital Costs	0.0387	0.0362	0.0359
Repair & Maintenance	0.0209	0.0204	0.0194
Levelized Replacement	0.0346	0.0249	0.0149
Total	0.1453	0.1308	0.1170
Difference		9.9%	19.5%

9.3.2.9 Prospect for Cost Benefits

The cost analysis preformed for this report has many limitations and assumptions, as well as insights and conclusions. Yet, two conclusions are worth discussing further:

1. Removing one blade reduces installation costs by 10.6%.
2. Two-bladed rotors offer the possibility of increasing the system availability. Increased system availability decreases the difference in net Annual energy production

Cost of Energy may be Reduced 19.5% using Two-Bladed Rotors Offshore

Installation cost is the largest cost barrier to the operation of offshore wind turbines. An offshore foundation affects both the capital and installation costs.

Table 9.39. Wind turbine capital cost difference between models.

	$/kW	difference
Capital Costs 3B	1859.21	0.00
Capital Costs 2BUT	1771.07	88.14
Capital Costs 2BOPT	1697.65	161.56

Table 9.40. Installation capital cost difference between models.

	$/kW	difference
Installation 3B	640.45	
Installation 2BUT	572.81	67.65
Installation 2BOPT	572.81	67.65

Offshore Two-Bladed Rotors Increase System Availability

The system availability is both the strongest and weakest argument in this cost analysis. It is the strongest because it shows the link between reducing the number of components needed to be fixed increases the net annual energy production. Large gains in system availability came from assuming that a higher rpm rotor speed will reduce the torque transferred to the gearbox thereby increasing the life of the gearbox.

It is the weakest argument because the failure rates and average days down are based on three bladed land wind turbines. The analysis further alters the onland, three-bladed failure rates to accommodate a two-bladed wind turbine. The decreased annual failure rates for a two-bladed rotor may be considered optimistic in this study. The blade loads on a two-bladed rotor are higher than on a three-bladed rotor and periodic. The higher loads may decrease the time to failure, eliminating the advantage of having one-less blade to fix. This could be true for all the components whose annual failure rate was changed in this study.

The number of days down due to failure data was not changed to reflect working in an offshore environment. Due to the complexity of working offshore, it is certain that the number of days down will increase in an offshore environment. Moving past this important assumption, if the

failure rates used in this study could be considered optimistic, the number of days down due to failure could be considered conservative.

Like the annual failure rates, the number of days down due to failure is based on studies done on land-based three-bladed wind turbines. Unlike the annual failure rates, the days down due to failure were not changed for two-bladed rotors. It is certain that the number of days down per failure would decrease with a two bladed rotor. As shown earlier in this report regarding the installation of the wind turbine, the symmetry of a two-bladed rotor holds advantages with moving, or removing the rotor.

9.3.3 Proposed Final Design

Based on parametric studies reported in Section 9.1, a 5MW wind turbine design is proposed. This design was designated the name 5MW2DBUTT2C0TipBrk according to the naming convention adopted in Appendix 1. Table 9.41 shows the design configuration of the 5MW wind turbine final design. Compared to other 2-bladed design studied in this project, the selected final design can produce the largest AEP without experiencing significantly larger load effects. Specifically, the final design produces 16,360 MWh AEP, which is 3.84% more than the AEP of the basic 5MW 2-bladed downwind design (5MW2DB00), and only 3.26% less than the AEP of the 3-bladed upwind baseline turbine. The detailed AEP calculations were introduced in Section 4.7, and more AEP results can be found in Section 9.3.1.

Table 9.41. Configuration of final design.

Model Name	5MW2DBUTT2C0TipBrk
Rating	5MW
Number of Blades	2
Wind Direction	Downwind
Blade Design	BUT
Shaft Tilt	2°
Conning Angle	0°
Teeter	Enabled
Tip-brake	Enabled

Table 9.42. Major attributes and responses of final design.

Model Name	5MW2DBUTT2C0TipBrk	% difference
Annual Energy Production	16360 MWh	-3.26
Minimum Tower-to-Blade Clearance	3.634 m	-47.9
Maximum Teeter Angles	3.24°	N/A

Major performance attributes and responses of the final design as well as a comparison with the baseline turbine are presented in Table 9.42. The load effect and torque results of the final design are tabulated in Table 9.43 and Table 9.44, respectively. The fatigue damage results of this turbine design are listed in Table 9.45.

The rotor blade of the proposed design has a 0° conning angle and a 2° tilt angle. The minimum tower-to-blade clearance for this design is 3.6 m, which satisfies the minimum clearance specification of 3.5 m.

The teeter mechanism for the final design has a teeter parameter set of 0.3, which is suitable for the 2-bladed machines. The details of teeter parameter sets are described in Section 6.2.5. The teeter set 0.3 is found from the parametric study that is performed in Section 6.2.5 and Section 9.1.5. The selected teeter set reduces loads transferred from the rotor to LSS efficiently with the acceptable teeter angle range. The tip-brake is mounted for the safe emergency shutdown. According to the parametric study of Section 9.1.6, application of tip-brake efficiently reduces load effects under fault conditions. In addition, the tip-brakes allow larger minimum tower-to-blade clearance. Because of the increased tower-to-blade clearance, the conning angle and the shaft tilt angles could be reduced to near 0°, which yield higher AEP.

Most of the load effects of the final design are within the safe region. However, the axial force and the torsional moment at the blade root require careful investigation in the detailed design because these load effects exceeded the safe limit. That does not necessarily mean that the axial forces and torsional moments are exceeding structural capacity. The safe limits can confirm that a structure is 100% safe when the load effects on the structure are under the safe limits as long as the baseline design is 100% safe. The detailed description of the safe limit is presented in Appendix 5. The shear force, bending moment, and torsional moment at the tower base did not exceed the safe limit, but they are close. Other load effects and torques are within the safe limit.

The weighted percent differences of load effects for the final designs are shown in Figure 9.42 and Figure 9.43. The concept of the weighted percent difference as a useful measure for load comparison is described in Appendix 7. The graphs show that the final design has smaller load effects than the baseline design in most cases. A careful examination of the maximum load effects at the base of the tower in normal condition in Figure 9.44 show that that all load effect types are within the safe limit (green horizontal line). The maximum shear force and bending moment at the tower base of the final 5MW machine occurred in DLC1.4, at an average wind speed of 9.4 m/s.

The load effect at the blade root is presented in Figure 9.45 and Figure 9.46 for the normal operating conditions and fault conditions respectively. The graphs show that the blade root axial forces and torsional moments of the final designs exceed the safe limit in both conditions. The maximum axial force at the blade root occurred in DLC1.3 at 25 m/s, the cut-out speed case for the 5MW machine under the normal operating conditions. The maximum axial force occurred in DLC2.3 at the cut-out speed for both the final design and baseline turbines under the fault conditions. The maximum torsional moment occurred in DLC1.4 at an average wind speed of 13.4 m/s for the final 5MW machine in the normal operating conditions. The maximum torsional moment under fault conditions occurred in DLC2.3 at 11.4 m/s rated speed for the 5MW machine.

Finally Figure 9.47 shows the torque values in the high speed shaft. These values are below the safe limit under all operating conditions.

As presented in Table 9.45, fatigue damage analysis on 5MW2DBUTT2C0TipBrk turbine shows that the damage values caused by different loads at critical turbine locations are considerably lower than one. Fatigue damage of the final design was estimated using the same technique that was used for all the other designs considered in this study. The fatigue damage calculation methodology is described in Section 4.4.

Table 9.43. Load effects of final design.

		Shear Force				Bending Moment				Axial Force				Torsional Moment			
		Maximum		Average		Maximum		Average		Maximum		Average		Maximum		Average	
Location	Condition	Value (kN)	%diff (%)	Value (kN)	%diff (%)	Value (kN m)	%diff (%)	Value (kN m)	%diff (%)	Value (kN)	%diff (%)	Value (kN)	%diff (%)	Value (kN m)	%diff (%)	Value (kN m)	%diff (%)
Tower Base	Normal Operating	1570	32.9	678	-1.1	123959	32.0	55393	2.7	-5723	-1.9	-5560	-3.9	11540	26.5	2667	1.6
	Fault	1201	-13.4	309	-21.2	95078	-14.7	24915	-19.0	-5719	-1.9	-5576	-2.8	4450	-49.9	1170	-37.4
	Parked	790	-9.9	283	-17.2	59767	-11.8	21878	-22.9	-5606	-2.6	-5605	-2.6	3360	-20.9	3258	-14.3
Tower Top	Normal Operating	1431	21.1	704	-1.1	8887	-15.3	4451	-14.1	-3429	-2.9	-3265	-6.4	11540	26.5	2667	1.6
	Fault	1208	-8.4	311	-14.3	8265	-35.5	3839	29.1	-3422	-2.9	-3281	-4.7	4450	-49.9	1170	-37.4
	Parked	652	-12.9	252	-29.2	1787	-70.4	1236	-69.4	-3312	-4.4	-3312	-4.4	3360	-20.9	3258	-14.3
Blade Roots	Normal Operating	573	22.4	360	20.2	21896	23.5	12618	24.9	1683	66.1	1087	74.1	304	50.3	87	55.7
	Fault	579	28.8	244	22.0	18919	25.8	6938	36.5	1716	64.7	487	60.0	611	243.6	55	44.7
	Parked	242	-15.8	216	-23.3	7265	-5.6	4985	-33.7	-5	-97.4	-2	-98.8	153	-24.4	108	-44.5
LSS	Normal Operating	1077	-4.5	921	-15.0	10826	-19.3	4122	-16.3	1000	-8.3	653	-17.3	5272	-5.0	3199	-23.6
	Fault	1085	-5.9	935	-12.6	6815	-47.6	2766	7.1	1055	-13.5	235	-15.7	6772	-5.2	2959	37.7
	Parked	959	-16.4	958	-15.9	3760	-34.3	3676	-21.3	-368	-181.8	83	-62.8	1278	-55.0	1206	-51.9

Table 9.44. Torques of final design.

	LSS				HSS				Generator			
	Maximum		Average		Maximum		Average		Maximum		Average	
Condition	Value (kN)	%diff (%)	Value (kN)	%diff (%)	Value (kN m)	%diff (%)	Value (kN m)	%diff (%)	Value (kN m)	%diff (%)	Value (kN m)	%diff (%)
Normal Operating	5272	-5.0	3199	-23.6	54	-5.0	33	-23.6	36	-23.6	33	-23.6
Fault	6772	-5.2	2959	37.7	70	-5.2	31	37.7	36	-23.6	17	10.6
Parked	1278	-55.0	1206	-148.1	13	-55.0	12	-51.9	N/A		N/A	

Table 9.45. Fatigue life result of final design.

	Shear Force		Bending Moment		Axial Force		Torsional Moment	
Location	Damage	%diff (%)	Damage	%diff (%)	Damage	%diff (%)	Damage	%diff (%)
Tower Base	3.4944E-02	1.45E+02	3.0043E-02	1.46E+02	6.6411E-22	6.63E-22	1.2935E-10	4.20E+03
Tower Top	1.7402E-02	1.19E+02	1.0015E-07	2.44E+04	1.1039E-19	1.10E-19	1.2937E-10	4.19E+03
Blade Roots	7.4303E-02	2.55E+04	1.6400E-01	2.01E+04	4.2424E-04	4.21E-04	5.9758E-06	1.35E+04
LSS	1.5772E-14	1.02E+06	8.8560E-06	6.32E+03	2.0256E-04	1.00E-04	2.1552E-07	1.88E+03

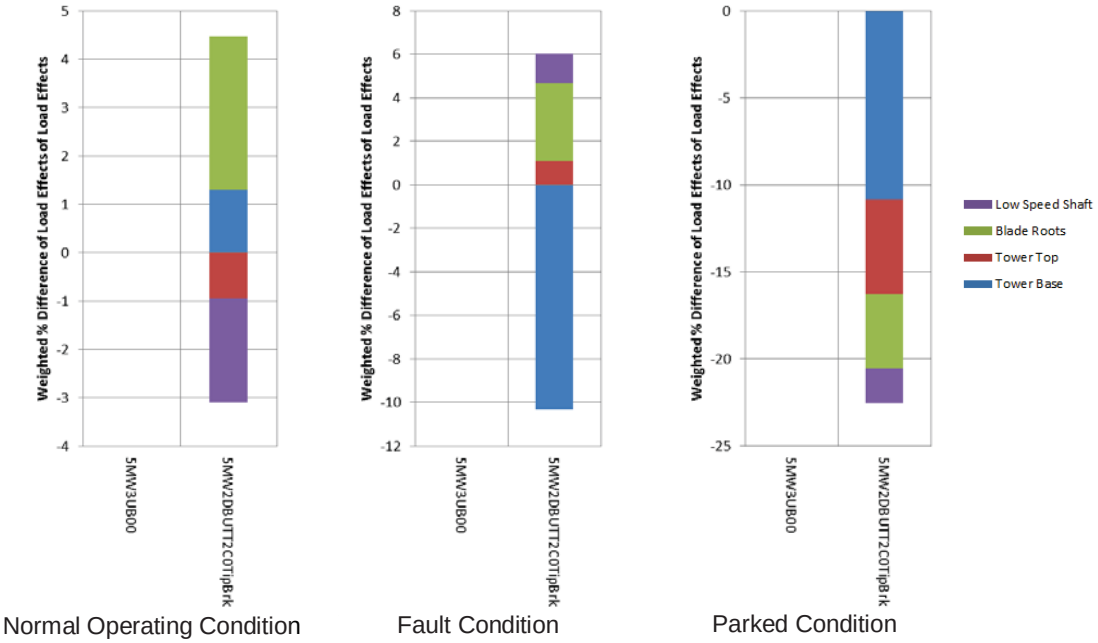

Figure 9.42. Weighted % difference of average loads of final design.

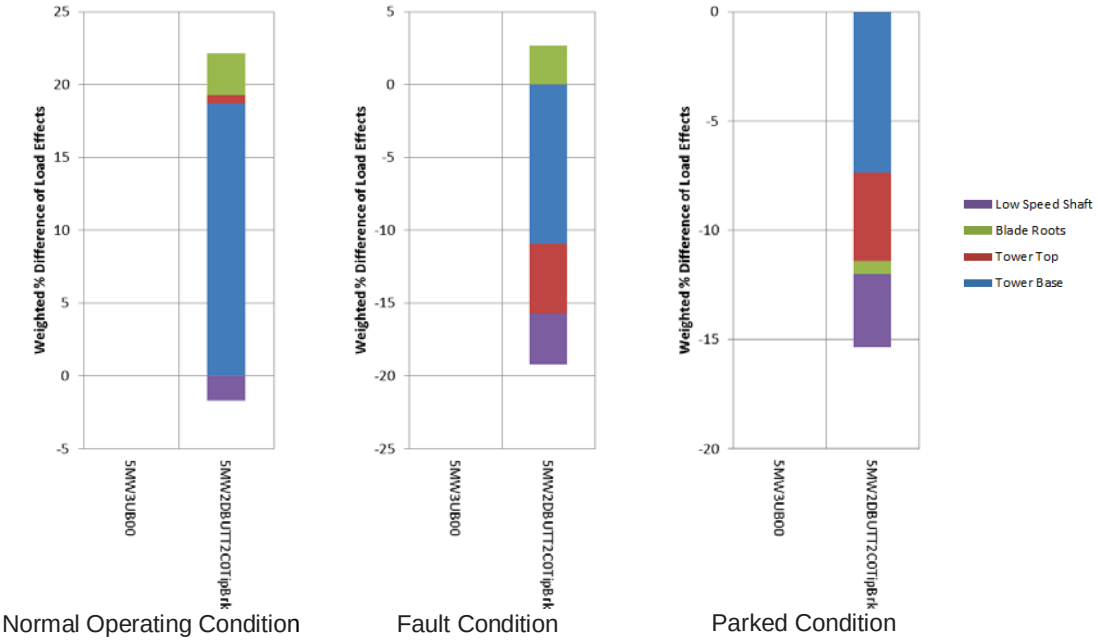

Figure 9.43. Weighted % difference of maximum loads of final design.

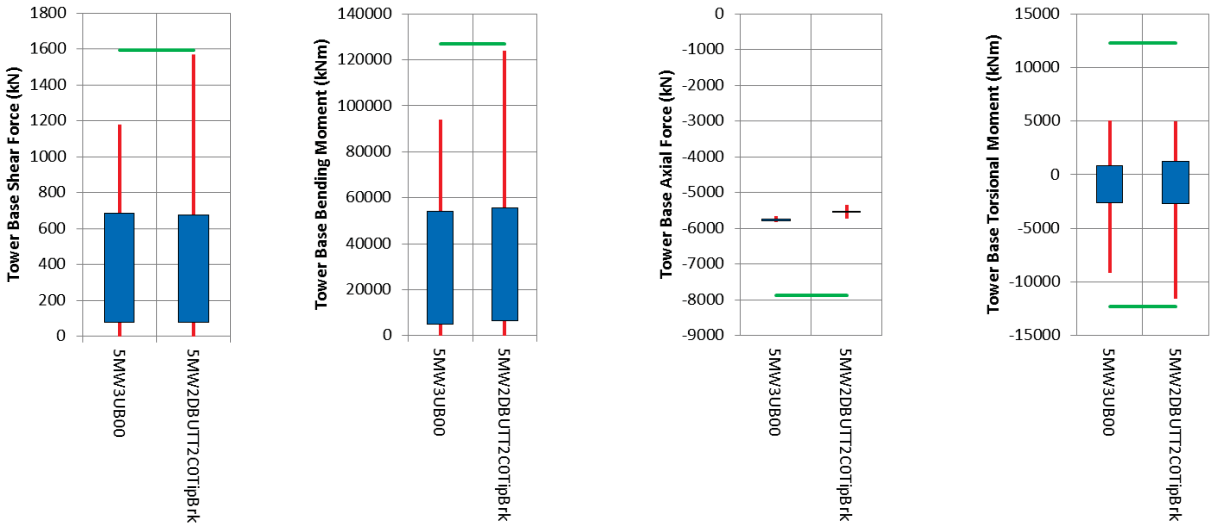

Figure 9.44. Tower base load effects of final design under normal operating conditions.

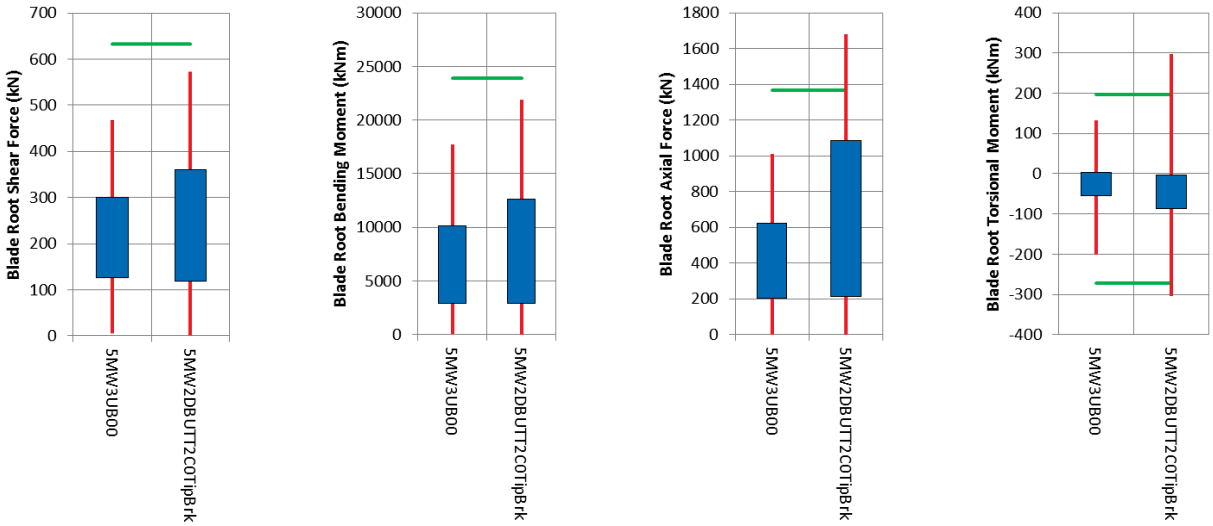

Figure 9.45. Blade root load effects of final design under normal operating conditions.

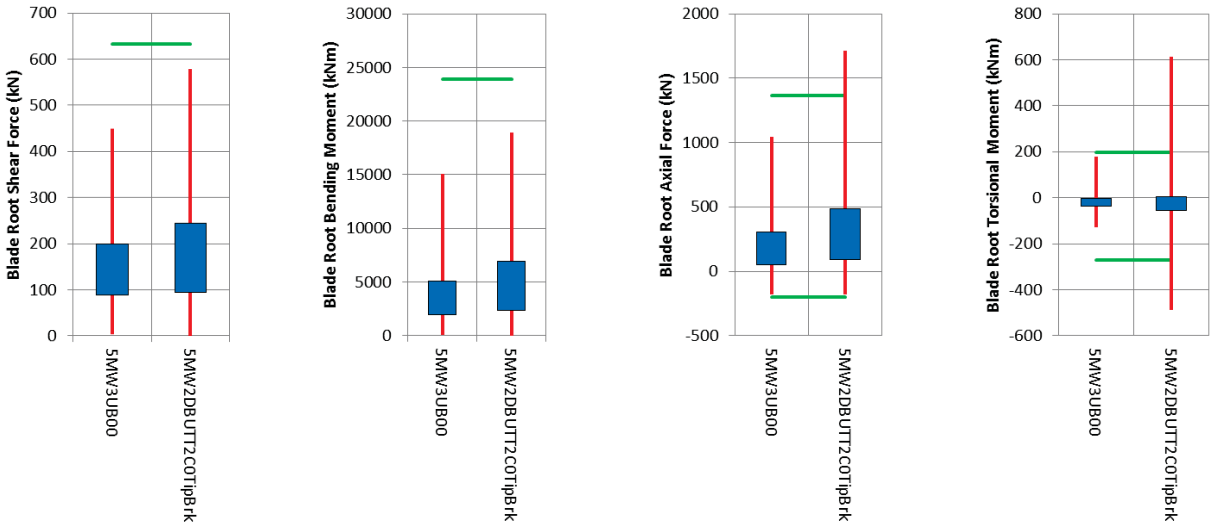

Figure 9.46. Blade root load effects of final design under fault conditions.

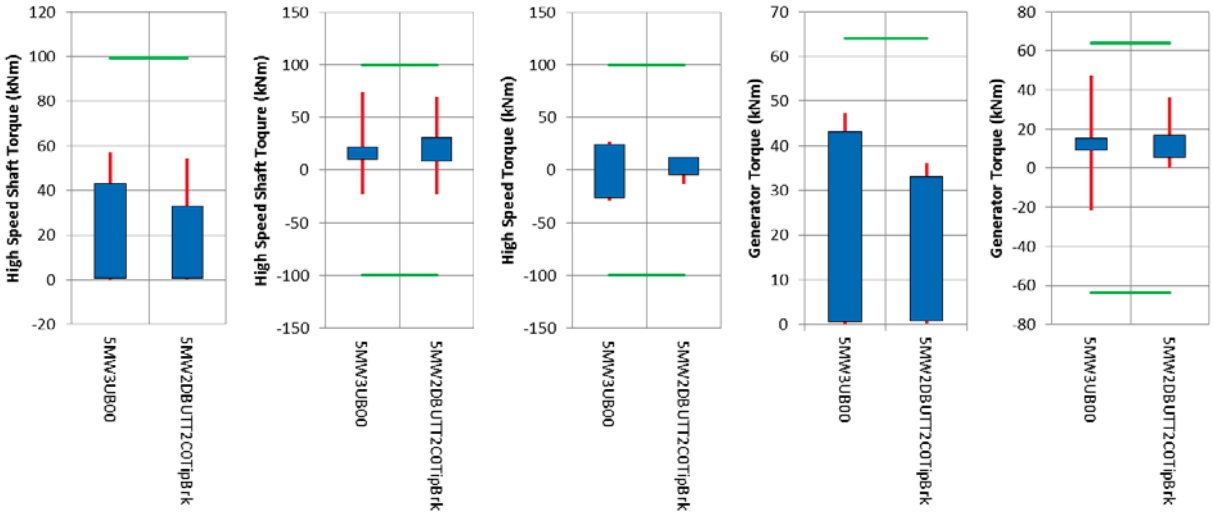

Figure 9.47. Torques of final design.

9.4 Summary

The computational results presented in this chapter demonstrate that the proposed downwind, 2-bladed wind turbine concept is a creditable and practical wind turbine design for offshore applications. This notwithstanding, the 2-bladed downwind concept has both advantages and disadvantages over its 2-bladed or 3-bladed upwind counterparts.

10 Educational Program Development

The educational program developed in this project consisted of curriculum development, new course offerings and outreach, which are described below.

10.1 Curriculum Development

Major curriculum development activities were as follows:

a) An existing course on Alternative Energy (MIME 4980/5980) was redesigned with a greater wind energy topical content to emphasize wind energy education.

b) A new course (MIME4980/5980) Wind Energy for Science Educators was developed and offered for the first time in summer 2012.

c) Acquired new computer-controlled wind energy laboratory equipment for incorporating wind energy related hands-on experiments in the department teaching labs.

d) One faculty member of the project team served as a faculty panel reviewer for the Ohio Board of Regents and the Ohio Articulation and Transfer Network for the wind energy and alternative energy curricula.

e) Participated as a founding institution for the North American Wind Energy Academy (NAWEA)

a) The Alternative Energy course is offered as a technical elective for the Mechanical, Industrial, and Manufacturing Engineering (MIME) students at the University of Toledo, but it is also included in the curriculum for a minor in Alternative Energy offered across the university. Students from other engineering majors have also taken this course in the past. Currently, more than 35% of this course covers the subjects of wind energy (up from about 20% before this course redesign). A few new elements related to wind turbine design were incorporated in the course curriculum after discussions with the engineers from Nordic Windpower, one of the project's original industry partners.

b) The *Wind Energy for Science Educators* course (MIME4980/5980) is aimed at and was delivered to a select group of K-12 math and science educators from Ohio and Michigan. The course participants earn college credit for taking this course as part of their master's degree in education curriculum. In 2012 two faculty members of the project team (Drs. Afjeh and Cioc), with the assistance of a graduate student (Mr. Zhang) and a faculty member from the Toledo Technology Academy (Mr. Ted Richardson), developed and delivered a workshop/course focused on wind energy. The two-week program was designed to comprise both hands-on and demonstration projects. The topics under consideration were broad in scope and included wind resource measurement, wind turbine siting, and basic experiments on aerodynamic concepts of lift and drag, as it pertains to wind turbines, energy conversion, and power generation from wind.

c) The equipment acquired (Computer Controlled Wind Energy Unit with SCADA "EEEC") is a turnkey, laboratory-scale unit designed for studying wind energy and the influence of specific factors on wind power generation. The unit consists of the following components: a tunnel, a wind turbine with angle-adjustable and removable blades to permit experiments with different blade numbers, axial fan to produce the wind, load and battery charger regulator, auxiliary battery charger, battery, DC Loads Module for power measurements, sensors, and EDIBON Supervisory Control and Data Acquisition system (SCADA).

The system measures and monitors in real time the voltage and current produced by the wind turbine, the wind speed, the rotational speed of the wind turbine, and the temperature of the air. This Computer Control System (SCADA) supplied by EDIBON includes a control interface box, a data acquisition board, computer control and data acquisition software for controlling the system and measuring all the physical quantities of interest.

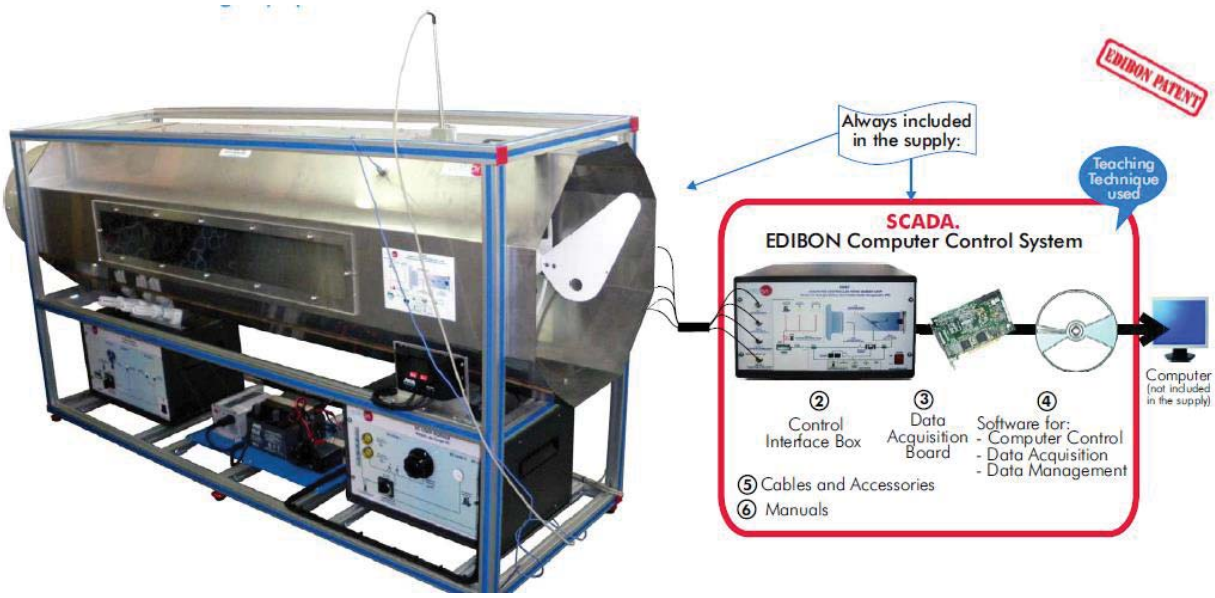

Figure 10.1. The Computer Controlled Wind Energy Unit with SCADA (Courtesy of EDIBON).

The unit was delivered in 2011 and has been used since then in the *Alternative Energy* and the *Wind Energy for Science Educators* courses. Using this unit, the students can measure the power output from the turbine model, generate the power curve (turbine power as a function of the wind speed), and vary the blade pitch, the number of blades (2, 3, or 6), and the load. Using these quantities, other parameters of interest, such as the variation of power coefficient with the tip speed ratio for various rotor configurations (number of blades, blade geometry) can be determined. For example, in the case of a 6-blade rotor set at various pitch angles, the power produced by the rotor is shown in Figure 10.2.

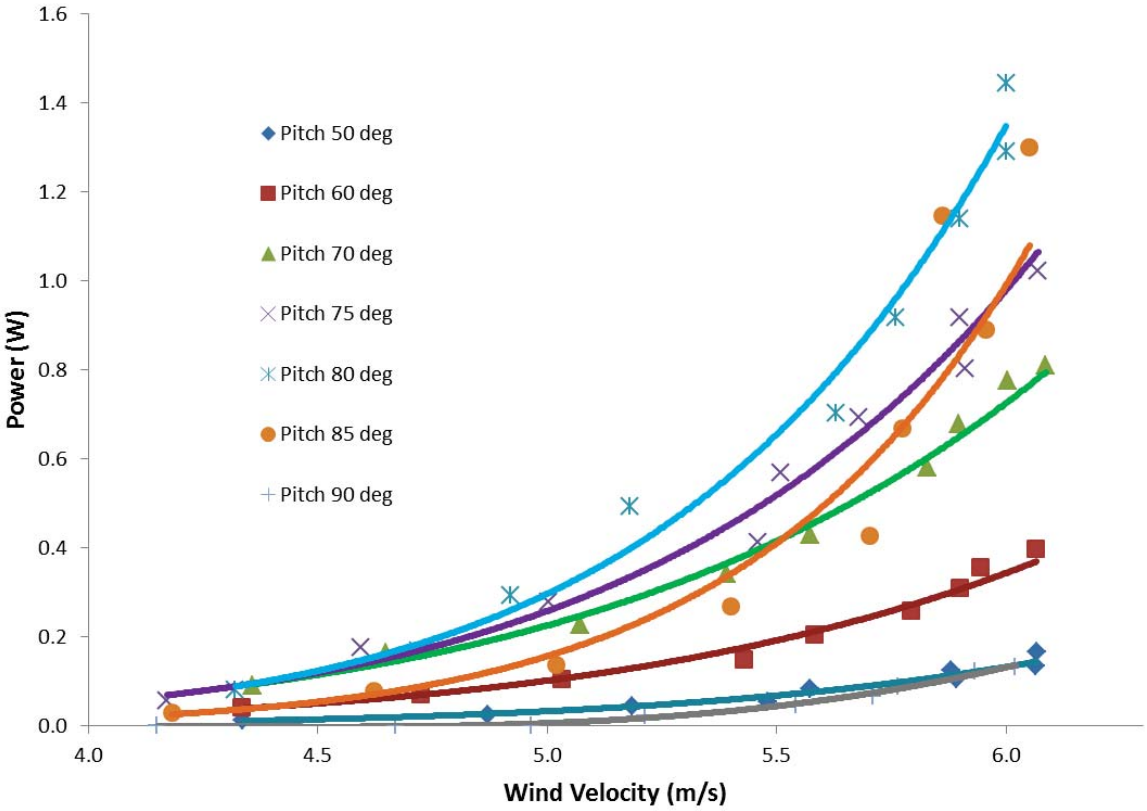

Figure 10.2. Power produced by the wind turbine (W) as a function of the wind speed (m/s) for a six-bladed rotor at various pitch angles.

The same experimental data are shown in Figure 10.3, this time using the non-dimensional parameters, the coefficient of power (C_p) and the tip speed ratio (TSR).

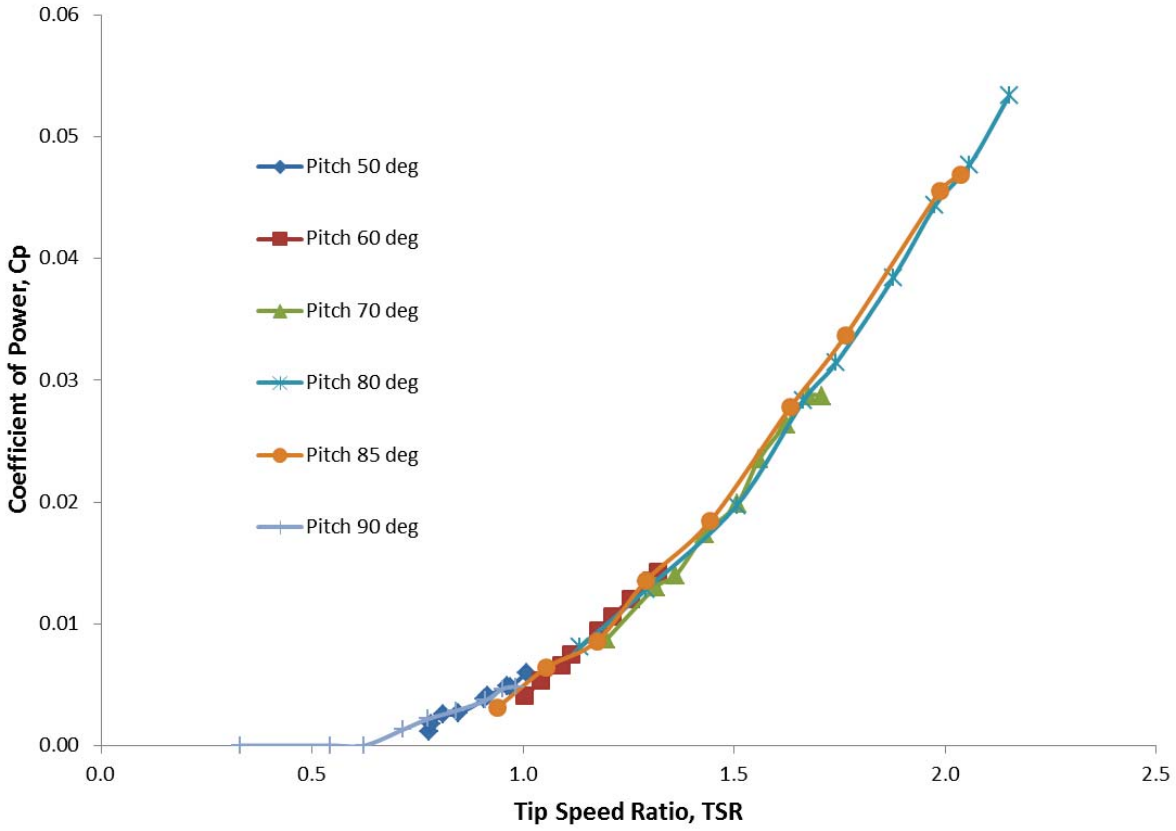

Figure 10.3. Same data as in the previous figure shown in non-dimensional variables.

d) A project team member (Dr. Cioc) used the experience gained during this project to serve as a panel reviewer for Transfer Assurance Guides (TAG) courses in Wind Energy or Renewable Energy for the University System of Ohio Board of Regents. The faculty review panel for the TAG in Renewable Energy guarantees that if a student takes an approved TAG course then that course will transfer as major credit to any of Ohio's public institutions. TAG courses are equivalent when they have been matched to the same set of learning outcomes and have been approved during the same time period. The panel receives course proposals from affiliated Ohio institutions, analyzes and discusses them to determine "extent of match" to learning outcomes, rigor and credit hours. During the past year, this project's team member (Dr. Cioc) was involved in the review of more than 10 courses in wind energy and two courses in alternative energy.

e) The North American Wind Energy Academy, NAWEA,is composed of universities, research laboratories, and industry participants dedicated to coordinating wind energy research and education activities in order to advance the state of wind energy technology and to develop the next generation of wind energy engineers, researchers, scientists, and innovators. Academy members coalesce around the vision, collaborate, and share their knowledge, skills, and capabilities to promote wind energy education and technologies. (Extracted from

http://www.nawea.org). Two faculty and three student members of the team actively participated in the 2012 inaugural meeting of NAWEA by presenting UT wind turbine research results, and by contributing to and supported the NAWEA concept, charter and by-laws.

10.2 Training and Outreach

Major training and dissemination of the educational program development are as follows:

a) K-12 teacher training in wind energy during summer 2012.

b) Undergraduate and graduate Students trained in wind energy research

c) A subset of the project team members participated at the NAWEA inaugural meeting (2012, Amherst, MA).

The teacher-training course was conducted for the first time in July 2012 on the main campus of The University of Toledo, with visits to UT's engineering laboratories. Twenty-four teacher leaders from Ohio and Michigan attended this course (two Toledo, Ohio school districts, one Akron, Ohio school district, and a Monroe, Michigan school district). The two-week program developed for teacher training was designed to train the teachers to be "teacher leaders." The course consists of both hands-on and demonstration projects. The teacher leaders were prepared to include the wind energy-related concepts learned in this course as part of a project-based science curriculum in their own schools, and to disseminate the knowledge and methods learned to other science teachers (thus becoming teacher leaders.) The course participants were recruited in collaboration with the LEADERS project (Leadership for Educators Academy for Driving Economic Revitalization in Science) at The University of Toledo. The LEADERS program, which is partially funded by the NSF, has a goal of making science education more relevant to students by incorporating Project-Based Science (PBS) that is linked to the renewable energies industry and its environmental impacts. The renewable energies industry, along with its environmental impacts, has been identified as a vital element in the economic development strategy for the Great Lakes Region (http://leaders.utoledo.edu).

11 Summary and Conclusion

The computational results presented in Chapter 9 demonstrate that the proposed downwind, 2-bladed wind turbine concept is a creditable and practical wind turbine design for offshore applications. This notwithstanding, the 2-bladed downwind concept has both advantages and disadvantages over its 2-bladed or 3-bladed upwind counterparts.

The results shown in Chapter 8 and in Section 9.3.2 confirmed that the levelized cost of energy of the 2-bladed downwind design is considerably lower than that of the baseline design (3-bladed). Specifically, the cost of the 2-bladed design with redesigned blades (BUT blades) is \$0.1308 /kWh and that of the optimized design is \$0.117 /kWh. These values are considerably lower than those of the 3-bladed baseline design, which is \$0.1453 /kWh. It could be possible to reduce the cost even more to \$0.0868 by replacing the gravity foundation with a floating one.

A 2-bladed turbine has one less blade. This can reduce the capital cost of the turbine by approximately 4% (Section 9.3.2). Additionally, assuming the same rated power, the higher RPM of the rotor of this turbine reduces the torque that is applied to the LSS and to the gearbox. This can potentially increase the reliability of the gearbox, which is a critical component of the power transmission. On the other hand, the higher rotational speed of 2-bladed turbines increases the blades loads.

Another important advantage of 2-bladed turbine concepts is the possibility of adding teeter degree of freedom to the system (Section 9.1.5). The teeter mechanism can effectively reduce the loads effects the tower and shaft. However, the teeter mechanism would increase the complexity of the design and the likelihood of failure in this mechanism.

Because the downwind configuration has larger clearance the designer has more options to modify the design to increase AEP. For example, the designer can increase the AEP by reducing the shaft tilt and cone angles thereby increasing the swept area.

Unlike the upwind design, for the downwind configuration, the bending moments due to wind loads and the mass of the rotor are in the same direction. Therefore, higher loads are expected at the base of the tower. Because these two bending moments oppose each other in an upwind configuration, lower bending moments are observed for the upwind configuration. However, this disadvantage of the 2-bladed downwind design compared to the 3-bladed upwind design was found to be minimal because the position of the tower top center of mass is close to the yaw axis and the tower top mass is lower (Section 9.1.2).

An appropriate braking strategy can effectively mitigate the load effects that are applied to the rotor, the blades and the tower of a 2-bladed design under fault conditions.

Fatigue damage analysis on critical turbine components demonstrated that the baseline 3-bladed turbine has relatively less damage than 2-bladed upwind and downwind turbines considered in this project. The results indicated that among all the load effects considered, bending moment on the blade root contributes most to damage accumulation. Increasing the coning angle and introducing a teeter mechanism considerably reduces fatigue damage on 2-bladed turbine

components. Increase in tilt angle reduces the damage associated with torsional moment at the blade root and torsional moment at the LSS.

References

Bir, G. S. (2005). *User's Guide to BModes.* National Renewable Energy Laboratory, Golden, CO.

Bir, G. S. (2005). *User's Guide to PreComp*. Tech. rep. National Renewable Energy Laboratory, Golden, CO.

Brown, T., & El Seify, M. (2005). A unified model for rubble ice load and behaviour. *PERD/CHC 5-119.*

Buhl, M. L. (2004). *WT_Perf user's guide.* National Renewable Energy Laboratory, Golden, CO.

Bush, E. A. (2009). *A comparison of alternative foundation models for offshore wind turbines and resulting long-term loads.* M.Sc. Thesis, University of Texas at Austin.

C-CORE. (2008). *Ice loads on wind turbine structures in Lake Erie.* C-Core Report R-08-014-566 v2.

Dames & Moore. (1974). *Lake bottom geotechnical and geophysical studies.* Reports No. 5-1 & 5-2, for the First Phase Airport Feasibility Study for Lake Erie Regional Transportation Authority, under contract to Howard, Needles, Tammen and Bergendoff.

DNV-OS-J101 (2013). *Design of Offshore Wind Turbine Structures*.

Driedger-Marschall, B., Endres, P. K., Krueger, R. M., & van den Bruck, C. (2009). *Great lakes wind energy center feasibility study: final feasibility report*. Cleveland, OH: juwi GmbH.

Downing, S. D., & Socie, D. F. (1982). Simple rainflow counting algorithms. *International Journal of Fatigue*, *4*(1), 31-40.

Dykes, K., Miller, F., Weinberg, B., Godwin, A. & Sautter, E., (2008). *A wind resource assessment for near-shore lake Erie*. Cleveland Water Crib Monitoring Site Two-Year Report, Green Energy Ohio.

Fingersh, L. J., Hand, M. M., & Laxson, A. S. (2006). *Wind turbine design cost and scaling model*. National Renewable Energy Laboratory, Golden, CO.

Faulstich, S., Hahn, B., Jung, H., Rafik, K., & Ringhandt, A. (2008). Appropriate failure statistics and reliability characteristics. *Proc. of DEWEK*.

Faulstich, S., Lyding, P., & Hahn, B. (2010). *Component reliability ranking with respect to WT concept and external environmental conditions. Kassel*: Fraunhofer Institute for Wind energy and Energy System Technology (IWES).

Griffith, D. T., & Ashwill, T. D. (2011). *The Sandia 100-meter all-glass baseline wind turbine blade: Snl100-00.* Sandia National Laboratories Technical Report.

Griffin, D. A. (1997). *Investigation of aerodynamic braking devices for wind turbine applications.* National Renewable Energy Lab., Golden, CO.

Hayman, G. J., & Buhl Jr, M. (2012). *MLife User's Guide for Version 1.00*. National Renewable Energy Lab., Golden, CO.

Hansen,C. *NWTC Computer-Aided Engineering Tools, AirfoilPrep*. http://wind.nrel.gov/designcodes/preprocessors/airfoilprep/.Last modified 14-December-2012; accessed 29-August-2013.

International Electrotechnical Committee. (2005). *IEC 61400-1: Wind turbines part 1: Design requirements.*

International Electrotechnical Commission. (2009). *IEC 61400-3. Wind Turbines—Part 3: Design Requirements for Offshore Wind Turbines.*

ISO, I. (2005). 19901-1: *Petroleum and natural gas industries-specific requirements for offshore structures-Part 1: Metocean design and operating conditions*. British Standards Institute.

Jonkman, J. M., & Buhl Jr, M. L. (2005). *FAST user's guide.* National Renewable Energy Laboratory, Golden, CO.

Jonkman, J. M., & Buhl Jr, M. L. (2007). Loads analysis of a floating offshore wind turbine using fully coupled simulation. In *WINDPOWER Conference and Exhibition*, Los Angeles, California, 3–6 June 2007.

Jonkman, J. M., Butterfield, S., Musial, W., & Scott, G. (2009). *Definition of a 5-MW reference wind turbine for offshore system development*. National Renewable Energy Laboratory, Golden, CO.

Jonkman, J., & Kilcher, L. (2012). *TurbSim User's Guide: Version 1.06. 00*. *NREL/TP-xxx-xxxx (Draft Version).* National Renewable Energy Laboratory, Golden, CO.

Jonkman, J. M., & Matha, D. (2010). *A quantitative comparison of the responses of three floating platforms*. National Renewable Energy Laboratory, Golden, CO.

Kaiser, M. J., & Snyder, B. (2010). *Offshore Wind Energy Installation and Decommissioning Cost Estimation in the US Outer Continental Shelf*.

Kelley, N. D., & Jonkman, B. J. (2005). *Overview of the TurbSim stochastic inflow turbulence simulator*. National Renewable Energy Laboratory, Golden, CO.

Kooijman, H. J. T., Lindenburg, C., Winkelaar, D., & van der Hooft, E. L. (2003). *Dowec 6 MW pre-design*. Energy Research Center of the Netherlands (ECN).

Laino, D. J., & Hansen, A. C. (2001). *User's guide to the computer software routines AeroDyn interface for ADAMS®*. Salt Lake City, UT: Windward Engineering, Prepared for the National Renewable Energy Laboratory under Subcontract No. TCX-9-29209-01.

Lever, J. H. (2000). *Assessment of Millennium Pipeline Project Lake Erie Crossing* (No. ERDC/CRREL-TR-00-13). Engineer Research and Development Center Hanover NH Cold Regions Research and Engineering Lab.

Lindenburg, C. (2002). Aeroelastic modeling of the LMH64-5 blade. *ECN, Petten*.

Link, H., LaCava, W., van Dam, J., McNiff, B., Sheng, S., Wallen, R., ... & Oyague, F. (2011). *Gearbox reliability collaborative project report: findings from phase 1 and phase 2 testing*. Contract, 303, 275-3000.

Manwell, J. F., McGowan, J. G., & Rogers, A. L. (2002). *Wind energy explained: theory, design and application*. John Wiley&Sons Ltd, UK.

Marrone, Joseph F., Sharma, Ravi M.S. & Cooper, Brent D. (2013). *Advanced offshore wind turbine/foundation concept for the Great Lakes.* DOE Project DE-EE0003540; Foundation Conceptual Design Report. Prepared by Ocean & Coastal Consultants, Inc., a COWI Company, for Nautica Windpower LLC.

Nelsen, R. B. (2006). *An introduction to copulas*. Springer.

Nikolaidis, E., Mourelatos, Z. P., & Pandey, V. (2011). *Design decisions under uncertainty with limited information* (Vol. 7). Taylor & Francis US.

NOAA. National Oceanic and Atmospheric Administration. *Department of Commerce*. http://www.noaa.gov/

Norouzi, M. (2012). *An efficient method for reliability assessment under dynamic stochastic loads.* Ph.D. Dissertation, The University of Toledo, OH, USA.

Norouzi, M. & Nikolaidis, E. (2013). Modeling dependence between wind and wave in an offshore wind turbine site. *In Proceedings of the 23rd International Offshore and Polar Engineering Conference*, Anchorage, Alaska.

Ochi, M. K. (2005). *Ocean waves: the stochastic approach* (Vol. 6). Cambridge University Press.

Powles, S. R. J. (1983). The effects of tower shadow on the dynamics of a horizontal-axis wind turbine. *Wind Engineering*, *7*, 26-42.

Ralston, T. D. (1977). Ice force design considerations for conical offshore structures. In *Proceedings of the 4th International Conference on Port and Ocean Engineering under Arctic Conditions,* Newfoundland Memorial University, Canada.

Senjyu, T., Sakamoto, R., Urasaki, N., Funabashi, T., Fujita, H., & Sekine, H. (2006). Output power leveling of wind turbine generator for all operating regions by pitch angle control. *Energy Conversion, IEEE Transactions on*, *21*(2), 467-475.

Timco, G., Frederking, R., Kamesaki, K., & Tada, H. (1999). Comparison of ice load calculation algorithms for first-year ridges. In *Proceedings International Workshop on Rational Evaluation of Ice Forces on Structures, REIFS'99* (pp. 88-102).

Wells, E. (2012). *An assessment of surface ice sheet loads and their effects on an offshore wind turbine structure.* M.Sc. Thesis, The University of Toledo, OH, USA.

White, K. (2004) .*Method to estimate river ice thickness based on meteorological data*. ERDC/CRREL Technical Note 04-3.

Appendix

Appendix 1: Wind Turbine Models

A total of 23 different wind turbine models were developed for parametric studies. The following design parameters were changed in these models in order to investigate the effects of design changes on performance and safety.

- Power rating
- Number of blades
- Upwind/downwind configuration
- Blade model
- Shaft tilt angle
- Conning angle
- Teeter parameters
- Application of tip-brake

Table A1.1 shows the wind turbine models employed in this investigation. Table A1.1 includes the design changes of each wind turbine model. Figure A1.1 shows how these design settings were established for each model. For example, the first row shows that turbines with three and two blades were studied. According to the second row, an upwind design with three blades, and two designs with upwind and downwind configuration were studied. The rest of the rows of the Figure A1.1 can be extended with same logic for the various models. Acronyms for each design are shown at the bottom of the figure.

The wind turbine models numbered from 1 to 16 are used for the wind turbine model comparison studies that includes aspects of load effects, fatigue life estimation, tower-to-blade clearance, and teeter angle. The comparison studies of wind turbine models are covered in section 9.1. The wind turbine models numbered 6, and from 16 to 21 were used to find a proper teeter parameter that is discussed in section 6.2.4. The turbine model number 22 is used only for the AEP comparisons, presented in section 9.3.1. This model was used to find how much the tower shadow affects to the AEP of upwind and downwind turbines. The wind turbine model numbered 23 is the final selected design that is discussed in section 9.3.3. The detail designs of wind turbine models can be found in chapter 6.

The acronym for each model was defined according to the rules described in Table A1.2. The first three characters specify the rating of the wind turbine. For example, “5MW” denotes a wind turbine with a rating of 5MW. The next number shows the number of blades; for example “3” indicates a three blade rotor. The next symbol is for the wind direction for the wind turbine (“U” means upwind machine and “D” means downwind). The next three letters indicates blade model. “B00” denotes the original NREL 5MW wind turbine blade. Acronym “BUT” denotes the blade that has improved twist angle from The University of Toledo. The next letters are optional settings. If there are no characters after the 9th letter, it means that the wind turbine has a 5° shaft tilt angle, 2.5° conning angle, and no tip-brake. Also, if the wind turbine model is a 3-bladed machine, teeter is not used. A wind turbine model of a 2-bladed machine uses the teeter parameter set 0.3. The list of teeter parameter sets can be found from Table 6.6. Moreover, if the

wind turbine is a downwind machine, tower shadow effect is applied. If there is "NoTwrShdw" mark in the acronyms of a downwind machine, it means that the tower shadow effect was not considered. If there is a "TipBrk" mark in the model name, it means the model includes tip-brakes. If there is a "T#C#" mark, where the "#" denotes a number, in the acronyms of a wind turbine model, it means the wind turbine model has changes on shaft tilt or conning angle from the baseline design settings, which is 5° shaft tilt angle and 2.5° conning angle. Character "T" denotes the shaft tilt angle, and "C" denotes the conning angle. The shaft tilt angle used in the wind turbine model is the same as the number after the character "T". The conning angle of the wind turbine model is the same as the number after character "C". For example, "T0C2.5" means that the wind turbine model has 0° shaft tilt and 2.5° conning angles. If there is a "Teeter#" mark, where the "#" denotes a number, in the acronyms of a wind turbine model, it means the wind turbine model uses other than the teeter parameter set 0.3 for the 2-bladed machines. For example, if there is "Teeter0.5" mark in the acronyms of a wind turbine model, the wind turbine model uses teeter set "Teeter0.5". The "TeeterNo" mark is used for the model that has no teeter mechanism for the 2-bladed wind turbine. The details of the teeter parameter sets are explained in section 6.2.4.

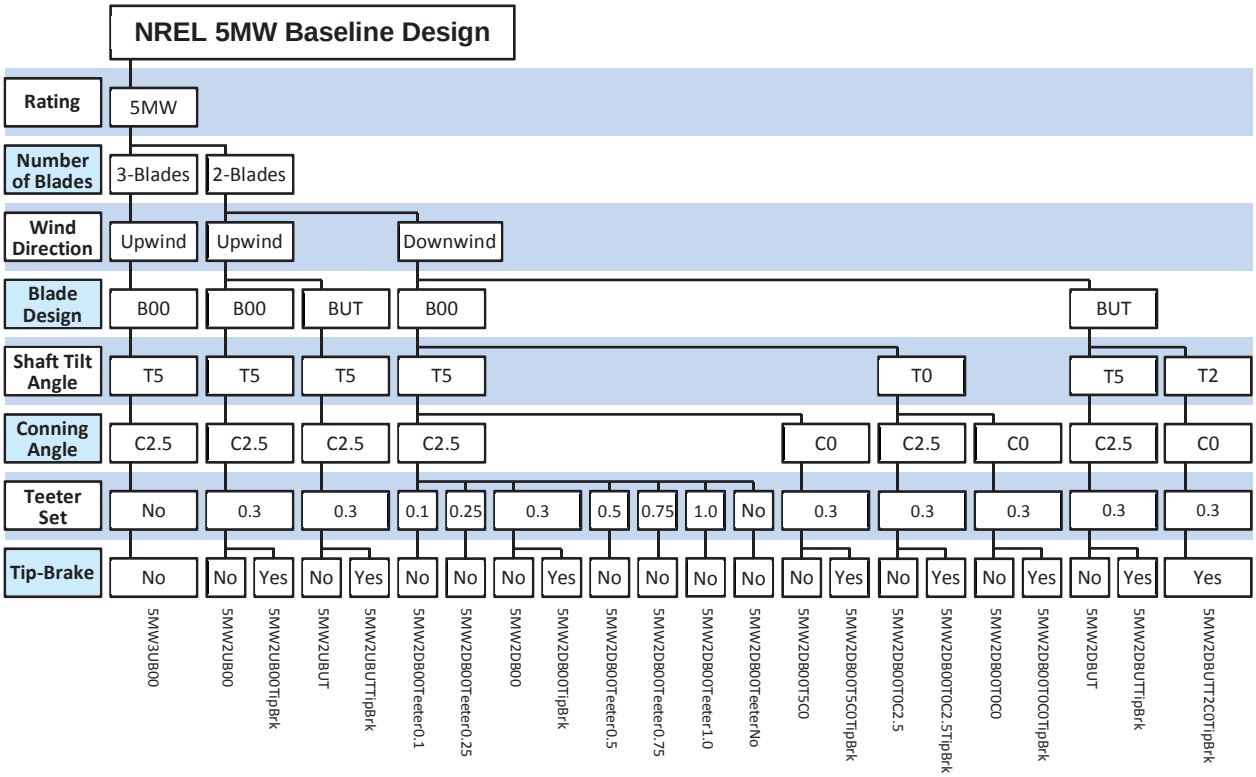

Figure A1.1. Description of alternative designs.

Table A1.1. List of simulated models.

#	Model	Power Rating	Num. of Blades	Wind Direction	Blade Model	Tilt (deg)	Cone (deg)	Teeter Set	Tip Brake	Tower Shadow
1	5MW3UB00	5MW	3	Up	Baseline	5	2.5	No	No	No
2	5MW2UB00	5MW	2	Up	Baseline	5	2.5	0.3	No	No
3	5MW2UB00TipBrk	5MW	2	Up	Baseline	5	2.5	0.3	Yes	No
4	5MW2UBUT	5MW	2	Up	BUT	5	2.5	0.3	No	No
5	5MW2UBUTTipBrk	5MW	2	Up	BUT	5	2.5	0.3	Yes	No
6	5MW2DB00	5MW	2	Down	Baseline	5	2.5	0.3	No	Yes
7	5MW2DB00TipBrk	5MW	2	Down	Baseline	5	2.5	0.3	Yes	Yes
8	5MW2DBUT	5MW	2	Down	BUT	5	2.5	0.3	No	Yes
9	5MW2DBUTTipBrk	5MW	2	Down	BUT	5	2.5	0.3	Yes	Yes
10	5MW2DB00T5C0	5MW	2	Down	Baseline	5	0	0.3	No	Yes
11	5MW2DB00T5C0TipBrk	5MW	2	Down	Baseline	5	0	0.3	Yes	Yes
12	5MW2DB00T0C2.5	5MW	2	Down	Baseline	0	2.5	0.3	No	Yes
13	5MW2DB00T0C2.5TipBrk	5MW	2	Down	Baseline	0	2.5	0.3	Yes	Yes
14	5MW2DB00T0C0	5MW	2	Down	Baseline	0	0	0.3	No	Yes
15	5MW2DB00T0C0TipBrk	5MW	2	Down	Baseline	0	0	0.3	Yes	Yes
16	5MW2DB00TeeterNo	5MW	2	Down	Baseline	5	2.5	No	No	Yes
17	5MW2DB00Teeter0.1	5MW	2	Down	Baseline	5	2.5	0.1	No	Yes
18	5MW2DB00Teeter0.25	5MW	2	Down	Baseline	5	2.5	0.25	No	Yes
19	5MW2DB00Teeter0.5	5MW	2	Down	Baseline	5	2.5	0.5	No	Yes
20	5MW2DB00Teeter0.75	5MW	2	Down	Baseline	5	2.5	0.75	No	Yes
21	5MW2DB00Teeter1.0	5MW	2	Down	Baseline	5	2.5	1.0	No	Yes
22	5MW2DB00NoTwrShdw	5MW	2	Down	Baseline	5	2.5	0.3	No	No
23	5MW2DBUTT2C0TipBrk	5MW	2	Down	BUT	2	0	0.3	Yes	Yes

Table A1.2. Model name acronyms descriptions.

Acronym	Location	Description
#MW	1~3	Rating in MW. The number “#” denotes a wind turbine rating.
“2” or “3”	4	Number of blades on the rotor.
“U” or “D”	5	Wind direction. “U” denotes upwind, and “D” denotes downwind.
“B00” or “BUT”	6~8	Blade design. “B00” denotes the baseline blade, and “BUT” denotes the improved blade from The University of Toledo
T#C#	after 8	Shaft tilt angle and conning angle. The number “#” after character “T” denotes shaft tilt angle in degree, and the number “#” after character “C” denotes conning angle in degree.
Teeter#	after 8	Teeter set other than the “Teeter0.3” teeter parameter set for the 2-bladed machines. The number “#” denotes teeter set number. If “No” is placed at “#”, teeter is disabled. Teeter is disabled for all 3-bladed machines.
TipBrk	after 8	If “TipBrk” is placed in a model name, tip-brake is enabled. If not, tip-brake is disabled.
NoTwrShdw	after 8	If “NoTwrShdw” is placed in a model name of a downwind machine, tower shadow effect is disabled. If not, tower shadow effect is enabled. Tower shadow effect is disabled for all upwind machines.

Appendix 2: Tower Structural Models

The tower structural properties along the height of the tower are listed in Table A2.1. The abbreviations are the same as thoses used in FAST tower input file. Refer to FAST User's Guide [Jonkman & Buhl, 2005] for the detailed descriptions of the structural properties.

Table A2.1. Tower structural properties.

Elevation	HtFract	TMassDen	TwFAStif	TwSSStif	TwGJStif	TwEAStif	TwFAIner	TwSSIner	TwFAcgOf	TwSScgOf
(m)	(-)	(kg/m)	(Nm^2)	(Nm^2)	(Nm^2)	(N)	(kg m)	(kg m)	(m)	(m)
11.00	0	4270.42	1.8871E+04	1.8871E+04	4.6622E+11	4.6622E+11	3.5877E+11	1.0550E+11	0	0
17.76	0.088251	4030.44	1.6720E+04	1.6720E+04	4.1308E+11	4.1308E+11	3.1788E+11	9.9576E+10	0	0
25.52	0.189556	3763.45	1.4483E+04	1.4483E+04	3.5783E+11	3.5783E+11	2.7536E+11	9.2979E+10	0	0
33.28	0.290862	3505.52	1.2479E+04	1.2479E+04	3.0830E+11	3.0830E+11	2.3724E+11	8.6607E+10	0	0
41.04	0.392167	3256.66	1.0689E+04	1.0689E+04	2.6408E+11	2.6408E+11	2.0322E+11	8.0459E+10	0	0
48.80	0.493473	3016.86	9.0989E+03	9.0989E+03	2.2480E+11	2.2480E+11	1.7299E+11	7.4534E+10	0	0
56.56	0.594778	2786.13	7.6927E+03	7.6927E+03	1.9006E+11	1.9006E+11	1.4625E+11	6.8834E+10	0	0
64.32	0.696084	2564.46	6.4557E+03	6.4557E+03	1.5949E+11	1.5949E+11	1.2273E+11	6.3357E+10	0	0
72.08	0.797389	2351.87	5.3739E+03	5.3739E+03	1.3277E+11	1.3277E+11	1.0217E+11	5.8105E+10	0	0
79.84	0.898695	2148.34	4.4336E+03	4.4336E+03	1.0954E+11	1.0954E+11	8.4291E+10	5.3077E+10	0	0
87.60	1	1953.87	3.6221E+03	3.6221E+03	8.9488E+10	8.9488E+10	6.8863E+10	4.8272E+10	0	0

The masses and CM information of the tower top components are listed in Table A2.2. Similar to the acronyms of wind turbine model names in Appendix 1, the model names with 3U, 2U, and 2D stand for three-bladed upwind, two-bladed upwind, and two-bladed downwind configuration respectively. The models whose names include "TipBrk" include a tip-brake. The model whose names include "T5C0", "T0C2.5", and "T0C0" have 5° shaft tilt with 0° precone, 0° shaft tilt with 2.5° precone, and 0° shaft tilt with 0° precone angle, respectively. Otherwise, shaft tilt and precone angles are 5° and 2.5° respectively.

Most of the abbreviations used in Table A2.2 are the same as those used in FAST input file. NumBl means number of blades, and TipBrk mass means tip-brake mass. Blade CM means the CM location of a blade measured from the blade root parallel to the blade z axis, according to the FAST blade coordinate system. HubRad means radius of rotor hub, and HubMass means mass of rotor hub. Rotor mass is the summation of blade masses and hub mass. NacMass is the mass of the nacelle, and YawBrMass is the yaw bearing mass. Twr2Shft is the distance from the tower top to the shaft along the tower axis in the height direction. OverHang is the overhang length, and UndSling is the distance between the end point of overhang and the apex of the cone of rotation. HubCM is the distance between the apex of the cone of rotation and the hub center of mass. ShftTilt is the shaft tilt angle and the PreCone is the precone angles of all blades. NacCMxn, NacCMyn, and NacCMzn are the nacelle center of mass location in x, y, and z directions according to the tower top coordinate system given in [Bir, 2007]. These distances are measured from the yaw bearing CM that is located at the top of the tower and the yaw axis. The positive x direction is the same direction as the wind direction. The y direction is perpendicular to the x direction. The z direction is the height direction of the tower. Hub CM x, Hub CM y, and Hub CM z are the hub center of mass location from the yaw bearing CM location in x, y, and z directions, respectively. Blades CM x, Blades CM y, and Blades CM z are the CM location of all blades from the yaw bearing CM in each direction.

Table A2.2. Tower top masses and center of mass locations.

Model	3U	3U TipBrk	2U	2U TipBrk	2D	2D TipBrk
NumBl	3	3	2	2	2	2
TipBrk mass (kg)	0	77.8	0	77.8	0	77.8
Blade mass (kg)	17740	17818	17740	17818	17740	17818
Blade CM (m)	20.475	20.654	20.475	20.654	20.475	20.654
HubRad (m)	1.5	1.5	1.5	1.5	1.5	1.5
HubMass (kg)	56780	56780	56780	56780	56780	56780
Rotor mass (kg)	110000	110233	92260	92416	92260	92416
NacMass (kg)	240000	240000	240000	240000	240000	240000
YawBrMass (kg)	0	0	0	0	0	0
Twr2Shft (m)	1.96256	1.96256	1.96256	1.96256	1.96256	1.96256
OverHang (m)	-5.0191	-5.0191	-5.0191	-5.0191	5.0191	5.0191
UndSling (m)	0	0	0	0	0	0
HubCM (m)	0	0	0	0	0	0
ShftTilt (deg)	-5	-5	-5	-5	5	5
PreCone (deg)	-2.5	-2.5	-2.5	-2.5	2.5	2.5
NacCMxn (m)	1.9	1.9	1.9	1.9	-1.9	-1.9
NacCMyn (m)	0	0	0	0	0	0
NacCMzn (m)	1.75	1.75	1.75	1.75	1.75	1.75
Hub CM x (m)	-5	-5	-5	-5	5	5
Hub CM y (m)	0	0	0	0	0	0
Hub CM z (m)	2.4	2.4	2.4	2.4	2.4	2.4
Blades CM x (m)	-5.9576	-5.9654	-5.9576	-5.9654	5.9576	5.9654
Blades CM y (m)	0	0	0	0	0	0
Blades CM z (m)	2.4418	2.4422	2.4418	2.4422	2.4418	2.4422

Model	2D T5C0	2D T5C0 TipBrk	2D T0C2.5	2D T0C2.5 TipBrk	2D T0C0	2D T0C0 TipBrk
NumBl	2	2	2	2	2	2
TipBrk mass (kg)	0	77.8	0	77.8	0	77.8
Blade mass (kg)	17740	17818	17740	17818	17740	17818
Blade CM (m)	20.475	20.654	20.475	20.654	20.475	20.654
HubRad (m)	1.5	1.5	1.5	1.5	1.5	1.5
HubMass (kg)	56780	56780	56780	56780	56780	56780
Rotor mass (kg)	92260	92416	92260	92416	92260	92416
NacMass (kg)	240000	240000	240000	240000	240000	240000
YawBrMass (kg)	0	0	0	0	0	0
Twr2Shft (m)	1.96256	1.96256	1.96256	1.96256	1.96256	1.96256
OverHang (m)	5.0191	5.0191	5.0191	5.0191	5.0191	5.0191
UndSling (m)	0	0	0	0	0	0
HubCM (m)	0	0	0	0	0	0
ShftTilt (deg)	5	5	0	0	0	0
PreCone (deg)	0	0	2.5	2.5	0	0
NacCMxn (m)	-1.9	-1.9	-1.9	-1.9	-1.9	-1.9
NacCMyn (m)	0	0	0	0	0	0
NacCMzn (m)	1.75	1.75	1.75	1.75	1.75	1.75
Hub CM x (m)	5	5	5	5	5	5
Hub CM y (m)	0	0	0	0	0	0
Hub CM z (m)	2.4	2.4	2.0	2.0	2.0	2.0
Blades CM x (m)	5.0000	5.0000	5.9767	5.9845	5.0191	5.0191
Blades CM y (m)	0	0	0	0	0	0
Blades CM z (m)	2.4000	2.4000	2.0044	2.0047	1.9626	1.96256

The same abbreviations used in the BModes input file are used in Table A2.3. The definitions of the terms are introduced in BModes user's guide [Bir, 2007].

Table A2.3. Tower top mass, CM, and mass moment of inertia for BModes input file.

Models	3U	3U TipBrk	2U	2U TipBrk	2D	2D TipBrk
NumBl	3	3	2	2	2	2
Wind direction	Up	Up	Up	Up	Down	Down
Tip-brake	No	Yes	No	Yes	No	Yes
tip_mass (kg)	350000	350233	332260	332416	332260	332416
cm_loc (m)	-0.4142	-0.4191	-0.1182	-0.1218	0.1182	0.1218
cm_axial (m)	1.9606	1.9610	1.9350	1.9352	1.9350	1.9352
ixx_tip (kg m^2)	1379376	1380856	1273602	1274589	1273602	1274589
iyy_tip (kg m^2)	5554229	5568969	4818804	4828631	4818804	4828631
izz_tip (kg m^2)	4174853	4188113	3545202	3554042	3545202	3554042
ixy_tip (kg m^2)	0	0	0	0	0	0
izx_tip (kg m^2)	-657574	-662097	-399503	-402519	399503	402519
iyz_tip (kg m^2)	0	0	0	0	0	0

Models	2D T5C0	2D T5C0 TipBrk	2D T0C2.5	2D T0C2.5 TipBrk	2D T0C0	2D T0C0 TipBrk
NumBl	2	2	2	2	2	2
Wind direction	Down	Down	Down	Down	Down	Down
Tip-brake	No	Yes	No	Yes	No	Yes
tip_mass (kg)	332260	332416	332260	332416	332260	332416
cm_loc (m)	0.0160	0.0183	0.1235	0.1271	0.0213	0.0236
cm_axial (m)	1.9305	1.9307	1.8135	1.8136	1.8090	1.8091
ixx_tip (kg m^2)	1266419	1267315	1096237	1096911	1090352	1090952
iyy_tip (kg m^2)	4439320	4444106	4660392	4669951	4280908	4285427
izz_tip (kg m^2)	3172901	3176791	3564155	3573040	3190555	3194475
ixy_tip (kg m^2)	0	0	0	0	0	0
izx_tip (kg m^2)	-657574	-399503	399503	-662097	-402519	402519
iyz_tip (kg m^2)	0	0	0	0	0	0

References

Jonkman, J. M., & Buhl Jr, M. L. (2005). *FAST user's guide.* National Renewable Energy Laboratory, Golden, CO.

Bir, G. S. (2005). *User's Guide to BModes.* National Renewable Energy Laboratory, Golden, CO.

Appendix 3: NREL 5MW Baseline Blade Geometry

The NREL 5MW baseline blade geometry data are listed in following table. The values marked in pink are interpolated values.

Table A3.1. Baseline blade geometry data long span.

Radius (m)	Span (m)	Span (Fraction)	Chord (m)	Twist (deg)	Pitch Axis (Fraction)	Airfoil (-)	Thickness / Chord Ratio (%)	Source (-)
1.500	0.000	0.000	3.500	13.308	0.500	Cylinder	100.000	All
1.808	0.308	0.005	3.500	13.308	0.500	Cylinder	100.000	SNL100-00
1.931	0.431	0.007	3.500	13.308	0.500	Translation	99.250	SNL100-00
2.054	0.554	0.009	3.500	13.308	0.500	Translation	98.500	SNL100-00
2.177	0.677	0.011	3.500	13.308	0.500	Translation	97.750	SNL100-00
2.300	0.800	0.013	3.500	13.308	0.500	Ellipse	97.000	SNL100-00
2.502	1.002	0.016	3.500	13.308	0.500	N/A	95.833	LMH64-5
2.867	1.367	0.022	3.542	13.308	0.499	N/A	93.730	NREL5MW
2.976	1.476	0.024	3.554	13.308	0.499	Ellipse	93.100	SNL100-00
3.099	1.599	0.026	3.568	13.308	0.498	Ellipse	92.500	SNL100-00
3.501	2.001	0.033	3.614	13.308	0.493	N/A	89.854	LMH64-5
4.391	2.891	0.047	3.716	13.308	0.483	Translation	84.000	SNL100-00
5.600	4.100	0.067	3.854	13.308	0.469	N/A	76.508	NREL5MW
5.682	4.182	0.068	3.863	13.308	0.468	Translation	76.000	SNL100-00
6.974	5.474	0.089	4.011	13.308	0.453	Translation	68.000	SNL100-00
8.333	6.833	0.111	4.167	13.308	0.437	N/A	60.925	NREL5MW
8.511	7.011	0.114	4.187	13.308	0.435	Translation	60.000	SNL100-00
10.479	8.979	0.146	4.412	13.308	0.410	Translation	51.000	SNL100-00
11.525	10.025	0.163	4.531	13.308	0.400	Translation	47.000	SNL100-00
11.750	10.250	0.167	4.557	13.308	0.398	N/A	46.198	NREL5MW
12.001	10.501	0.171	4.586	13.274	0.395	N/A	45.305	LMH64-5
12.201	10.701	0.174	4.609	13.248	0.393	N/A	44.594	LMH64-5
12.509	11.009	0.179	4.629	13.207	0.390	Translation	43.500	SNL100-00
12.700	11.200	0.182	4.641	13.181	0.388	N/A	42.906	NREL5MW
13.493	11.993	0.195	4.691	12.917	0.380	DU99-W-405	40.448	SNL100-00
13.501	12.001	0.195	4.692	12.914	0.380	N/A	40.435	LMH64-5
13.700	12.200	0.198	4.689	12.848	0.380	N/A	40.142	NREL5MW
14.700	13.200	0.215	4.673	12.192	0.379	N/A	38.668	NREL5MW
15.153	13.653	0.222	4.666	11.906	0.378	DU99-W-405 Adj	38.000	SNL100-00
15.501	14.001	0.228	4.661	11.687	0.378	N/A	37.581	LMH64-5
15.700	14.200	0.231	4.656	11.561	0.378	N/A	37.341	NREL5MW
15.850	14.350	0.233	4.652	11.480	0.378	N/A	37.160	NREL5MW
16.501	15.001	0.244	4.635	11.168	0.377	N/A	36.376	LMH64-5
16.700	15.200	0.247	4.625	11.072	0.377	N/A	36.137	NREL5MW
16.814	15.314	0.249	4.619	11.040	0.377	DU99-W-350 Adj	36.000	SNL100-00
17.700	16.200	0.263	4.573	10.792	0.376	N/A	34.932	NREL5MW
18.474	16.974	0.276	4.534	10.575	0.375	DU99-W-350 Adj	34.000	SNL100-00
19.700	18.200	0.296	4.471	10.232	0.375	N/A	33.026	NREL5MW
19.950	18.450	0.300	4.458	10.162	0.375	N/A	32.827	NREL5MW
21.501	20.001	0.325	4.379	9.728	0.375	N/A	31.595	LMH64-5
21.700	20.200	0.328	4.369	9.672	0.375	N/A	31.437	NREL5MW
23.517	22.017	0.358	4.276	9.161	0.375	DU97-W-300	29.993	SNL100-00
23.700	22.200	0.361	4.267	9.110	0.375	N/A	29.846	NREL5MW
24.050	22.550	0.367	4.249	9.011	0.375	N/A	29.566	NREL5MW
24.701	23.201	0.377	4.216	8.823	0.375	N/A	29.044	LMH64-5
25.700	24.200	0.393	4.158	8.534	0.375	N/A	28.243	NREL5MW
26.501	25.001	0.407	4.111	8.293	0.375	N/A	27.601	LMH64-5
27.700	26.200	0.426	4.035	7.932	0.375	N/A	26.640	NREL5MW
28.150	26.650	0.433	4.007	7.795	0.375	N/A	26.279	NREL5MW
28.499	26.999	0.439	3.985	7.688	0.375	DU91-W2-250	26.000	SNL100-00
29.700	28.200	0.459	3.909	7.321	0.375	N/A	25.276	NREL5MW
31.700	30.200	0.491	3.783	6.711	0.375	N/A	24.072	NREL5MW
32.201	30.701	0.499	3.751	6.559	0.375	N/A	23.770	LMH64-5
32.250	30.750	0.500	3.748	6.544	0.375	N/A	23.741	NREL5MW
33.480	31.980	0.520	3.674	6.186	0.375	DU93-W-210 Adj	23.000	SNL100-00
33.700	32.200	0.524	3.661	6.122	0.375	N/A	22.913	NREL5MW
34.501	33.001	0.537	3.613	5.891	0.375	N/A	22.598	LMH64-5
35.700	34.200	0.556	3.541	5.546	0.375	N/A	22.125	NREL5MW

Table A3.1. Baseline blade geometry data long span (continue).

Radius (m)	Span (m)	Span (Fraction)	Chord (m)	Twist (deg)	Pitch Axis (Fraction)	Airfoil (-)	Thickness / Chord Ratio (%)	Source (-)
36.350	34.850	0.567	3.502	5.361	0.375	N/A	21.869	NREL5MW
36.501	35.001	0.569	3.493	5.317	0.375	N/A	21.810	LMH64-5
37.501	36.001	0.585	3.433	5.028	0.375	N/A	21.416	LMH64-5
37.700	36.200	0.589	3.421	4.971	0.375	N/A	21.337	NREL5MW
38.523	37.023	0.602	3.372	4.736	0.375	DU93-W-210	21.013	SNL100-00
39.700	38.200	0.621	3.301	4.401	0.375	N/A	20.420	NREL5MW
40.450	38.950	0.633	3.256	4.188	0.375	N/A	20.043	NREL5MW
41.501	40.001	0.650	3.193	3.890	0.375	N/A	19.513	LMH64-5
41.700	40.200	0.654	3.181	3.834	0.375	N/A	19.413	NREL5MW
42.201	40.701	0.662	3.151	3.708	0.375	N/A	19.161	LMH64-5
42.521	41.021	0.667	3.132	3.628	0.375	NACA 64-618 Adj	19.000	SNL100-00
43.505	42.005	0.683	3.073	3.381	0.375	NACA 64-618 Adj	18.500	SNL100-00
43.700	42.200	0.686	3.061	3.332	0.375	N/A	18.468	NREL5MW
44.550	43.050	0.700	3.010	3.125	0.375	N/A	18.327	NREL5MW
44.701	43.201	0.702	3.001	3.094	0.375	N/A	18.301	LMH64-5
45.501	44.001	0.715	2.953	2.931	0.375	N/A	18.169	LMH64-5
45.700	44.200	0.719	2.941	2.890	0.375	N/A	18.136	NREL5MW
46.518	45.018	0.732	2.892	2.732	0.375	NACA 64-618	18.000	SNL100-00
47.700	46.200	0.751	2.821	2.503	0.375	N/A	18.000	NREL5MW
48.486	46.986	0.764	2.774	2.351	0.375	NACA 64-618	18.000	SNL100-00
48.650	47.150	0.767	2.764	2.319	0.375	N/A	18.000	NREL5MW
49.700	48.200	0.784	2.701	2.116	0.375	N/A	18.000	NREL5MW
51.501	50.001	0.813	2.593	1.768	0.375	N/A	18.000	LMH64-5
51.700	50.200	0.816	2.581	1.730	0.375	N/A	18.000	NREL5MW
52.750	51.250	0.833	2.518	1.526	0.375	N/A	18.000	NREL5MW
53.529	52.029	0.846	2.471	1.375	0.375	NACA 64-618	18.000	SNL100-00
53.700	52.200	0.849	2.461	1.342	0.375	N/A	18.000	NREL5MW
55.700	54.200	0.881	2.341	0.954	0.375	N/A	18.000	NREL5MW
56.167	54.667	0.889	2.313	0.863	0.375	N/A	18.000	NREL5MW
56.481	54.981	0.894	2.294	0.802	0.375	NACA 64-618	18.000	SNL100-00
56.501	55.001	0.894	2.293	0.798	0.375	N/A	18.000	LMH64-5
56.700	55.200	0.898	2.281	0.760	0.375	N/A	18.000	NREL5MW
57.501	56.001	0.911	2.232	0.611	0.375	N/A	18.000	LMH64-5
57.700	56.200	0.914	2.211	0.574	0.375	N/A	18.000	NREL5MW
58.700	57.200	0.930	2.107	0.404	0.375	N/A	18.000	NREL5MW
58.900	57.400	0.933	2.086	0.370	0.375	N/A	18.000	NREL5MW
59.200	57.700	0.938	2.055	0.319	0.375	N/A	18.000	NREL5MW
59.495	57.995	0.943	2.024	0.280	0.375	NACA 64-618	18.000	SNL100-00
59.501	58.001	0.943	2.023	0.279	0.375	N/A	18.000	LMH64-5
59.700	58.200	0.946	1.972	0.253	0.375	N/A	18.000	NREL5MW
60.200	58.700	0.954	1.846	0.216	0.375	N/A	18.000	NREL5MW
60.356	58.856	0.957	1.806	0.204	0.375	NACA 64-618	18.000	SNL100-00
60.700	59.200	0.963	1.719	0.178	0.375	N/A	18.000	NREL5MW
61.100	59.600	0.969	1.617	0.148	0.375	N/A	18.000	LMH64-5
61.200	59.700	0.971	1.580	0.140	0.375	N/A	18.000	NREL5MW
61.278	59.778	0.972	1.551	0.134	0.375	NACA 64-618	18.000	SNL100-00
61.633	60.133	0.978	1.419	0.106	0.375	N/A	18.000	NREL5MW
61.700	60.200	0.979	1.394	0.101	0.375	N/A	18.000	NREL5MW
62.139	60.639	0.986	1.231	0.067	0.375	NACA 64-618	18.000	SNL100-00
62.200	60.700	0.987	1.209	0.062	0.375	N/A	18.000	NREL5MW
62.501	61.001	0.992	1.097	0.039	0.375	N/A	18.000	LMH64-5
62.700	61.200	0.995	0.684	0.023	0.375	N/A	18.000	NREL5MW
63.000	61.500	1.000	0.061	0.023	0.375	NACA 64-618	18.000	SNL100-00

References

Griffith, D. T., & Ashwill, T. D. (2011). *The Sandia 100-meter all-glass baseline wind turbine blade: Snl100-00.* Sandia National Laboratories Technical Report.

Lindenburg, C. (2002). Aeroelastic modeling of the LMH64-5 blade. *ECN, Petten*.

Jonkman, J. M., Butterfield, S., Musial, W., & Scott, G. (2009). *Definition of a 5-MW reference wind turbine for offshore system development*. National Renewable Energy Laboratory, Golden, CO.

Appendix 4: Definition of Load Effects

Load effects are determined by performing FAST simulations. The term *load effect* is used in this report to denote internal forces and moments in wind turbine structures that are found from FAST simulations. The term *load effect* distinguishes the internal forces and moments in a wind turbine structure from the term *external load* on a wind turbine structure. More specifically for this report, the term *load effect* denotes the post-processed internal loads that will be introduced in later in this section. Maximum, minimum, and average load effects were calculated using Fast simulations and by sorting the time marching output of FAST for various DLCs, and used for the ultimate load effect analyses. The time marching output of FAST simulation in DLC1.2 were used for estimating the fatigue life.

The detailed theory of load effect calculations from external loads in FAST simulation can be found from Jonkman & Buhl [2004], Jonkman [2003], Moriarty & Hansen [2005], and Jonkman & Buhl [2005]. The detailed output descriptions of FAST simulation can be found in Jonkman & Buhl [2005] or released FAST archives. The design load cases (DLC) for normal operation conditions, fault conditions, and parked conditions were considered to perform the simulation. The DLCs are explained in section 5.4. The detailed description of models used in simulations is explained in chapter 6.

In this research, there are 4 types of load effects of interest (shear forces, bending moments, axial forces, torsional moments) at 4 different locations (tower base, tower top, each blade root, LSS), 3 torques on LSS, HSS, and generator. The load effects found from FAST simulations are post-processed for easier analysis. The root mean squared (RMS) values were used for shear forces and bending moments because the cross-sections of the locations of interest have a circular shape and the structural properties are homogeneous. Although a composite material is used in the rotor blade, it is assumed that the structural properties are homogeneous at the blade root. The post-processed load effects for each locations of interest are listed in Table A4.1 to Table A4.4.

The coordinate systems used in this report follow Jonkman and Buhl [2005]. The tower base coordinate system is fixed at the top of the platform, which is located 11m above the water surface. The tower top location is loaded at the yaw bearing height. The tower top coordinate system does not rotate along the yaw rotation. The LSS coordinate system does not rotate along the rotor. The LSS bending moments are measured at 1.912m location from the rotor apex (for 3 blades machines) or teeter pin (for 2 blades machines). The LSS torsional moment and the LSS torque (rotor torque) are the same concept and are used interchangeably.

Table A4.1. Tower base load effects.

Internal Load	Unit	Internal Load Description	Coordinate	Load Effect	Load Effect Description
F_{xt}	kN	Tower base fore-aft shear force	Along x_t	$F_{xyt} = \sqrt{{F_{xt}}^2 + {F_{yt}}^2}$	Tower base shear force
F_{yt}	kN	Tower base side-to-side shear force	Along y_t		
F_{zt}	kN	Tower base axial force	Along z_t	F_{zt}	Tower base axial force
M_{xt}	kN·m	Tower base side-to-side (roll) moment	About x_t	$M_{xyt} = \sqrt{{M_{xt}}^2 + {M_{yt}}^2}$	Tower base bending moment
M_{yt}	kN·m	Tower base fore-aft (pitching) moment	About y_t		
M_{zt}	kN·m	Tower base torsional (yaw) moment	About z_t	M_{zt}	Tower base torsional moment

Table A4.2. Tower top load effects.

Internal Load	Unit	Internal Load Description	Coordinate	Load Effect	Load Effect Description
F_{xp}	kN	Tower top fore-aft shear force	Along x_p	$F_{xyp} = \sqrt{{F_{xp}}^2 + {F_{yp}}^2}$	Tower top shear force
F_{yp}	kN	Tower top side-to-side shear force	Along y_p		
F_{zp}	kN	Tower top axial force	Along z_p	F_{zp}	Tower top axial force
M_{xp}	kN·m	Tower top roll moment	About x_p	$M_{xyp} = \sqrt{{M_{xp}}^2 + {M_{yp}}^2}$	Tower top bending moment
M_{yp}	kN·m	Tower top pitch moment	About y_p		
M_{zp}	kN·m	Tower top yaw moment	About z_p	M_{zp}	Tower top torsional moment

Table A4.3. Blade root load effects.

Internal Load	Unit	Internal Load Description	Coordinate	Load Effect	Load Effect Description
F_{xb}	kN	Blade root flapwise shear force	Along x_b	$F_{xyb} = \sqrt{{F_{xb}}^2 + {F_{yb}}^2}$	Blade root shear force
F_{yb}	kN	Blade root edgewise shear	Along y_b		
F_{zb}	kN	Blade root axial force	Along z_b	F_{zb}	Blade root axial force
M_{xb}	kN·m	Blade root flapwise bending moment	About x_b	$M_{xyb} = \sqrt{{M_{xb}}^2 + {M_{yb}}^2}$	Blade root bending moment
M_{yb}	kN·m	Blade root edgewise bending moment	About y_b		
M_{zb}	kN·m	Blade root torsional moment	About z_b	M_{zb}	Blade root torsional moment

Table A4.4. LSS load effects.

Internal Load	Unit	Internal Load Description	Coordinate	Load Effect	Load Effect Description
F_{xs}	kN	LSS axial force (thrust)	Along x_s	F_{xs}	LSS axial force
F_{ys}	kN	LSS shear force	Along y_s	$F_{yzs} = \sqrt{{F_{ys}}^2 + {F_{zs}}^2}$	LSS shear force
F_{zs}	kN	LSS shear force	Along z_s		
M_{xs}	kN·m	LSS torsional moment (rotor torque)	About x_s	M_{xs}	LSS torsional moment
M_{ys}	kN·m	LSS bending moment at the shaft's strain gage	About y_s	$M_{yzs} = \sqrt{{M_{ys}}^2 + {M_{zb}}^2}$	LSS bending moment
M_{zs}	kN·m	LSS bending moment at the shaft's strain gage	About z_s		

References

Jonkman, J. M., & Buhl Jr, M. L. (2004). New developments for the NWTC's FAST aeroelastic HAWT simulator. In *The 23rd ASME Wind Energy Symposium, Reno, Nevada*.

Jonkman, J. M. (2003). *Modeling of the UAE Wind Turbine for Refinement of FAST_AD*. Colorado: National Renewable Energy Laboratory.

Moriarty, P. J., & Hansen, A. C. (2005). *AeroDyn theory manual*. National Renewable Energy Laboratory. Golden, Co.

Jonkman, J. M., & Buhl Jr, M. L. (2005). *FAST user's guide*. National Renewable Energy Laboratory, Golden, CO.

Appendix 5: Safe Limit

The safe limits were determined according to the calculated load effects on the baseline model, assuming that the baseline design is safe. First, to determine a safe limit load effect, the maximum and minimum load effects of the baseline model are multiplied by the load factor for the corresponding DLC. Then, the load effects that have largest magnitude are selected for the shear force, bending moment, axial force, and torsional moment from the locations at the tower base, tower top, LSS, and torques from the locations at the HSS, and generator. The safe limit is determined using the load effect with the largest magnitude for both positive and negative value regions on the tower, and shafts that are made of isotropic material. For the blades, maximum and minimum loads are collected from both blades, because the blades are not made of an isotropic material.

The load capacity of the wind turbine structure in reality may be larger than the safe limits calculated using the above procedure and indicated by the green line in load effects graphs. However, if a load effect for a particular model does not exceed the safe limits, this is considered as conclusive evidence that the model is safe. The models in which the load effects exceed the safe limit may still be safe because the load capacity of the structure may be much larger than the safe limit. However, these models need to be carefully considered in the detailed design stage.

Table A5.1. Safe limits according to the baseline model.

	Shear Force	Bending Moment	Axial Force		Torsional Moment	
	Max	Max	Max	Min	Max	Min
Tower Base	1595	126821	7878	-7878	12311	-12311
Tower Top	1595	17308	4767	-4767	12311	-12311
Blade Roots	632	23940	1367	-201	197	-273
LSS	1557	18113	1473	-1473	9641	-9641
HSS Torque					99	-99
Generator Torque					64	-64

Appendix 6: Load Effect Graph

Graphs showing the range of maximum and minimum average load effects, and maximum and minimum load effects were also used to demonstrate the load effect results from various models. Figure A6.1 and Figure A6.2 are examples of this type of graphs. The blue bars indicate ranges of maximum and minimum average values for the load effect. The red lines specify ranges of maximum and minimum values for the load effect. These values do not include load factors. Similar to the maximum and minimum load effects, the average load effects are also shown as a range using maximum and minimum average load effects. This presentation stylewas selected because the load effects are obtained from different DLCs. The green horizontal lines indicate the safe limit for each load effect.

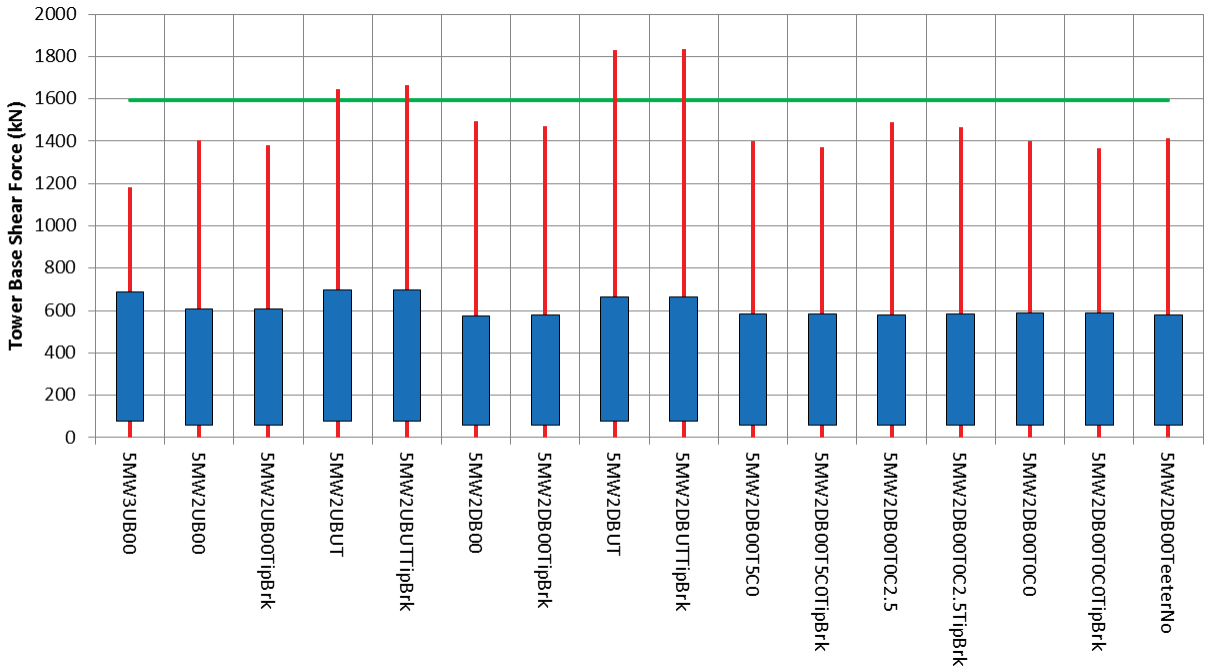

Figure A6.1. An example of load effect graph of tower base shear force.

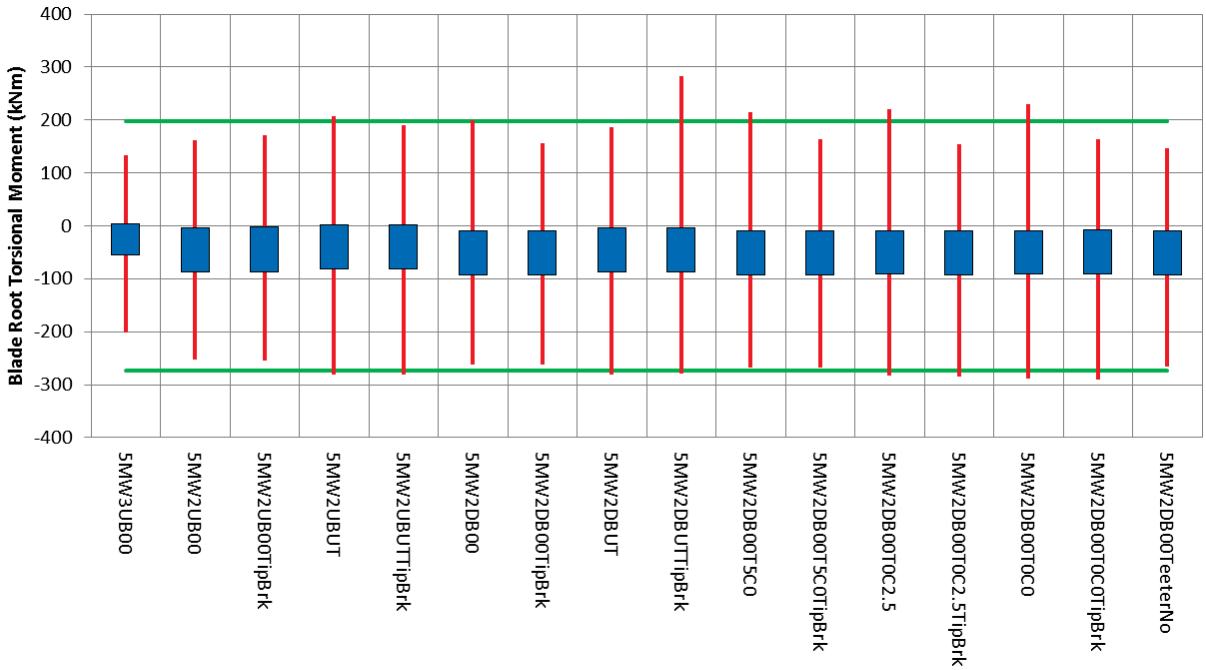

Figure A6.2. An example of load effect graph of blade root torsional moment.

Appendix 7: Weighted Percent Difference Graph

The weighted percent difference values were used to compare load effects of parametric design models to the load effects of the baseline model. The weighted percent difference, η_m, of load effects of a model relative to the baseline model is defined in Eq. (A7.1). Weights are used to scale the percent differences depending on their own baseline magnitude. Only the magnitudes of the load effect valuesare considered for the weighted percent difference calculations. This is because the low magnitude of a load effect is always better than a high value, regardless of the sign. Between a maximum and a minimum value of a load effect , the larger magnitude value is used for calculations. The same logic is used for the maximum of average values and the minimum of average values.

$$\eta_m = \sum_{i=1}^{N} \frac{[q_i|(\xi_i)_b|]^p \left[\left(\frac{\left|(\xi_i)_j\right| - |(\xi_i)_b|}{|(\xi_i)_b|}\right) s\right]}{\sum_{i=1}^{N}[q_n|(\xi_i)_b|]^p} \tag{A7.1}$$

In the above equation, ξ is a load effect value, j is the model number, and b denotes the baseline model. Variable i specifies the load effect for various load effect types at locations of interest. N is the total number of kinds of load effects considered. Variable q is a factor that determines the importance of each load effect, which is set to 1 in this research, which means that all load effects are considered equally important. The magnitude of exponent p determines the importance of the weight term, which is $[q_i|(\xi_i)_b|]$ term, relative to the difference of load effects term, which is $\left[\left(\frac{|(\xi_i)_j|-|(\xi_i)_b|}{|(\xi_i)_b|}\right) s\right]$ term. In this research, this factor is set to 1, which means that the weight term and the difference of load effects term are considered equally important. s is the scale for normalization. In this research, s is set to 100%.

There are three reasons why the weighted percent difference is used: a) An index is required to quantify the aggregate difference of the load effects of a model relative to the baseline model. The weighted percent difference converts load effect results to dimensionless values and enables putting all weighted percent differences into one value for different types of load effects on the locations of interest. The weighted percent difference in Eq. (A7.1) summarizes the differences in 192 load effect values, that are maximum and minimum, and maximum and minimum of averages of 4 different types of load effects (shear force, bending moment, axial force, torsional moment) at 4 different locations of interest (tower base, tower top, blade roots, LSS) in normal operating, fault, and parked conditions, into 6 values ,that are weighted percent differences of maximum load effects and average load effects in the 3 different condition groups, for each wind turbine model. (Refer Appendix 4, and section 9.1) This helps readers analyze and understand load effect results more easily. b) An index is required that express the cumulative difference of many load effects in a design relative to the load effects in a baseline model. c) That index also requires capability to reflect the magnitude of load effects at the same time. The problem of traditional percent difference is when the value of interest is too small (near zero), the percent difference becomes too sensitive to the load value. For example, if the baseline design has 1N value and an alternative design has 10N value, the percent difference will be 900%. However, a 9N difference is negligible for a large wind turbine structure. Thus, the reader may misinterpret that 900% difference is a significant difference, although the difference in the actual magnitude is just 9N. Because of this, the product of the magnitude of load effects and the percent

difference is used to compare the load effects of various wind turbine models. As a result, the percent differences of load effects that have small magnitude are minimized in the weighted percent difference value. On the other hand, the percent differences of load effects that have larger magnitudes relative to the other load effects are maximized and this contributes more to determining the weighted percent difference value.

The weighted percent difference is made for an index that can compare the differences of load effects relative to the baseline model. This allows comparing changes in load effects of other alternative designs. The weighted percent difference value does not show the exact value of load effect differences. However, it is a good index that can be used to compare changes in load effect values in one model to those in other models. By examining weighted percent difference graphs, the reader easily understands which design is subjected to higher loads. It also shows what location contributes more to increase or decrease the total load effects relative to other models or other measurement locations.

Using the weighted percent difference, the load effects at the tower base, tower top, blades, and LSS from the simulations of the selected 16 different models of section 9.1 are summarized into 6 graphs: maximum values and maximum of average values for normal operation, fault, and parked conditions. These graphs are listed in Figure 9.2 and Figure 9.3 The NREL 5MW 3-bladed upwind baseline model (5MW3UB00) is the baseline model for these graphs. Each bar graph is divided into 4 portions to show how much the tower base, tower top, blades, and LSS load effects contribute to total weighted percent difference from the baseline model. The line graph indicates the total weighted percent difference. This reflects changes in the load effects from the baseline model from all different locations. The total weighted percent difference is equal to the sum of all weighted percent differences at each location.

An example of the percent difference graphs is shown in Figure A7.1. Each color of bar represents a location of interest. In the Figure A7.1, the blue bars denote tower base, the red bars denote the tower top, the green bars denote the blade roots, and the purple bars denote the LSS. The orange line denotes the total weighted percent difference. This line can be used when it is necessary.

For example, the overall average load effect in normal operating conditions decreases relative to the baseline in design 5MW2UB00 (represented by the second column in Figure A7.1). The total weighted percent difference of average load effects (orange line) is 8.41% lower than the average load effects in the baseline design (5MW3UB00). The load effects on a blade (green bar) contribute to an increase of 3.55% to the total load effect compared to the baseline design. On the other hand, the tower base load effects (blue bar) contribute to decrease the total load effect of 6.63%. The load effects in the tower top (red bar) and the LSS (purple bar) reduce the total load effect by 2.57% and 2.76%, respectively. The total change in the load effects is equal to the sum of weighted percent differences, and it is equal to 3.55% - 6.63% - 2.57% - 2.76% = -8.41%. In this way, it can be determined approximately what locations contribute to the total change in the overall load effect relative to the baseline model.

For a more detailed example, consider the blade root load effect comparisons of the baseline design and the 5MW2UB00 design shown in Figure A7.2. The blue bars are ranges of the average load effect and the red lines are ranges of the maximum load effect. Because the average

load effects are calculated from various DLC, the average load effects are shown as a range rather than a single value. The green line is the safe limit that will be explained later in this section. In this example, only the average load effects (blue bars) will be considered because we are considering Figure A7.1. As shown in Table 9.12, the percent difference of the maximum average blade root shear force of the 5MW2UB00 wind turbine model is 28.57%. The percent difference of the maximum average blade root bending moment is 28.34%, and the axial force is 74.56%. The minimum average blade root torsion moments have maximum magnitude values. Thus, the absolute values of these values are used to calculate percent difference, which is equal to 55.06%. All four different percent differences are positive values in this case. The weights of each load effect at blade root are 300, 10101, 624, and 56 for the shear force, bending moment, axial force, and torsional moment, respectively. These values are the $[a_n|(x_n)_b|]^p$ terms of the numerator in Eq. (A7.1). Because the a_n and p are set to 1, and the maximum magnitudes of average load effects of baseline model are used as weights, $(x_n)_b$, these values are same as the average load effects of 5MW3UB00 in Table 9.12. The total weight of all locations for average load effects is 97106 that is the denominator of Eq. (A7.1). The weighted percent difference of each type of load effects in the blade root are 0.088%, 2.948%, 0.479%, and 0.032% respectively. The summation of these four values is 3.55%. This value is the same as the weighted percent difference of the blade root that contributed to increase total weighted percent difference. It is the value of the green bar in Figure A7.1 at the third column for the model 5MW2UB00. Using the same procedure, weighted percent differences at other locations can be found.

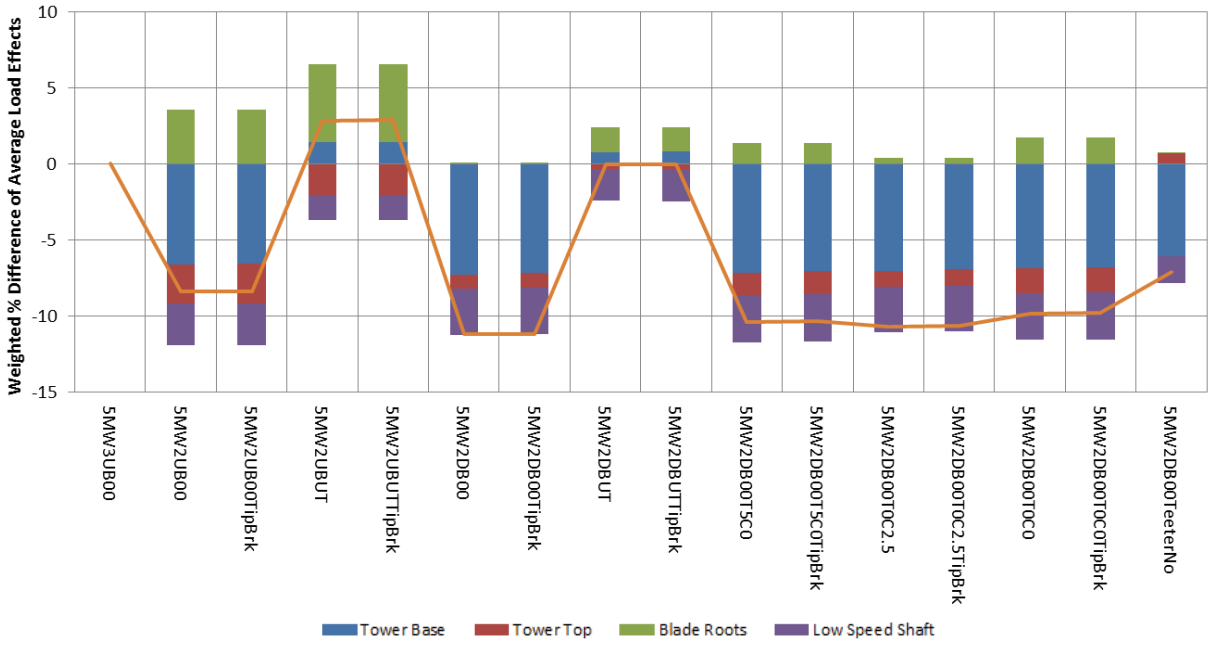

Figure A7.1. Weighted % difference of maximum of average load effects in normal operation conditions.

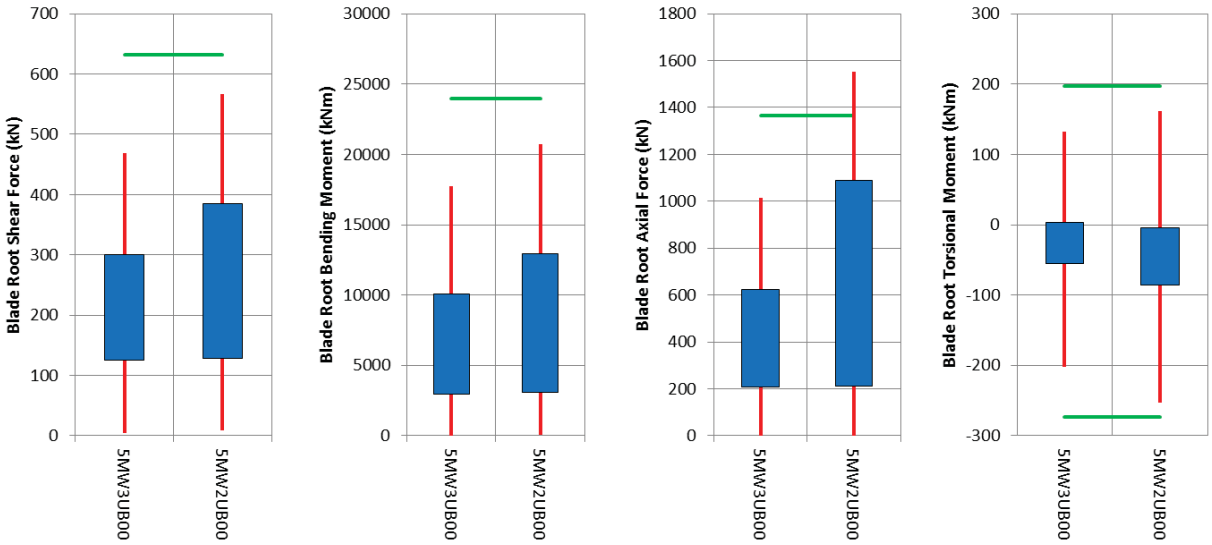

Figure A7.2. Blade root load effect comparisons for 3-bladed and 2-bladed configurations in normal operating conditions.

Appendix 8: Load Effect Results

The load effect results at the tower base, tower top, blade roots, LSS, and torques at LSS, HSS, and generator, in normal operating, fault, and parked conditions are listed in the tables below. Also, data for minimum tower-to-blade clearance, and maximum and minimum teeter angle in each condition are presented in following tables.

Table A8.1. Load effect result data at tower base in normal operating conditions.

Load Effects		Shear Force			Bending Moment			Axial Force			Torsional Moment		
		Value (kN)	DLC (-)	Vs (m/s)	Value (kN m)	DLC (-)	Vs (m/s)	Value (kN)	DLC (-)	Vs (m/s)	Value (kN m)	DLC (-)	Vs (m/s)
Model		5MW3UB00											
Maximums	Max	1181	DLC1.3	15.0	93942	DLC1.3	15.0	-5654	DLC1.3	25.0	5090	DLC1.4	13.4
	Min	1	DLC1.3	21.0	100	DLC1.3	25.0	-5836	DLC1.3	17.0	-9119	DLC1.4	11.4
Averages	Max	685	DLC1.5H	11.0	53934	DLC1.5V	11.0	-5730	DLC1.5H	25.0	827	DLC1.4	13.4
	Min	77	DLC1.3	3.0	4816	DLC1.3	3.0	-5788	DLC1.5V	11.0	-2625	DLC1.4	9.4
Model		5MW2UB00											
Maximums	Max	1405	DLC1.4	9.4	109496	DLC1.4	9.4	-5498	DLC1.3	25.0	4418	DLC1.4	13.4
	Min	1	DLC1.3	21.0	95	DLC1.3	25.0	-5679	DLC1.3	25.0	-7922	DLC1.4	11.4
Averages	Max	606	DLC1.5H	11.0	48577	DLC1.5V	11.0	-5556	DLC1.3	3.0	453	DLC1.4	13.4
	Min	61	DLC1.3	3.0	4595	DLC1.3	3.0	-5608	DLC1.3	11.0	-1802	DLC1.4	9.4
Model		5MW2IB00TipBrk											
Maximums	Max	1379	DLC1.4	9.4	107410	DLC1.4	9.4	-5500	DLC1.3	25.0	4437	DLC1.4	13.4
	Min	1	DLC1.3	21.0	80	DLC1.3	25.0	-5681	DLC1.3	25.0	-7951	DLC1.4	11.4
Averages	Max	607	DLC1.5H	11.0	48674	DLC1.5V	11.0	-5558	DLC1.5H	3.0	458	DLC1.4	13.4
	Min	61	DLC1.3	3.0	4578	DLC1.3	3.0	-5610	DLC1.3	11.0	-1771	DLC1.4	9.4
Model		5MW2UBUT											
Maximums	Max	1645	DLC1.4	11.4	128540	DLC1.4	9.4	-5468	DLC1.4	11.4	5153	DLC1.4	13.4
	Min	1	DLC1.3	25.0	57	DLC1.3	25.0	-5684	DLC1.3	13.0	-9773	DLC1.4	9.4
Averages	Max	696	DLC1.5V	11.0	55820	DLC1.5V	11.0	-5558	DLC1.3	3.0	497	DLC1.4	13.4
	Min	78	DLC1.3	3.0	5930	DLC1.3	3.0	-5615	DLC1.3	11.0	-2262	DLC1.4	9.4
Model		5MW2UBUTTipBrk											
Maximums	Max	1664	DLC1.4	11.4	129283	DLC1.4	9.4	-5476	DLC1.4	11.4	5148	DLC1.4	13.4
	Min	1	DLC1.3	23.0	98	DLC1.3	23.0	-5684	DLC1.3	15.0	-9729	DLC1.4	9.4
Averages	Max	696	DLC1.5V	11.0	55852	DLC1.5V	11.0	-5560	DLC1.5H	3.0	495	DLC1.4	13.4
	Min	78	DLC1.3	3.0	5917	DLC1.3	3.0	-5616	DLC1.3	11.0	-2261	DLC1.4	9.4
Model		5MW2DB00											
Maximums	Max	1495	DLC1.4	9.4	118349	DLC1.4	9.4	-5353	DLC1.4	9.4	5079	DLC1.3	25.0
	Min	1	DLC1.3	25.0	84	DLC1.3	21.0	-5718	DLC1.3	25.0	-9307	DLC1.4	11.4
Averages	Max	576	DLC1.5V	11.0	47465	DLC1.5V	11.0	-5514	DLC1.5H	11.0	1588	DLC1.3	25.0
	Min	59	DLC1.3	3.0	5374	DLC1.5H	3.0	-5551	DLC1.3	25.0	-2354	DLC1.4	9.4
Model		5MW2DB00TipBrk											
Maximums	Max	1469	DLC1.4	9.4	116337	DLC1.4	9.4	-5393	DLC1.4	11.4	5083	DLC1.3	25.0
	Min	1	DLC1.3	21.0	64	DLC1.4	11.4	-5720	DLC1.3	25.0	-9308	DLC1.4	11.4
Averages	Max	578	DLC1.5V	11.0	47619	DLC1.5V	11.0	-5516	DLC1.5H	11.0	1585	DLC1.3	25.0
	Min	59	DLC1.3	3.0	5374	DLC1.5H	3.0	-5552	DLC1.3	25.0	-2321	DLC1.4	9.4
Model		5MW2DBUT											
Maximums	Max	1831	DLC1.4	9.4	144619	DLC1.4	9.4	-5329	DLC1.4	11.4	4950	DLC1.3	25.0
	Min	0	DLC1.4	11.4	87	DLC1.3	23.0	-5710	DLC1.3	25.0	-12250	DLC1.4	11.4
Averages	Max	663	DLC1.5H	11.0	54675	DLC1.5V	11.0	-5510	DLC1.5H	11.0	1574	DLC1.3	25.0
	Min	77	DLC1.3	3.0	6821	DLC1.5H	3.0	-5550	DLC1.3	25.0	-2861	DLC1.4	9.4
Model		5MW2DBUTTipBrk											
Maximums	Max	1836	DLC1.4	9.4	145193	DLC1.4	9.4	-5287	DLC1.4	9.4	4936	DLC1.3	25.0
	Min	1	DLC1.3	23.0	54	DLC1.3	21.0	-5716	DLC1.3	25.0	-12250	DLC1.4	11.4
Averages	Max	664	DLC1.5H	11.0	54761	DLC1.5V	11.0	-5512	DLC1.5H	11.0	1569	DLC1.3	25.0
	Min	77	DLC1.3	3.0	6826	DLC1.5H	3.0	-5552	DLC1.3	25.0	-2847	DLC1.4	9.4
Model		5MW2DB00T5C0											
Maximums	Max	1400	DLC1.4	11.4	106981	DLC1.4	11.4	-5364	DLC1.4	9.4	4994	DLC1.3	25.0
	Min	1	DLC1.3	21.0	85	DLC1.3	25.0	-5724	DLC1.3	25.0	-8816	DLC1.4	11.4
Averages	Max	584	DLC1.5V	11.0	47828	DLC1.5V	11.0	-5513	DLC1.5H	11.0	1545	DLC1.3	25.0
	Min	59	DLC1.3	3.0	5083	DLC1.5H	3.0	-5549	DLC1.3	25.0	-2126	DLC1.4	9.4

Table A8.1. Load effect result data at tower base in normal operating conditions (continue).

Load Effects		Shear Force			Bending Moment			Axial Force			Torsional Moment		
		Value (kN)	DLC (-)	Vs (m/s)	Value (kN m)	DLC (-)	Vs (m/s)	Value (kN)	DLC (-)	Vs (m/s)	Value (kN m)	DLC (-)	Vs (m/s)
Model		5MW2DB00T5C0TipBrk											
Maximums	Max	1371	DLC1.4	11.4	104812	DLC1.4	11.4	-5416	DLC1.4	11.4	4992	DLC1.3	25.0
	Min	1	DLC1.3	25.0	83	DLC1.3	21.0	-5727	DLC1.3	25.0	-8790	DLC1.4	11.4
Averages	Max	585	DLC1.5V	11.0	47954	DLC1.5V	11.0	-5514	DLC1.5H	11.0	1542	DLC1.3	25.0
	Min	59	DLC1.3	3.0	5076	DLC1.5H	3.0	-5551	DLC1.3	3.0	-2100	DLC1.4	9.4
Model		5MW2DB00T0C2.5											
Maximums	Max	1492	DLC1.4	9.4	117768	DLC1.4	9.4	-5392	DLC1.4	9.4	4495	DLC1.3	25.0
	Min	1	DLC1.3	21.0	66	DLC1.3	21.0	-5714	DLC1.4	9.4	-9493	DLC1.4	11.4
Averages	Max	580	DLC1.5V	11.0	47584	DLC1.5V	11.0	-5545	DLC1.4	9.4	1026	DLC1.3	25.0
	Min	60	DLC1.3	3.0	5400	DLC1.3	3.0	-5568	DLC1.3	11.0	-2449	DLC1.4	9.4
Model		5MW2DB00T0C2.5TipBrk											
Maximums	Max	1467	DLC1.4	9.4	115986	DLC1.4	9.4	-5461	DLC1.4	11.4	4482	DLC1.3	25.0
	Min	1	DLC1.4	9.4	106	DLC1.3	25.0	-5716	DLC1.3	25.0	-9459	DLC1.4	11.4
Averages	Max	582	DLC1.5V	11.0	47736	DLC1.5V	11.0	-5547	DLC1.4	9.4	1022	DLC1.3	25.0
	Min	60	DLC1.3	3.0	5407	DLC1.3	3.0	-5569	DLC1.3	11.0	-2417	DLC1.4	9.4
Model		5MW2DB00T0C0											
Maximums	Max	1399	DLC1.4	11.4	106416	DLC1.4	11.4	-5412	DLC1.4	9.4	4515	DLC1.3	25.0
	Min	1	DLC1.4	9.4	72	DLC1.3	25.0	-5720	DLC1.3	25.0	-8972	DLC1.4	9.4
Averages	Max	588	DLC1.5V	11.0	47974	DLC1.5V	11.0	-5546	DLC1.4	9.4	1023	DLC1.3	25.0
	Min	60	DLC1.3	3.0	5092	DLC1.3	3.0	-5568	DLC1.4	13.4	-2199	DLC1.4	9.4
Model		5MW2DB00T0C0TipBrk											
Maximums	Max	1365	DLC1.4	11.4	103507	DLC1.4	11.4	-5471	DLC1.3	25.0	4502	DLC1.3	25.0
	Min	1	DLC1.3	19.0	54	DLC1.3	25.0	-5725	DLC1.3	25.0	-8869	DLC1.4	11.4
Averages	Max	590	DLC1.5V	11.0	48105	DLC1.5V	11.0	-5548	DLC1.4	9.4	1019	DLC1.3	25.0
	Min	60	DLC1.3	3.0	5094	DLC1.3	3.0	-5570	DLC1.4	13.4	-2173	DLC1.4	9.4
Model		5MW2DB00TeeterNo											
Maximums	Max	1412	DLC1.4	11.4	110809	DLC1.4	9.4	-5390	DLC1.4	11.4	7188	DLC1.3	25.0
	Min	1	DLC1.3	19.0	95	DLC1.3	21.0	-5686	DLC1.3	25.0	-13790	DLC1.4	11.4
Averages	Max	577	DLC1.5V	11.0	47891	DLC1.5V	11.0	-5512	DLC1.4	11.4	1595	DLC1.3	25.0
	Min	59	DLC1.3	3.0	5403	DLC1.5H	3.0	-5552	DLC1.3	25.0	-3114	DLC1.4	11.4
Model		5MW2UBUTT2C0TipBrk											
Maximums	Max	1570	DLC1.4	9.4	123959	DLC1.4	9.4	-5347	DLC1.4	9.4	4972	DLC1.4	13.4
	Min	1	DLC1.3	25.0	97	DLC1.3	23.0	-5723	DLC1.3	25.0	-11540	DLC1.4	11.4
Averages	Max	678	DLC1.5H	11.0	55393	DLC1.5V	11.0	-5534	DLC1.4	9.4	1217	DLC1.3	25.0
	Min	77	DLC1.3	3.0	6558	DLC1.3	3.0	-5560	DLC1.3	25.0	-2667	DLC1.4	9.4

Table A8.2. Load effect result data at tower base in fault conditions.

Load Effects		Shear Force			Bending Moment			Axial Force			Torsional Moment		
		Value (kN)	DLC (-)	Vs (m/s)	Value (kN m)	DLC (-)	Vs (m/s)	Value (kN)	DLC (-)	Vs (m/s)	Value (kN m)	DLC (-)	Vs (m/s)
Model		5MW3UB00											
Maximums	Max	1386	DLC2.3	25.0	111495	DLC2.3	25.0	-5526	DLC2.1P	25.0	7782	DLC2.1P	11.4
	Min	0	DLC2.3	11.4	38	DLC2.3	9.4	-5828	DLC2.3	11.4	-8876	DLC2.1P	25.0
Averages	Max	392	DLC2.3	25.0	30759	DLC2.3	25.0	-5671	DLC2.1P	25.0	27	DLC2.1G	11.4
	Min	222	DLC2.1P	11.4	17788	DLC2.1P	11.4	-5737	DLC2.1P	11.4	-1868	DLC2.1P	25.0
Model		5MW2UB00											
Maximums	Max	1498	DLC2.3	25.0	115128	DLC2.3	25.0	-5211	DLC2.1P	25.0	10261	DLC2.1P	11.4
	Min	0	DLC2.3	11.4	40	DLC2.3	25.0	-5750	DLC2.1P	25.0	-17278	DLC2.1P	25.0
Averages	Max	347	DLC2.3	13.4	27228	DLC2.3	13.4	-5552	DLC2.1G	25.0	1576	DLC2.1P	25.0
	Min	192	DLC2.1G	11.4	15465	DLC2.1G	11.4	-5596	DLC2.1P	25.0	-238	DLC2.3	25.0
Model		5MW2IB00TipBrk											
Maximums	Max	1443	DLC2.3	25.0	112975	DLC2.3	25.0	-5425	DLC2.1P	25.0	3685	DLC2.1P	25.0
	Min	0	DLC2.3	11.4	3	DLC2.3	11.4	-5686	DLC2.3	25.0	-4323	DLC2.1P	25.0
Averages	Max	284	DLC2.3	11.4	22503	DLC2.3	11.4	-5539	DLC2.3	25.0	568	DLC2.1P	25.0
	Min	139	DLC2.3	9.4	11004	DLC2.3	9.4	-5583	DLC2.1P	25.0	-878	DLC2.1P	25.0
Model		5MW2UBUT											
Maximums	Max	1451	DLC2.3	25.0	112531	DLC2.3	25.0	-5305	DLC2.1P	25.0	9993	DLC2.1P	11.4
	Min	0	DLC2.3	13.4	12	DLC2.3	13.4	-5761	DLC2.1P	25.0	-11310	DLC2.1P	25.0
Averages	Max	332	DLC2.3	25.0	26145	DLC2.3	25.0	-5523	DLC2.3	25.0	207	DLC2.1P	25.0
	Min	203	DLC2.3	9.4	16188	DLC2.3	9.4	-5571	DLC2.3	11.4	-160	DLC2.3	13.4

Table A8.2. Load effect result data at tower base in fault conditions (continue).

Load Effects		Shear Force			Bending Moment			Axial Force			Torsional Moment		
		Value (kN)	DLC (-)	Vs (m/s)	Value (kN m)	DLC (-)	Vs (m/s)	Value (kN)	DLC (-)	Vs (m/s)	Value (kN m)	DLC (-)	Vs (m/s)
Model		5MW2UBUTTipBrk											
Maximums	Max	1179	DLC2.3	11.4	93868	DLC2.3	11.4	-5413	DLC2.1G	25.0	4462	DLC2.1P	25.0
	Min	0	DLC2.3	11.4	2	DLC2.3	9.4	-5693	DLC2.1P	25.0	-4402	DLC2.1P	25.0
Averages	Max	281	DLC2.3	11.4	22415	DLC2.3	11.4	-5538	DLC2.3	25.0	677	DLC2.1P	25.0
	Min	165	DLC2.3	9.4	13078	DLC2.3	9.4	-5584	DLC2.1P	25.0	-1129	DLC2.1P	25.0
Model		5MW2DB00											
Maximums	Max	1380	DLC2.3	25.0	110466	DLC2.3	25.0	-5291	DLC2.1P	25.0	9330	DLC2.1P	11.4
	Min	1	DLC2.3	13.4	37	DLC2.3	13.4	-5745	DLC2.1P	25.0	-13638	DLC2.1P	25.0
Averages	Max	309	DLC2.3	13.4	24630	DLC2.3	13.4	-5544	DLC2.3	11.4	2431	DLC2.1P	25.0
	Min	177	DLC2.3	9.4	14527	DLC2.3	9.4	-5610	DLC2.1P	25.0	142	DLC2.3	9.4
Model		5MW2DB00TipBrk											
Maximums	Max	1466	DLC2.3	25.0	118227	DLC2.3	25.0	-5409	DLC2.3	25.0	4938	DLC2.1P	25.0
	Min	0	DLC2.3	9.4	4	DLC2.3	9.4	-5718	DLC2.1G	25.0	-6259	DLC2.1G	25.0
Averages	Max	262	DLC2.1P	25.0	22606	DLC2.1P	25.0	-5535	DLC2.1P	25.0	1446	DLC2.1P	25.0
	Min	144	DLC2.3	9.4	11914	DLC2.3	9.4	-5570	DLC2.3	25.0	-92	DLC2.1P	25.0
Model		5MW2DBUT											
Maximums	Max	1517	DLC2.3	25.0	116346	DLC2.3	25.0	-5326	DLC2.1P	25.0	13267	DLC2.1P	25.0
	Min	1	DLC2.3	13.4	28	DLC2.1G	11.4	-5812	DLC2.1P	25.0	-10665	DLC2.1P	11.4
Averages	Max	301	DLC2.3	11.4	24412	DLC2.3	11.4	-5543	DLC2.3	13.4	489	DLC2.1G	25.0
	Min	192	DLC2.3	9.4	15719	DLC2.3	9.4	-5585	DLC2.3	25.0	166	DLC2.3	9.4
Model		5MW2DBUTTipBrk											
Maximums	Max	1178	DLC2.3	11.4	93647	DLC2.3	11.4	-5370	DLC2.3	9.4	4942	DLC2.1P	25.0
	Min	0	DLC2.3	13.4	2	DLC2.3	9.4	-5717	DLC2.1G	25.0	-5721	DLC2.1G	25.0
Averages	Max	295	DLC2.3	11.4	24059	DLC2.3	11.4	-5537	DLC2.3	11.4	1539	DLC2.1P	25.0
	Min	156	DLC2.3	9.4	13032	DLC2.3	9.4	-5570	DLC2.1G	25.0	-39	DLC2.1P	25.0
Model		5MW2DB00T5C0											
Maximums	Max	1405	DLC2.3	25.0	112574	DLC2.3	25.0	-5281	DLC2.1P	25.0	9394	DLC2.1P	11.4
	Min	0	DLC2.3	25.0	9	DLC2.3	9.4	-5744	DLC2.1P	25.0	-13635	DLC2.1P	25.0
Averages	Max	318	DLC2.3	13.4	25220	DLC2.3	13.4	-5541	DLC2.3	11.4	2456	DLC2.1P	25.0
	Min	183	DLC2.3	9.4	14849	DLC2.3	9.4	-5609	DLC2.1P	25.0	120	DLC2.3	9.4
Model		5MW2DB00T5C0TipBrk											
Maximums	Max	1488	DLC2.3	25.0	119434	DLC2.3	25.0	-5411	DLC2.3	25.0	4592	DLC2.1P	25.0
	Min	0	DLC2.3	9.4	4	DLC2.3	9.4	-5720	DLC2.1G	25.0	-6266	DLC2.1G	25.0
Averages	Max	259	DLC2.1P	25.0	22240	DLC2.1P	25.0	-5536	DLC2.1P	25.0	1310	DLC2.1P	25.0
	Min	140	DLC2.3	9.4	11432	DLC2.3	9.4	-5570	DLC2.3	25.0	-120	DLC2.1P	25.0
Model		5MW2DB00T0C2.5											
Maximums	Max	1416	DLC2.3	25.0	111228	DLC2.3	25.0	-5268	DLC2.1P	25.0	9325	DLC2.1P	11.4
	Min	0	DLC2.3	9.4	16	DLC2.3	9.4	-5742	DLC2.1P	25.0	-15583	DLC2.1P	25.0
Averages	Max	326	DLC2.3	13.4	25890	DLC2.3	13.4	-5554	DLC2.3	9.4	2194	DLC2.1P	25.0
	Min	180	DLC2.3	9.4	14663	DLC2.3	9.4	-5606	DLC2.1P	25.0	66	DLC2.3	9.4
Model		5MW2DB00T0C2.5TipBrk											
Maximums	Max	1491	DLC2.3	25.0	117709	DLC2.3	25.0	-5437	DLC2.1P	25.0	4293	DLC2.1P	25.0
	Min	0	DLC2.3	13.4	4	DLC2.3	13.4	-5691	DLC2.1P	25.0	-4795	DLC2.1P	25.0
Averages	Max	258	DLC2.1P	25.0	21970	DLC2.1P	25.0	-5547	DLC2.1P	25.0	795	DLC2.1P	25.0
	Min	136	DLC2.3	9.4	11398	DLC2.3	9.4	-5573	DLC2.1P	25.0	-320	DLC2.1P	25.0
Model		5MW2DB00T0C0											
Maximums	Max	1438	DLC2.3	25.0	113130	DLC2.3	25.0	-5259	DLC2.1P	25.0	9355	DLC2.1P	11.4
	Min	0	DLC2.3	11.4	39	DLC2.3	11.4	-5742	DLC2.1P	25.0	-15555	DLC2.1P	25.0
Averages	Max	338	DLC2.3	13.4	26757	DLC2.3	13.4	-5553	DLC2.3	9.4	2225	DLC2.1P	25.0
	Min	188	DLC2.3	9.4	15248	DLC2.3	9.4	-5606	DLC2.1P	25.0	52	DLC2.3	9.4
Model		5MW2DB00T0C0TipBrk											
Maximums	Max	1509	DLC2.3	25.0	118812	DLC2.3	25.0	-5436	DLC2.1P	25.0	4274	DLC2.1P	25.0
	Min	0	DLC2.3	9.4	1	DLC2.3	9.4	-5694	DLC2.1P	25.0	-4614	DLC2.1P	25.0
Averages	Max	260	DLC2.3	11.4	22030	DLC2.1P	25.0	-5546	DLC2.1P	25.0	658	DLC2.1P	25.0
	Min	137	DLC2.3	9.4	11143	DLC2.3	9.4	-5570	DLC2.1P	25.0	-320	DLC2.1P	25.0
Model		5MW2DB00TeeterNo											
Maximums	Max	1407	DLC2.3	25.0	112319	DLC2.3	25.0	-5248	DLC2.1P	25.0	11714	DLC2.1P	25.0
	Min	0	DLC2.3	9.4	55	DLC2.3	9.4	-5751	DLC2.1P	25.0	-15572	DLC2.1P	25.0
Averages	Max	449	DLC2.3	25.0	35761	DLC2.3	25.0	-5543	DLC2.3	11.4	2464	DLC2.1P	25.0
	Min	202	DLC2.1G	11.4	16728	DLC2.1G	11.4	-5610	DLC2.1P	25.0	85	DLC2.3	9.4

Table A8.2. Load effect result data at tower base in fault conditions (continue).

Load Effects		Shear Force			Bending Moment			Axial Force			Torsional Moment		
		Value (kN)	DLC (-)	Vs (m/s)	Value (kN m)	DLC (-)	Vs (m/s)	Value (kN)	DLC (-)	Vs (m/s)	Value (kN m)	DLC (-)	Vs (m/s)
Model		5MW2UBUTT2C0TipBrk											
Maximums	Max	1201	DLC2.3	11.4	95078	DLC2.3	11.4	-5401	DLC2.3	9.4	4446	DLC2.1P	25.0
	Min	0	DLC2.3	9.4	1	DLC2.3	13.4	-5719	DLC2.3	9.4	-4450	DLC2.1G	25.0
Averages	Max	309	DLC2.3	11.4	24915	DLC2.3	11.4	-5540	DLC2.1P	25.0	1170	DLC2.1P	25.0
	Min	161	DLC2.3	25.0	13191	DLC2.3	9.4	-5576	DLC2.1P	25.0	-393	DLC2.1P	25.0

Table A8.3. Load effect result data at tower base in parked conditions.

Load Effects		Shear Force			Bending Moment			Axial Force			Torsional Moment		
		Value (kN)	DLC (-)	Vs (m/s)	Value (kN m)	DLC (-)	Vs (m/s)	Value (kN)	DLC (-)	Vs (m/s)	Value (kN m)	DLC (-)	Vs (m/s)
Model		5MW3UB00											
Maximums	Max	877	DLC6.2a	37.4	67766	DLC6.2a	37.4	-5636	DLC6.1a	37.4	3901	DLC7.1a	25.0
	Min	0	DLC6.2a	37.4	41	DLC6.2a	37.4	-5758	DLC6.2a	37.4	-4250	DLC6.2a	37.4
Averages	Max	342	DLC6.2a	37.4	28359	DLC6.2a	37.4	-5636	DLC6.1a	37.4	3800	DLC7.1a	25.0
	Min	24	DLC6.3a	25.0	959	DLC6.3a	25.0	-5756	DLC7.1a	25.0	-1989	DLC6.2a	37.4
Model		5MW2UB00											
Maximums	Max	539	DLC6.2a	37.4	41614	DLC6.2a	37.4	-5429	DLC6.2a	37.4	3354	DLC7.1a	25.0
	Min	0	DLC6.2a	37.4	6	DLC6.2a	37.4	-5583	DLC6.2a	37.4	-186	DLC6.2a	37.4
Averages	Max	181	DLC6.2a	37.4	13970	DLC6.2a	37.4	-5431	DLC6.2a	37.4	3265	DLC7.1a	25.0
	Min	8	DLC6.2a	37.4	658	DLC6.2a	37.4	-5568	DLC7.1a	25.0	-51	DLC6.2a	37.4
Model		5MW2IB00TipBrk											
Maximums	Max	581	DLC6.2a	37.4	44334	DLC6.2a	37.4	-5431	DLC6.2a	37.4	3352	DLC7.1a	25.0
	Min	0	DLC6.2a	37.4	2	DLC6.2a	37.4	-5584	DLC6.2a	37.4	-184	DLC6.2a	37.4
Averages	Max	179	DLC6.2a	37.4	13886	DLC6.2a	37.4	-5432	DLC6.2a	37.4	3262	DLC7.1a	25.0
	Min	8	DLC6.2a	37.4	683	DLC6.2a	37.4	-5569	DLC7.1a	25.0	-52	DLC6.2a	37.4
Model		5MW2UBUT											
Maximums	Max	611	DLC6.2a	37.4	46547	DLC6.2a	37.4	-5422	DLC6.2a	37.4	3368	DLC7.1a	25.0
	Min	0	DLC6.2a	37.4	2	DLC6.2a	37.4	-5585	DLC6.2a	37.4	-150	DLC6.2a	37.4
Averages	Max	189	DLC6.2a	37.4	14629	DLC6.2a	37.4	-5423	DLC6.2a	37.4	3274	DLC7.1a	25.0
	Min	8	DLC6.2a	37.4	679	DLC6.2a	37.4	-5560	DLC6.2a	37.4	-37	DLC6.2a	37.4
Model		5MW2UBUTTipBrk											
Maximums	Max	619	DLC6.2a	37.4	47130	DLC6.2a	37.4	-5423	DLC6.2a	37.4	3368	DLC7.1a	25.0
	Min	0	DLC6.2a	37.4	1	DLC6.2a	37.4	-5587	DLC6.2a	37.4	-151	DLC6.2a	37.4
Averages	Max	187	DLC6.2a	37.4	14537	DLC6.2a	37.4	-5424	DLC6.2a	37.4	3274	DLC7.1a	25.0
	Min	9	DLC6.2a	37.4	709	DLC6.2a	37.4	-5561	DLC6.2a	37.4	-38	DLC6.2a	37.4
Model		5MW2DB00											
Maximums	Max	596	DLC6.2a	37.4	45467	DLC6.2a	37.4	-5519	DLC6.2a	37.4	3565	DLC7.1a	25.0
	Min	0	DLC6.2a	37.4	2	DLC6.2a	37.4	-5671	DLC6.2a	37.4	-153	DLC6.2a	37.4
Averages	Max	228	DLC6.2a	37.4	17594	DLC6.2a	37.4	-5544	DLC6.2a	37.4	3280	DLC7.1a	25.0
	Min	4	DLC6.2a	37.4	462	DLC6.2a	37.4	-5669	DLC6.2a	37.4	-118	DLC6.1a	37.4
Model		5MW2DB00TipBrk											
Maximums	Max	637	DLC6.2a	37.4	48102	DLC6.2a	37.4	-5522	DLC6.2a	37.4	3542	DLC7.1a	25.0
	Min	0	DLC6.2a	37.4	6	DLC6.2a	37.4	-5672	DLC6.2a	37.4	-162	DLC6.2a	37.4
Averages	Max	228	DLC6.2a	37.4	17644	DLC6.2a	37.4	-5545	DLC6.2a	37.4	3278	DLC7.1a	25.0
	Min	5	DLC6.2a	37.4	494	DLC6.2a	37.4	-5671	DLC6.2a	37.4	-118	DLC6.1a	37.4
Model		5MW2DBUT											
Maximums	Max	704	DLC6.2a	37.4	53004	DLC6.2a	37.4	-5514	DLC7.1a	25.0	3579	DLC7.1a	25.0
	Min	0	DLC6.2a	37.4	3	DLC6.2a	37.4	-5678	DLC6.2a	37.4	-157	DLC6.2a	37.4
Averages	Max	255	DLC6.2a	37.4	19632	DLC6.2a	37.4	-5545	DLC6.2a	37.4	3292	DLC7.1a	25.0
	Min	4	DLC6.2a	37.4	438	DLC6.2a	37.4	-5676	DLC6.1a	37.4	-96	DLC6.2a	37.4
Model		5MW2DBUTTipBrk											
Maximums	Max	714	DLC6.2a	37.4	53672	DLC6.2a	37.4	-5517	DLC6.2a	37.4	3579	DLC7.1a	25.0
	Min	0	DLC6.2a	37.4	1	DLC6.2a	37.4	-5680	DLC6.1a	37.4	-148	DLC6.2a	37.4
Averages	Max	255	DLC6.2a	37.4	19728	DLC6.2a	37.4	-5546	DLC6.2a	37.4	3290	DLC7.1a	25.0
	Min	4	DLC6.2a	37.4	461	DLC6.2a	37.4	-5679	DLC6.1a	37.4	-99	DLC6.2a	37.4
Model		5MW2DB00T5C0											
Maximums	Max	594	DLC6.2a	37.4	45672	DLC6.2a	37.4	-5517	DLC6.2a	37.4	3532	DLC7.1a	25.0
	Min	0	DLC6.2a	37.4	2	DLC6.2a	37.4	-5673	DLC6.2a	37.4	-172	DLC6.2a	37.4
Averages	Max	229	DLC6.2a	37.4	17664	DLC6.2a	37.4	-5544	DLC6.2a	37.4	3252	DLC7.1a	25.0
	Min	5	DLC6.2a	37.4	359	DLC6.2a	37.4	-5672	DLC6.2a	37.4	-134	DLC6.2a	37.4

Table A8.3. Load effect result data at tower base in parked conditions (continue).

Load Effects		Shear Force			Bending Moment			Axial Force			Torsional Moment		
		Value (kN)	DLC (-)	Vs (m/s)	Value (kN m)	DLC (-)	Vs (m/s)	Value (kN)	DLC (-)	Vs (m/s)	Value (kN m)	DLC (-)	Vs (m/s)
Model		5MW2DB00T5C0TipBrk											
Maximums	Max	640	DLC6.2a	37.4	48636	DLC6.2a	37.4	-5512	DLC6.2a	37.4	3506	DLC7.1a	25.0
	Min	0	DLC6.2a	37.4	1	DLC6.2a	37.4	-5675	DLC6.2a	37.4	-194	DLC6.2a	37.4
Averages	Max	230	DLC6.2a	37.4	17751	DLC6.2a	37.4	-5545	DLC6.2a	37.4	3250	DLC7.1a	25.0
	Min	5	DLC6.2a	37.4	390	DLC6.2a	37.4	-5673	DLC6.2a	37.4	-133	DLC6.2a	37.4
Model		5MW2DB00T0C2.5											
Maximums	Max	668	DLC6.2a	37.4	50814	DLC6.2a	37.4	-5534	DLC6.2a	37.4	3411	DLC7.1a	25.0
	Min	0	DLC6.2a	37.4	2	DLC6.2a	37.4	-5586	DLC7.1a	25.0	-236	DLC6.2a	37.4
Averages	Max	264	DLC6.2a	37.4	20312	DLC6.2a	37.4	-5548	DLC6.2a	37.4	3310	DLC7.1a	25.0
	Min	3	DLC6.2a	37.4	458	DLC6.2a	37.4	-5585	DLC7.1a	25.0	-41	DLC6.2a	37.4
Model		5MW2DB00T0C2.5TipBrk											
Maximums	Max	746	DLC6.2a	37.4	55724	DLC6.2a	37.4	-5532	DLC6.2a	37.4	3419	DLC7.1a	25.0
	Min	0	DLC6.3a	25.0	1	DLC6.2a	37.4	-5588	DLC7.1a	25.0	-261	DLC6.2a	37.4
Averages	Max	267	DLC6.2a	37.4	20533	DLC6.2a	37.4	-5551	DLC6.2a	37.4	3311	DLC7.1a	25.0
	Min	4	DLC6.2a	37.4	489	DLC6.2a	37.4	-5588	DLC7.1a	25.0	-41	DLC6.2a	37.4
Model		5MW2DB00T0C0											
Maximums	Max	665	DLC6.2a	37.4	51096	DLC6.2a	37.4	-5523	DLC6.2a	37.4	3370	DLC7.1a	25.0
	Min	0	DLC6.2a	37.4	5	DLC6.2a	37.4	-5587	DLC7.1a	25.0	-223	DLC6.2a	37.4
Averages	Max	266	DLC6.2a	37.4	20507	DLC6.2a	37.4	-5549	DLC6.2a	37.4	3283	DLC7.1a	25.0
	Min	4	DLC6.2a	37.4	293	DLC6.2a	37.4	-5585	DLC7.1a	25.0	-26	DLC6.2a	37.4
Model		5MW2DB00T0C0TipBrk											
Maximums	Max	740	DLC6.2a	37.4	56083	DLC6.2a	37.4	-5521	DLC6.2a	37.4	3377	DLC7.1a	25.0
	Min	0	DLC6.2a	37.4	2	DLC6.2a	37.4	-5589	DLC7.1a	25.0	-247	DLC6.2a	37.4
Averages	Max	270	DLC6.2a	37.4	20790	DLC6.2a	37.4	-5552	DLC6.2a	37.4	3284	DLC7.1a	25.0
	Min	4	DLC6.2a	37.4	318	DLC6.2a	37.4	-5588	DLC7.1a	25.0	-26	DLC6.2a	37.4
Model		5MW2DB00TeeterNo											
Maximums	Max	602	DLC6.2a	37.4	45857	DLC6.2a	37.4	-5517	DLC6.2a	37.4	3749	DLC7.1a	25.0
	Min	0	DLC6.3a	25.0	2	DLC6.2a	37.4	-5670	DLC6.2a	37.4	-1634	DLC6.2a	37.4
Averages	Max	231	DLC6.2a	37.4	17786	DLC6.2a	37.4	-5544	DLC6.2a	37.4	3262	DLC7.1a	25.0
	Min	5	DLC6.2a	37.4	481	DLC6.2a	37.4	-5669	DLC6.2a	37.4	-118	DLC6.1a	37.4
Model		5MW2UBUTT2C0TipBrk											
Maximums	Max	790	DLC6.2a	37.4	59767	DLC6.2a	37.4	-5518	DLC6.2a	37.4	3360	DLC7.1a	25.0
	Min	0	DLC6.3a	25.0	3	DLC6.2a	37.4	-5606	DLC6.1a	37.4	-132	DLC6.2a	37.4
Averages	Max	283	DLC6.2a	37.4	21878	DLC6.2a	37.4	-5550	DLC6.2a	37.4	3258	DLC7.1a	25.0
	Min	5	DLC6.2a	37.4	372	DLC6.2a	37.4	-5605	DLC6.1a	37.4	-46	DLC6.2a	37.4

Table A8.4. Load effect result data at tower top in normal operating conditions.

Load Effects		Shear Force			Bending Moment			Axial Force			Torsional Moment		
		Value (kN)	DLC (-)	Vs (m/s)	Value (kN m)	DLC (-)	Vs (m/s)	Value (kN)	DLC (-)	Vs (m/s)	Value (kN m)	DLC (-)	Vs (m/s)
Model		5MW3UB00											
Maximums	Max	1181	DLC1.3	15.0	10492	DLC1.4	11.4	-3359	DLC1.3	25.0	5090	DLC1.4	13.4
	Min	1	DLC1.3	23.0	17	DLC1.5V	3.0	-3531	DLC1.3	17.0	-9119	DLC1.4	11.4
Averages	Max	712	DLC1.5V	11.0	5180	DLC1.4	13.4	-3436	DLC1.5H	25.0	828	DLC1.4	13.4
	Min	78	DLC1.3	3.0	997	DLC1.3	5.0	-3489	DLC1.5V	11.0	-2625	DLC1.4	9.4
Model		5MW2UB00											
Maximums	Max	1269	DLC1.4	9.4	8068	DLC1.4	9.4	-3204	DLC1.3	25.0	4418	DLC1.4	13.4
	Min	1	DLC1.3	25.0	8	DLC1.3	3.0	-3381	DLC1.3	25.0	-7922	DLC1.4	11.4
Averages	Max	629	DLC1.5H	11.0	3768	DLC1.4	13.4	-3263	DLC1.5H	3.0	453	DLC1.4	13.4
	Min	63	DLC1.3	3.0	213	DLC1.3	3.0	-3311	DLC1.3	11.0	-1802	DLC1.4	9.4
Model		5MW2IB00TipBrk											
Maximums	Max	1246	DLC1.4	9.4	7952	DLC1.4	9.4	-3207	DLC1.3	25.0	4437	DLC1.4	13.4
	Min	1	DLC1.3	21.0	10	DLC1.5H	3.0	-3384	DLC1.3	25.0	-7951	DLC1.4	11.4
Averages	Max	630	DLC1.5H	11.0	3750	DLC1.4	13.4	-3265	DLC1.3	3.0	458	DLC1.4	13.4
	Min	62	DLC1.3	3.0	221	DLC1.3	3.0	-3312	DLC1.3	11.0	-1771	DLC1.4	9.4
Model		5MW2UBUT											
Maximums	Max	1513	DLC1.4	11.4	7718	DLC1.4	11.4	-3169	DLC1.4	11.4	5153	DLC1.4	13.4
	Min	1	DLC1.3	21.0	3	DLC1.3	3.0	-3383	DLC1.3	25.0	-9773	DLC1.4	9.4
Averages	Max	722	DLC1.5V	11.0	3725	DLC1.4	13.4	-3265	DLC1.3	3.0	497	DLC1.4	13.4
	Min	80	DLC1.3	3.0	238	DLC1.3	3.0	-3316	DLC1.3	11.0	-2262	DLC1.4	9.4

Table A8.4. Load effect result data at tower top in normal operating conditions (continue).

Load Effects		Shear Force			Bending Moment			Axial Force			Torsional Moment		
		Value (kN)	DLC (-)	Vs (m/s)	Value (kN m)	DLC (-)	Vs (m/s)	Value (kN)	DLC (-)	Vs (m/s)	Value (kN m)	DLC (-)	Vs (m/s)
Model		5MW2UBUTTipBrk											
Maximums	Max	1528	DLC1.4	11.4	7811	DLC1.4	11.4	-3179	DLC1.4	11.4	5148	DLC1.4	13.4
	Min	1	DLC1.3	21.0	3	DLC1.3	3.0	-3385	DLC1.3	25.0	-9729	DLC1.4	9.4
Averages	Max	723	DLC1.5V	11.0	3720	DLC1.4	13.4	-3266	DLC1.3	3.0	496	DLC1.4	13.4
	Min	80	DLC1.3	3.0	246	DLC1.3	3.0	-3318	DLC1.3	11.0	-2261	DLC1.4	9.4
Model		5MW2DB00											
Maximums	Max	1344	DLC1.4	9.4	9830	DLC1.4	9.4	-3054	DLC1.4	9.4	5079	DLC1.3	25.0
	Min	0	DLC1.4	13.4	155	DLC1.5H	3.0	-3424	DLC1.3	25.0	-9307	DLC1.4	11.4
Averages	Max	598	DLC1.5V	11.0	4881	DLC1.4	11.4	-3216	DLC1.5H	11.0	1588	DLC1.3	25.0
	Min	62	DLC1.3	3.0	641	DLC1.5H	3.0	-3255	DLC1.3	25.0	-2354	DLC1.4	9.4
Model		5MW2DB00TipBrk											
Maximums	Max	1323	DLC1.4	9.4	9572	DLC1.4	9.4	-3096	DLC1.4	11.4	5083	DLC1.3	25.0
	Min	1	DLC1.3	23.0	154	DLC1.5H	3.0	-3426	DLC1.3	25.0	-9307	DLC1.4	11.4
Averages	Max	600	DLC1.5V	11.0	4860	DLC1.4	11.4	-3218	DLC1.5H	11.0	1585	DLC1.3	25.0
	Min	62	DLC1.3	3.0	653	DLC1.5H	3.0	-3257	DLC1.3	25.0	-2321	DLC1.4	9.4
Model		5MW2DBUT											
Maximums	Max	1644	DLC1.4	9.4	9570	DLC1.4	9.4	-3028	DLC1.4	11.4	4950	DLC1.3	25.0
	Min	1	DLC1.3	21.0	179	DLC1.3	3.0	-3416	DLC1.3	25.0	-12250	DLC1.4	11.4
Averages	Max	689	DLC1.5H	11.0	4870	DLC1.4	11.4	-3211	DLC1.5H	11.0	1574	DLC1.3	25.0
	Min	80	DLC1.3	3.0	734	DLC1.5H	3.0	-3255	DLC1.3	25.0	-2861	DLC1.4	9.4
Model		5MW2DBUTTipBrk											
Maximums	Max	1651	DLC1.4	9.4	9609	DLC1.4	9.4	-2990	DLC1.4	9.4	4936	DLC1.3	25.0
	Min	1	DLC1.3	21.0	193	DLC1.5H	3.0	-3421	DLC1.3	25.0	-12250	DLC1.4	11.4
Averages	Max	690	DLC1.5H	11.0	4864	DLC1.4	11.4	-3212	DLC1.5H	11.0	1569	DLC1.3	25.0
	Min	80	DLC1.3	3.0	746	DLC1.5H	3.0	-3257	DLC1.3	25.0	-2847	DLC1.4	9.4
Model		5MW2DB00T5C0											
Maximums	Max	1295	DLC1.4	11.4	9182	DLC1.4	9.4	-3065	DLC1.4	9.4	4994	DLC1.3	25.0
	Min	1	DLC1.3	23.0	54	DLC1.3	3.0	-3430	DLC1.3	25.0	-8816	DLC1.4	11.4
Averages	Max	606	DLC1.5V	11.0	4587	DLC1.4	11.4	-3215	DLC1.5H	11.0	1545	DLC1.3	25.0
	Min	62	DLC1.3	3.0	330	DLC1.5H	3.0	-3254	DLC1.3	25.0	-2126	DLC1.4	9.4
Model		5MW2DB00T5C0TipBrk											
Maximums	Max	1272	DLC1.4	11.4	9018	DLC1.4	9.4	-3116	DLC1.4	11.4	4992	DLC1.3	25.0
	Min	1	DLC1.3	25.0	58	DLC1.3	3.0	-3433	DLC1.3	25.0	-8790	DLC1.4	11.4
Averages	Max	608	DLC1.5V	11.0	4567	DLC1.4	11.4	-3216	DLC1.5H	11.0	1542	DLC1.3	25.0
	Min	62	DLC1.3	3.0	337	DLC1.5H	3.0	-3255	DLC1.3	25.0	-2100	DLC1.4	9.4
Model		5MW2DB00T0C2.5											
Maximums	Max	1344	DLC1.4	9.4	9828	DLC1.4	9.4	-3093	DLC1.4	9.4	4495	DLC1.3	25.0
	Min	1	DLC1.3	25.0	77	DLC1.5H	3.0	-3418	DLC1.3	25.0	-9493	DLC1.4	11.4
Averages	Max	603	DLC1.5H	11.0	4672	DLC1.4	13.4	-3249	DLC1.4	9.4	1026	DLC1.3	25.0
	Min	62	DLC1.3	3.0	592	DLC1.5H	3.0	-3272	DLC1.4	13.4	-2449	DLC1.4	9.4
Model		5MW2DB00T0C2.5TipBrk											
Maximums	Max	1323	DLC1.4	9.4	9434	DLC1.4	9.4	-3164	DLC1.4	11.4	4482	DLC1.3	25.0
	Min	1	DLC1.3	25.0	96	DLC1.5H	3.0	-3422	DLC1.3	25.0	-9459	DLC1.4	11.4
Averages	Max	605	DLC1.5V	11.0	4653	DLC1.4	13.4	-3251	DLC1.4	9.4	1022	DLC1.3	25.0
	Min	62	DLC1.3	3.0	604	DLC1.5H	3.0	-3273	DLC1.4	13.4	-2417	DLC1.4	9.4
Model		5MW2DB00T0C0											
Maximums	Max	1281	DLC1.4	11.4	9170	DLC1.4	9.4	-3113	DLC1.4	9.4	4515	DLC1.3	25.0
	Min	1	DLC1.3	25.0	44	DLC1.3	3.0	-3426	DLC1.3	25.0	-8972	DLC1.4	9.4
Averages	Max	611	DLC1.5V	11.0	4375	DLC1.4	11.4	-3251	DLC1.4	9.4	1023	DLC1.3	25.0
	Min	62	DLC1.3	3.0	283	DLC1.5H	3.0	-3273	DLC1.4	13.4	-2199	DLC1.4	9.4
Model		5MW2DB00T0C0TipBrk											
Maximums	Max	1249	DLC1.4	11.4	8827	DLC1.4	9.4	-3177	DLC1.3	25.0	4502	DLC1.3	25.0
	Min	1	DLC1.3	25.0	42	DLC1.3	3.0	-3431	DLC1.3	25.0	-8869	DLC1.4	11.4
Averages	Max	613	DLC1.5V	11.0	4355	DLC1.4	11.4	-3252	DLC1.4	9.4	1019	DLC1.3	25.0
	Min	62	DLC1.3	3.0	290	DLC1.5H	3.0	-3274	DLC1.4	13.4	-2173	DLC1.4	9.4
Model		5MW2DB00TeeterNo											
Maximums	Max	1277	DLC1.4	11.4	11831	DLC1.3	25.0	-3094	DLC1.4	11.4	7188	DLC1.3	25.0
	Min	1	DLC1.3	25.0	97	DLC1.5H	3.0	-3391	DLC1.3	25.0	-13790	DLC1.4	11.4
Averages	Max	600	DLC1.5V	11.0	5696	DLC1.4	13.4	-3215	DLC1.4	11.4	1595	DLC1.3	25.0
	Min	62	DLC1.3	3.0	652	DLC1.5H	3.0	-3256	DLC1.3	25.0	-3114	DLC1.4	11.4

Table A8.4. Load effect result data at tower top in normal operating conditions (continue).

Load Effects		Shear Force			Bending Moment			Axial Force			Torsional Moment		
		Value (kN)	DLC (-)	Vs (m/s)	Value (kN m)	DLC (-)	Vs (m/s)	Value (kN)	DLC (-)	Vs (m/s)	Value (kN m)	DLC (-)	Vs (m/s)
Model		5MW2UBUTT2C0TipBrk											
Maximums	Max	1431	DLC1.4	9.4	8887	DLC1.4	9.4	-3049	DLC1.4	9.4	4972	DLC1.4	13.4
	Min	1	DLC1.4	11.4	8	DLC1.3	3.0	-3429	DLC1.3	25.0	-11540	DLC1.4	11.4
Averages	Max	704	DLC1.5H	11.0	4451	DLC1.4	11.4	-3238	DLC1.4	9.4	1218	DLC1.3	25.0
	Min	81	DLC1.3	3.0	371	DLC1.5H	3.0	-3265	DLC1.3	25.0	-2667	DLC1.4	9.4

Table A8.5. Load effect result data at tower top in fault conditions.

Load Effects		Shear Force			Bending Moment			Axial Force			Torsional Moment		
		Value (kN)	DLC (-)	Vs (m/s)	Value (kN m)	DLC (-)	Vs (m/s)	Value (kN)	DLC (-)	Vs (m/s)	Value (kN m)	DLC (-)	Vs (m/s)
Model		5MW3UB00											
Maximums	Max	1318	DLC2.3	25.0	12821	DLC2.1P	11.4	-3229	DLC2.1P	25.0	7782	DLC2.1P	11.4
	Min	1	DLC2.1G	11.4	11	DLC2.3	13.4	-3525	DLC2.1P	25.0	-8876	DLC2.1P	25.0
Averages	Max	363	DLC2.3	25.0	2974	DLC2.1P	25.0	-3376	DLC2.1P	25.0	27	DLC2.1G	11.4
	Min	223	DLC2.1P	11.4	1899	DLC2.1P	11.4	-3442	DLC2.1P	11.4	-1868	DLC2.1P	25.0
Model		5MW2UB00											
Maximums	Max	1414	DLC2.3	25.0	13935	DLC2.1P	11.4	-2916	DLC2.1P	25.0	10261	DLC2.1P	11.4
	Min	0	DLC2.3	25.0	1	DLC2.3	9.4	-3454	DLC2.1P	25.0	-17278	DLC2.1P	25.0
Averages	Max	331	DLC2.3	13.4	3507	DLC2.1P	25.0	-3258	DLC2.1G	25.0	1576	DLC2.1P	25.0
	Min	193	DLC2.1G	11.4	1039	DLC2.3	9.4	-3301	DLC2.1P	25.0	-238	DLC2.3	25.0
Model		5MW2IB00TipBrk											
Maximums	Max	1434	DLC2.3	25.0	7162	DLC2.1P	25.0	-3130	DLC2.1P	25.0	3685	DLC2.1P	25.0
	Min	0	DLC2.3	9.4	2	DLC2.3	25.0	-3388	DLC2.1P	25.0	-4323	DLC2.1P	25.0
Averages	Max	283	DLC2.3	11.4	3878	DLC2.1P	25.0	-3245	DLC2.3	25.0	568	DLC2.1P	25.0
	Min	143	DLC2.3	9.4	1037	DLC2.3	9.4	-3289	DLC2.1P	25.0	-878	DLC2.1P	25.0
Model		5MW2UBUT											
Maximums	Max	1367	DLC2.3	25.0	14300	DLC2.1P	25.0	-3009	DLC2.1P	25.0	9993	DLC2.1P	11.4
	Min	0	DLC2.3	11.4	7	DLC2.3	13.4	-3467	DLC2.1P	25.0	-11310	DLC2.1P	25.0
Averages	Max	306	DLC2.3	25.0	3887	DLC2.1P	25.0	-3228	DLC2.3	25.0	208	DLC2.1P	25.0
	Min	204	DLC2.3	9.4	1113	DLC2.3	9.4	-3275	DLC2.3	11.4	-160	DLC2.3	13.4
Model		5MW2UBUTTipBrk											
Maximums	Max	1207	DLC2.3	11.4	7100	DLC2.1P	25.0	-3119	DLC2.1G	25.0	4462	DLC2.1P	25.0
	Min	0	DLC2.3	25.0	6	DLC2.3	25.0	-3399	DLC2.1P	25.0	-4403	DLC2.1P	25.0
Averages	Max	287	DLC2.3	11.4	3864	DLC2.1P	25.0	-3244	DLC2.3	25.0	677	DLC2.1P	25.0
	Min	169	DLC2.3	9.4	1080	DLC2.3	9.4	-3290	DLC2.1P	25.0	-1129	DLC2.1P	25.0
Model		5MW2DB00											
Maximums	Max	1313	DLC2.3	25.0	14113	DLC2.1P	25.0	-2996	DLC2.1P	25.0	9331	DLC2.1P	11.4
	Min	0	DLC2.3	9.4	3	DLC2.3	9.4	-3451	DLC2.1P	25.0	-13638	DLC2.1P	25.0
Averages	Max	298	DLC2.3	13.4	3066	DLC2.1P	25.0	-3249	DLC2.3	11.4	2431	DLC2.1P	25.0
	Min	178	DLC2.3	9.4	1258	DLC2.3	9.4	-3315	DLC2.1P	25.0	142	DLC2.3	9.4
Model		5MW2DB00TipBrk											
Maximums	Max	1460	DLC2.3	25.0	8339	DLC2.1P	25.0	-3110	DLC2.3	25.0	4938	DLC2.1P	25.0
	Min	0	DLC2.3	9.4	11	DLC2.3	13.4	-3424	DLC2.1G	25.0	-6259	DLC2.1G	25.0
Averages	Max	257	DLC2.1P	25.0	4142	DLC2.1P	25.0	-3240	DLC2.1P	25.0	1446	DLC2.1P	25.0
	Min	146	DLC2.3	9.4	1244	DLC2.3	9.4	-3275	DLC2.3	25.0	-92	DLC2.1P	25.0
Model		5MW2DBUT											
Maximums	Max	1398	DLC2.3	25.0	13616	DLC2.1P	25.0	-3029	DLC2.1P	25.0	13267	DLC2.1P	25.0
	Min	1	DLC2.1G	11.4	4	DLC2.3	11.4	-3517	DLC2.1P	25.0	-10665	DLC2.1P	11.4
Averages	Max	301	DLC2.3	11.4	4432	DLC2.1P	25.0	-3248	DLC2.3	13.4	489	DLC2.1G	25.0
	Min	194	DLC2.3	9.4	1328	DLC2.3	9.4	-3290	DLC2.3	25.0	166	DLC2.3	9.4
Model		5MW2DBUTTipBrk											
Maximums	Max	1185	DLC2.3	11.4	8156	DLC2.1P	25.0	-3068	DLC2.3	9.4	4942	DLC2.1P	25.0
	Min	0	DLC2.3	11.4	4	DLC2.3	25.0	-3423	DLC2.1G	25.0	-5721	DLC2.1G	25.0
Averages	Max	299	DLC2.3	11.4	4195	DLC2.1P	25.0	-3241	DLC2.3	11.4	1539	DLC2.1P	25.0
	Min	161	DLC2.3	9.4	1316	DLC2.3	9.4	-3276	DLC2.1G	25.0	-39	DLC2.1P	25.0
Model		5MW2DB00T5C0											
Maximums	Max	1336	DLC2.3	25.0	13949	DLC2.1P	25.0	-2987	DLC2.1P	25.0	9394	DLC2.1P	11.4
	Min	0	DLC2.3	9.4	6	DLC2.1G	11.4	-3449	DLC2.1P	25.0	-13637	DLC2.1P	25.0
Averages	Max	306	DLC2.3	13.4	2763	DLC2.1P	25.0	-3246	DLC2.3	11.4	2456	DLC2.1P	25.0
	Min	182	DLC2.3	9.4	1089	DLC2.3	9.4	-3314	DLC2.1P	25.0	120	DLC2.3	9.4

Table A8.5. Load effect result data at tower top in fault conditions (continue).

Load Effects		Shear Force			Bending Moment			Axial Force			Torsional Moment		
		Value (kN)	DLC (-)	Vs (m/s)	Value (kN m)	DLC (-)	Vs (m/s)	Value (kN)	DLC (-)	Vs (m/s)	Value (kN m)	DLC (-)	Vs (m/s)
Model		5MW2DB00T5C0TipBrk											
Maximums	Max	1476	DLC2.3	25.0	8151	DLC2.1P	25.0	-3111	DLC2.3	25.0	4592	DLC2.1P	25.0
	Min	0	DLC2.3	13.4	1	DLC2.3	13.4	-3425	DLC2.1G	25.0	-6265	DLC2.1G	25.0
Averages	Max	257	DLC2.3	11.4	3978	DLC2.1P	25.0	-3241	DLC2.1P	25.0	1310	DLC2.1P	25.0
	Min	143	DLC2.3	9.4	998	DLC2.3	9.4	-3275	DLC2.3	25.0	-120	DLC2.1P	25.0
Model		5MW2DB00T0C2.5											
Maximums	Max	1343	DLC2.3	25.0	13370	DLC2.1P	25.0	-2974	DLC2.1P	25.0	9325	DLC2.1P	11.4
	Min	0	DLC2.3	11.4	5	DLC2.3	9.4	-3447	DLC2.1P	25.0	-15583	DLC2.1P	25.0
Averages	Max	313	DLC2.3	13.4	3270	DLC2.1P	25.0	-3258	DLC2.3	13.4	2195	DLC2.1P	25.0
	Min	180	DLC2.3	9.4	1239	DLC2.3	9.4	-3312	DLC2.1P	25.0	66	DLC2.3	9.4
Model		5MW2DB00T0C2.5TipBrk											
Maximums	Max	1472	DLC2.3	25.0	8226	DLC2.1P	25.0	-3143	DLC2.1P	25.0	4293	DLC2.1P	25.0
	Min	0	DLC2.3	9.4	15	DLC2.3	11.4	-3395	DLC2.1P	25.0	-4795	DLC2.1P	25.0
Averages	Max	259	DLC2.3	11.4	4066	DLC2.1P	25.0	-3253	DLC2.1P	25.0	795	DLC2.1P	25.0
	Min	140	DLC2.3	9.4	1204	DLC2.3	9.4	-3278	DLC2.1P	25.0	-320	DLC2.1P	25.0
Model		5MW2DB00T0C0											
Maximums	Max	1363	DLC2.3	25.0	13312	DLC2.1P	25.0	-2965	DLC2.1P	25.0	9355	DLC2.1P	11.4
	Min	0	DLC2.1G	11.4	3	DLC2.1G	11.4	-3446	DLC2.1P	25.0	-15555	DLC2.1P	25.0
Averages	Max	324	DLC2.3	13.4	3065	DLC2.1P	25.0	-3258	DLC2.3	13.4	2225	DLC2.1P	25.0
	Min	188	DLC2.3	9.4	1070	DLC2.3	9.4	-3311	DLC2.1P	25.0	52	DLC2.3	9.4
Model		5MW2DB00T0C0TipBrk											
Maximums	Max	1486	DLC2.3	25.0	8246	DLC2.1P	25.0	-3141	DLC2.1P	25.0	4274	DLC2.1P	25.0
	Min	0	DLC2.3	9.4	0	DLC2.3	13.4	-3398	DLC2.1P	25.0	-4614	DLC2.1P	25.0
Averages	Max	264	DLC2.3	11.4	3823	DLC2.1P	25.0	-3252	DLC2.1P	25.0	659	DLC2.1P	25.0
	Min	141	DLC2.3	9.4	977	DLC2.3	9.4	-3275	DLC2.1P	25.0	-320	DLC2.1P	25.0
Model		5MW2DB00TeeterNo											
Maximums	Max	1344	DLC2.3	25.0	17167	DLC2.1P	25.0	-2951	DLC2.1P	25.0	11714	DLC2.1P	25.0
	Min	0	DLC2.3	9.4	3	DLC2.3	13.4	-3455	DLC2.1P	25.0	-15572	DLC2.1P	25.0
Averages	Max	409	DLC2.3	25.0	3212	DLC2.1P	25.0	-3247	DLC2.3	11.4	2464	DLC2.1P	25.0
	Min	202	DLC2.1G	11.4	1357	DLC2.3	9.4	-3315	DLC2.1P	25.0	85	DLC2.3	9.4
Model		5MW2UBUTT2C0TipBrk											
Maximums	Max	1208	DLC2.3	11.4	8265	DLC2.1P	25.0	-3103	DLC2.3	9.4	4446	DLC2.1P	25.0
	Min	0	DLC2.3	13.4	1	DLC2.3	13.4	-3422	DLC2.3	9.4	-4450	DLC2.1G	25.0
Averages	Max	311	DLC2.3	11.4	3839	DLC2.1P	25.0	-3245	DLC2.1P	25.0	1170	DLC2.1P	25.0
	Min	165	DLC2.3	25.0	1070	DLC2.3	9.4	-3281	DLC2.1P	25.0	-393	DLC2.1P	25.0

Table A8.6. Load effect result data at tower top in parked conditions.

Load Effects		Shear Force			Bending Moment			Axial Force			Torsional Moment		
		Value (kN)	DLC (-)	Vs (m/s)	Value (kN m)	DLC (-)	Vs (m/s)	Value (kN)	DLC (-)	Vs (m/s)	Value (kN m)	DLC (-)	Vs (m/s)
Model		5MW3UB00											
Maximums	Max	748	DLC6.2a	37.4	6040	DLC6.2a	37.4	-3342	DLC6.1a	37.4	3901	DLC7.1a	25.0
	Min	1	DLC6.2a	37.4	27	DLC6.2a	37.4	-3464	DLC7.1a	25.0	-4250	DLC6.2a	37.4
Averages	Max	355	DLC6.2a	37.4	4036	DLC6.2a	37.4	-3343	DLC6.1a	37.4	3800	DLC7.1a	25.0
	Min	24	DLC6.3a	25.0	228	DLC6.2a	37.4	-3464	DLC7.1a	25.0	-1989	DLC6.2a	37.4
Model		5MW2UB00											
Maximums	Max	474	DLC6.2a	37.4	1787	DLC7.1a	25.0	-3135	DLC6.2a	37.4	3354	DLC7.1a	25.0
	Min	0	DLC6.2a	37.4	5	DLC6.2a	37.4	-3287	DLC6.2a	37.4	-186	DLC6.2a	37.4
Averages	Max	160	DLC6.2a	37.4	1708	DLC7.1a	25.0	-3136	DLC6.2a	37.4	3265	DLC7.1a	25.0
	Min	7	DLC6.2a	37.4	49	DLC6.3a	25.0	-3274	DLC7.1a	25.0	-51	DLC6.2a	37.4
Model		5MW2IB00TipBrk											
Maximums	Max	480	DLC6.2a	37.4	1830	DLC6.2a	37.4	-3137	DLC6.2a	37.4	3352	DLC7.1a	25.0
	Min	0	DLC6.2a	37.4	10	DLC6.2a	37.4	-3287	DLC6.2a	37.4	-184	DLC6.2a	37.4
Averages	Max	160	DLC6.2a	37.4	1722	DLC7.1a	25.0	-3138	DLC6.2a	37.4	3262	DLC7.1a	25.0
	Min	7	DLC6.2a	37.4	58	DLC6.3a	25.0	-3276	DLC7.1a	25.0	-52	DLC6.2a	37.4
Model		5MW2UBUT											
Maximums	Max	503	DLC6.2a	37.4	2067	DLC7.1a	25.0	-3128	DLC6.2a	37.4	3368	DLC7.1a	25.0
	Min	0	DLC6.2a	37.4	2	DLC6.2a	37.4	-3288	DLC6.2a	37.4	-150	DLC6.2a	37.4
Averages	Max	167	DLC6.2a	37.4	1972	DLC7.1a	25.0	-3128	DLC6.2a	37.4	3274	DLC7.1a	25.0
	Min	7	DLC6.2a	37.4	115	DLC6.2a	37.4	-3265	DLC6.2a	37.4	-37	DLC6.2a	37.4

Table A8.6. Load effect result data at tower top in parked conditions (continue).

Load Effects		Shear Force			Bending Moment			Axial Force			Torsional Moment		
		Value (kN)	DLC (-)	Vs (m/s)	Value (kN m)	DLC (-)	Vs (m/s)	Value (kN)	DLC (-)	Vs (m/s)	Value (kN m)	DLC (-)	Vs (m/s)
Model		5MW2UBUTTipBrk											
Maximums	Max	507	DLC6.2a	37.4	2060	DLC7.1a	25.0	-3129	DLC6.2a	37.4	3368	DLC7.1a	25.0
	Min	0	DLC6.2a	37.4	1	DLC6.2a	37.4	-3290	DLC6.2a	37.4	-152	DLC6.2a	37.4
Averages	Max	167	DLC6.2a	37.4	1971	DLC7.1a	25.0	-3131	DLC6.2a	37.4	3274	DLC7.1a	25.0
	Min	8	DLC6.2a	37.4	97	DLC6.2a	37.4	-3267	DLC6.2a	37.4	-38	DLC6.2a	37.4
Model		5MW2DB00											
Maximums	Max	520	DLC6.2a	37.4	3105	DLC7.1a	25.0	-3224	DLC6.2a	37.4	3565	DLC7.1a	25.0
	Min	0	DLC6.2a	37.4	5	DLC6.2a	37.4	-3377	DLC6.2a	37.4	-153	DLC6.2a	37.4
Averages	Max	201	DLC6.2a	37.4	1921	DLC7.1a	25.0	-3249	DLC6.2a	37.4	3280	DLC7.1a	25.0
	Min	3	DLC6.2a	37.4	392	DLC6.2a	37.4	-3376	DLC6.2a	37.4	-118	DLC6.1a	37.4
Model		5MW2DB00TipBrk											
Maximums	Max	529	DLC6.2a	37.4	3107	DLC7.1a	25.0	-3224	DLC6.2a	37.4	3542	DLC7.1a	25.0
	Min	0	DLC6.2a	37.4	3	DLC6.2a	37.4	-3378	DLC6.2a	37.4	-162	DLC6.2a	37.4
Averages	Max	203	DLC6.2a	37.4	1931	DLC7.1a	25.0	-3251	DLC6.2a	37.4	3278	DLC7.1a	25.0
	Min	4	DLC6.2a	37.4	406	DLC6.2a	37.4	-3376	DLC6.2a	37.4	-118	DLC6.1a	37.4
Model		5MW2DBUT											
Maximums	Max	578	DLC6.2a	37.4	3237	DLC7.1a	25.0	-3219	DLC6.2a	37.4	3579	DLC7.1a	25.0
	Min	0	DLC6.2a	37.4	1	DLC6.2a	37.4	-3384	DLC6.2a	37.4	-157	DLC6.2a	37.4
Averages	Max	224	DLC6.2a	37.4	2079	DLC7.1a	25.0	-3250	DLC6.2a	37.4	3292	DLC7.1a	25.0
	Min	3	DLC6.2a	37.4	394	DLC6.2a	37.4	-3383	DLC6.1a	37.4	-96	DLC6.2a	37.4
Model		5MW2DBUTTipBrk											
Maximums	Max	584	DLC6.2a	37.4	3255	DLC7.1a	25.0	-3219	DLC6.2a	37.4	3579	DLC7.1a	25.0
	Min	0	DLC6.2a	37.4	1	DLC6.2a	37.4	-3386	DLC6.1a	37.4	-148	DLC6.2a	37.4
Averages	Max	227	DLC6.2a	37.4	2062	DLC7.1a	25.0	-3251	DLC6.2a	37.4	3290	DLC7.1a	25.0
	Min	4	DLC6.2a	37.4	407	DLC6.2a	37.4	-3384	DLC6.1a	37.4	-99	DLC6.2a	37.4
Model		5MW2DB00T5C0											
Maximums	Max	522	DLC6.2a	37.4	3041	DLC7.1a	25.0	-3223	DLC6.2a	37.4	3532	DLC7.1a	25.0
	Min	0	DLC6.2a	37.4	6	DLC6.2a	37.4	-3380	DLC6.2a	37.4	-172	DLC6.2a	37.4
Averages	Max	202	DLC6.2a	37.4	1675	DLC7.1a	25.0	-3249	DLC6.2a	37.4	3252	DLC7.1a	25.0
	Min	4	DLC6.2a	37.4	70	DLC6.2a	37.4	-3378	DLC6.2a	37.4	-134	DLC6.2a	37.4
Model		5MW2DB00T5C0TipBrk											
Maximums	Max	533	DLC6.2a	37.4	2974	DLC7.1a	25.0	-3218	DLC6.2a	37.4	3506	DLC7.1a	25.0
	Min	0	DLC6.2a	37.4	19	DLC6.2a	37.4	-3381	DLC6.2a	37.4	-194	DLC6.2a	37.4
Averages	Max	204	DLC6.2a	37.4	1677	DLC7.1a	25.0	-3251	DLC6.2a	37.4	3250	DLC7.1a	25.0
	Min	5	DLC6.2a	37.4	83	DLC6.2a	37.4	-3380	DLC6.2a	37.4	-133	DLC6.2a	37.4
Model		5MW2DB00T0C2.5											
Maximums	Max	603	DLC6.2a	37.4	1906	DLC6.2a	37.4	-3240	DLC6.2a	37.4	3411	DLC7.1a	25.0
	Min	0	DLC6.3a	25.0	5	DLC6.2a	37.4	-3292	DLC7.1a	25.0	-236	DLC6.2a	37.4
Averages	Max	232	DLC6.2a	37.4	1070	DLC6.2a	37.4	-3255	DLC6.2a	37.4	3310	DLC7.1a	25.0
	Min	3	DLC6.2a	37.4	408	DLC6.2a	37.4	-3292	DLC7.1a	25.0	-41	DLC6.2a	37.4
Model		5MW2DB00T0C2.5TipBrk											
Maximums	Max	612	DLC6.2a	37.4	1890	DLC6.2a	37.4	-3238	DLC6.2a	37.4	3419	DLC7.1a	25.0
	Min	0	DLC6.2a	37.4	3	DLC6.2a	37.4	-3294	DLC7.1a	25.0	-261	DLC6.2a	37.4
Averages	Max	235	DLC6.2a	37.4	1093	DLC6.2a	37.4	-3256	DLC6.2a	37.4	3311	DLC7.1a	25.0
	Min	3	DLC6.2a	37.4	421	DLC6.2a	37.4	-3293	DLC7.1a	25.0	-41	DLC6.2a	37.4
Model		5MW2DB00T0C0											
Maximums	Max	606	DLC6.2a	37.4	1699	DLC6.2a	37.4	-3229	DLC6.2a	37.4	3370	DLC7.1a	25.0
	Min	0	DLC6.2a	37.4	2	DLC6.2a	37.4	-3293	DLC7.1a	25.0	-223	DLC6.2a	37.4
Averages	Max	234	DLC6.2a	37.4	981	DLC6.2a	37.4	-3256	DLC6.2a	37.4	3283	DLC7.1a	25.0
	Min	3	DLC6.2a	37.4	82	DLC6.2a	37.4	-3292	DLC7.1a	25.0	-26	DLC6.2a	37.4
Model		5MW2DB00T0C0TipBrk											
Maximums	Max	619	DLC6.2a	37.4	1863	DLC6.2a	37.4	-3227	DLC6.2a	37.4	3377	DLC7.1a	25.0
	Min	0	DLC6.2a	37.4	5	DLC6.2a	37.4	-3295	DLC7.1a	25.0	-247	DLC6.2a	37.4
Averages	Max	238	DLC6.2a	37.4	1011	DLC6.2a	37.4	-3257	DLC6.2a	37.4	3284	DLC7.1a	25.0
	Min	4	DLC6.2a	37.4	94	DLC6.2a	37.4	-3294	DLC7.1a	25.0	-26	DLC6.2a	37.4
Model		5MW2DB00TeeterNo											
Maximums	Max	525	DLC6.2a	37.4	3137	DLC7.1a	25.0	-3222	DLC6.2a	37.4	3749	DLC7.1a	25.0
	Min	0	DLC6.2a	37.4	2	DLC6.2a	37.4	-3376	DLC6.2a	37.4	-1634	DLC6.2a	37.4
Averages	Max	204	DLC6.2a	37.4	1944	DLC7.1a	25.0	-3249	DLC6.2a	37.4	3262	DLC7.1a	25.0
	Min	4	DLC6.2a	37.4	393	DLC6.2a	37.4	-3376	DLC6.2a	37.4	-118	DLC6.1a	37.4

Table A8.6. Load effect result data at tower top in parked conditions (continue).

Load Effects		Shear Force			Bending Moment			Axial Force			Torsional Moment		
		Value (kN)	DLC (-)	Vs (m/s)	Value (kN m)	DLC (-)	Vs (m/s)	Value (kN)	DLC (-)	Vs (m/s)	Value (kN m)	DLC (-)	Vs (m/s)
Model		5MW2UBUTT2C0TipBrk											
Maximums	Max	652	DLC6.2a	37.4	1787	DLC6.2a	37.4	-3225	DLC6.2a	37.4	3360	DLC7.1a	25.0
	Min	0	DLC6.2a	37.4	1	DLC6.2a	37.4	-3312	DLC6.1a	37.4	-132	DLC6.2a	37.4
Averages	Max	252	DLC6.2a	37.4	1236	DLC6.2a	37.4	-3255	DLC6.2a	37.4	3258	DLC7.1a	25.0
	Min	4	DLC6.2a	37.4	97	DLC6.2a	37.4	-3312	DLC6.1a	37.4	-46	DLC6.2a	37.4

Table A8.7. Load effect result data at blade roots in normal operating conditions.

Load Effects		Shear Force			Bending Moment			Axial Force			Torsional Moment		
		Value (kN)	DLC (-)	Vs (m/s)	Value (kN m)	DLC (-)	Vs (m/s)	Value (kN)	DLC (-)	Vs (m/s)	Value (kN m)	DLC (-)	Vs (m/s)
Model		5MW3UB00											
Maximums	Max	468	DLC1.4	11.4	17734	DLC1.4	11.4	1013	DLC1.3	23.0	133	DLC1.3	15.0
	Min	5	DLC1.3	25.0	23	DLC1.3	23.0	0	DLC1.1	3.0	-202	DLC1.4	13.4
Averages	Max	300	DLC1.5V	11.0	10101	DLC1.5V	11.0	624	DLC1.5V	25.0	4	DLC1.5H	11.0
	Min	125	DLC1.3	3.0	2939	DLC1.3	3.0	206	DLC1.3	3.0	-56	DLC1.4	13.4
Model		5MW2UB00											
Maximums	Max	566	DLC1.3	15.0	20723	DLC1.4	11.4	1552	DLC1.3	25.0	162	DLC1.3	15.0
	Min	8	DLC1.4	11.4	44	DLC1.3	25.0	0	DLC1.3	3.0	-253	DLC1.4	11.4
Averages	Max	385	DLC1.5V	11.0	12963	DLC1.5V	11.0	1090	DLC1.5H	25.0	-4	DLC1.5H	11.0
	Min	128	DLC1.3	3.0	3079	DLC1.3	3.0	213	DLC1.5V	3.0	-86	DLC1.5V	25.0
Model		5MW2IB00TipBrk											
Maximums	Max	569	DLC1.3	15.0	20672	DLC1.4	11.4	1567	DLC1.3	25.0	172	DLC1.4	11.4
	Min	8	DLC1.4	11.4	33	DLC1.3	25.0	0	DLC1.1	3.0	-254	DLC1.4	11.4
Averages	Max	387	DLC1.5V	11.0	12978	DLC1.5V	11.0	1104	DLC1.5H	25.0	-3	DLC1.5H	11.0
	Min	128	DLC1.3	3.0	3108	DLC1.3	3.0	215	DLC1.5V	3.0	-86	DLC1.5V	25.0
Model		5MW2UBUT											
Maximums	Max	646	DLC1.4	11.4	24036	DLC1.4	11.4	1658	DLC1.3	25.0	207	DLC1.4	11.4
	Min	9	DLC1.4	11.4	47	DLC1.3	25.0	0	DLC1.3	3.0	-281	DLC1.4	11.4
Averages	Max	427	DLC1.5V	11.0	14479	DLC1.5V	11.0	1070	DLC1.3	23.0	1	DLC1.5H	11.0
	Min	132	DLC1.3	3.0	3303	DLC1.3	3.0	210	DLC1.3	3.0	-82	DLC1.5V	25.0
Model		5MW2UBUTTipBrk											
Maximums	Max	644	DLC1.4	11.4	23987	DLC1.4	11.4	1674	DLC1.3	25.0	191	DLC1.4	11.4
	Min	12	DLC1.4	11.4	49	DLC1.3	25.0	0	DLC1.1	3.0	-281	DLC1.4	11.4
Averages	Max	428	DLC1.5V	11.0	14460	DLC1.5V	11.0	1084	DLC1.3	23.0	1	DLC1.5H	11.0
	Min	133	DLC1.3	3.0	3332	DLC1.3	3.0	213	DLC1.3	3.0	-82	DLC1.5V	25.0
Model		5MW2DB00											
Maximums	Max	469	DLC1.3	15.0	17953	DLC1.4	11.4	1540	DLC1.3	25.0	200	DLC1.4	9.4
	Min	0	DLC1.4	9.4	14	DLC1.3	25.0	0	DLC1.1	3.0	-262	DLC1.4	13.4
Averages	Max	269	DLC1.5V	11.0	9672	DLC1.5V	11.0	1091	DLC1.5H	25.0	-10	DLC1.5H	7.0
	Min	113	DLC1.3	3.0	2456	DLC1.5H	3.0	212	DLC1.5H	3.0	-93	DLC1.5V	25.0
Model		5MW2DB00TipBrk											
Maximums	Max	473	DLC1.3	15.0	17827	DLC1.4	11.4	1556	DLC1.3	25.0	155	DLC1.4	9.4
	Min	0	DLC1.5H	25.0	10	DLC1.3	3.0	0	DLC1.1	3.0	-262	DLC1.4	13.4
Averages	Max	269	DLC1.5V	11.0	9638	DLC1.5V	11.0	1105	DLC1.5H	25.0	-10	DLC1.5H	7.0
	Min	113	DLC1.5H	3.0	2476	DLC1.5H	3.0	215	DLC1.5H	3.0	-93	DLC1.5V	25.0
Model		5MW2DBUT											
Maximums	Max	538	DLC1.4	11.4	20880	DLC1.4	11.4	1658	DLC1.3	25.0	187	DLC1.4	9.4
	Min	0	DLC1.3	3.0	13	DLC1.3	21.0	0	DLC1.1	3.0	-280	DLC1.4	13.4
Averages	Max	310	DLC1.5V	11.0	11207	DLC1.5V	11.0	1071	DLC1.3	23.0	-4	DLC1.5H	7.0
	Min	114	DLC1.5H	3.0	2598	DLC1.5H	3.0	210	DLC1.5H	3.0	-87	DLC1.5V	25.0
Model		5MW2DBUTTipBrk											
Maximums	Max	534	DLC1.4	11.4	20700	DLC1.4	11.4	1674	DLC1.3	25.0	282	DLC1.4	9.4
	Min	0	DLC1.3	3.0	13	DLC1.3	25.0	0	DLC1.1	3.0	-279	DLC1.4	13.4
Averages	Max	310	DLC1.5V	11.0	11147	DLC1.5V	11.0	1085	DLC1.3	23.0	-4	DLC1.5H	7.0
	Min	114	DLC1.5H	3.0	2623	DLC1.5H	3.0	213	DLC1.3	3.0	-88	DLC1.5V	25.0
Model		5MW2DB00T5C0											
Maximums	Max	514	DLC1.3	15.0	18891	DLC1.4	11.4	1545	DLC1.3	25.0	216	DLC1.4	9.4
	Min	1	DLC1.3	23.0	17	DLC1.3	23.0	0	DLC1.1	3.0	-267	DLC1.4	13.4
Averages	Max	308	DLC1.5V	11.0	10913	DLC1.5V	11.0	1093	DLC1.5H	25.0	-9	DLC1.5H	7.0
	Min	113	DLC1.3	3.0	2565	DLC1.3	3.0	214	DLC1.5H	3.0	-92	DLC1.5V	25.0

Table A8.7. Load effect result data at blade roots in normal operating conditions (continue).

Load Effects		Shear Force			Bending Moment			Axial Force			Torsional Moment		
		Value (kN)	DLC (-)	Vs (m/s)	Value (kN m)	DLC (-)	Vs (m/s)	Value (kN)	DLC (-)	Vs (m/s)	Value (kN m)	DLC (-)	Vs (m/s)
Model		5MW2DB00T5C0TipBrk											
Maximums	Max	518	DLC1.3	15.0	18763	DLC1.4	11.4	1561	DLC1.3	25.0	163	DLC1.4	9.4
	Min	0	DLC1.5V	3.0	13	DLC1.3	23.0	0	DLC1.1	3.0	-269	DLC1.4	13.4
Averages	Max	309	DLC1.5V	11.0	10899	DLC1.5V	11.0	1107	DLC1.5H	25.0	-9	DLC1.5H	7.0
	Min	114	DLC1.3	3.0	2590	DLC1.3	3.0	216	DLC1.5H	3.0	-92	DLC1.5V	25.0
Model		5MW2DB00T0C2.5											
Maximums	Max	481	DLC1.3	15.0	18030	DLC1.4	11.4	1548	DLC1.3	25.0	220	DLC1.4	9.4
	Min	0	DLC1.5V	3.0	4	DLC1.4	9.4	0	DLC1.1	3.0	-284	DLC1.4	13.4
Averages	Max	283	DLC1.5V	11.0	9979	DLC1.5V	11.0	1092	DLC1.5H	25.0	-10	DLC1.5H	7.0
	Min	115	DLC1.3	3.0	2584	DLC1.3	3.0	213	DLC1.5V	3.0	-92	DLC1.5V	25.0
Model		5MW2DB00T0C2.5TipBrk											
Maximums	Max	484	DLC1.3	15.0	17912	DLC1.4	11.4	1563	DLC1.3	25.0	155	DLC1.4	9.4
	Min	0	DLC1.3	3.0	3	DLC1.4	13.4	0	DLC1.1	3.0	-284	DLC1.4	13.4
Averages	Max	283	DLC1.5V	11.0	9947	DLC1.5V	11.0	1105	DLC1.5H	25.0	-10	DLC1.5H	7.0
	Min	116	DLC1.3	3.0	2608	DLC1.3	3.0	216	DLC1.5V	3.0	-92	DLC1.5V	25.0
Model		5MW2DB00T0C0											
Maximums	Max	526	DLC1.3	15.0	18940	DLC1.4	11.4	1552	DLC1.3	25.0	230	DLC1.4	9.4
	Min	1	DLC1.3	23.0	16	DLC1.3	25.0	0	DLC1.1	3.0	-289	DLC1.4	13.4
Averages	Max	323	DLC1.5V	11.0	11236	DLC1.5V	11.0	1093	DLC1.5H	25.0	-9	DLC1.5H	7.0
	Min	118	DLC1.3	3.0	2724	DLC1.3	3.0	214	DLC1.5V	3.0	-91	DLC1.5V	25.0
Model		5MW2DB00T0C0TipBrk											
Maximums	Max	530	DLC1.3	15.0	18850	DLC1.4	11.4	1568	DLC1.3	25.0	164	DLC1.4	9.4
	Min	1	DLC1.3	25.0	17	DLC1.3	23.0	0	DLC1.1	3.0	-291	DLC1.4	13.4
Averages	Max	324	DLC1.5V	11.0	11227	DLC1.5V	11.0	1107	DLC1.5H	25.0	-8	DLC1.5H	7.0
	Min	118	DLC1.3	3.0	2749	DLC1.3	3.0	216	DLC1.5V	3.0	-91	DLC1.5V	25.0
Model		5MW2DB00TeeterNo											
Maximums	Max	508	DLC1.4	11.4	19770	DLC1.4	11.4	1534	DLC1.3	25.0	147	DLC1.4	9.4
	Min	1	DLC1.3	17.0	9	DLC1.3	3.0	0	DLC1.1	3.0	-266	DLC1.4	13.4
Averages	Max	268	DLC1.5V	11.0	9675	DLC1.5V	11.0	1091	DLC1.5H	25.0	-10	DLC1.5H	7.0
	Min	113	DLC1.5H	3.0	2452	DLC1.5H	3.0	212	DLC1.5H	3.0	-93	DLC1.5V	25.0
Model		5MW2UBUTT2C0TipBrk											
Maximums	Max	573	DLC1.4	11.4	21896	DLC1.4	11.4	1683	DLC1.3	25.0	298	DLC1.4	9.4
	Min	1	DLC1.3	23.0	16	DLC1.3	25.0	0	DLC1.1	3.0	-304	DLC1.4	13.4
Averages	Max	360	DLC1.5V	11.0	12618	DLC1.5V	11.0	1087	DLC1.3	23.0	-3	DLC1.5H	7.0
	Min	119	DLC1.3	3.0	2873	DLC1.3	3.0	214	DLC1.3	3.0	-87	DLC1.5V	25.0

Table A8.8. Load effect result data at blade roots in fault conditions.

Load Effects		Shear Force			Bending Moment			Axial Force			Torsional Moment		
		Value (kN)	DLC (-)	Vs (m/s)	Value (kN m)	DLC (-)	Vs (m/s)	Value (kN)	DLC (-)	Vs (m/s)	Value (kN m)	DLC (-)	Vs (m/s)
Model		5MW3UB00											
Maximums	Max	450	DLC2.3	11.4	15045	DLC2.3	11.4	1042	DLC2.3	25.0	178	DLC2.3	9.4
	Min	3	DLC2.3	25.0	43	DLC2.1G	25.0	-180	DLC2.3	25.0	-130	DLC2.3	25.0
Averages	Max	200	DLC2.3	11.4	5084	DLC2.3	11.4	304	DLC2.3	13.4	-3	DLC2.3	9.4
	Min	89	DLC2.3	25.0	1937	DLC2.3	25.0	51	DLC2.1G	11.4	-38	DLC2.1P	25.0
Model		5MW2UB00											
Maximums	Max	588	DLC2.3	13.4	18580	DLC2.3	13.4	1636	DLC2.3	25.0	323	DLC2.3	13.4
	Min	0	DLC2.3	25.0	17	DLC2.3	25.0	-177	DLC2.3	25.0	-193	DLC2.3	25.0
Averages	Max	245	DLC2.1P	25.0	5862	DLC2.1P	25.0	462	DLC2.3	25.0	-2	DLC2.3	9.4
	Min	96	DLC2.3	25.0	2317	DLC2.3	25.0	188	DLC2.1G	25.0	-59	DLC2.1P	25.0
Model		5MW2IB00TipBrk											
Maximums	Max	655	DLC2.3	25.0	20930	DLC2.3	25.0	1723	DLC2.3	25.0	609	DLC2.3	11.4
	Min	3	DLC2.3	13.4	4	DLC2.3	13.4	-178	DLC2.3	25.0	-496	DLC2.3	25.0
Averages	Max	249	DLC2.3	11.4	6997	DLC2.3	11.4	489	DLC2.3	25.0	4	DLC2.3	11.4
	Min	115	DLC2.3	9.4	3067	DLC2.3	25.0	90	DLC2.3	9.4	-49	DLC2.1P	25.0
Model		5MW2UBUT											
Maximums	Max	607	DLC2.3	11.4	20435	DLC2.3	11.4	1551	DLC2.3	25.0	287	DLC2.3	25.0
	Min	0	DLC2.3	11.4	4	DLC2.3	11.4	-176	DLC2.3	11.4	-175	DLC2.3	25.0
Averages	Max	210	DLC2.1G	11.4	5667	DLC2.1G	11.4	450	DLC2.3	13.4	-1	DLC2.3	9.4
	Min	132	DLC2.1P	25.0	2831	DLC2.1P	25.0	146	DLC2.3	9.4	-52	DLC2.1P	25.0

Table A8.8. Load effect result data at blade roots in fault conditions (continue).

Load Effects		Shear Force			Bending Moment			Axial Force			Torsional Moment		
		Value (kN)	DLC (-)	Vs (m/s)	Value (kN m)	DLC (-)	Vs (m/s)	Value (kN)	DLC (-)	Vs (m/s)	Value (kN m)	DLC (-)	Vs (m/s)
Model		5MW2UBUTTipBrk											
Maximums	Max	622	DLC2.3	11.4	20842	DLC2.3	11.4	1692	DLC2.3	25.0	692	DLC2.3	11.4
	Min	3	DLC2.3	9.4	7	DLC2.3	9.4	-176	DLC2.3	25.0	-439	DLC2.3	25.0
Averages	Max	251	DLC2.3	11.4	7066	DLC2.3	11.4	479	DLC2.3	25.0	6	DLC2.3	11.4
	Min	121	DLC2.3	9.4	3202	DLC2.3	25.0	89	DLC2.3	9.4	-50	DLC2.1P	25.0
Model		5MW2DB00											
Maximums	Max	497	DLC2.3	13.4	18397	DLC2.3	25.0	1651	DLC2.3	25.0	404	DLC2.3	25.0
	Min	2	DLC2.3	25.0	2	DLC2.3	25.0	-177	DLC2.3	25.0	-257	DLC2.3	25.0
Averages	Max	226	DLC2.1P	25.0	5427	DLC2.1P	25.0	463	DLC2.3	25.0	-6	DLC2.3	9.4
	Min	72	DLC2.3	25.0	1681	DLC2.3	25.0	116	DLC2.3	9.4	-69	DLC2.1P	25.0
Model		5MW2DB00TipBrk											
Maximums	Max	621	DLC2.3	25.0	20249	DLC2.3	25.0	1724	DLC2.3	25.0	566	DLC2.3	25.0
	Min	0	DLC2.3	9.4	6	DLC2.3	9.4	-178	DLC2.3	25.0	-483	DLC2.3	25.0
Averages	Max	205	DLC2.3	11.4	5586	DLC2.3	11.4	489	DLC2.3	25.0	-2	DLC2.3	11.4
	Min	85	DLC2.3	9.4	2360	DLC2.3	25.0	95	DLC2.3	9.4	-58	DLC2.1P	25.0
Model		5MW2DBUT											
Maximums	Max	508	DLC2.3	11.4	17522	DLC2.3	25.0	1541	DLC2.3	25.0	358	DLC2.3	13.4
	Min	1	DLC2.3	13.4	43	DLC2.1P	25.0	-175	DLC2.3	13.4	-200	DLC2.1G	25.0
Averages	Max	223	DLC2.3	11.4	6349	DLC2.3	11.4	452	DLC2.3	13.4	-3	DLC2.3	9.4
	Min	103	DLC2.3	13.4	2691	DLC2.1P	25.0	133	DLC2.3	9.4	-55	DLC2.1P	25.0
Model		5MW2DBUTTipBrk											
Maximums	Max	540	DLC2.3	25.0	17291	DLC2.3	11.4	1710	DLC2.3	25.0	577	DLC2.3	11.4
	Min	0	DLC2.3	9.4	2	DLC2.3	9.4	-178	DLC2.3	25.0	-514	DLC2.3	25.0
Averages	Max	224	DLC2.3	11.4	6443	DLC2.3	11.4	486	DLC2.3	25.0	1	DLC2.3	11.4
	Min	92	DLC2.3	9.4	2253	DLC2.3	25.0	102	DLC2.3	9.4	-57	DLC2.1P	25.0
Model		5MW2DB00T5C0											
Maximums	Max	542	DLC2.3	13.4	17727	DLC2.3	13.4	1657	DLC2.3	25.0	374	DLC2.3	25.0
	Min	1	DLC2.3	25.0	7	DLC2.3	25.0	-178	DLC2.3	25.0	-264	DLC2.3	25.0
Averages	Max	232	DLC2.1P	25.0	5665	DLC2.3	13.4	464	DLC2.3	25.0	-6	DLC2.3	11.4
	Min	79	DLC2.3	25.0	1904	DLC2.3	25.0	125	DLC2.3	9.4	-69	DLC2.1P	25.0
Model		5MW2DB00T5C0TipBrk											
Maximums	Max	644	DLC2.3	25.0	21083	DLC2.3	25.0	1734	DLC2.3	25.0	622	DLC2.3	25.0
	Min	0	DLC2.3	9.4	9	DLC2.3	9.4	-178	DLC2.3	25.0	-477	DLC2.3	25.0
Averages	Max	213	DLC2.3	11.4	6143	DLC2.3	11.4	490	DLC2.3	25.0	1	DLC2.3	11.4
	Min	100	DLC2.3	9.4	2674	DLC2.3	25.0	110	DLC2.3	9.4	-57	DLC2.1P	25.0
Model		5MW2DB00T0C2.5											
Maximums	Max	508	DLC2.3	13.4	17114	DLC2.3	13.4	1655	DLC2.3	25.0	349	DLC2.3	25.0
	Min	0	DLC2.3	25.0	7	DLC2.3	25.0	-175	DLC2.3	25.0	-278	DLC2.3	25.0
Averages	Max	232	DLC2.1P	25.0	5540	DLC2.1P	25.0	464	DLC2.3	25.0	-6	DLC2.3	9.4
	Min	68	DLC2.3	25.0	1623	DLC2.3	25.0	124	DLC2.3	9.4	-66	DLC2.1P	25.0
Model		5MW2DB00T0C2.5TipBrk											
Maximums	Max	613	DLC2.3	25.0	19989	DLC2.3	25.0	1730	DLC2.3	25.0	566	DLC2.3	25.0
	Min	1	DLC2.3	25.0	8	DLC2.3	13.4	-179	DLC2.3	25.0	-484	DLC2.3	25.0
Averages	Max	203	DLC2.3	11.4	5743	DLC2.3	11.4	492	DLC2.3	25.0	-2	DLC2.3	11.4
	Min	87	DLC2.3	25.0	2133	DLC2.3	25.0	109	DLC2.3	9.4	-54	DLC2.1P	25.0
Model		5MW2DB00T0C0											
Maximums	Max	554	DLC2.3	13.4	17892	DLC2.3	13.4	1661	DLC2.3	25.0	326	DLC2.3	13.4
	Min	1	DLC2.3	25.0	10	DLC2.3	25.0	-176	DLC2.3	25.0	-289	DLC2.3	25.0
Averages	Max	239	DLC2.1P	25.0	5746	DLC2.1P	25.0	464	DLC2.3	25.0	-5	DLC2.3	9.4
	Min	76	DLC2.3	25.0	1847	DLC2.3	25.0	140	DLC2.3	9.4	-66	DLC2.1P	25.0
Model		5MW2DB00T0C0TipBrk											
Maximums	Max	637	DLC2.3	25.0	20831	DLC2.3	25.0	1739	DLC2.3	25.0	622	DLC2.3	25.0
	Min	0	DLC2.3	25.0	1	DLC2.3	25.0	-180	DLC2.3	25.0	-479	DLC2.3	25.0
Averages	Max	221	DLC2.3	11.4	6290	DLC2.3	11.4	493	DLC2.3	25.0	1	DLC2.3	11.4
	Min	97	DLC2.3	25.0	2443	DLC2.3	25.0	95	DLC2.3	9.4	-53	DLC2.1P	25.0
Model		5MW2DB00TeeterNo											
Maximums	Max	500	DLC2.3	13.4	18744	DLC2.3	25.0	1638	DLC2.3	25.0	415	DLC2.3	25.0
	Min	0	DLC2.3	25.0	2	DLC2.3	25.0	-181	DLC2.3	25.0	-255	DLC2.3	25.0
Averages	Max	229	DLC2.1P	25.0	5521	DLC2.1P	25.0	462	DLC2.3	25.0	-6	DLC2.3	9.4
	Min	77	DLC2.3	25.0	1793	DLC2.3	25.0	117	DLC2.3	9.4	-69	DLC2.1P	25.0

Table A8.8. Load effect result data at blade roots in fault conditions (continue).

Load Effects		Shear Force			Bending Moment			Axial Force			Torsional Moment		
		Value (kN)	DLC (-)	Vs (m/s)	Value (kN m)	DLC (-)	Vs (m/s)	Value (kN)	DLC (-)	Vs (m/s)	Value (kN m)	DLC (-)	Vs (m/s)
Model		5MW2UBUTT2C0TipBrk											
Maximums	Max	579	DLC2.3	25.0	18919	DLC2.3	11.4	1716	DLC2.3	25.0	611	DLC2.3	11.4
	Min	0	DLC2.3	11.4	1	DLC2.3	11.4	-178	DLC2.3	25.0	-489	DLC2.3	25.0
Averages	Max	244	DLC2.3	11.4	6938	DLC2.3	11.4	487	DLC2.3	25.0	5	DLC2.3	11.4
	Min	93	DLC2.3	25.0	2378	DLC2.3	25.0	92	DLC2.3	9.4	-55	DLC2.1P	25.0

Table A8.9. Load effect result data at blade roots in parked conditions.

Load Effects		Shear Force			Bending Moment			Axial Force			Torsional Moment		
		Value (kN)	DLC (-)	Vs (m/s)	Value (kN m)	DLC (-)	Vs (m/s)	Value (kN)	DLC (-)	Vs (m/s)	Value (kN m)	DLC (-)	Vs (m/s)
Model		5MW3UB00											
Maximums	Max	288	DLC6.2a	37.4	7696	DLC6.2a	37.4	149	DLC7.1a	25.0	179	DLC6.2a	37.4
	Min	15	DLC6.2a	37.4	192	DLC6.3a	25.0	-183	DLC6.2a	37.4	-202	DLC6.2a	37.4
Averages	Max	282	DLC6.2a	37.4	7514	DLC6.2a	37.4	149	DLC7.1a	25.0	176	DLC6.2a	37.4
	Min	22	DLC6.3a	25.0	261	DLC6.3a	25.0	-183	DLC6.2a	37.4	-194	DLC6.2a	37.4
Model		5MW2UB00											
Maximums	Max	233	DLC7.1a	25.0	6204	DLC6.2a	37.4	6	DLC6.2a	37.4	6	DLC6.2a	37.4
	Min	86	DLC6.2a	37.4	1211	DLC6.1a	37.4	-10	DLC6.2a	37.4	-185	DLC6.2a	37.4
Averages	Max	232	DLC7.1a	25.0	5329	DLC7.1a	25.0	3	DLC6.2a	37.4	4	DLC6.2a	37.4
	Min	87	DLC6.2a	37.4	1236	DLC6.1a	37.4	-4	DLC6.2a	37.4	-147	DLC6.2a	37.4
Model		5MW2IB00TipBrk											
Maximums	Max	234	DLC7.1a	25.0	6390	DLC6.2a	37.4	6	DLC6.2a	37.4	8	DLC6.2a	37.4
	Min	87	DLC6.2a	37.4	1259	DLC6.1a	37.4	-9	DLC6.2a	37.4	-188	DLC6.2a	37.4
Averages	Max	233	DLC7.1a	25.0	5377	DLC7.1a	25.0	2	DLC6.2a	37.4	4	DLC6.2a	37.4
	Min	88	DLC6.2a	37.4	1280	DLC6.1a	37.4	-3	DLC6.2a	37.4	-146	DLC6.2a	37.4
Model		5MW2UBUT											
Maximums	Max	230	DLC7.1a	25.0	6711	DLC6.2a	37.4	5	DLC6.2a	37.4	23	DLC6.2a	37.4
	Min	104	DLC6.1a	37.4	782	DLC6.2a	37.4	-8	DLC6.2a	37.4	-178	DLC6.2a	37.4
Averages	Max	229	DLC7.1a	25.0	5266	DLC7.1a	25.0	1	DLC6.2a	37.4	3	DLC6.2a	37.4
	Min	104	DLC6.1a	37.4	803	DLC6.2a	37.4	-3	DLC6.2a	37.4	-135	DLC6.2a	37.4
Model		5MW2UBUTTipBrk											
Maximums	Max	234	DLC6.2a	37.4	7011	DLC6.2a	37.4	5	DLC6.2a	37.4	27	DLC6.2a	37.4
	Min	104	DLC6.1a	37.4	831	DLC6.2a	37.4	-9	DLC6.2a	37.4	-182	DLC6.2a	37.4
Averages	Max	230	DLC7.1a	25.0	5303	DLC7.1a	25.0	1	DLC6.2a	37.4	3	DLC6.2a	37.4
	Min	105	DLC6.1a	37.4	851	DLC6.2a	37.4	-2	DLC6.2a	37.4	-134	DLC6.2a	37.4
Model		5MW2DB00											
Maximums	Max	268	DLC7.1a	25.0	6868	DLC7.1a	25.0	5	DLC7.1a	25.0	13	DLC6.2a	37.4
	Min	145	DLC6.2a	37.4	2728	DLC6.2a	37.4	-10	DLC7.1a	25.0	-178	DLC6.2a	37.4
Averages	Max	265	DLC6.1a	37.4	5957	DLC6.1a	37.4	1	DLC7.1a	25.0	4	DLC6.2a	37.4
	Min	167	DLC6.2a	37.4	3446	DLC6.2a	37.4	-5	DLC7.1a	25.0	-148	DLC6.2a	37.4
Model		5MW2DB00TipBrk											
Maximums	Max	267	DLC6.1a	37.4	6832	DLC7.1a	25.0	5	DLC7.1a	25.0	9	DLC6.2a	37.4
	Min	145	DLC6.2a	37.4	2711	DLC6.2a	37.4	-10	DLC7.1a	25.0	-182	DLC6.2a	37.4
Averages	Max	266	DLC6.1a	37.4	6006	DLC6.1a	37.4	1	DLC7.1a	25.0	4	DLC6.2a	37.4
	Min	168	DLC6.2a	37.4	3506	DLC6.2a	37.4	-5	DLC7.1a	25.0	-148	DLC6.2a	37.4
Model		5MW2DBUT											
Maximums	Max	273	DLC7.1a	25.0	7149	DLC7.1a	25.0	14	DLC7.1a	25.0	25	DLC6.2a	37.4
	Min	146	DLC6.2a	37.4	2891	DLC6.2a	37.4	-19	DLC7.1a	25.0	-173	DLC6.2a	37.4
Averages	Max	247	DLC6.1a	37.4	6382	DLC6.1a	37.4	6	DLC7.1a	25.0	3	DLC6.2a	37.4
	Min	169	DLC6.2a	37.4	3525	DLC6.2a	37.4	-10	DLC7.1a	25.0	-135	DLC6.2a	37.4
Model		5MW2DBUTTipBrk											
Maximums	Max	272	DLC7.1a	25.0	7177	DLC7.1a	25.0	14	DLC7.1a	25.0	30	DLC6.2a	37.4
	Min	148	DLC6.2a	37.4	2966	DLC6.2a	37.4	-19	DLC7.1a	25.0	-177	DLC6.2a	37.4
Averages	Max	247	DLC6.1a	37.4	6432	DLC6.1a	37.4	6	DLC7.1a	25.0	4	DLC6.2a	37.4
	Min	170	DLC6.2a	37.4	3584	DLC6.2a	37.4	-10	DLC7.1a	25.0	-135	DLC6.2a	37.4
Model		5MW2DB00T5C0											
Maximums	Max	266	DLC6.1a	37.4	6804	DLC7.1a	25.0	5	DLC7.1a	25.0	9	DLC6.2a	37.4
	Min	143	DLC6.2a	37.4	2243	DLC6.2a	37.4	-9	DLC7.1a	25.0	-178	DLC6.2a	37.4
Averages	Max	266	DLC6.1a	37.4	5994	DLC6.1a	37.4	2	DLC7.1a	25.0	4	DLC6.2a	37.4
	Min	167	DLC6.2a	37.4	3443	DLC6.2a	37.4	-5	DLC7.1a	25.0	-148	DLC6.2a	37.4

Table A8.9. Load effect result data at blade roots in parked conditions (continue).

Load Effects		Shear Force			Bending Moment			Axial Force			Torsional Moment		
		Value (kN)	DLC (-)	Vs (m/s)	Value (kN m)	DLC (-)	Vs (m/s)	Value (kN)	DLC (-)	Vs (m/s)	Value (kN m)	DLC (-)	Vs (m/s)
Model		5MW2DB00T5C0TipBrk											
Maximums	Max	267	DLC6.1a	37.4	6806	DLC7.1a	25.0	6	DLC7.1a	25.0	14	DLC6.2a	37.4
	Min	141	DLC6.2a	37.4	2190	DLC6.2a	37.4	-9	DLC7.1a	25.0	-182	DLC6.2a	37.4
Averages	Max	267	DLC6.1a	37.4	6044	DLC6.1a	37.4	2	DLC7.1a	25.0	4	DLC6.2a	37.4
	Min	168	DLC6.2a	37.4	3503	DLC6.2a	37.4	-5	DLC7.1a	25.0	-148	DLC6.2a	37.4
Model		5MW2DB00T0C2.5											
Maximums	Max	234	DLC6.2a	37.4	6630	DLC6.2a	37.4	6	DLC6.2a	37.4	5	DLC6.2a	37.4
	Min	139	DLC6.1a	37.4	2806	DLC6.2a	37.4	-5	DLC6.2a	37.4	-188	DLC6.2a	37.4
Averages	Max	222	DLC7.1a	25.0	5102	DLC7.1a	25.0	2	DLC6.2a	37.4	3	DLC6.2a	37.4
	Min	139	DLC6.1a	37.4	3115	DLC6.1a	37.4	-2	DLC6.2a	37.4	-110	DLC6.2a	37.4
Model		5MW2DB00T0C2.5TipBrk											
Maximums	Max	228	DLC6.2a	37.4	6610	DLC6.2a	37.4	6	DLC6.2a	37.4	6	DLC6.2a	37.4
	Min	139	DLC6.1a	37.4	2747	DLC6.2a	37.4	-6	DLC6.2a	37.4	-194	DLC6.2a	37.4
Averages	Max	223	DLC7.1a	25.0	5139	DLC7.1a	25.0	3	DLC6.2a	37.4	3	DLC6.2a	37.4
	Min	140	DLC6.1a	37.4	3160	DLC6.1a	37.4	-3	DLC6.2a	37.4	-110	DLC6.2a	37.4
Model		5MW2DB00T0C0											
Maximums	Max	235	DLC6.2a	37.4	6651	DLC6.2a	37.4	5	DLC6.2a	37.4	18	DLC6.2a	37.4
	Min	139	DLC6.1a	37.4	2418	DLC6.2a	37.4	-6	DLC6.2a	37.4	-186	DLC6.2a	37.4
Averages	Max	222	DLC7.1a	25.0	5103	DLC7.1a	25.0	2	DLC6.2a	37.4	2	DLC6.2a	37.4
	Min	139	DLC6.1a	37.4	3118	DLC6.2a	37.4	-2	DLC6.2a	37.4	-110	DLC6.2a	37.4
Model		5MW2DB00T0C0TipBrk											
Maximums	Max	229	DLC6.2a	37.4	6597	DLC6.2a	37.4	5	DLC6.2a	37.4	7	DLC6.2a	37.4
	Min	139	DLC6.1a	37.4	2422	DLC6.2a	37.4	-6	DLC6.2a	37.4	-194	DLC6.2a	37.4
Averages	Max	223	DLC7.1a	25.0	5141	DLC7.1a	25.0	3	DLC6.2a	37.4	3	DLC6.2a	37.4
	Min	140	DLC6.1a	37.4	3156	DLC6.2a	37.4	-3	DLC6.2a	37.4	-110	DLC6.2a	37.4
Model		5MW2DB00TeeterNo											
Maximums	Max	267	DLC7.1a	25.0	6855	DLC7.1a	25.0	5	DLC7.1a	25.0	7	DLC6.2a	37.4
	Min	145	DLC6.2a	37.4	2679	DLC6.2a	37.4	-10	DLC7.1a	25.0	-180	DLC6.2a	37.4
Averages	Max	265	DLC6.1a	37.4	5957	DLC6.1a	37.4	1	DLC7.1a	25.0	4	DLC6.2a	37.4
	Min	167	DLC6.2a	37.4	3433	DLC6.2a	37.4	-5	DLC7.1a	25.0	-148	DLC6.2a	37.4
Model		5MW2UBUTT2C0TipBrk											
Maximums	Max	242	DLC6.2a	37.4	7265	DLC6.2a	37.4	4	DLC6.2a	37.4	11	DLC6.2a	37.4
	Min	144	DLC6.2a	37.4	2304	DLC6.2a	37.4	-5	DLC6.2a	37.4	-153	DLC6.2a	37.4
Averages	Max	216	DLC7.1a	25.0	4985	DLC7.1a	25.0	1	DLC6.2a	37.4	3	DLC6.2a	37.4
	Min	171	DLC6.2a	37.4	3603	DLC6.2a	37.4	-2	DLC6.1a	37.4	-108	DLC6.2a	37.4

Table A8.10. Load effect result data at LSS in normal operating conditions.

Load Effects		Shear Force			Bending Moment			Axial Force			Torsional Moment		
		Value (kN)	DLC (-)	Vs (m/s)	Value (kN m)	DLC (-)	Vs (m/s)	Value (kN)	DLC (-)	Vs (m/s)	Value (kN m)	DLC (-)	Vs (m/s)
Model		5MW3UB00											
Maximums	Max	1128	DLC1.3	25.0	13417	DLC1.4	11.4	1091	DLC1.3	15.0	5549	DLC1.3	25.0
	Min	975	DLC1.3	25.0	4	DLC1.3	23.0	-39	DLC1.3	25.0	-9	DLC1.3	3.0
Averages	Max	1085	DLC1.4	13.4	4924	DLC1.4	9.4	790	DLC1.5V	11.0	4189	DLC1.3	25.0
	Min	1054	DLC1.5H	25.0	1008	DLC1.3	21.0	170	DLC1.3	3.0	57	DLC1.3	3.0
Model		5MW2UB00											
Maximums	Max	1005	DLC1.3	25.0	8572	DLC1.4	11.4	1023	DLC1.3	15.0	4458	DLC1.3	25.0
	Min	811	DLC1.4	11.4	5	DLC1.4	13.4	-44	DLC1.4	9.4	0	DLC1.4	9.4
Averages	Max	914	DLC1.4	13.4	3537	DLC1.4	9.4	693	DLC1.5V	11.0	3168	DLC1.3	25.0
	Min	892	DLC1.5H	25.0	1554	DLC1.3	21.0	140	DLC1.3	3.0	85	DLC1.3	3.0
Model		5MW2IB00TipBrk											
Maximums	Max	1007	DLC1.3	25.0	8581	DLC1.4	11.4	1028	DLC1.3	15.0	4471	DLC1.3	25.0
	Min	806	DLC1.4	11.4	6	DLC1.3	23.0	-38	DLC1.3	25.0	0	DLC1.1	3.0
Averages	Max	916	DLC1.4	13.4	3508	DLC1.4	9.4	694	DLC1.5V	11.0	3168	DLC1.3	25.0
	Min	894	DLC1.5H	25.0	1557	DLC1.3	21.0	140	DLC1.3	3.0	85	DLC1.3	3.0
Model		5MW2UBUT											
Maximums	Max	1001	DLC1.3	25.0	11852	DLC1.4	11.4	1114	DLC1.3	15.0	4489	DLC1.3	25.0
	Min	745	DLC1.4	11.4	5	DLC1.3	21.0	-65	DLC1.4	9.4	-1	DLC1.3	3.0
Averages	Max	914	DLC1.4	13.4	4496	DLC1.4	9.4	784	DLC1.5V	11.0	3198	DLC1.3	25.0
	Min	889	DLC1.4	9.4	1546	DLC1.3	21.0	157	DLC1.3	3.0	77	DLC1.3	3.0

Table A8.10. Load effect result data at LSS in normal operating conditions (continue).

Load Effects		Shear Force			Bending Moment			Axial Force			Torsional Moment		
		Value (kN)	DLC (-)	Vs (m/s)	Value (kN m)	DLC (-)	Vs (m/s)	Value (kN)	DLC (-)	Vs (m/s)	Value (kN m)	DLC (-)	Vs (m/s)
Model		5MW2UBUTTipBrk											
Maximums	Max	1004	DLC1.3	25.0	11988	DLC1.4	11.4	1117	DLC1.3	15.0	4519	DLC1.3	25.0
	Min	759	DLC1.4	11.4	5	DLC1.3	23.0	-67	DLC1.4	9.4	-1	DLC1.3	3.0
Averages	Max	915	DLC1.4	13.4	4477	DLC1.4	9.4	785	DLC1.5V	11.0	3198	DLC1.3	25.0
	Min	891	DLC1.4	9.4	1549	DLC1.3	21.0	157	DLC1.3	3.0	77	DLC1.3	3.0
Model		5MW2DB00											
Maximums	Max	1081	DLC1.3	25.0	9083	DLC1.4	9.4	842	DLC1.3	15.0	5005	DLC1.3	25.0
	Min	757	DLC1.4	9.4	4	DLC1.3	9.0	-224	DLC1.3	25.0	0	DLC1.3	3.0
Averages	Max	922	DLC1.3	25.0	3472	DLC1.4	9.4	504	DLC1.5H	11.0	3167	DLC1.3	25.0
	Min	896	DLC1.4	9.4	1009	DLC1.3	7.0	-19	DLC1.3	3.0	80	DLC1.3	3.0
Model		5MW2DB00TipBrk											
Maximums	Max	1080	DLC1.3	25.0	9052	DLC1.4	9.4	847	DLC1.3	15.0	5145	DLC1.3	25.0
	Min	799	DLC1.4	11.4	4	DLC1.3	9.0	-222	DLC1.3	25.0	0	DLC1.3	3.0
Averages	Max	924	DLC1.3	25.0	3432	DLC1.4	9.4	506	DLC1.5H	11.0	3167	DLC1.3	25.0
	Min	897	DLC1.4	9.4	1005	DLC1.3	7.0	-19	DLC1.3	3.0	80	DLC1.3	3.0
Model		5MW2DBUT											
Maximums	Max	1074	DLC1.3	25.0	11532	DLC1.4	11.4	935	DLC1.3	15.0	4983	DLC1.3	25.0
	Min	756	DLC1.4	9.4	5	DLC1.3	11.0	-247	DLC1.4	9.4	-2	DLC1.3	3.0
Averages	Max	922	DLC1.3	25.0	4237	DLC1.4	9.4	593	DLC1.5V	11.0	3199	DLC1.3	25.0
	Min	891	DLC1.4	9.4	1008	DLC1.3	5.0	-2	DLC1.3	3.0	75	DLC1.3	3.0
Model		5MW2DBUTTipBrk											
Maximums	Max	1081	DLC1.3	25.0	11526	DLC1.4	11.4	938	DLC1.3	15.0	5089	DLC1.3	25.0
	Min	685	DLC1.4	9.4	6	DLC1.3	7.0	-248	DLC1.4	9.4	-2	DLC1.3	3.0
Averages	Max	924	DLC1.3	25.0	4220	DLC1.4	9.4	594	DLC1.5V	11.0	3199	DLC1.3	25.0
	Min	893	DLC1.4	9.4	1006	DLC1.3	5.0	-2	DLC1.3	3.0	75	DLC1.3	3.0
Model		5MW2DB00T5C0											
Maximums	Max	1086	DLC1.3	25.0	8742	DLC1.4	9.4	856	DLC1.3	15.0	5091	DLC1.3	25.0
	Min	769	DLC1.4	9.4	5	DLC1.3	11.0	-231	DLC1.3	25.0	0	DLC1.1	3.0
Averages	Max	921	DLC1.3	25.0	3360	DLC1.4	9.4	512	DLC1.5H	11.0	3167	DLC1.3	25.0
	Min	897	DLC1.4	9.4	1242	DLC1.3	7.0	-19	DLC1.3	3.0	81	DLC1.3	3.0
Model		5MW2DB00T5C0TipBrk											
Maximums	Max	1086	DLC1.3	25.0	8710	DLC1.4	9.4	861	DLC1.3	15.0	5228	DLC1.3	25.0
	Min	810	DLC1.4	11.4	4	DLC1.3	9.0	-228	DLC1.3	25.0	0	DLC1.1	3.0
Averages	Max	922	DLC1.3	25.0	3328	DLC1.4	9.4	513	DLC1.5H	11.0	3167	DLC1.3	25.0
	Min	898	DLC1.4	9.4	1241	DLC1.3	7.0	-19	DLC1.3	3.0	82	DLC1.3	3.0
Model		5MW2DB00T0C2.5											
Maximums	Max	1064	DLC1.4	9.4	8839	DLC1.4	9.4	925	DLC1.3	15.0	5106	DLC1.3	25.0
	Min	735	DLC1.4	9.4	5	DLC1.3	9.0	-158	DLC1.3	25.0	0	DLC1.3	3.0
Averages	Max	920	DLC1.4	13.4	3420	DLC1.4	9.4	586	DLC1.5H	11.0	3167	DLC1.3	25.0
	Min	898	DLC1.4	9.4	1040	DLC1.3	7.0	60	DLC1.3	3.0	80	DLC1.3	3.0
Model		5MW2DB00T0C2.5TipBrk											
Maximums	Max	1063	DLC1.3	25.0	8857	DLC1.4	9.4	930	DLC1.3	15.0	5269	DLC1.3	25.0
	Min	813	DLC1.4	11.4	6	DLC1.3	25.0	-157	DLC1.3	25.0	0	DLC1.3	3.0
Averages	Max	921	DLC1.4	13.4	3381	DLC1.4	9.4	587	DLC1.5H	11.0	3167	DLC1.3	25.0
	Min	899	DLC1.4	9.4	1037	DLC1.3	7.0	60	DLC1.3	3.0	80	DLC1.3	3.0
Model		5MW2DB00T0C0											
Maximums	Max	1069	DLC1.3	25.0	8590	DLC1.4	9.4	937	DLC1.3	15.0	5235	DLC1.3	25.0
	Min	753	DLC1.4	9.4	4	DLC1.3	23.0	-169	DLC1.3	25.0	0	DLC1.3	3.0
Averages	Max	921	DLC1.4	13.4	3308	DLC1.4	9.4	594	DLC1.5H	11.0	3167	DLC1.3	25.0
	Min	899	DLC1.4	9.4	1293	DLC1.3	7.0	60	DLC1.3	3.0	81	DLC1.3	3.0
Model		5MW2DB00T0C0TipBrk											
Maximums	Max	1072	DLC1.3	25.0	8602	DLC1.4	9.4	942	DLC1.3	15.0	5391	DLC1.3	25.0
	Min	815	DLC1.3	25.0	7	DLC1.3	23.0	-166	DLC1.3	25.0	0	DLC1.3	3.0
Averages	Max	922	DLC1.4	13.4	3278	DLC1.4	9.4	596	DLC1.5H	11.0	3167	DLC1.3	25.0
	Min	900	DLC1.4	9.4	1293	DLC1.3	7.0	60	DLC1.3	3.0	81	DLC1.3	3.0
Model		5MW2DB00TeeterNo											
Maximums	Max	1073	DLC1.3	25.0	13073	DLC1.4	11.4	847	DLC1.3	15.0	4956	DLC1.3	25.0
	Min	782	DLC1.4	11.4	4	DLC1.3	7.0	-240	DLC1.3	25.0	0	DLC1.1	3.0
Averages	Max	924	DLC1.3	25.0	4674	DLC1.4	11.4	505	DLC1.5V	11.0	3167	DLC1.3	25.0
	Min	891	DLC1.4	9.4	1010	DLC1.3	5.0	-19	DLC1.3	3.0	81	DLC1.3	3.0

Table A8.10. Load effect result data at LSS in normal operating conditions (continue).

Load Effects		Shear Force			Bending Moment			Axial Force			Torsional Moment		
		Value (kN)	DLC (-)	Vs (m/s)	Value (kN m)	DLC (-)	Vs (m/s)	Value (kN)	DLC (-)	Vs (m/s)	Value (kN m)	DLC (-)	Vs (m/s)
Model		5MW2UBUTT2C0TipBrk											
Maximums	Max	1077	DLC1.3	25.0	10826	DLC1.4	11.4	1000	DLC1.3	15.0	5272	DLC1.3	25.0
	Min	716	DLC1.4	9.4	6	DLC1.3	9.0	-204	DLC1.4	9.4	-2	DLC1.3	3.0
Averages	Max	921	DLC1.4	13.4	4122	DLC1.4	9.4	653	DLC1.5V	11.0	3199	DLC1.3	25.0
	Min	896	DLC1.4	9.4	1242	DLC1.3	7.0	46	DLC1.3	3.0	75	DLC1.3	3.0

Table A8.11. Load effect result data at LSS in fault conditions.

Load Effects		Shear Force			Bending Moment			Axial Force			Torsional Moment		
		Value (kN)	DLC (-)	Vs (m/s)	Value (kN m)	DLC (-)	Vs (m/s)	Value (kN)	DLC (-)	Vs (m/s)	Value (kN m)	DLC (-)	Vs (m/s)
Model		5MW3UB00											
Maximums	Max	1153	DLC2.1P	25.0	13018	DLC2.1P	25.0	1219	DLC2.3	11.4	7142	DLC2.1P	25.0
	Min	854	DLC2.1P	25.0	22	DLC2.3	25.0	-778	DLC2.3	25.0	-2215	DLC2.3	9.4
Averages	Max	1070	DLC2.1G	11.4	2581	DLC2.3	9.4	278	DLC2.1P	11.4	2149	DLC2.1P	25.0
	Min	1006	DLC2.1P	25.0	2148	DLC2.1P	11.4	174	DLC2.1G	25.0	940	DLC2.1G	25.0
Model		5MW2UB00											
Maximums	Max	1103	DLC2.1P	25.0	17106	DLC2.1P	25.0	1066	DLC2.3	13.4	5924	DLC2.1P	25.0
	Min	581	DLC2.1P	25.0	29	DLC2.1G	25.0	-831	DLC2.3	25.0	-1812	DLC2.3	25.0
Averages	Max	933	DLC2.1P	25.0	3786	DLC2.1P	25.0	267	DLC2.3	11.4	2639	DLC2.1P	25.0
	Min	890	DLC2.3	13.4	1952	DLC2.1G	11.4	152	DLC2.1G	25.0	680	DLC2.1G	25.0
Model		5MW2IB00TipBrk											
Maximums	Max	1009	DLC2.1P	25.0	7310	DLC2.1P	25.0	1266	DLC2.3	25.0	6337	DLC2.1P	25.0
	Min	761	DLC2.1P	25.0	33	DLC2.1P	25.0	-301	DLC2.3	25.0	-1806	DLC2.3	25.0
Averages	Max	915	DLC2.1P	25.0	3034	DLC2.1P	25.0	318	DLC2.3	11.4	2880	DLC2.1P	25.0
	Min	874	DLC2.3	25.0	1767	DLC2.1P	11.4	216	DLC2.3	9.4	769	DLC2.3	9.4
Model		5MW2UBUT											
Maximums	Max	1100	DLC2.1P	25.0	15613	DLC2.1P	25.0	1161	DLC2.3	11.4	6009	DLC2.1P	25.0
	Min	641	DLC2.1P	25.0	51	DLC2.1P	25.0	-771	DLC2.3	25.0	-1668	DLC2.3	25.0
Averages	Max	900	DLC2.1P	11.4	2556	DLC2.1P	25.0	297	DLC2.3	11.4	2384	DLC2.1P	25.0
	Min	865	DLC2.3	25.0	1941	DLC2.1G	11.4	151	DLC2.1G	25.0	845	DLC2.3	9.4
Model		5MW2UBUTTipBrk											
Maximums	Max	1028	DLC2.1P	25.0	7194	DLC2.1P	25.0	1187	DLC2.3	11.4	6357	DLC2.1P	25.0
	Min	765	DLC2.1G	25.0	17	DLC2.1G	25.0	-212	DLC2.3	25.0	-1818	DLC2.3	9.4
Averages	Max	916	DLC2.1P	25.0	3085	DLC2.1P	25.0	350	DLC2.3	11.4	3022	DLC2.1P	25.0
	Min	873	DLC2.3	25.0	1774	DLC2.1P	11.4	231	DLC2.3	25.0	808	DLC2.3	9.4
Model		5MW2DB00											
Maximums	Max	1117	DLC2.1P	25.0	14296	DLC2.1P	25.0	910	DLC2.3	13.4	6214	DLC2.1P	25.0
	Min	643	DLC2.1P	25.0	8	DLC2.3	25.0	-974	DLC2.3	25.0	-1845	DLC2.1P	25.0
Averages	Max	974	DLC2.1P	25.0	3331	DLC2.1P	25.0	100	DLC2.3	11.4	1553	DLC2.1P	25.0
	Min	904	DLC2.3	9.4	1303	DLC2.3	9.4	-11	DLC2.1G	25.0	729	DLC2.3	9.4
Model		5MW2DB00TipBrk											
Maximums	Max	1073	DLC2.1G	25.0	6349	DLC2.1G	25.0	1100	DLC2.3	25.0	6584	DLC2.1P	25.0
	Min	775	DLC2.1P	25.0	4	DLC2.3	11.4	-438	DLC2.3	25.0	-2395	DLC2.3	25.0
Averages	Max	937	DLC2.1P	25.0	2708	DLC2.1P	25.0	154	DLC2.3	11.4	2922	DLC2.1P	25.0
	Min	902	DLC2.1P	25.0	1223	DLC2.1P	11.4	52	DLC2.3	9.4	723	DLC2.3	9.4
Model		5MW2DBUT											
Maximums	Max	1175	DLC2.1P	25.0	15931	DLC2.1P	25.0	966	DLC2.3	11.4	6365	DLC2.1P	25.0
	Min	698	DLC2.1P	25.0	8	DLC2.3	13.4	-948	DLC2.3	25.0	-1942	DLC2.3	25.0
Averages	Max	941	DLC2.3	25.0	2786	DLC2.1P	25.0	129	DLC2.3	11.4	2331	DLC2.1P	25.0
	Min	904	DLC2.3	13.4	1283	DLC2.3	9.4	-10	DLC2.1G	25.0	788	DLC2.3	9.4
Model		5MW2DBUTTipBrk											
Maximums	Max	1079	DLC2.3	9.4	5884	DLC2.1G	25.0	995	DLC2.3	11.4	6644	DLC2.1P	25.0
	Min	772	DLC2.3	9.4	16	DLC2.3	25.0	-440	DLC2.3	25.0	-2121	DLC2.3	25.0
Averages	Max	937	DLC2.1P	25.0	2662	DLC2.1P	25.0	184	DLC2.3	11.4	2973	DLC2.1P	25.0
	Min	905	DLC2.3	13.4	1204	DLC2.3	9.4	67	DLC2.3	25.0	801	DLC2.3	9.4
Model		5MW2DB00T5C0											
Maximums	Max	1115	DLC2.1P	25.0	14530	DLC2.1P	25.0	926	DLC2.3	13.4	6269	DLC2.1P	25.0
	Min	639	DLC2.1P	25.0	5	DLC2.3	25.0	-986	DLC2.3	25.0	-1954	DLC2.3	25.0
Averages	Max	974	DLC2.1P	25.0	3510	DLC2.1P	25.0	102	DLC2.3	11.4	1550	DLC2.1P	25.0
	Min	904	DLC2.3	9.4	1612	DLC2.3	11.4	-11	DLC2.1G	25.0	733	DLC2.3	9.4

Table A8.11. Load effect result data at LSS in fault conditions (continue).

Load Effects		Shear Force			Bending Moment			Axial Force			Torsional Moment		
		Value (kN)	DLC (-)	Vs (m/s)	Value (kN m)	DLC (-)	Vs (m/s)	Value (kN)	DLC (-)	Vs (m/s)	Value (kN m)	DLC (-)	Vs (m/s)
Model		5MW2DB00T5C0TipBrk											
Maximums	Max	1074	DLC2.1G	25.0	6495	DLC2.1G	25.0	1121	DLC2.3	25.0	6641	DLC2.1P	25.0
	Min	780	DLC2.1P	25.0	19	DLC2.1G	11.4	-451	DLC2.3	25.0	-2438	DLC2.3	25.0
Averages	Max	936	DLC2.1P	25.0	2913	DLC2.1P	25.0	156	DLC2.3	11.4	2882	DLC2.1P	25.0
	Min	903	DLC2.1P	25.0	1472	DLC2.1P	11.4	53	DLC2.3	9.4	725	DLC2.3	9.4
Model		5MW2DB00T0C2.5											
Maximums	Max	1097	DLC2.1P	25.0	15661	DLC2.1P	25.0	989	DLC2.3	13.4	6307	DLC2.1P	25.0
	Min	623	DLC2.1P	25.0	5	DLC2.3	25.0	-903	DLC2.3	25.0	-1901	DLC2.3	25.0
Averages	Max	960	DLC2.1P	25.0	3223	DLC2.1P	25.0	180	DLC2.3	11.4	2134	DLC2.1P	25.0
	Min	905	DLC2.3	13.4	1344	DLC2.3	9.4	69	DLC2.1G	25.0	725	DLC2.3	9.4
Model		5MW2DB00T0C2.5TipBrk											
Maximums	Max	1044	DLC2.1P	25.0	6151	DLC2.1P	25.0	1191	DLC2.3	25.0	6698	DLC2.1P	25.0
	Min	785	DLC2.1P	25.0	4	DLC2.3	25.0	-356	DLC2.3	25.0	-2451	DLC2.3	25.0
Averages	Max	926	DLC2.1P	25.0	2562	DLC2.1P	25.0	234	DLC2.3	11.4	2750	DLC2.1P	25.0
	Min	900	DLC2.1P	25.0	1219	DLC2.1P	11.4	132	DLC2.3	9.4	722	DLC2.3	9.4
Model		5MW2DB00T0C0											
Maximums	Max	1097	DLC2.1P	25.0	15851	DLC2.1P	25.0	1004	DLC2.3	13.4	6433	DLC2.1P	25.0
	Min	616	DLC2.1P	25.0	3	DLC2.3	25.0	-915	DLC2.3	25.0	-2023	DLC2.3	25.0
Averages	Max	960	DLC2.1P	25.0	3407	DLC2.1P	25.0	182	DLC2.3	11.4	2144	DLC2.1P	25.0
	Min	905	DLC2.3	13.4	1644	DLC2.3	11.4	69	DLC2.1G	25.0	733	DLC2.3	9.4
Model		5MW2DB00T0C0TipBrk											
Maximums	Max	1048	DLC2.1P	25.0	6888	DLC2.1P	25.0	1211	DLC2.3	25.0	6742	DLC2.1P	25.0
	Min	788	DLC2.1P	25.0	14	DLC2.3	25.0	-369	DLC2.3	25.0	-2508	DLC2.3	25.0
Averages	Max	924	DLC2.1P	25.0	2799	DLC2.1P	25.0	236	DLC2.3	11.4	2803	DLC2.1P	25.0
	Min	900	DLC2.1P	25.0	1476	DLC2.1P	11.4	133	DLC2.3	9.4	728	DLC2.3	9.4
Model		5MW2DB00TeeterNo											
Maximums	Max	1128	DLC2.1P	25.0	18026	DLC2.1P	25.0	917	DLC2.3	13.4	6101	DLC2.1P	25.0
	Min	584	DLC2.1P	25.0	3	DLC2.3	25.0	-971	DLC2.3	25.0	-1781	DLC2.3	25.0
Averages	Max	974	DLC2.1P	25.0	3608	DLC2.1P	25.0	101	DLC2.3	11.4	1557	DLC2.1P	25.0
	Min	903	DLC2.3	9.4	1291	DLC2.3	9.4	-11	DLC2.1G	25.0	726	DLC2.3	9.4
Model		5MW2UBUTT2C0TipBrk											
Maximums	Max	1085	DLC2.3	9.4	6815	DLC2.1P	25.0	1055	DLC2.3	11.4	6772	DLC2.1P	25.0
	Min	768	DLC2.3	9.4	4	DLC2.3	11.4	-412	DLC2.3	25.0	-2200	DLC2.3	25.0
Averages	Max	935	DLC2.1P	25.0	2766	DLC2.1P	25.0	235	DLC2.3	11.4	2959	DLC2.1P	25.0
	Min	899	DLC2.1P	25.0	1490	DLC2.1P	11.4	116	DLC2.3	25.0	806	DLC2.3	9.4

Table A8.12. Load effect result data at LSS in parked conditions.

Load Effects		Shear Force			Bending Moment			Axial Force			Torsional Moment		
		Value (kN)	DLC (-)	Vs (m/s)	Value (kN m)	DLC (-)	Vs (m/s)	Value (kN)	DLC (-)	Vs (m/s)	Value (kN m)	DLC (-)	Vs (m/s)
Model		5MW3UB00											
Maximums	Max	1147	DLC6.2a	37.4	5723	DLC6.2a	37.4	450	DLC6.2a	37.4	2629	DLC6.2a	37.4
	Min	986	DLC6.2a	37.4	99	DLC6.2a	37.4	-333	DLC6.2a	37.4	-2840	DLC6.2a	37.4
Averages	Max	1140	DLC6.2a	37.4	4671	DLC7.1a	25.0	222	DLC7.1a	25.0	2406	DLC6.2a	37.4
	Min	988	DLC6.2a	37.4	1488	DLC6.2a	37.4	51	DLC6.2a	37.4	-2508	DLC6.2a	37.4
Model		5MW2UB00											
Maximums	Max	945	DLC6.2a	37.4	4036	DLC7.1a	25.0	308	DLC6.2a	37.4	1455	DLC7.1a	25.0
	Min	775	DLC6.2a	37.4	1619	DLC6.2a	37.4	-221	DLC6.2a	37.4	-702	DLC6.2a	37.4
Averages	Max	912	DLC6.2a	37.4	3952	DLC7.1a	25.0	199	DLC7.1a	25.0	1409	DLC7.1a	25.0
	Min	776	DLC6.2a	37.4	1625	DLC6.2a	37.4	50	DLC6.2a	37.4	-687	DLC6.2a	37.4
Model		5MW2IB00TipBrk											
Maximums	Max	950	DLC6.2a	37.4	4039	DLC7.1a	25.0	278	DLC6.2a	37.4	1477	DLC7.1a	25.0
	Min	776	DLC6.2a	37.4	1626	DLC6.2a	37.4	-174	DLC6.2a	37.4	-744	DLC6.2a	37.4
Averages	Max	914	DLC6.2a	37.4	3955	DLC7.1a	25.0	199	DLC7.1a	25.0	1423	DLC7.1a	25.0
	Min	778	DLC6.2a	37.4	1632	DLC6.2a	37.4	51	DLC6.2a	37.4	-725	DLC6.2a	37.4
Model		5MW2UBUT											
Maximums	Max	951	DLC6.2a	37.4	4040	DLC7.1a	25.0	302	DLC6.2a	37.4	1734	DLC7.1a	25.0
	Min	767	DLC6.2a	37.4	1592	DLC6.1a	37.4	-218	DLC6.2a	37.4	-677	DLC6.2a	37.4
Averages	Max	911	DLC6.2a	37.4	3952	DLC7.1a	25.0	197	DLC7.1a	25.0	1675	DLC7.1a	25.0
	Min	769	DLC6.2a	37.4	1598	DLC6.1a	37.4	51	DLC6.2a	37.4	-15	DLC6.2a	37.4

Table A8.12. Load effect result data at LSS in parked conditions (continue).

Load Effects		Shear Force			Bending Moment			Axial Force			Torsional Moment		
		Value (kN)	DLC (-)	Vs (m/s)	Value (kN m)	DLC (-)	Vs (m/s)	Value (kN)	DLC (-)	Vs (m/s)	Value (kN m)	DLC (-)	Vs (m/s)
Model		5MW2UBUTTipBrk											
Maximums	Max	952	DLC6.2a	37.4	4044	DLC7.1a	25.0	319	DLC6.2a	37.4	1728	DLC7.1a	25.0
	Min	769	DLC6.2a	37.4	1600	DLC6.1a	37.4	-207	DLC6.2a	37.4	-698	DLC6.2a	37.4
Averages	Max	913	DLC6.2a	37.4	3955	DLC7.1a	25.0	197	DLC7.1a	25.0	1674	DLC7.1a	25.0
	Min	771	DLC6.2a	37.4	1605	DLC6.1a	37.4	51	DLC6.2a	37.4	-17	DLC6.2a	37.4
Model		5MW2DB00											
Maximums	Max	1023	DLC6.2a	37.4	3655	DLC7.1a	25.0	162	DLC6.2a	37.4	1824	DLC7.1a	25.0
	Min	851	DLC6.2a	37.4	1374	DLC6.2a	37.4	-391	DLC6.2a	37.4	-2826	DLC7.1a	25.0
Averages	Max	1021	DLC6.2a	37.4	3554	DLC7.1a	25.0	34	DLC7.1a	25.0	879	DLC6.2a	37.4
	Min	890	DLC6.2a	37.4	1389	DLC6.2a	37.4	-107	DLC6.2a	37.4	-1300	DLC6.2a	37.4
Model		5MW2DB00TipBrk											
Maximums	Max	1024	DLC6.2a	37.4	3684	DLC7.1a	25.0	137	DLC6.2a	37.4	1772	DLC7.1a	25.0
	Min	846	DLC6.2a	37.4	1378	DLC6.2a	37.4	-342	DLC6.2a	37.4	-2826	DLC7.1a	25.0
Averages	Max	1022	DLC6.2a	37.4	3553	DLC7.1a	25.0	34	DLC7.1a	25.0	895	DLC6.2a	37.4
	Min	892	DLC6.2a	37.4	1387	DLC6.2a	37.4	-107	DLC6.2a	37.4	-1320	DLC6.2a	37.4
Model		5MW2DBUT											
Maximums	Max	1030	DLC6.1a	37.4	3661	DLC7.1a	25.0	157	DLC6.2a	37.4	2503	DLC7.1a	25.0
	Min	842	DLC6.2a	37.4	1383	DLC6.2a	37.4	-392	DLC6.2a	37.4	-2972	DLC7.1a	25.0
Averages	Max	1028	DLC6.1a	37.4	3518	DLC7.1a	25.0	34	DLC7.1a	25.0	1546	DLC6.2a	37.4
	Min	891	DLC6.2a	37.4	1389	DLC6.2a	37.4	-107	DLC6.2a	37.4	-579	DLC6.2a	37.4
Model		5MW2DBUTTipBrk											
Maximums	Max	1031	DLC6.1a	37.4	3663	DLC7.1a	25.0	193	DLC6.2a	37.4	2498	DLC7.1a	25.0
	Min	842	DLC6.2a	37.4	1380	DLC6.2a	37.4	-397	DLC6.2a	37.4	-2975	DLC7.1a	25.0
Averages	Max	1030	DLC6.1a	37.4	3516	DLC7.1a	25.0	34	DLC7.1a	25.0	1579	DLC6.2a	37.4
	Min	893	DLC6.2a	37.4	1387	DLC6.2a	37.4	-107	DLC6.2a	37.4	-618	DLC6.2a	37.4
Model		5MW2DB00T5C0											
Maximums	Max	1025	DLC6.2a	37.4	3837	DLC7.1a	25.0	165	DLC6.2a	37.4	1787	DLC7.1a	25.0
	Min	853	DLC6.2a	37.4	1645	DLC6.2a	37.4	-394	DLC6.2a	37.4	-2813	DLC7.1a	25.0
Averages	Max	1024	DLC6.2a	37.4	3738	DLC7.1a	25.0	35	DLC7.1a	25.0	775	DLC6.2a	37.4
	Min	890	DLC6.2a	37.4	1721	DLC6.2a	37.4	-107	DLC6.2a	37.4	-1216	DLC6.2a	37.4
Model		5MW2DB00T5C0TipBrk											
Maximums	Max	1027	DLC6.2a	37.4	3828	DLC7.1a	25.0	133	DLC6.2a	37.4	1729	DLC7.1a	25.0
	Min	848	DLC6.2a	37.4	1641	DLC6.2a	37.4	-343	DLC6.2a	37.4	-2745	DLC7.1a	25.0
Averages	Max	1025	DLC6.2a	37.4	3738	DLC7.1a	25.0	35	DLC7.1a	25.0	792	DLC6.2a	37.4
	Min	892	DLC6.2a	37.4	1724	DLC6.2a	37.4	-107	DLC6.2a	37.4	-1236	DLC6.2a	37.4
Model		5MW2DB00T0C2.5											
Maximums	Max	939	DLC7.1a	25.0	3625	DLC7.1a	25.0	292	DLC6.2a	37.4	1291	DLC6.2a	37.4
	Min	873	DLC6.2a	37.4	1312	DLC6.2a	37.4	-364	DLC6.2a	37.4	-986	DLC6.2a	37.4
Averages	Max	938	DLC7.1a	25.0	3536	DLC7.1a	25.0	116	DLC7.1a	25.0	394	DLC6.2a	37.4
	Min	901	DLC6.2a	37.4	1384	DLC6.2a	37.4	-28	DLC6.2a	37.4	-971	DLC6.2a	37.4
Model		5MW2DB00T0C2.5TipBrk											
Maximums	Max	942	DLC6.2a	37.4	3631	DLC7.1a	25.0	250	DLC6.2a	37.4	1429	DLC6.2a	37.4
	Min	872	DLC6.2a	37.4	1305	DLC6.2a	37.4	-318	DLC6.2a	37.4	-1010	DLC6.2a	37.4
Averages	Max	939	DLC7.1a	25.0	3535	DLC7.1a	25.0	116	DLC7.1a	25.0	415	DLC6.2a	37.4
	Min	902	DLC6.2a	37.4	1383	DLC6.2a	37.4	-28	DLC6.2a	37.4	-992	DLC6.2a	37.4
Model		5MW2DB00T0C0											
Maximums	Max	940	DLC7.1a	25.0	3774	DLC7.1a	25.0	294	DLC6.2a	37.4	1327	DLC6.2a	37.4
	Min	875	DLC6.2a	37.4	1628	DLC6.2a	37.4	-365	DLC6.2a	37.4	-1067	DLC6.2a	37.4
Averages	Max	938	DLC7.1a	25.0	3698	DLC7.1a	25.0	117	DLC7.1a	25.0	394	DLC6.2a	37.4
	Min	902	DLC6.2a	37.4	1729	DLC6.2a	37.4	-28	DLC6.2a	37.4	-975	DLC6.2a	37.4
Model		5MW2DB00T0C0TipBrk											
Maximums	Max	942	DLC7.1a	25.0	3780	DLC7.1a	25.0	253	DLC6.2a	37.4	1416	DLC6.2a	37.4
	Min	873	DLC6.2a	37.4	1619	DLC6.2a	37.4	-320	DLC6.2a	37.4	-1114	DLC6.2a	37.4
Averages	Max	940	DLC7.1a	25.0	3699	DLC7.1a	25.0	117	DLC7.1a	25.0	415	DLC6.2a	37.4
	Min	904	DLC6.2a	37.4	1732	DLC6.2a	37.4	-28	DLC6.2a	37.4	-1004	DLC6.2a	37.4
Model		5MW2DB00TeeterNo											
Maximums	Max	1022	DLC6.2a	37.4	4004	DLC7.1a	25.0	165	DLC6.2a	37.4	1893	DLC7.1a	25.0
	Min	849	DLC6.2a	37.4	1373	DLC6.2a	37.4	-394	DLC6.2a	37.4	-2845	DLC7.1a	25.0
Averages	Max	1021	DLC6.2a	37.4	3548	DLC7.1a	25.0	34	DLC7.1a	25.0	878	DLC6.2a	37.4
	Min	890	DLC6.2a	37.4	1389	DLC6.2a	37.4	-107	DLC6.2a	37.4	-1300	DLC6.2a	37.4

Table A8.12. Load effect result data at LSS in parked conditions (continue).

Load Effects		Shear Force			Bending Moment			Axial Force			Torsional Moment		
		Value (kN)	DLC (-)	Vs (m/s)	Value (kN m)	DLC (-)	Vs (m/s)	Value (kN)	DLC (-)	Vs (m/s)	Value (kN m)	DLC (-)	Vs (m/s)
Model		5MW2UBUTT2C0TipBrk											
Maximums	Max	959	DLC6.1a	37.4	3760	DLC7.1a	25.0	241	DLC6.2a	37.4	1229	DLC6.2a	37.4
	Min	858	DLC6.2a	37.4	1642	DLC6.2a	37.4	-368	DLC6.2a	37.4	-1278	DLC6.2a	37.4
Averages	Max	958	DLC6.1a	37.4	3676	DLC7.1a	25.0	83	DLC7.1a	25.0	1206	DLC6.2a	37.4
	Min	901	DLC6.2a	37.4	1731	DLC6.2a	37.4	-59	DLC6.2a	37.4	-444	DLC6.2a	37.4

Table A8.13. Torque result data in normal operating conditions.

Torques		LSS			HSS			Generator		
		Value (kN m)	DLC (-)	Vs (m/s)	Value (kN m)	DLC (-)	Vs (m/s)	Value (kN m)	DLC (-)	Vs (m/s)
Model		5MW3UB00								
Maximums	Max	5549	DLC1.3	25.0	57	DLC1.3	25.0	47	DLC1.4	11.4
	Min	-9	DLC1.3	3.0	0	DLC1.3	3.0	0	DLC1.3	3.0
Averages	Max	4189	DLC1.3	25.0	43	DLC1.3	25.0	43	DLC1.3	25.0
	Min	57	DLC1.3	3.0	1	DLC1.3	3.0	1	DLC1.3	3.0
Model		5MW2UB00								
Maximums	Max	4458	DLC1.3	25.0	46	DLC1.3	25.0	36	DLC1.3	17.0
	Min	18	DLC1.3	3.0	0	DLC1.3	3.0	0	DLC1.3	3.0
Averages	Max	3168	DLC1.3	25.0	33	DLC1.3	25.0	33	DLC1.3	25.0
	Min	85	DLC1.3	3.0	1	DLC1.3	3.0	1	DLC1.3	3.0
Model		5MW2UB00TipBrk								
Maximums	Max	4471	DLC1.3	25.0	46	DLC1.3	25.0	36	DLC1.3	17.0
	Min	18	DLC1.3	3.0	0	DLC1.3	3.0	0	DLC1.3	3.0
Averages	Max	3168	DLC1.3	25.0	33	DLC1.3	25.0	33	DLC1.3	25.0
	Min	85	DLC1.3	3.0	1	DLC1.3	3.0	1	DLC1.3	3.0
Model		5MW2UBUT								
Maximums	Max	4489	DLC1.3	25.0	46	DLC1.3	25.0	36	DLC1.3	13.0
	Min	10	DLC1.3	3.0	0	DLC1.3	3.0	0	DLC1.3	3.0
Averages	Max	3198	DLC1.3	25.0	33	DLC1.3	25.0	33	DLC1.3	25.0
	Min	77	DLC1.3	3.0	1	DLC1.3	3.0	1	DLC1.3	3.0
Model		5MW2UBUTTipBrk								
Maximums	Max	4519	DLC1.3	25.0	47	DLC1.3	25.0	36	DLC1.3	13.0
	Min	10	DLC1.3	3.0	0	DLC1.3	3.0	0	DLC1.3	3.0
Averages	Max	3198	DLC1.3	25.0	33	DLC1.3	25.0	33	DLC1.3	25.0
	Min	77	DLC1.3	3.0	1	DLC1.3	3.0	1	DLC1.3	3.0
Model		5MW2DB00								
Maximums	Max	5005	DLC1.3	25.0	52	DLC1.3	25.0	36	DLC1.3	21.0
	Min	12	DLC1.3	3.0	0	DLC1.3	3.0	0	DLC1.3	3.0
Averages	Max	3167	DLC1.3	25.0	33	DLC1.3	25.0	33	DLC1.3	25.0
	Min	80	DLC1.3	3.0	1	DLC1.3	3.0	1	DLC1.3	3.0
Model		5MW2DB00TipBrk								
Maximums	Max	5145	DLC1.3	25.0	53	DLC1.3	25.0	36	DLC1.3	21.0
	Min	12	DLC1.3	3.0	0	DLC1.3	3.0	0	DLC1.3	3.0
Averages	Max	3167	DLC1.3	25.0	33	DLC1.3	25.0	33	DLC1.3	25.0
	Min	80	DLC1.3	3.0	1	DLC1.3	3.0	1	DLC1.3	3.0
Model		5MW2DBUT								
Maximums	Max	4983	DLC1.3	25.0	51	DLC1.3	25.0	36	DLC1.3	15.0
	Min	8	DLC1.3	3.0	0	DLC1.3	3.0	0	DLC1.3	3.0
Averages	Max	3199	DLC1.3	25.0	33	DLC1.3	25.0	33	DLC1.3	25.0
	Min	75	DLC1.3	3.0	1	DLC1.3	3.0	1	DLC1.3	3.0
Model		5MW2DBUTTipBrk								
Maximums	Max	5089	DLC1.3	25.0	52	DLC1.3	25.0	36	DLC1.3	15.0
	Min	8	DLC1.3	3.0	0	DLC1.3	3.0	0	DLC1.3	3.0
Averages	Max	3199	DLC1.3	25.0	33	DLC1.3	25.0	33	DLC1.3	25.0
	Min	75	DLC1.3	3.0	1	DLC1.3	3.0	1	DLC1.3	3.0
Model		5MW2DB00T5C0								
Maximums	Max	5091	DLC1.3	25.0	52	DLC1.3	25.0	36	DLC1.3	21.0
	Min	14	DLC1.3	3.0	0	DLC1.3	3.0	0	DLC1.3	3.0
Averages	Max	3167	DLC1.3	25.0	33	DLC1.3	25.0	33	DLC1.3	25.0
	Min	81	DLC1.3	3.0	1	DLC1.3	3.0	1	DLC1.3	3.0

Table A8.13. Torque result data in normal operating conditions (continue).

Torques		LSS			HSS			Generator		
		Value (kN m)	DLC (-)	Vs (m/s)	Value (kN m)	DLC (-)	Vs (m/s)	Value (kN m)	DLC (-)	Vs (m/s)
Model		5MW2DB00T5C0TipBrk								
Maximums	Max	5228	DLC1.3	25.0	54	DLC1.3	25.0	36	DLC1.3	21.0
	Min	14	DLC1.3	3.0	0	DLC1.3	3.0	0	DLC1.3	3.0
Averages	Max	3167	DLC1.3	25.0	33	DLC1.3	25.0	33	DLC1.3	25.0
	Min	82	DLC1.3	3.0	1	DLC1.3	3.0	1	DLC1.3	3.0
Model		5MW2UB00T0C2.5								
Maximums	Max	5106	DLC1.3	25.0	53	DLC1.3	25.0	36	DLC1.3	19.0
	Min	11	DLC1.3	3.0	0	DLC1.3	3.0	0	DLC1.3	3.0
Averages	Max	3167	DLC1.3	25.0	33	DLC1.3	25.0	33	DLC1.3	25.0
	Min	80	DLC1.3	3.0	1	DLC1.3	3.0	1	DLC1.3	3.0
Model		5MW2UB00 T0C2.5TipBrk								
Maximums	Max	5269	DLC1.3	25.0	54	DLC1.3	25.0	36	DLC1.3	19.0
	Min	11	DLC1.3	3.0	0	DLC1.3	3.0	0	DLC1.3	3.0
Averages	Max	3167	DLC1.3	25.0	33	DLC1.3	25.0	33	DLC1.3	25.0
	Min	80	DLC1.3	3.0	1	DLC1.3	3.0	1	DLC1.3	3.0
Model		5MW2UB00T0C0								
Maximums	Max	5235	DLC1.3	25.0	54	DLC1.3	25.0	36	DLC1.3	17.0
	Min	13	DLC1.3	3.0	0	DLC1.3	3.0	0	DLC1.3	3.0
Averages	Max	3167	DLC1.3	25.0	33	DLC1.3	25.0	33	DLC1.3	25.0
	Min	81	DLC1.3	3.0	1	DLC1.3	3.0	1	DLC1.3	3.0
Model		5MW2UB00T0C0TipBrk								
Maximums	Max	5391	DLC1.3	25.0	56	DLC1.3	25.0	36	DLC1.3	19.0
	Min	12	DLC1.3	3.0	0	DLC1.3	3.0	0	DLC1.3	3.0
Averages	Max	3167	DLC1.3	25.0	33	DLC1.3	25.0	33	DLC1.3	25.0
	Min	81	DLC1.3	3.0	1	DLC1.3	3.0	1	DLC1.3	3.0
Model		5MW2DB00TeeterNo								
Maximums	Max	4956	DLC1.3	25.0	51	DLC1.3	25.0	36	DLC1.3	21.0
	Min	13	DLC1.3	3.0	0	DLC1.3	3.0	0	DLC1.3	3.0
Averages	Max	3167	DLC1.3	25.0	33	DLC1.3	25.0	33	DLC1.3	25.0
	Min	81	DLC1.3	3.0	1	DLC1.3	3.0	1	DLC1.3	3.0
Model		5MW2UBUTT2C0TipBrk								
Maximums	Max	5272	DLC1.3	25.0	54	DLC1.3	25.0	36	DLC1.3	15.0
	Min	8	DLC1.3	3.0	0	DLC1.3	3.0	0	DLC1.3	3.0
Averages	Max	3199	DLC1.3	25.0	33	DLC1.3	25.0	33	DLC1.3	25.0
	Min	75	DLC1.3	3.0	1	DLC1.3	3.0	1	DLC1.3	3.0

Table A8.14. Torque result data in fault conditions.

Torques		LSS			HSS			Generator		
		Value (kN m)	DLC (-)	Vs (m/s)	Value (kN m)	DLC (-)	Vs (m/s)	Value (kN m)	DLC (-)	Vs (m/s)
Model		5MW3UB00								
Maximums	Max	7142	DLC2.1P	25.0	74	DLC2.1P	25.0	47	DLC2.1P	25.0
	Min	-2215	DLC2.3	9.4	-23	DLC2.3	9.4	-21	DLC2.1P	25.0
Averages	Max	2149	DLC2.1P	25.0	22	DLC2.1P	25.0	15	DLC2.1P	25.0
	Min	940	DLC2.1G	25.0	10	DLC2.1G	25.0	9	DLC2.1G	11.4
Model		5MW2UB00								
Maximums	Max	5924	DLC2.1P	25.0	61	DLC2.1P	25.0	36	DLC2.1P	25.0
	Min	-1812	DLC2.3	25.0	-19	DLC2.3	25.0	-7	DLC2.1P	25.0
Averages	Max	2639	DLC2.1P	25.0	27	DLC2.1P	25.0	13	DLC2.1P	25.0
	Min	680	DLC2.1G	25.0	7	DLC2.1G	25.0	6	DLC2.3	9.4
Model		5MW2UB00TipBrk								
Maximums	Max	6337	DLC2.1P	25.0	65	DLC2.1P	25.0	36	DLC2.1P	25.0
	Min	-1806	DLC2.3	25.0	-19	DLC2.3	25.0	0	DLC2.1P	11.4
Averages	Max	2880	DLC2.1P	25.0	30	DLC2.1P	25.0	17	DLC2.1P	25.0
	Min	769	DLC2.3	9.4	8	DLC2.3	9.4	5	DLC2.3	9.4
Model		5MW2UBUT								
Maximums	Max	6009	DLC2.1P	25.0	62	DLC2.1P	25.0	36	DLC2.1P	25.0
	Min	-1668	DLC2.3	25.0	-17	DLC2.3	25.0	-15	DLC2.1P	25.0
Averages	Max	2384	DLC2.1P	25.0	25	DLC2.1P	25.0	13	DLC2.1P	25.0
	Min	845	DLC2.3	9.4	9	DLC2.3	9.4	6	DLC2.3	9.4

Table A8.14. Torque result data in fault conditions (continue).

Torques		LSS			HSS			Generator		
		Value (kN m)	DLC (-)	Vs (m/s)	Value (kN m)	DLC (-)	Vs (m/s)	Value (kN m)	DLC (-)	Vs (m/s)
Model		5MW2UBUTTipBrk								
Maximums	Max	6357	DLC2.1P	25.0	66	DLC2.1P	25.0	36	DLC2.1P	25.0
	Min	-1818	DLC2.3	9.4	-19	DLC2.3	9.4	0	DLC2.1P	11.4
Averages	Max	3022	DLC2.1P	25.0	31	DLC2.1P	25.0	17	DLC2.1P	25.0
	Min	808	DLC2.3	9.4	8	DLC2.3	9.4	6	DLC2.3	9.4
Model		5MW2DB00								
Maximums	Max	6214	DLC2.1P	25.0	64	DLC2.1P	25.0	36	DLC2.1P	25.0
	Min	-1845	DLC2.1P	25.0	-19	DLC2.1P	25.0	-25	DLC2.1P	25.0
Averages	Max	1553	DLC2.1P	25.0	16	DLC2.1P	25.0	12	DLC2.1P	25.0
	Min	729	DLC2.3	9.4	8	DLC2.3	9.4	6	DLC2.3	9.4
Model		5MW2DB00TipBrk								
Maximums	Max	6584	DLC2.1P	25.0	68	DLC2.1P	25.0	36	DLC2.1P	25.0
	Min	-2395	DLC2.3	25.0	-25	DLC2.3	25.0	0	DLC2.1P	11.4
Averages	Max	2922	DLC2.1P	25.0	30	DLC2.1P	25.0	17	DLC2.1P	25.0
	Min	723	DLC2.3	9.4	7	DLC2.3	9.4	5	DLC2.3	9.4
Model		5MW2DBUT								
Maximums	Max	6365	DLC2.1P	25.0	66	DLC2.1P	25.0	36	DLC2.1P	25.0
	Min	-1942	DLC2.3	25.0	-20	DLC2.3	25.0	-14	DLC2.1P	25.0
Averages	Max	2331	DLC2.1P	25.0	24	DLC2.1P	25.0	13	DLC2.1P	25.0
	Min	788	DLC2.3	9.4	8	DLC2.3	9.4	6	DLC2.3	9.4
Model		5MW2DBUTTipBrk								
Maximums	Max	6644	DLC2.1P	25.0	68	DLC2.1P	25.0	36	DLC2.1P	25.0
	Min	-2121	DLC2.3	25.0	-22	DLC2.3	25.0	0	DLC2.1P	11.4
Averages	Max	2973	DLC2.1P	25.0	31	DLC2.1P	25.0	17	DLC2.1P	25.0
	Min	801	DLC2.3	9.4	8	DLC2.3	9.4	5	DLC2.3	9.4
Model		5MW2DB00T5C0								
Maximums	Max	6269	DLC2.1P	25.0	65	DLC2.1P	25.0	36	DLC2.1P	25.0
	Min	-1954	DLC2.3	25.0	-20	DLC2.3	25.0	-25	DLC2.1P	25.0
Averages	Max	1550	DLC2.1P	25.0	16	DLC2.1P	25.0	12	DLC2.1P	25.0
	Min	733	DLC2.3	9.4	8	DLC2.3	9.4	6	DLC2.3	9.4
Model		5MW2DB00T5C0TipBrk								
Maximums	Max	6641	DLC2.1P	25.0	68	DLC2.1P	25.0	36	DLC2.1P	25.0
	Min	-2438	DLC2.3	25.0	-25	DLC2.3	25.0	0	DLC2.1P	11.4
Averages	Max	2882	DLC2.1P	25.0	30	DLC2.1P	25.0	17	DLC2.1P	25.0
	Min	725	DLC2.3	9.4	7	DLC2.3	9.4	5	DLC2.3	9.4
Model		5MW2UB00T0C2.5								
Maximums	Max	6307	DLC2.1P	25.0	65	DLC2.1P	25.0	36	DLC2.1P	25.0
	Min	-1901	DLC2.3	25.0	-20	DLC2.3	25.0	-19	DLC2.1P	25.0
Averages	Max	2134	DLC2.1P	25.0	22	DLC2.1P	25.0	12	DLC2.1P	25.0
	Min	725	DLC2.3	9.4	7	DLC2.3	9.4	6	DLC2.3	9.4
Model		5MW2UB00 T0C2.5TipBrk								
Maximums	Max	6698	DLC2.1P	25.0	69	DLC2.1P	25.0	36	DLC2.1P	25.0
	Min	-2451	DLC2.3	25.0	-25	DLC2.3	25.0	-2	DLC2.1P	25.0
Averages	Max	2750	DLC2.1P	25.0	28	DLC2.1P	25.0	17	DLC2.1P	25.0
	Min	722	DLC2.3	9.4	7	DLC2.3	9.4	5	DLC2.3	9.4
Model		5MW2UB00T0C0								
Maximums	Max	6433	DLC2.1P	25.0	66	DLC2.1P	25.0	36	DLC2.1P	25.0
	Min	-2023	DLC2.3	25.0	-21	DLC2.3	25.0	-19	DLC2.1P	25.0
Averages	Max	2144	DLC2.1P	25.0	22	DLC2.1P	25.0	12	DLC2.1P	25.0
	Min	733	DLC2.3	9.4	8	DLC2.3	9.4	6	DLC2.3	9.4
Model		5MW2UB00T0C0TipBrk								
Maximums	Max	6742	DLC2.1P	25.0	70	DLC2.1P	25.0	36	DLC2.1P	25.0
	Min	-2508	DLC2.3	25.0	-26	DLC2.3	25.0	0	DLC2.1P	11.4
Averages	Max	2803	DLC2.1P	25.0	29	DLC2.1P	25.0	17	DLC2.1P	25.0
	Min	728	DLC2.3	9.4	8	DLC2.3	9.4	5	DLC2.3	9.4
Model		5MW2DB00TeeterNo								
Maximums	Max	6101	DLC2.1P	25.0	63	DLC2.1P	25.0	36	DLC2.1P	25.0
	Min	-1781	DLC2.3	25.0	-18	DLC2.3	25.0	-25	DLC2.1P	25.0
Averages	Max	1557	DLC2.1P	25.0	16	DLC2.1P	25.0	12	DLC2.1P	25.0
	Min	726	DLC2.3	9.4	7	DLC2.3	9.4	6	DLC2.3	9.4

Table A8.14. Torque result data in fault conditions (continue).

Torques		LSS			HSS			Generator		
		Value (kN m)	DLC (-)	Vs (m/s)	Value (kN m)	DLC (-)	Vs (m/s)	Value (kN m)	DLC (-)	Vs (m/s)
Model		5MW2UBUTT2C0TipBrk								
Maximums	Max	6772	DLC2.1P	25.0	70	DLC2.1P	25.0	36	DLC2.1P	25.0
	Min	-2200	DLC2.3	25.0	-23	DLC2.3	25.0	0	DLC2.1P	11.4
Averages	Max	2959	DLC2.1P	25.0	31	DLC2.1P	25.0	17	DLC2.1P	25.0
	Min	806	DLC2.3	9.4	8	DLC2.3	9.4	5	DLC2.3	9.4

Table A8.15. Torque result data in parked conditions.

Torques		LSS			HSS		
		Value (kN m)	DLC (-)	Vs (m/s)	Value (kN m)	DLC (-)	Vs (m/s)
Model		5MW3UB00					
Maximums	Max	2629	DLC6.2a	37.4	27	DLC6.2a	37.4
	Min	-2840	DLC6.2a	37.4	-29	DLC6.2a	37.4
Averages	Max	2406	DLC6.2a	37.4	25	DLC6.2a	37.4
	Min	-2508	DLC6.2a	37.4	-26	DLC6.2a	37.4
Model		5MW2UB00					
Maximums	Max	1455	DLC7.1a	25.0	15	DLC7.1a	25.0
	Min	-702	DLC6.2a	37.4	-7	DLC6.2a	37.4
Averages	Max	1409	DLC7.1a	25.0	15	DLC7.1a	25.0
	Min	-687	DLC6.2a	37.4	-7	DLC6.2a	37.4
Model		5MW2UB00TipBrk					
Maximums	Max	1477	DLC7.1a	25.0	15	DLC7.1a	25.0
	Min	-744	DLC6.2a	37.4	-8	DLC6.2a	37.4
Averages	Max	1423	DLC7.1a	25.0	15	DLC7.1a	25.0
	Min	-725	DLC6.2a	37.4	-7	DLC6.2a	37.4
Model		5MW2UBUT					
Maximums	Max	1734	DLC7.1a	25.0	18	DLC7.1a	25.0
	Min	-677	DLC6.2a	37.4	-7	DLC6.2a	37.4
Averages	Max	1675	DLC7.1a	25.0	17	DLC7.1a	25.0
	Min	-15	DLC6.2a	37.4	0	DLC6.2a	37.4
Model		5MW2UBUTTipBrk					
Maximums	Max	1728	DLC7.1a	25.0	18	DLC7.1a	25.0
	Min	-698	DLC6.2a	37.4	-7	DLC6.2a	37.4
Averages	Max	1674	DLC7.1a	25.0	17	DLC7.1a	25.0
	Min	-17	DLC6.2a	37.4	0	DLC6.2a	37.4
Model		5MW2DB00					
Maximums	Max	1824	DLC7.1a	25.0	19	DLC7.1a	25.0
	Min	-2826	DLC7.1a	25.0	-29	DLC7.1a	25.0
Averages	Max	879	DLC6.2a	37.4	9	DLC6.2a	37.4
	Min	-1300	DLC6.2a	37.4	-13	DLC6.2a	37.4
Model		5MW2DB00TipBrk					
Maximums	Max	1772	DLC7.1a	25.0	18	DLC7.1a	25.0
	Min	-2826	DLC7.1a	25.0	-29	DLC7.1a	25.0
Averages	Max	895	DLC6.2a	37.4	9	DLC6.2a	37.4
	Min	-1320	DLC6.2a	37.4	-14	DLC6.2a	37.4
Model		5MW2DBUT					
Maximums	Max	2503	DLC7.1a	25.0	26	DLC7.1a	25.0
	Min	-2972	DLC7.1a	25.0	-31	DLC7.1a	25.0
Averages	Max	1546	DLC6.2a	37.4	16	DLC6.2a	37.4
	Min	-579	DLC6.2a	37.4	-6	DLC6.2a	37.4
Model		5MW2DBUTTipBrk					
Maximums	Max	2498	DLC7.1a	25.0	26	DLC7.1a	25.0
	Min	-2975	DLC7.1a	25.0	-31	DLC7.1a	25.0
Averages	Max	1579	DLC6.2a	37.4	16	DLC6.2a	37.4
	Min	-618	DLC6.2a	37.4	-6	DLC6.2a	37.4
Model		5MW2DB00T5C0					
Maximums	Max	1787	DLC7.1a	25.0	18	DLC7.1a	25.0
	Min	-2813	DLC7.1a	25.0	-29	DLC7.1a	25.0
Averages	Max	775	DLC6.2a	37.4	8	DLC6.2a	37.4
	Min	-1216	DLC6.2a	37.4	-13	DLC6.2a	37.4

Table A8.15. Torque result data in parked conditions (continue).

Torques		LSS			HSS		
		Value (kN m)	DLC (-)	Vs (m/s)	Value (kN m)	DLC (-)	Vs (m/s)
Model		5MW2DB00T5C0TipBrk					
Maximums	Max	1729	DLC7.1a	25.0	18	DLC7.1a	25.0
	Min	-2745	DLC7.1a	25.0	-28	DLC7.1a	25.0
Averages	Max	792	DLC6.2a	37.4	8	DLC6.2a	37.4
	Min	-1236	DLC6.2a	37.4	-13	DLC6.2a	37.4
Model		5MW2UB00T0C2.5					
Maximums	Max	1291	DLC6.2a	37.4	13	DLC6.2a	37.4
	Min	-986	DLC6.2a	37.4	-10	DLC6.2a	37.4
Averages	Max	394	DLC6.2a	37.4	4	DLC6.2a	37.4
	Min	-971	DLC6.2a	37.4	-10	DLC6.2a	37.4
Model		5MW2UB00 T0C2.5TipBrk					
Maximums	Max	1429	DLC6.2a	37.4	15	DLC6.2a	37.4
	Min	-1010	DLC6.2a	37.4	-10	DLC6.2a	37.4
Averages	Max	415	DLC6.2a	37.4	4	DLC6.2a	37.4
	Min	-992	DLC6.2a	37.4	-10	DLC6.2a	37.4
Model		5MW2UB00T0C0					
Maximums	Max	1327	DLC6.2a	37.4	14	DLC6.2a	37.4
	Min	-1067	DLC6.2a	37.4	-11	DLC6.2a	37.4
Averages	Max	394	DLC6.2a	37.4	4	DLC6.2a	37.4
	Min	-975	DLC6.2a	37.4	-10	DLC6.2a	37.4
Model		5MW2UB00T0C0TipBrk					
Maximums	Max	1416	DLC6.2a	37.4	15	DLC6.2a	37.4
	Min	-1114	DLC6.2a	37.4	-11	DLC6.2a	37.4
Averages	Max	415	DLC6.2a	37.4	4	DLC6.2a	37.4
	Min	-1004	DLC6.2a	37.4	-10	DLC6.2a	37.4
Model		5MW2DB00TeeterNo					
Maximums	Max	1893	DLC7.1a	25.0	20	DLC7.1a	25.0
	Min	-2845	DLC7.1a	25.0	-29	DLC7.1a	25.0
Averages	Max	878	DLC6.2a	37.4	9	DLC6.2a	37.4
	Min	-1300	DLC6.2a	37.4	-13	DLC6.2a	37.4
Model		5MW2UBUTT2C0TipBrk					
Maximums	Max	1229	DLC6.2a	37.4	13	DLC6.2a	37.4
	Min	-1278	DLC6.2a	37.4	-13	DLC6.2a	37.4
Averages	Max	1206	DLC6.2a	37.4	12	DLC6.2a	37.4
	Min	-444	DLC6.2a	37.4	-5	DLC6.2a	37.4

Table A8.16. Tower-to-blade clearance result data in normal operating conditions.

	Blade 1 Minimum Clearance			Blade 2 Minimum Clearance		
Model	Value (m)	DLC (-)	Vs (m/s)	Value (m)	DLC (-)	Vs (m/s)
5MW3UB00	6.59	DLC1.3	17.0	6.70	DLC1.4	11.4
5MW2UB00	4.04	DLC1.3	19.0	4.40	DLC1.3	21.0
5MW2UB00TipBrk	4.36	DLC1.3	19.0	4.67	DLC1.3	21.0
5MW2UBUT	3.89	DLC1.3	17.0	3.08	DLC1.3	17.0
5MW2UBUTTipBrk	4.06	DLC1.3	17.0	3.29	DLC1.3	17.0
5MW2DB00	10.30	DLC1.3	25.0	10.66	DLC1.3	25.0
5MW2DB00TipBrk	10.37	DLC1.3	25.0	10.75	DLC1.3	25.0
5MW2DBUT	10.46	DLC1.3	25.0	10.24	DLC1.3	25.0
5MW2DBUTTipBrk	10.45	DLC1.3	25.0	10.24	DLC1.3	25.0
5MW2DB00T5C0	8.19	DLC1.3	25.0	8.49	DLC1.3	25.0
5MW2DB00T5C0TipBrk	8.28	DLC1.3	25.0	8.59	DLC1.3	25.0
5MW2DB00T0C2.5	4.62	DLC1.3	25.0	4.74	DLC1.3	23.0
5MW2DB00T0C2.5TipBrk	4.69	DLC1.3	25.0	4.78	DLC1.3	23.0
5MW2DB00T0C0	2.48	DLC1.3	25.0	2.53	DLC1.3	23.0
5MW2DB00T0C0TipBrk	2.54	DLC1.3	25.0	2.58	DLC1.3	23.0
5MW2DB00TeeterNo	10.26	DLC1.3	25.0	10.37	DLC1.3	23.0
5MW2DBUTT2C0TipBrk	4.74	DLC1.3	25.0	4.44	DLC1.3	25.0

Table A8.17. Tower-to-blade clearance result data in fault conditions.

Model	Blade 1 Minimum Clearance			Blade 2 Minimum Clearance		
	Value (m)	DLC (-)	Vs (m/s)	Value (m)	DLC (-)	Vs (m/s)
5MW3UB00	6.97	DLC2.3	9.4	5.82	DLC2.3	11.4
5MW2UB00	4.50	DLC2.1P	11.4	3.89	DLC2.3	11.4
5MW2UB00TipBrk	2.66	DLC2.3	25.0	4.24	DLC2.1G	25.0
5MW2UBUT	4.37	DLC2.1P	11.4	2.65	DLC2.3	11.4
5MW2UBUTTipBrk	4.09	DLC2.3	25.0	2.66	DLC2.3	11.4
5MW2DB00	7.09	DLC2.1G	25.0	4.76	DLC2.1P	11.4
5MW2DB00TipBrk	10.01	DLC2.3	25.0	10.48	DLC2.1P	25.0
5MW2DBUT	8.37	DLC2.1G	11.4	6.28	DLC2.1P	11.4
5MW2DBUTTipBrk	9.38	DLC2.3	25.0	10.75	DLC2.1P	25.0
5MW2DB00T5C0	4.73	DLC2.1G	25.0	2.00	DLC2.1P	11.4
5MW2DB00T5C0TipBrk	7.65	DLC2.3	25.0	7.99	DLC2.1P	25.0
5MW2DB00T0C2.5	0.88	DLC2.1G	25.0	0.97	DLC2.1P	11.4
5MW2DB00T0C2.5TipBrk	3.99	DLC2.3	25.0	4.07	DLC2.1P	25.0
5MW2DB00T0C0	0.61	DLC2.1G	25.0	0.02	DLC2.1P	25.0
5MW2DB00T0C0TipBrk	1.67	DLC2.3	25.0	2.03	DLC2.1P	25.0
5MW2DB00TeeterNo	6.97	DLC2.1G	25.0	6.75	DLC2.3	25.0
5MW2DBUTT2C0TipBrk	3.63	DLC2.3	25.0	4.37	DLC2.1P	25.0

Table A8.18. Tower-to-blade clearance result data in parked conditions.

Model	Blade 1 Minimum Clearance			Blade 2 Minimum Clearance		
	Value (m)	DLC (-)	Vs (m/s)	Value (m)	DLC (-)	Vs (m/s)
5MW3UB00	63.31	DLC7.1a	25.0	33.47	DLC7.1a	25.0
5MW2UB00	63.21	DLC7.1a	25.0	63.38	DLC6.2a	37.4
5MW2UB00TipBrk	63.21	DLC7.1a	25.0	63.37	DLC6.2a	37.4
5MW2UBUT	63.21	DLC7.1a	25.0	63.37	DLC6.2a	37.4
5MW2UBUTTipBrk	63.21	DLC7.1a	25.0	63.36	DLC6.2a	37.4
5MW2DB00	63.33	DLC6.1a	37.4	63.29	DLC7.1a	25.0
5MW2DB00TipBrk	63.33	DLC6.1a	37.4	63.29	DLC7.1a	25.0
5MW2DBUT	63.32	DLC6.1a	37.4	63.12	DLC7.1a	25.0
5MW2DBUTTipBrk	63.31	DLC6.1a	37.4	63.10	DLC7.1a	25.0
5MW2DB00T5C0	63.10	DLC6.1a	37.4	63.06	DLC7.1a	25.0
5MW2DB00T5C0TipBrk	63.10	DLC6.1a	37.4	63.06	DLC7.1a	25.0
5MW2DB00T0C2.5	63.31	DLC6.2a	37.4	63.34	DLC7.1a	25.0
5MW2DB00T0C2.5TipBrk	63.29	DLC6.2a	37.4	63.33	DLC7.1a	25.0
5MW2DB00T0C0	63.09	DLC6.2a	37.4	63.12	DLC7.1a	25.0
5MW2DB00T0C0TipBrk	63.08	DLC6.2a	37.4	63.12	DLC7.1a	25.0
5MW2DB00TeeterNo	63.33	DLC6.1a	37.4	63.37	DLC6.2a	37.4
5MW2DBUTT2C0TipBrk	63.11	DLC6.2a	37.4	63.10	DLC6.2a	37.4

Table A8.19. Teeter angle result data in normal operating conditions.

Model	Maximum Teeter Angle			Minimum Teeter Angle		
	Value (deg)	DLC (-)	Vs (m/s)	Value (deg)	DLC (-)	Vs (m/s)
5MW3UB00	0.00	DLC1.1	3.0	0.00	DLC1.1	3.0
5MW2UB00	2.38	DLC1.4	9.4	-2.69	DLC1.4	9.4
5MW2UB00TipBrk	2.36	DLC1.4	9.4	-2.65	DLC1.4	9.4
5MW2UBUT	2.99	DLC1.4	11.4	-3.17	DLC1.4	11.4
5MW2UBUTTipBrk	2.97	DLC1.4	11.4	-3.22	DLC1.4	11.4
5MW2DB00	2.74	DLC1.4	11.4	-3.09	DLC1.4	9.4
5MW2DB00TipBrk	2.71	DLC1.4	11.4	-3.04	DLC1.4	9.4
5MW2DBUT	3.44	DLC1.4	11.4	-3.24	DLC1.4	11.4
5MW2DBUTTipBrk	3.44	DLC1.4	11.4	-3.19	DLC1.4	11.4
5MW2DB00T5C0	2.57	DLC1.4	11.4	-2.96	DLC1.4	9.4
5MW2DB00T5C0TipBrk	2.54	DLC1.4	11.4	-2.91	DLC1.4	9.4
5MW2DB00T0C2.5	2.68	DLC1.4	11.4	-3.04	DLC1.4	9.4
5MW2DB00T0C2.5TipBrk	2.64	DLC1.4	11.4	-2.99	DLC1.4	9.4
5MW2DB00T0C0	2.52	DLC1.4	11.4	-2.93	DLC1.4	9.4
5MW2DB00T0C0TipBrk	2.48	DLC1.4	11.4	-2.89	DLC1.4	9.4
5MW2DB00TeeterNo	0.00	DLC1.1	3.0	0.00	DLC1.1	3.0
5MW2DBUTT2C0TipBrk	3.24	DLC1.4	11.4	-3.07	DLC1.4	9.4

Table A8.20. Teeter angle result data in fault conditions.

Model	Maximum Teeter Angle			Minimum Teeter Angle		
	Value (deg)	DLC (-)	Vs (m/s)	Value (deg)	DLC (-)	Vs (m/s)
5MW3UB00	0.00	DLC2.1G	11.4	0.00	DLC2.1G	11.4
5MW2UB00	5.94	DLC2.1P	25.0	-1.49	DLC2.3	25.0
5MW2UB00TipBrk	2.97	DLC2.1P	25.0	-1.82	DLC2.1G	25.0
5MW2UBUT	5.20	DLC2.1P	11.4	-1.63	DLC2.1G	25.0
5MW2UBUTTipBrk	3.00	DLC2.1P	25.0	-1.65	DLC2.1G	25.0
5MW2DB00	5.05	DLC2.1P	25.0	-1.49	DLC2.3	25.0
5MW2DB00TipBrk	3.19	DLC2.1P	25.0	-2.75	DLC2.1G	25.0
5MW2DBUT	4.77	DLC2.1P	25.0	-1.71	DLC2.1G	25.0
5MW2DBUTTipBrk	2.58	DLC2.1G	25.0	-2.62	DLC2.1G	25.0
5MW2DB00T5C0	5.14	DLC2.1P	25.0	-1.41	DLC2.3	25.0
5MW2DB00T5C0TipBrk	3.26	DLC2.1P	25.0	-2.77	DLC2.1G	25.0
5MW2DB00T0C2.5	5.47	DLC2.1P	25.0	-1.48	DLC2.1P	25.0
5MW2DB00T0C2.5TipBrk	2.58	DLC2.1P	25.0	-1.95	DLC2.1G	25.0
5MW2DB00T0C0	5.55	DLC2.1P	25.0	-1.45	DLC2.1P	25.0
5MW2DB00T0C0TipBrk	2.67	DLC2.1P	25.0	-1.93	DLC2.1G	25.0
5MW2DB00TeeterNo	0.00	DLC2.1G	11.4	0.00	DLC2.1G	11.4
5MW2DBUTT2C0TipBrk	3.02	DLC2.1P	25.0	-1.98	DLC2.1G	25.0

Table A8.21. Teeter angle result data in parked conditions.

Model	Maximum Teeter Angle			Minimum Teeter Angle		
	Value (deg)	DLC (-)	Vs (m/s)	Value (deg)	DLC (-)	Vs (m/s)
5MW3UB00	0.00	DLC6.1a	37.4	0.00	DLC6.1a	37.4
5MW2UB00	1.04	DLC7.1a	25.0	-0.02	DLC6.2a	37.4
5MW2UB00TipBrk	1.04	DLC7.1a	25.0	-0.02	DLC6.2a	37.4
5MW2UBUT	1.05	DLC7.1a	25.0	-0.02	DLC6.2a	37.4
5MW2UBUTTipBrk	1.05	DLC7.1a	25.0	-0.02	DLC6.2a	37.4
5MW2DB00	1.01	DLC7.1a	25.0	-0.06	DLC6.2a	37.4
5MW2DB00TipBrk	1.01	DLC7.1a	25.0	-0.06	DLC6.2a	37.4
5MW2DBUT	1.01	DLC7.1a	25.0	-0.08	DLC6.2a	37.4
5MW2DBUTTipBrk	1.01	DLC7.1a	25.0	-0.08	DLC6.2a	37.4
5MW2DB00T5C0	1.02	DLC7.1a	25.0	-0.07	DLC6.2a	37.4
5MW2DB00T5C0TipBrk	1.01	DLC7.1a	25.0	-0.07	DLC6.2a	37.4
5MW2DB00T0C2.5	1.00	DLC7.1a	25.0	-0.07	DLC6.2a	37.4
5MW2DB00T0C2.5TipBrk	1.01	DLC7.1a	25.0	-0.08	DLC6.2a	37.4
5MW2DB00T0C0	1.00	DLC7.1a	25.0	-0.07	DLC6.2a	37.4
5MW2DB00T0C0TipBrk	1.00	DLC7.1a	25.0	-0.07	DLC6.2a	37.4
5MW2DB00TeeterNo	0.00	DLC6.1a	37.4	0.00	DLC6.1a	37.4
5MW2DBUTT2C0TipBrk	0.99	DLC7.1a	25.0	-0.03	DLC6.2a	37.4

Appendix 9: Publications

Already Published/Presented

1. Andersen, B., Norouzi, M., Sescu, A., Wells, E., Nikolaidis, E., Cioc, S. & Afjeh, A. (2011). Advancing Offshore Freshwater Wind Energy Development. *Keynote paper presented at 5th International HNICEM Conference* in Manila, Philippines.

2. Sescu, A., Anderson, B. & Afjeh, A. (2011). Computational Investigation of Tower Shadow Effects on Wind Turbines, IMECE2011-62313, *Proceedings of the ASME International Mechanical Engineering Congress and Exposition*, Denver, CO.

3. Norouzi, M., Wells, E., Cioc, S. & Nikolaidis, E. (2011). Simulation of a Monopile 5MW Wind Turbine under Ice Impact Loads, *AWEA Offshore Windpower 2011 Conference & Exhibition*, Baltimore, MD.

4. Norouzi, M. & Nikolaidis, E. (2012). Efficient Estimation of First Excursion Failure by PRRA. *14th AIAA/ISSMO Multidisciplinary Analysis and Optimization (MAO) Conference*, 2012, Indianapolis, IN.

5. Norouzi, M. & Nikolaidis, E. (2012). Efficient Method for Reliability Assessment Under High-Cycle Fatigue. *International Journal of Reliability, Quality and Safety Engineering*, 19(5):2012, pp. 1-27, doi:10.1142/S0218539312500222

6. Norouzi, M. & Nikolaidis, E. (2012). Importance Sampling for Estimation of the Probability of Failure of Dynamic Systems, *SAE Int. J. Mater. Manf.* , 6(3):2013, doi:10.4271/2013-01-0607

7. Lee, J.W., (2012). Preliminary Studies of Structural Design Optimization for Composite Wind Turbine Blades, *Inaugural Meeting of the North American Wind Energy Academy (NAWEA)*, Amherst, MA.

8. Norouzi, M., (2012). Probabilistic Design of an Offshore Wind Turbine. *Inaugural Meeting of the North American Wind Energy Academy (NAWEA)*, Amherst, MA.

9. Norouzi, M. & Nikolaidis, E. (2012). Estimation of High-Cycle Fatigue Life by using Re-analysis. *SAE Int. J. Mater. Manf.* 5(1):2012, doi:10.4271/2012-01-0066

10. Norouzi, M. & Nikolaidis, E. (2012). Efficient Random Vibration Analysis Using Markov Chain Monte Carlo Simulation, *SAE Int. J. Mater. Manf.*, 5(1):2012, doi:10.4271/2012-01-0067.

11. Norouzi, M. & Nikolaidis, E., (2012). Modeling Dependence between Wind and Wave by Copula, *AWEA Offshore Windpower 2012 Conference & Exhibition*, Virginia Beach, VA.

12. Lee, J.W. & Jehan, M., (2012). First Excursion Failure and Fatigue Life Prediction and Damage Estimation of Composite Laminate Wind Turbine Blades, *AWEA Offshore Windpower 2012 Conference & Exhibition*, Virginia Beach, VA.

13. Sescu, A. & Afjeh, A. (2012). Evaluation of Aerodynamic Infrasound Radiating from Upwind and Downwind HAWT's. IMECE2012-86189, *Proceedings of the ASME 2012 International Mechanical Engineering Congress and Exposition*, Houston, TX.

14. Andersen, B., Lee, J.W., Norouzi, M., Jehan, M., Nikolaidis, E. & Afjeh, A. (2013). Advanced Concept Offshore Wind Turbine for the Great Lakes, *Clean Energy Manufacturing Initiative (CEMI) Summit*, Toledo, OH.

15. Norouzi, M. & Nikolaidis, E. (2013). Integrating Subset Simulation with Probabilistic Re-analysis to Estimate Reliability of Dynamic Systems. *Structural and Multidisciplinary Optimization*, DOI 10.1007/s00158-013-0914-9 2013

16. Norouzi, M., Wells, E., Cioc, S., Nikolaidis, E. & Afjeh, A. (2013). Significance of Ice Impact on Structural Integrity of a Monopile Offshore Wind Turbine in The Great Lakes, *23rd International Offshore (Ocean) and Polar Engineering Conference*, Alaska, Anchorage.

17. Norouzi, M. & Nikolaidis, E. (2013). Modeling Dependence between Wind and Wave in an Offshore Wind Turbine Site. *23rd International Offshore (Ocean) and Polar Engineering Conference*, Alaska, Anchorage.

18. Norouzi, M. & Nikolaidis, E. (2013). Efficient Sensitivity Reliability Analysis of Dynamic Systems Considering Change in Energy Content of Excitation. *11th International Conference On Structural Safety And Reliability (ICOSSAR)*, Columbia University, New York, NY, USA

Accepted for Publication/Presentation

1. Lee, J.W., Norouzi, M., Nikolaidis, E. & Afjeh, A. (2013, October). Comparison of the Loads on a 2-Bladed Downwind Turbine and a 3-Bladed Upwind Turbine, *AWEA Offshore WINDPOWER 2013 Conference*, Providence, RI

2. Lee, J.W., and Nikolaidis, E. (2013, October). Efficient Stress Estimation Method for Dynamic Wind Turbine Simulation Using FAST Results, *AWEA Offshore WINDPOWER 2013 Conference*, Providence, RI.

3. Norouzi, M., Lee, J.W., Nikolaidis,E. & Afjeh,A.A., (2013, October). Studying Effect of Soil and Structure Interaction on Load Estimates of a Monopile Offshore Turbine, *AWEA Offshore WINDPOWER 2013 Conference, Providence, RI.*